Stochastic Dynamic Response of Wood Structural Systems

by

Greg C. Foliente

Dissertation submitted to the Faculty of the
Virginia Polytechnic Institute and State University
in partial fulfillment of the requirements for the degree of

DOCTOR OF PHILOSOPHY

in

Wood Science and Forest Products

APPROVED :

J. Daniel Dolan, Co-chairman

Mahendra P. Singh, Co-chairman

Siegfried M. Holzer

D. Earl Kline

Joseph R. Loferski

December, 1993

Blacksburg, Virginia

Stochastic Dynamic Response of Wood Structural Systems

by

Greg C. Foliente

Committee Co-chairs: J. Daniel Dolan and Mahendra P. Singh

Wood Science and Forest Products

(Abstract)

Difficulties in characterizing the dynamic behavior of wood structures have hindered investigations into their performance under dynamic loading. Because of this, wood structures are treated unfavorably in seismic design codes, even though past damage assessment surveys after seismic events indicated generally satisfactory performance. To allow investigations into their performance and safety under dynamic loading, the energy dissipation mechanisms of wood joints and structural systems must be known and the hysteretic behavior modeled properly. This dissertation presents a general hysteresis model for wood joints and structural systems, based on a modification of the Bouc-Wen-Baber-Noori (BWBN) model. The hysteretic constitutive law, based on the endochronic theory of plasticity and characterized by a single mathematical form, produces a versatile, smoothly varying hysteresis that models previously observed behavior of wood joints and structural systems, namely, (*1*) nonlinear, inelastic behavior, (*2*) stiffness degradation, (*3*) strength degradation, (*4*) pinching, and (*5*) memory. The constitutive law takes into account the experimentally observed dependence of wood joints' response to their past history (i.e., the input and response at earlier times, or memory). Practical guidelines to estimate the hysteresis parameters of any wood joint or structural system are given. Hysteresis shapes produced by the proposed model are shown to compare favorably with experimental hysteresis of wood joints with: (*1*) yielding plates, (*2*) yielding nails, and (*3*) yielding bolts. To verify its behavior under arbitrary dynamic loadings, the proposed model is implemented in a nonlinear dynamic analysis program for single-degree-of-freedom (SDF) systems.

Three SDF wood systems are subjected to the Loma Prieta accelerogram to obtain their response time histories. Advantages of using the proposed model over currently available models in nonlinear dynamic analysis of more complex systems are identified. A multi-degree-of-freedom shear building model incorporating the proposed hysteresis model is formulated but not implemented on a computer.

For more realistic loadings, the random characteristics of earthquakes are modeled as a stochastic or random process. Nonlinear response statistics of SDF wood systems are obtained by Monte Carlo simulation and statistical linearization. The statistical linearization solutions are shown to give reasonably good estimates of mean-square response, for a range of practical system and model parameter values. An example verification procedure that can be used in applying the method to practical engineering problems is presented. The response analysis technique is general and can be applied not only in random vibration analysis of wood structural systems but also in the analysis of a wide variety of hysteretic systems with general pinching behavior, including reinforced concrete structures, braced steel frames and laterally loaded piles. Potential practical applications of the analysis method and of the response statistics obtained from the analysis are presented. The present work is the first known attempt to use random vibration techniques in studying the response of wood structures under natural hazard loadings.

Acknowledgements

I wish to express my gratitude to Drs. Mahendra P. Singh and J. Daniel Dolan for co-chairing my PhD committee. My interest in random vibrations and earthquake engineering was heightened by the teaching and research of Dr. Singh. Dr. Dolan provided support, friendship and encouragement throughout my program. I am also grateful to the members of my committee for their interest in my research and graduate education.

My special thanks go to Dr. Mohammad N. Noori of Worcester Polytechnic Institute in Massachusetts for his encouragement and for sharing with me information about his previous work on random vibration analysis of degrading and pinching hysteretic systems. Dr. Russi Yordanov of the Mathematics and Physics departments at Virginia Tech cheerfully entertained all my questions on various mathematical problems that I encountered in my graduate studies and research. I deeply appreciate his friendship. I also thank Dr. Y.-K. Wen of the University of Illinois at Urbana-Champaign and Dr. R.H. Sues of Applied Research Associates, Inc. in Raleigh, North Carolina for their cooperation in the initial stages of this work.

This project was funded by the U.S. Department of Agriculture National Research Initiative, Competitive Grants Program for Forest and Rangeland Renewable Resources. Dr. Thomas E. McLain served as my initial supervisor in this project. He was also my graduate advisor and mentor for five and a half years. I truly treasure the opportunity of being associated with him.

I am especially indebted to my wife, Tomoko, for her encouragement and abiding love. I am extremely blessed to have such a patient and supportive wife. My baby daughter, Megumi, has given me much joy, energy and inspiration. The elders and members of Blacksburg Christian Fellowship shared their love and fellowship to me and my family and made our stay in Blacksburg a very pleasant and memorable experience. Finally, I thank my parents and brothers, who have always been a constant source of love and support.

"Where is the Life we have lost in living?

Where is the wisdom we have lost in knowledge?

Where is the knowledge we have lost in information?"

– **(T.S. Eliot** 1888—1965) *Choruses from 'The Rock', I*

"For whoever finds me (wisdom) finds life and receives favor from the Lord ... The fear of the Lord is the beginning of wisdom, and knowledge of the Holy One is understanding."

– **Proverbs 8:35, 9:10**

Table of Contents

List of Tables

List of Figures

Notation

The following variables and symbols are used in the main part of this dissertation. Symbols used in the Appendices are defined where they appear.

A	=	parameter that affects the tangent stiffness and ultimate hysteretic strength;
A_o	=	initial value of A;
a_1, a_2, a_i	=	amplitude of cyclic excitation;
B	=	matrix of the expected values of the products of the forcing functions and the response vectors;
$[C]$	=	the damping matrix of a multi-degree-of-freedom (MDF) system;
C_{e3}	=	linearization coefficient of y_2;
C_i	=	expectations required to compute C_{e3};
c	=	viscous damping coefficient;
c_i	=	viscous damping coefficient of i^{th} mass;
c_1, c_2	=	viscous damping coefficient of generalized Maxwell model;
D	=	damage index;
D_i	=	damage index of the i^{th} storey;
D_T	=	global damage index;
$E(\cdot)$	=	expected value;
E_a	=	absorbed energy;
E_{a_i}	=	total absorbed energy of the i^{th} storey;
E_h	=	hysteretic energy;
E_i	=	input energy;
E_s	=	elastic strain energy;
E_ξ	=	damping energy;
e	=	error introduced by the linearization in random vibration analysis;

$\mathrm{erf}(\cdot)$ = error function (see Appendix B for details);

$\mathrm{erfc}(\cdot)$ = complementary error function (see Appendix B for details);

$F(t)$ = forcing function;

F_h = hysteretic restoring force;

F_{p_i} = peak factor;

F_T = total non-damping restoring force;

F_{T_y} = yield level of F_T;

$\mathbf{f}$ = vector of the dynamic actions;

$f(t), f_i(t)$ = mass-normalized forcing function;

f_s = non-damping restoring force;

$f_{Y_2Y_3}(y_2y_3)$= zero-mean joint Gaussian probability density function for y_2 and y_3;

$\mathbf{G}$ = matrix that contains the coefficients of $\mathbf{y}$;

g = acceleration of gravity (32.2 ft/s^2 or 9.807 m/s^2);

$H(\cdot)$ = the Heaviside function;

$[H^\alpha]$ = matrix that contains the hysteretic elements;

$h(\cdot)$ = an arbitrary function;

h_i^α = hysteretic coefficient of i^{th} element $[(1-\alpha_i)k_i]$;

$h(z)$ = pinching function;

h_1, h_2 = rate of u crossing U_{max} from below and from above, respectively;

$\{\mathcal{I}\}$ = the influence vector;

$I_{GL}(\cdot)$ = generalized Gauss-Laguerre quadrature;

I_{sn} = standard sin integral;

$I_{sum}(\cdot)$ = standard summation;

$[K^\alpha]$ = linear part of the stiffness matrix;

K_{e3} = linearization coefficient of y_3;

K_i = expectations required to compute K_{e3};

k = stiffness;

k_i, k_f = initial and final tangent stiffness, respectively;

k_i^{α} = linear spring coefficient of i^{th} element ($\alpha_i k_i$);

k_1, k_2 = spring stiffness of generalized Maxwell model;

$[M]$ = the mass matrix of a MDF system;

m = system mass;

m_i = mass of the i^{th} element;

n = hysteresis shape parameter that controls curve smoothness;

P = applied force;

$P(\cdot)$ = probability [$P_u(\cdot)$ is an upper bound and $P_l(\cdot)$ is a lower bound];

p = constant that controls the rate of initial drop in slope;

p_o = probability that the response will cross U_{max} in time t_d;

Q_i = total restoring force of the i^{th} mass;

Q_y = calculated joint yield strength;

q = fraction of ultimate hysteretic strength, z_u, where pinching occurs;

$\mathfrak{R}$ = differential operator;

$R_{XX}(t_1, t_2)$ = autocorrelation function of a random process $X(t)$ [also written as $R_{XX}(\tau)$ for stationary random processes; $\tau = t_2 - t_1$];

r = total number of lumped masses in a MDF model;

$\mathbf{S}$ = zero-mean time lag covariance matrix;

$\dot{\mathbf{S}}$ = time derivative of $\mathbf{S}$;

$\text{sgn}(\cdot)$ = the signum function;

S_o = white noise power spectral density level;

t, t_i = time;

$\bar{t}, t_d$ = time until U_{max} is crossed;

U_{max} = maximum displacement response level;

$\mathbf{u}$ = vector of system response;

u = relative displacement of the mass with respect to the base displacement;

$\dot{u}$ = relative velocity of the mass with respect to the base velocity;

$\ddot{u}$ = relative acceleration of the mass with respect to the base acceleration;

$\dddot{u}$ = relative jerk of the mass with respect to the base jerk;

u_g = earthquake ground displacement;

$\ddot{u}_g$ = earthquake ground acceleration;

u_i = interstorey drift, or relative displacement between floors;

u_{max} = maximum relative displacement;

u_o = relative displacement at $z = 0$;

u_{p_i} = peak displacement in i^{th} half cycle;

$u_{p_{i-1}}$ = peak displacement in $(i-1)^{th}$ half cycle (note that this is the peak opposite and immediately before that in the i^{th} half cycle);

u_t = absolute or total mass displacement $(u + u_g)$;

u_y = yield relative displacement;

$\mathbf{y}$ = vector of global response of a single-degree-of-freedom (SDF) system;

y_i = i^{th} element of response vector $\mathbf{y}$;

$\dot{y}_i$ = time derivative of y_i;

$\{X\}$ = vector of relative displacements;

$X(t)$ = random process;

x_i = relative displacement of the i^{th} mass with respect to the ground displacement;

$\dot{x}_i$ = relative velocity of the i^{th} mass with respect to the ground velocity;

$\ddot{x}_i$ = relative acceleration of the i^{th} mass with respect to the ground acceleration;

$\ddot{x}_g$ = ground acceleration;

$\ddot{x}_i^A$ = absolute acceleration $(\ddot{x}_i + \ddot{x}_g)$;

$\{Z\}$ = vector of the hysteretic components of the displacements;

z = hysteretic component of the displacement;

z_i = hysteretic displacement of the i^{th} mass;

z_{p_i} = peak z value in i^{th} half cycle;

$z_{p_{i-1}}$ = peak z value in $(i-1)^{th}$ half cycle;

z_u = ultimate value of z (or z at $\frac{dz}{du} = 0$);

α = a weighting constant representing the relative participations of the linear and nonlinear terms ($0< \alpha <1$); also known as rigidity ratio;

β = hysteresis shape parameter;

$\Gamma(\cdot)$ = Gamma function;

γ = hysteresis shape parameter;

$\gamma(\cdot)$ = incomplete Gamma function;

Δ_i = constants for expected values needed by C_{e3} and K_{e3};

$\delta(\cdot)$ = Dirac delta function;

δ_A = constant that controls the rate of strength and stiffness degradation;

δ_{ij} = Kronecker delta;

δ_m = maximum deformation under earthquake;

δ_u = ultimate deformation under monotonic loading;

δ_η = constant that controls the rate of stiffness degradation;

δ_ν = constant that controls the rate of strength degradation;

δ_ψ = parameter specified for the desired rate of change of ζ_2 based on ε;

ε = dissipated hysteretic energy;

$\dot{\varepsilon}$ = the rate of change of dissipated hysteretic energy;

ζ_1 = controls the magnitude of initial drop in slope, $\frac{dz}{du}$, ($\zeta_1 < 1.0$);

ζ_{1_o} = measure of total slip;

ζ_2 = controls the rate of change of the slope, $\frac{dz}{du}$;

η = stiffness degradation parameter;

η_i = value of η during the i^{th} half cycle;

θ_o = integration limit of I_{sn};

κ = non-negative parameter for determining damage index D;

λ = small parameter that controls the rate of change of ζ_2 as ζ_1 changes;

μ = ductility;

$\mu_X(t)$ = mean value function of random process $X(t)$;

$\mu_{U_{max}}$ = mean of U_{max};

μ_ε = mean of ε;

μ_{ζ_1} = mean of ζ_1;

μ_{ζ_2} = mean of ζ_2;

μ_η = mean of η;

μ_ν = mean of ν;

μ_{1*}, μ_{2*} = linearization coefficient constants;

ν = strength degradation parameter;

ξ = viscous damping ratio;

ξ_g = dominant damping ratio of the ground;

ξ_o = linear damping ratio ($c/2\sqrt{k_i m}$);

ρ, $\rho_{\dot{u}z}$, ρ_{23} = correlation coefficient of y_2 (or $\dot{u}$) and y_3 (or z);

$\rho_{u\dot{u}}$ = correlation coefficient of u and $\dot{u}$;

σ_u = root-mean-square (RMS) of y_1 (or u);

$\bar{\sigma}_u$ = maximum RMS of y_1 (or u) that occurs at $t = \bar{t}$;

$\sigma_{\dot{u}}$, σ_2 = RMS of y_2 (or $\dot{u}$);

σ_z, σ_3 = RMS of y_3 (or z);

σ_{1*}, σ_{2*} = linearization coefficient constants;

$\Phi(\cdot)$ = standard Gaussian cumulative distribution function;

$\Phi(\omega)$ = Kanai-Tajimi power spectral density function;

$\Phi_X(\omega)$ = power spectral density function of a random process $X(t)$;

ϕ_i = energy absorbing contribution factor to compute global damage D_T;

τ = time lag ($t_2 - t_1$);

ψ_o = parameter that contributes to the amount of pinching;

ω, ω_i = frequency of cyclic excitation;

ω_g = dominant frequency of the ground;

ω_n = natural frequency of undamped oscillation;

ω_o = preyield natural frequency of the system ($\sqrt{k_i/m}$).

Chapter 1

Introduction

1.1 General

Wood structures are generally recognized to perform well in seismic zones. This is attributed to wood's high specific strength (high strength to weight ratio), redundancy of non-load bearing elements including the presence of non-engineered shear walls and diaphragms and unit action of the system when the components are adequately fastened. Favorable system geometry, e.g. symmetrical plan for earthquake and steep roof slope for wind, also contribute to its performance.

Wood construction does not, however, guarantee earthquake- and/or hurricane-resistant structures. Assessments of collapsed or damaged wood buildings after earthquakes and typhoons have identified common failure modes and their possible causes and solutions (Soltis 1984; Falk and Soltis 1988; Conner et al. 1987). Most of what we know about wood structural behavior under dynamic loading, however, comes from qualitative field data and/or limited experimental data, with little theoretical understanding of actual behavior. Difficulties in characterizing wood system behavior (e.g., sensitivity of material properties to the rate and duration of loading and inelastic and nonlinear behavior) have hindered investigations into their performance under dynamic loading. Because of this, wood structures are treated unfavorably in seismic design codes. Stringent and unclear code requirements put wood at a disadvantage in competing with other traditional construction materials, such as steel and concrete, for the engineered structures market. Methods for dynamic analysis of wood structures

are needed to investigate the performance and safety of engineered wood systems under natural hazards.

A *dynamic analysis* or *dynamic response analysis* problem is one where the dynamic action (i.e., force) on a structural system- which is modeled mathematically by the assumed (or measured) mass, damping and stiffness properties of the actual system- is known and the corresponding system response is sought (Fig. 1.1). Accuracy of the computed response depends on the accuracy of the mathematical model used to describe the actual system and of the forcing function used to describe the dynamic action on the structure. Thus, the system model should provide as realistic a description of the actual structure's behavior as possible and the random nature of natural hazard loadings should be considered in the analysis.

1.2 Constitutive Modeling

With static monotonic loading, an appropriate load-displacement relation is normally sufficient to predict system response (Fig. 1.2a). With cyclic loading, the load-displacement trace produces *hysteresis* loops (Fig. 1.2b) caused by damping and/or inelastic deformation. (The area contained in the loop represents the *energy dissipated* by the structure.) Analytical modeling of an inelastic structure under dynamic loading ideally requires a force-displacement relation, or hysteresis model, that can produce the true behavior of the structure at all displacement levels and strain rates (Sozen 1974). Consequently, the energy dissipation mechanisms of wood joints and structural systems must be known and the hysteretic behavior modeled properly before we can accurately predict the overall system response of wood structures to dynamic loads.

Since (*1*) there are hundreds of combinations of materials and joint configurations in wood systems, and (*2*) wood-based products, fasteners and use of wood-based products continue to evolve, a general constitutive model is preferred over models derived from specific configurations. A completely empirical model will not only be expensive to

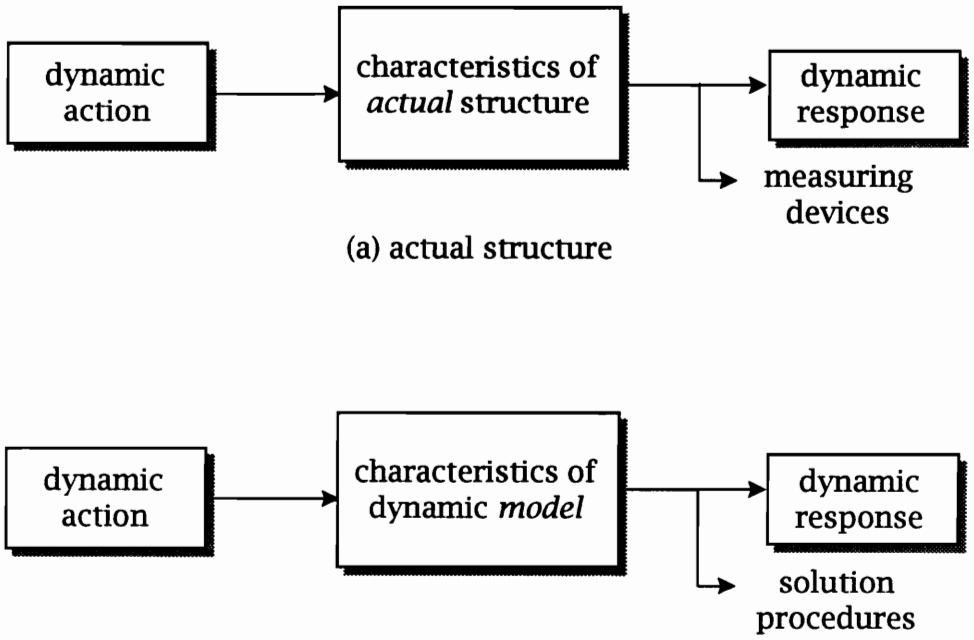

(a) actual structure

(b) equivalent dynamic model

Figure 1.1: Block scheme of the dynamic analysis process

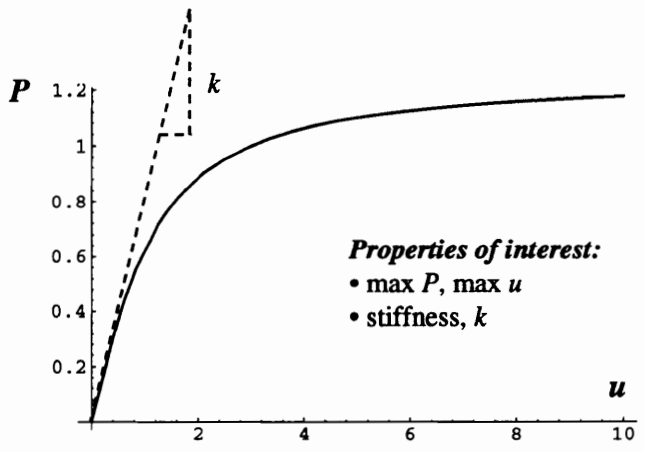

(a) due to monotonic loading

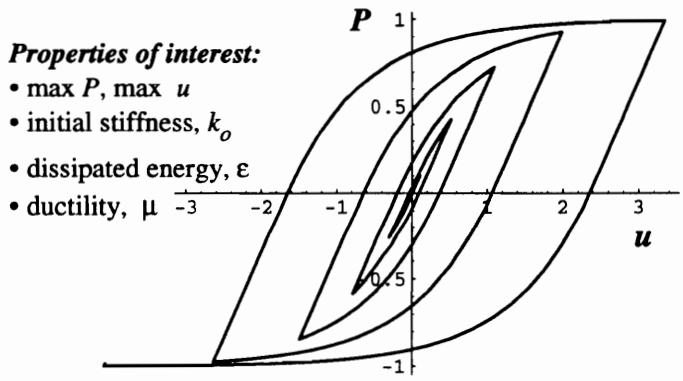

(b) due to cyclic loading

Figure 1.2: Typical load-displacement relations

obtain but may also be of limited use in dynamic analysis. A mathematical constitutive model, that simulates the general hysteretic features of wood systems, is preferred. Parameters of the new hysteresis model may be estimated from data obtained from previous tests of specific wood joints and assemblies.

1.3 Stochastic Dynamic Analysis

The orthodox viewpoint in engineering design "maintained that the objective of design was to prevent failure; it idealized variables as deterministic" (Newmark and Rosenblueth 1971). The traditional approach was to make convenient assumptions that allow the use of "equivalent" static loadings and analysis in place of the actual random dynamic characteristics of natural hazard loadings, such as earthquakes and wind gusts. Although actual recorded data of past earthquakes have been used to analyze structural properties and behavior, this approach is still strictly deterministic. A structure that has been analyzed and designed based on only one or two earthquake records may behave very differently when an earthquake with different characteristics occurs. Gross errors in analysis may lead to unsatisfactory designs, e.g. buildings can collapse during intense earthquakes or have excessive sways in severe winds, if the loadings are assumed to be deterministic, ignoring the inherent uncertainties in natural hazard loadings (Soong and Grigoriu 1993).

In seismic analysis and design, a large number of strong motion earthquake records is necessary to estimate response statistics. This approach is limited, however, by a relatively small number of available records of strong motion earthquakes. Even if artificial accelerograms are used, the cost and effort needed to perform these time history analyses may also be prohibitive. The random characteristics of natural hazard loadings, like earthquakes, and the corresponding structural response can be realistically represented by stochastic mathematical models. Random vibration analyses proved useful in estimating response statistics of structures subjected to loadings modeled as random processes [e.g., Amin and Ang (1968), Wen (1976), Baber and Noori (1986),

Sues et al. (1988), among others]. With a reliable estimate of response statistics, one may then design a structure based on accepted levels of safety, measured in terms of probability of failure.

Research on the dynamic analyses of wood structures has, so far, been limited to deterministic approaches (Ceccotti 1989). An appropriate hysteresis model for wood structures that is suited for both deterministic and random vibration analyses is needed. If this undertaking succeeds, the gap between advances in general structural dynamics and those in wood engineering would be narrowed down. It also opens future research opportunities, in the league of those in other structural materials, in the area of analysis and design of timber structures against natural hazards.

1.4 Objectives and Scope

The present work aims to pave the development of realistic and reliable analysis and design procedures for wood structures under natural hazard loadings. This is achieved by bringing together current know-how in the areas of stochastic structural dynamics and structural wood engineering.

The specific objectives are to:

1. develop a general hysteresis model that simulates experimentally observed behavior of wood joints and structural systems under cyclic and arbitrary dynamic loading, and

2. obtain the nonstationary response statistics of a single-degree-of-freedom (SDF) wood structural system under stochastic excitations representative of earthquake loadings.

Although the present analysis is limited to a SDF wood system, the hysteresis model will also be developed for multi-degree-of-freedom (MDF) structural systems. Extension of random vibration analysis to MDF systems will not be attempted here. Baber (1980) has shown that this extension is straightforward.

Newmark and Rosenblueth (1971) remarked: "It is our task to design engineeering systems- about whose pertinent properties we know little- to resist future earthquakes and tidal waves (and hurricanes)- about whose characteristics we know even less."

We have learned a great deal about engineering materials and systems and natural hazards and how to apply probabilistic methods to deal with uncertainties and risk since this remark was made. Branstetter et al. (1988), however, observed that, "The problem of highly nonlinear systems having random parameters as well as random loadings has been left largely unaddressed because of its mathematical complexity ..." Stochastic dynamic analysis of structural systems with uncertain parameters has been limited to linear systems (e.g., Jensen and Iwan 1992). Thus, the present work will be limited, for now, to analysis of nonlinear systems with "deterministic" properties under random loadings.

1.5 Dissertation Overview

A review of literature related to basic concepts of structural dynamics, observed behavior of wood joints and structural systems, and hysteresis modeling is presented in Chapter 2. Characteristic features of hysteresis behavior of wood joints are identified and current hysteresis models that have been used and proposed for dynamic analysis of wood structures are also reviewed. In Chapter 3, the approach taken in modeling the general hysteretic behavior of wood joints and structural systems, and the form and properties of the proposed model are discussed. Generalization of the pinching capability of the Bouc-Wen-Baber-Noori (BWBN) model, to complete the proposed hysteresis model for wood, is presented. Chapter 4 gives a summary of the proposed hysteresis model for SDF systems, presents the formulation for MDF shear building models, introduces the topic of systems identification, provides a general set of rules for identifying hysteresis model parameters for wood systems and presents nonlinear time history analysis results of three hypothetical SDF wood buildings subjected to the

Loma Prieta accelerogram. Model hysteresis is compared with experimental hysteresis of common wood joints. In Chapter 5, some basic concepts of random vibration theory, related to the present work, are reviewed. Nonlinear random vibration analyses of SDF wood structural systems, modeled by the modified BWBN restoring force model, are performed to obtain their nonstationary response statistics. An approximate analysis method, known as statistical linearization, is verified using Monte Carlo simulation. Potential practical applications of the analysis method and of the response statistics obtained from the analysis are discussed. Finally, Chapter 6 presents a set of conclusions for the present study and recommendations for future work.

Detailed derivations of formulas used in statistical linearization are given in the Appendices.

Chapter 2

Literature Review

2.1 General

Research on dynamic analysis of wood structures lags behind advances in general structural dynamics mainly because of (*1*) many factors affecting the collection of test data and (*2*) difficulties in characterizing the dynamic behavior of wood joints and structural systems. An international workshop on full-scale behavior of wood-framed buildings in earthquakes and high winds produced a document presenting the state-of-the-art and the specific research needs on the earthquake and wind performance of low-rise, light-framed wood construction (Gupta and Moss 1991). Summarizing the research needs in mathematical modeling of wood-framed buildings, Stalnaker and Gramatikov (1991) stressed the need for accurate hysteresis models for wood components, subcomponents and (both inter-element and inter-component) connections and for tests from which the hysteresis model can be derived. The hysteresis model should be incorporated into a dynamic analysis procedure that would allow response computations of wood structures under dynamic loading. The need for various types of parametric studies was also identified.

The objectives of this chapter are to elaborate on the need to accurately model the hysteretic behavior of wood joints and structural systems and to discuss the basis and limitations of current models for wood. Literature on other topics related to the present work will be mentioned in other chapters and sections as needed. To provide a background on dynamic behavior of wood structures and structural systems, some basic terms and concepts used in structural dynamic analysis and modeling are

first introduced. Review of the basic concepts of random vibrations is deferred until Chapter 5.

2.2 Basic Concepts of Structural Dynamics

2.2.1 Introduction

The mathematical expression, that describes the behavior of a structural system under dynamic loads, provides a quantitative expression of load-response relations. It may be written in the following synthetic form (Meirovitch 1985):

$$\mathfrak{R}\,\mathbf{u} = \mathbf{f} \tag{2.1}$$

where $\mathfrak{R}$ is a differential operator, $\mathbf{u}$ is the vector of the system response and $\mathbf{f}$ is the vector of the dynamic actions. Three fundamental cases can be studied:

1. The operation performed by the operator $\mathfrak{R}$ is known and the actions defined by the vector $\mathbf{f}$ are also known. The problem requires the solution of dynamic response, described by vector $\mathbf{u}$. This is known as a *dynamic analysis* or *dynamic response analysis* problem.

2. When the operator $\mathfrak{R}$ and the response $\mathbf{u}$ are known, the problem requires the solution of action vector $\mathbf{f}$ that produced the response $\mathbf{u}$. This is called an *action identification* or *action synthesis* problem.

3. When the vectors $\mathbf{f}$ and $\mathbf{u}$ are known, the problem is reduced to identifying the operator $\mathfrak{R}$. This is known as a *system identification* or *operator synthesis* problem.

The present work deals with dynamic analysis of wood structures. Two concepts can be used to define dynamic loads: (*1*) *deterministic*, or (*2*) *nondeterministic* or *stochastic* or *random*. When loading is deterministic, the forcing function is assumed as a known function of time. Its time variation is completely known at each time instant.

When loading is random, the forcing function is not completely known *a priori* and is, thus, defined statistically.

The first part of this dissertation deals with deterministic dynamic analysis of wood structures. After the proposed hysteresis model is verified to behave as intended and validated to represent experimental hysteresis plots of wood joints reasonably, random vibration analyses will be performed to compute response statistics.

2.2.2 Equation of Motion

Development of any mathematical model normally starts with the construction of an appropriate mechanical model of the actual system. In structural dynamics, a single-degree-of-freedom (SDF) mechanical model typically consists of the system mass, m, a dashpot with viscous damping coefficient, c, and a spring with stiffness, k (Fig. 2.1a).

The response of a SDF system to an earthquake ground motion will be analyzed. The SDF systems in Figs. 2.1a and b are assumed to behave in a linearly elastic-perfectly plastic fashion (Fig. 2.1c), with viscous damping.

The equation of motion for the system subjected to ground motion (Fig. 2.1a) is

$$m\ddot{u}_t + c\dot{u} + f_s = 0 \tag{2.2}$$

where m = mass, c = viscous damping coefficient, f_s = restoring force, $u_t = u + u_g$ = absolute (or total) displacement of the mass, u = relative displacement of the mass with respect to the ground motion, u_g = earthquake ground displacement, and dots designate time derivatives. In the linear elastic range, f_s may be expressed as ku, where k = stiffness (Fig. 2.1c).

Letting $\ddot{u}_t = \ddot{u} + \ddot{u}_g$, Eq. (2.2) may be rewritten as

$$m\ddot{u} + c\dot{u} + ku = -m\ddot{u}_g \tag{2.3}$$

With this equation, Fig. 2.1a is conveniently represented with the equivalent system in Fig. 2.1b having a fixed base and subjected to an effective horizontal dynamic force of

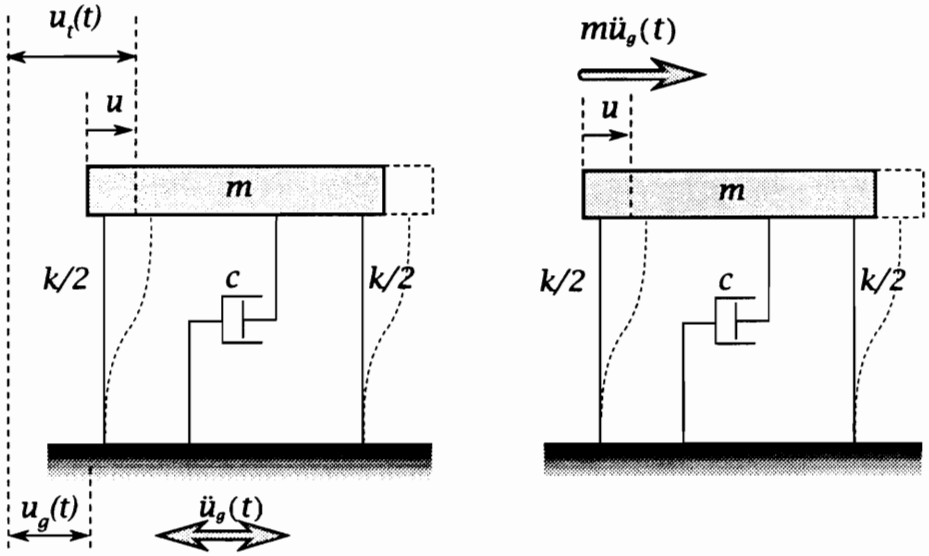

(a) moving base system

(b) equivalent fixed-base system

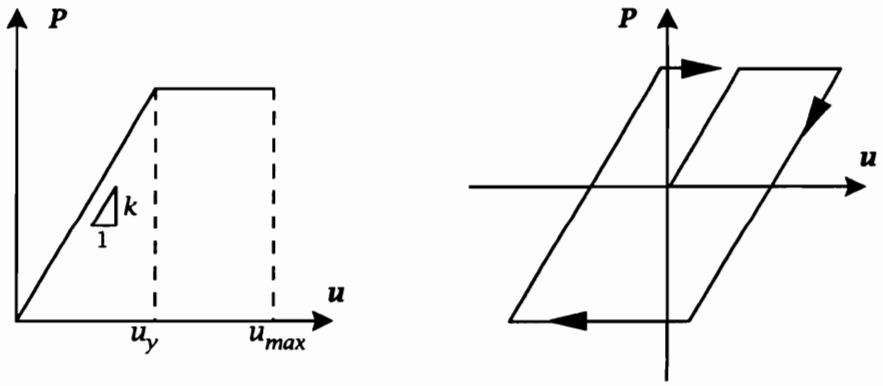

(c) monotonic load-displacement relations

(d) elasto-plastic hysteresis

Figure 2.1: A linearly elastic-perfectly plastic single-degree-of-freedom system

magnitude $-m\ddot{u}_g$. Dividing Eq. (2.3) by m, we obtain the differential equation

$$\ddot{u} + 2\xi\omega_n\dot{u} + \omega_n^2 u = -\ddot{u}_g \tag{2.4}$$

where $\omega_n = \sqrt{k/m}$ and $\xi = c/(2m\omega_n)$. The *natural frequency* of undamped oscillation is ω_n. The product $2m\omega_n$ is known as *critical damping* and ξ is a nondimensional quantity known as the *viscous damping factor* or *damping ratio.* When $\xi > 1$, the system is *overdamped* and oscillation is absent. When $\xi = 1$, system damping, c, equals critical damping. For a given initial excitation, a critically damped system "tends to approach the equilibrium position the fastest" (Meirovitch 1986). Most structures have the case $0 < \xi < 1$, referred to as the *underdamped case.* When $\xi = 0$ (or $c = 0$), known as the *undamped case*, the structure oscillates infinitely unless acted upon by an external force.

From the static monotonic load-displacement diagram, Fig. 2.1c, *displacement ductility* is

$$\mu = \frac{u_{max}}{u_y} \tag{2.5}$$

where u_{max} is maximum displacement and u_y is yield displacement. With cyclic loading, the load-displacement trace produces *hysteresis* loops, shown in Fig. 2.1d, caused by damping and/or inelastic system behavior. The area contained within the loop represents the *energy dissipated* by the structure.

2.2.3 Damping and Energy Dissipation

Damping is the mechanism by which energy is removed from a vibratory system; it is the property responsible for the eventual decay of free vibrations and for the fact that the response of a vibratory system excited at resonance (i.e., cyclic excitation with frequency, $\omega = \omega_n$) does not grow without limit (Crandall 1970). The origin and mechanism of damping, however, is complex and difficult to comprehend. For instance, damping can be (Srinivasan 1982): *(1)* of viscous origin, where the damping force is proportional to the first power of velocity [as in Eqs. (2.2) and (2.3)]; *(2)* of aerodynamic

origin, where the damping force is proportional to the square of the velocity; *(3)* of the Coulomb type, where the energy dissipated is constant in magnitude but changes direction with velocity (e.g., friction between dry sliding surfaces or interface effects in structures); *(4)* hysteretic in nature, where energy dissipation is a function of the stress amplitude; *(5)* due to imperfect elasticity of vibrating bodies (i.e., internal friction); etc. Analytical study of this phenomena is difficult because in real engineering systems, damping is a heterogeneous mix of these various mechanisms.

To simplify vibration analysis, viscous damping is normally assumed. In cases where damping forces are not proportional to velocity and have significant effect on response, an *equivalent viscous damping* concept is sometimes used (e.g., Medearis and Young 1964). To obtain the equivalent viscous damping ratio for a system, it is necessary to obtain the amount of energy dissipated per cycle measured by the area enclosed by the hysteresis loop and to divide this by the maximum stored energy. The dissipated energy of the actual damping force is assumed to be equivalent to that of a viscous damping force, $-c\dot{u}$. If the restoring force needed to bring the system back to equilibrium state at any given displacement is linear in the absence of damping, the use of equivalent viscous damping ratio simplifies the analysis. But in the case of systems with nonlinear restoring force, e.g. wood structural systems, actual damping is underestimated by the equivalent viscous damping approach (Polensek 1988). Note that most reported values of damping ratio of wood joints and components in the literature pertain to the equivalent viscous damping ratio.

References to damping in engineering literature should be clarified because different researchers use the term in slightly different ways. Some materials engineering researchers study damping as a nondestructive inspection tool to determine material properties while others use it as a macrostructural tool to investigate stress, strain and slip at interfaces within structural configurations and systems (Lazan 1968). They use the word damping to mean the total energy dissipation in a member, i.e. viscous and non-viscous types are combined. Researchers in structural dynamics, however,

normally refer to viscous damping alone when they use the word damping. Energy dissipation is, thus, attributed to "damping" *and* inelastic deformation. This is based on the evaluation of energy equations derived from the equation of motion [Eq. (2.2) or (2.3)].

Energy is *imparted* to a structure during seismic ground motion. The energy equations can be derived by using either Eq. (2.2) or (2.3) since both systems (Figs. 2.1a and b) give the same relative displacement. Many researchers used the derivation based on Eq. (2.3) in past studies. The choice of equation, however, may result in different definitions of input and kinetic energies. Uang and Bertero (1990) refer to the energy equation derived from Eq. (2.2) as "absolute" energy equation and that from Eq. (2.3) as "relative" energy equation. The absolute energy equations derived by Uang and Bertero are used in defining energy components.

By integrating Eq. (2.2) with respect to u from the time that ground motion excitation starts and replacing u by $(u_t - u_g)$, we obtain

$$\frac{m(\dot{u}_t)^2}{2} + \int c\dot{u}du + \int f_s du = \int m\ddot{u}_t du_g \tag{2.6}$$

The first term is the "absolute" kinetic energy (E_k),

$$E_k = \frac{m(\dot{u}_t)^2}{2} \tag{2.7}$$

because absolute velocity ($\dot{u}_t$) is used. The second term is the damping energy (E_ξ), which is always non-negative because

$$E_\xi = \int c\dot{u}du = \int c\dot{u}^2 dt \tag{2.8}$$

The third term is the absorbed energy (E_a), which is composed of recoverable elastic strain energy (E_s) and irrecoverable hysteretic energy (E_h):

$$E_a = \int f_s du = E_s + E_h \tag{2.9}$$

where $E_s = (f_s)^2/(2k)$.

The right-hand-side in Eq. (2.6) is the "absolute" input energy (E_i):

$$E_i = \int m\ddot{u}_t du_g \tag{2.10}$$

where $m\ddot{u}_t$ represents the inertia force applied to the structure which is the same as the total force applied to the structure foundation. Thus, E_i represents the work done by the total base shear at the foundation on the foundation displacement.

The absolute energy equation can be written as

$$E_i = E_k + E_\xi + E_a = E_k + E_\xi + E_s + E_h \tag{2.11}$$

The energy terms are illustrated in Fig. 2.2 for an elastic-perfectly plastic SDF system (with μ=5 and ξ=5%) subjected to the 1986 San Salvador earthquake (Uang and Bertero 1990).

2.3 Wood Structures and Components

2.3.1 Behavior of Wood Structural Systems

Wood structures consist of interacting components (or subassemblies) such as walls, floors, roofs and foundation that are fastened together by nails, bolts, steel straps and/or cleats forming a three-dimensional, highly indeterminate system. They normally incorporate some kind of lateral load resisting system that helps them to survive natural disasters, such as earthquakes and typhoons. The four most common systems, shown in Fig. 2.3a, are (Buchanan and Dean 1988): moment resisting frames, cantilever columns, diagonal bracing and shear walls. Horizontal bracing and/or diaphragms also contribute to a building's lateral load resistance. Typical light-frame residential wood buildings with diaphragm/shear and bearing wall construction (e.g., Fig. 2.3b) are not engineered.

Information from damage assessment surveys after natural disasters have traditionally served to indicate the performance of wood-framed buildings (Soltis 1984; Falk and Soltis 1988). Data from post-disaster surveys, however, are highly qualitative

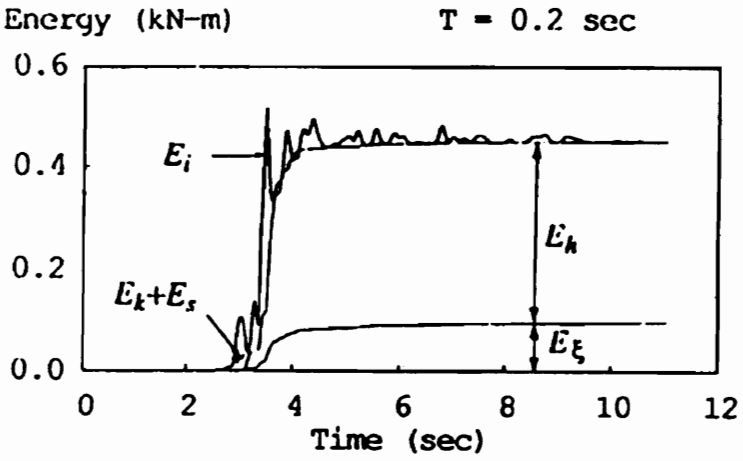

Figure 2.2: Energy terms using absolute energy formulation (from Uang and Bertero 1990)

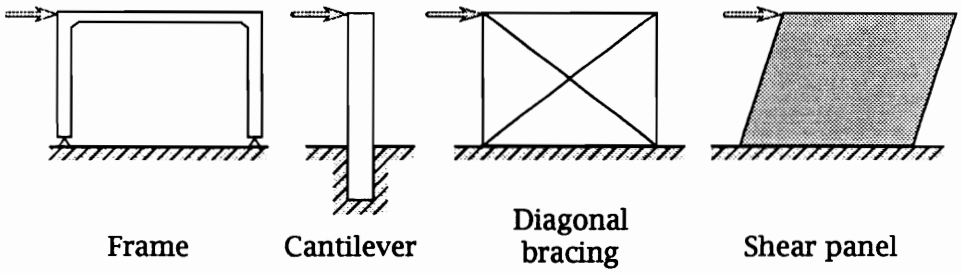

(a) lateral load resisting systems

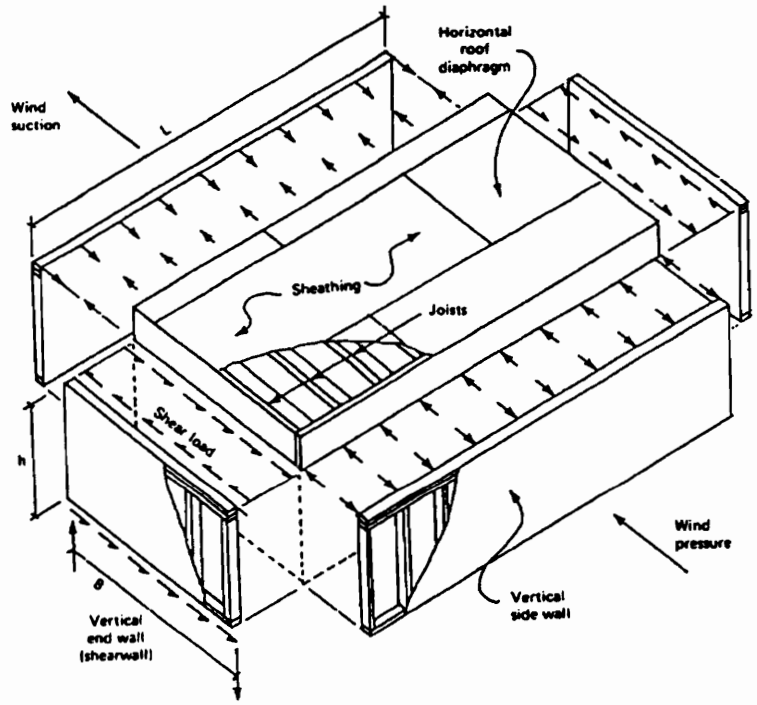

(b) typical wood diaphragm and shear wall construction (from Diekmann 1989)

Figure 2.3: Some common structural systems

and do not provide complete information on the dynamic behavior of the buildings under inspection. Recently, full-scale tests on houses have been used to observe building behavior and evaluate the failure mechanisms of the complete house and the major structural components. Three-storey wood houses have been tested in Japan under various types of loading including horizontal static, reverse cyclic and forced vibration (e.g. Yasumura et al. 1988, Hirashima 1988). Full-scale dynamic test of a 2-storey wood house using a 6-degree-of-freedom earthquake simulator has been performed in Greece (Touliatos 1989). Extensive reviews of full-scale testing around the world can be found in Gupta and Moss (1991).

Most available data are, however, based on tests of subassemblies such as shear walls (Medearis and Young 1964; Stewart 1987; Kamiya 1988; Dolan 1989; Filiatrault and Foschi 1991), diaphragms (Cheung et al. 1988; Polensek and Bastendorff 1979; Weyerhaeuser 1990) and truss systems (Gavrilović and Gramatikov 1991). A common observation from these tests is that the hysteresis trace of a wood subsystem or subassembly is governed by the hysterestic characteristics of its primary connection. Nailed sheathing behavior governs the hysteresis of shear walls and diaphragms (e.g., compare Figs. 2.4 and 2.5b); metal plate connections govern the hysteretic behavior of truss-frame systems. Dowrick (1986) also noted this when he collected cyclic test data of wood joints and structural systems in New Zealand, Japan and North America and examined common hysteresis loops for timber structures. Thus, we only need to characterize the hysteretic behavior of wood joints to characterize the behavior of wood structures and structural systems.

For analytical purposes, Dowrick classified the hysteresis loops for timber structures, based on their shape characteristics, into joints with: (*1*) yielding plate, (*2*) yielding nails, and (*3*) yielding bolts (Fig. 2.5). Similarities in the hysteresis shapes of the dowel-type fasteners, i.e. nails and bolts, can be seen in Figs. 2.5b and c.

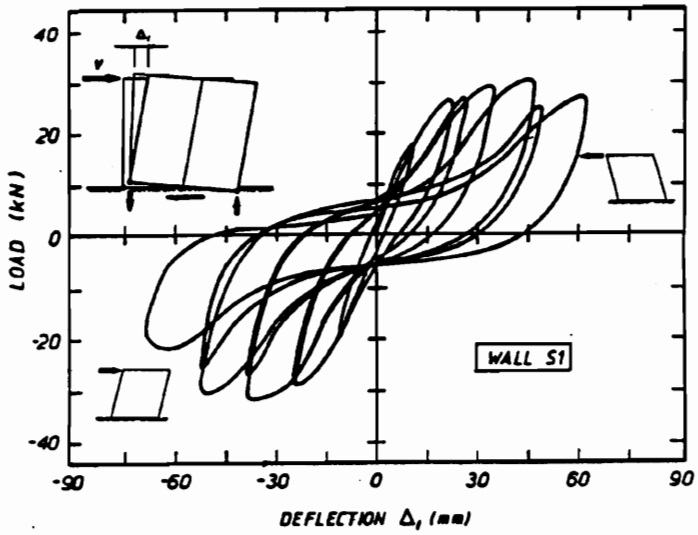

(a) plywood shear wall (from Stewart 1987)

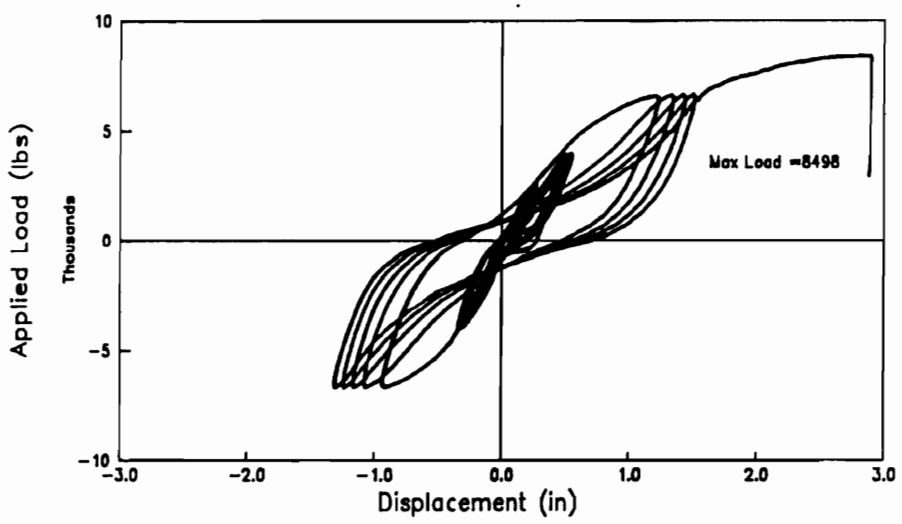

(b) oriented strand board diaphragm (from Weyerhaeuser 1990)

Figure 2.4: Typical hysteresis of wood subassemblies

(a) joint with yielding plate (from Dowrick, 1986)

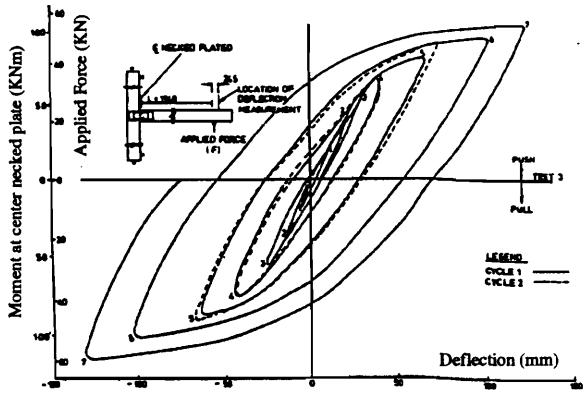

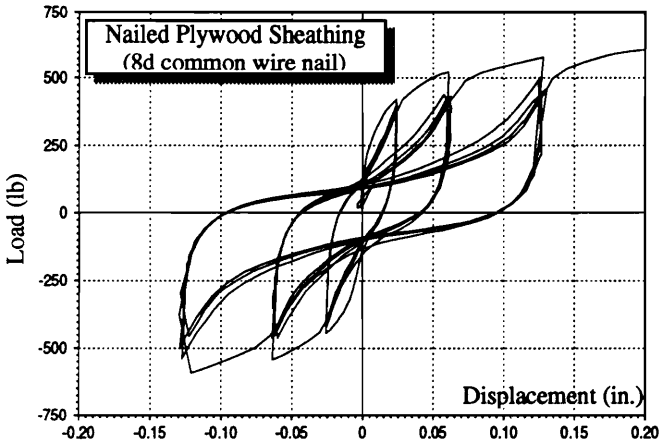

(b) joint with yielding nail

(c) joint with yielding bolt (from Dowrick, 1986)

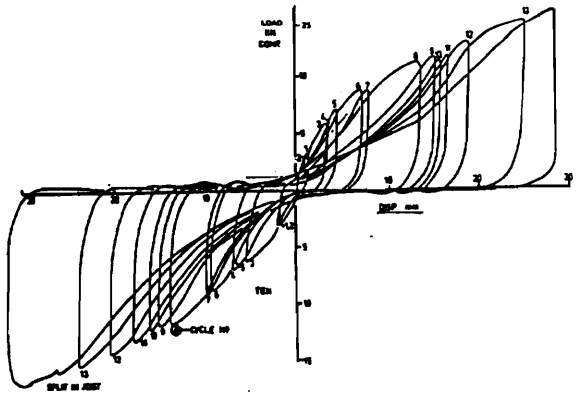

Figure 2.5: Typical hysteresis loops for wood joints

2.3.2 Hysteretic Characteristics

Equation (2.5) shows that ductility is mathematically defined in terms of material yield behavior. This poses no problem for steel and some reinforced concrete structures, but requires an alternative concept for timber structures since they do not demonstrate typical yield behavior.

Figure 2.5b shows hysteresis loops from static cyclic loading of a nailed plywood sheathing, typical of those observed in timber shear walls and diaphragms. Several characteristic features of cyclic response of these systems can be noted from the figure: (*1*) nonlinear, inelastic load-displacement relationship without a distinct yield point, (*2*) progressive loss of lateral stiffness in each loading cycle (will be referred to as *stiffness degradation*), (*3*) degradation of strength when cyclically loaded to the same displacement level (will be referred to as *strength degradation*), and (*4*) *pinched* hysteresis loops. A very important feature, not observed in the figure, is that the response of a wood joint, and possibly wood structures in general, at a given time depends not only on instantaneous displacement but also on its past history (i.e., the input and response at earlier times). This is known as *memory*. Whale (1988) observed that nailed or bolted timber joints under irregular short or medium term lateral loading have memory. In some tests, Dean et al. (1989) also noted the presence of initial slackness due to shrinkage clearances at bolt holes or deformation at supports. Stiffness degradation and hysteresis pinching in joints with dowel-type fasteners (e.g., Figs. 2.5b and c) are attributed to slackness or loosening of the joints caused by initial or previous cyclic loadings. The pinching effect is primarily due to slipping during force reversal.

Any hysteresis or constitutive model for timber structures should incorporate experimentally observed characteristics such as those given above.

2.4 Hysteresis Models

2.4.1 Models for General Dynamic Analysis

Analytical modeling of an inelastic structure under seismic loading requires a force-displacement relation that can produce the true behavior of the structure at all displacement levels and strain rates. This is a very stringent requirement considering that numerous factors contribute to the hysteresis behavior of different structural systems (Sozen 1974). Besides, most structural systems have hysteretic restoring forces that are difficult to compute because the response depends not only on instantaneous displacement but also on its past history. Thus, simplified hysteresis models are used in practice to obtain estimates of bounds to dynamic response in the inelastic range. Some models incorporate strength and/or stiffness degradation and pinching in an attempt to more accurately represent actual system behavior. This is important because degradation might lead to progressive weakening and total failure of structures.

Some piecewise linear hysteresis models that were developed for reinforced concrete and steel structures to represent their earthquake response have also been used in seismic analysis of timber structures. A summary is shown in Fig. 2.6 and briefly presented below (Loh and Ho 1990):

- *Elasto-plastic model* (Fig. 2.6a)- is used for a linearly elastic-perfectly plastic system and normally applied to steel frame structures with large deformation capacities.
- *Bilinear model* (Fig. 2.6b)- has a finite positive stiffness slope after yielding to simulate the strain hardening characteristics of steel and reinforced concrete structures. The elasto-plastic model is a special case of the bilinear model.
- *Modified Clough model* (Fig. 2.6c)- has a bilinear primary curve and an unloading stiffness that is updated for each loop by an unloading stiffness degradation parameter.

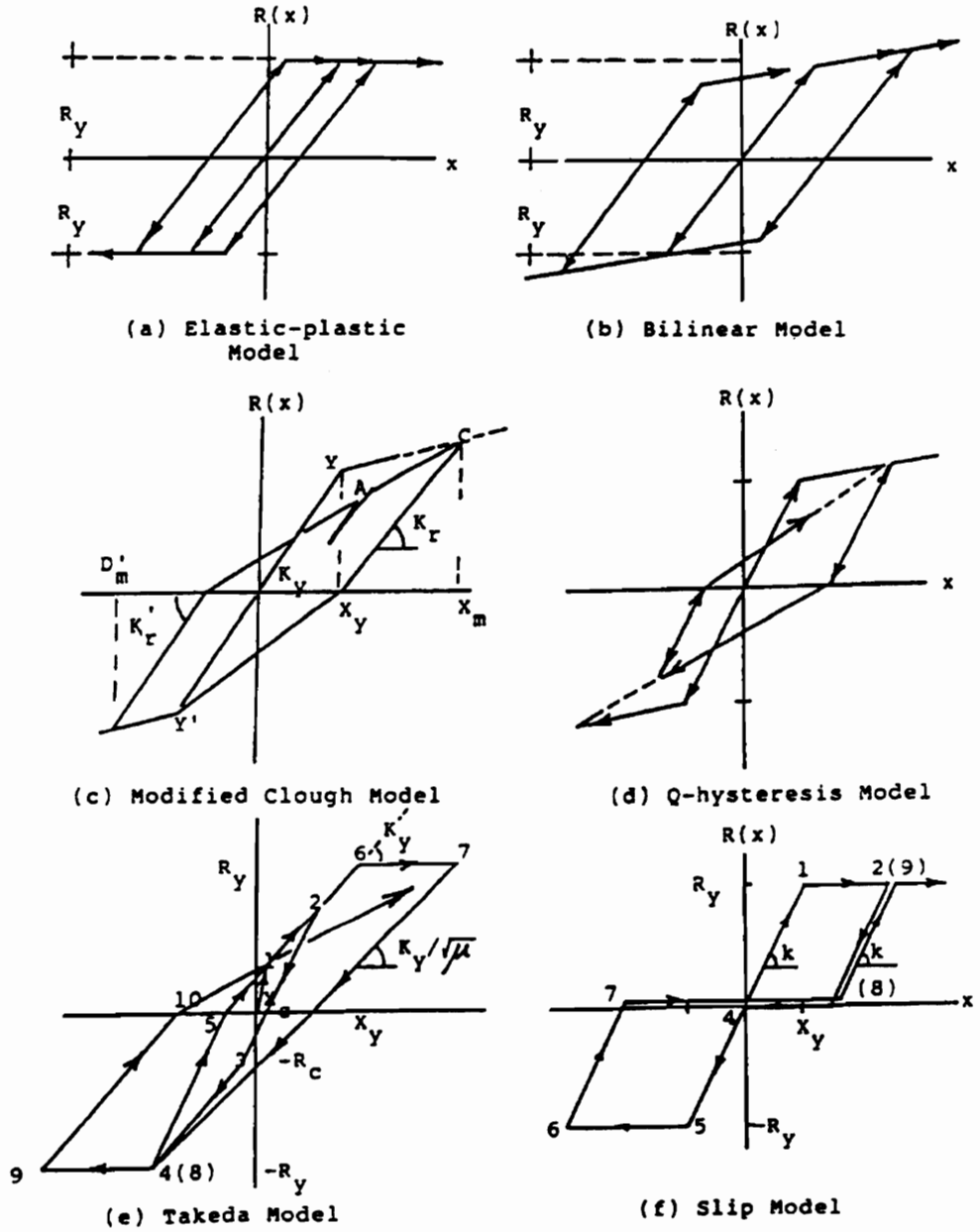

Figure 2.6: Illustrations of hysteresis models for various structures (from Loh and Ho 1990)

- *Q-hysteresis model* (Fig. 2.6d)- is a modified bilinear hysteresis model incorporating stiffness degradation during load reversals.
- *Takeda model* (Fig. 2.6e)- is based on experimentally observed behavior of reinforced concrete members tested under lateral load reversals with axial load.
- *Slip model* (Fig. 2.6f)- is commonly used to model the pinching effects in reinforced concrete structures with large vertical stresses.

The elasto-plastic and bilinear models are probably the simplest and most widely used in dynamic analysis of structures under complex deterministic and random excitations. But the exact solution for random vibration analysis, even for these simple models, has not been obtained. Previous researchers have used a variety of approximate solution techniques with varying degrees of success [see, for example, Noori's (1984) review]. The main problem with the elasto-plastic and bilinear models is their inability to accurately represent actual material behavior. Other piecewise linear models that allow various forms of degradation, however, are computationally inefficient, especially for random vibration analysis, in that they require one to keep track of all stiffness transition points. Ideally, a hysteresis model should be given in a form suited for random vibration analysis to allow researchers to investigate structural performance under natural hazards, with the random characteristics of the loading modeled as random processes. Estimates of response statistics may then be used to design a structure based on accepted levels of safety, measured in terms of probability of failure.

Another commonly used model, with smoothly varying hysteresis loops, is the *Ramberg-Osgood* model. It is based on a simple function defined by three parameters: a characteristic or yield load, a characteristic or yield displacement and an exponent. When the exponent is equal to unity, the model is elastic and when it approaches infinity, the elasto-plastic case is obtained. It has been used in modeling structural steel

members and connections and is most applicable for systems exhibiting stable, nondeteriorating hysteresis loops (Kaldjian and Fan 1968). But this is not suitable for random vibration analysis in its original form (Bhatti and Pister 1981). Jennings (1965), Iwan (1969) and Iemura (1977) have proposed variations of the Ramberg-Osgood model.

Other smoothly varying hysteresis models have been proposed (Iwan 1977; Bouc 1967) but one that has gained wide acceptance is Wen's (1976; 1980) modification of Bouc's model. The hysteretic restoring force is given by a nonlinear first order differential equation; thus, it is characterized by a single mathematical form. Baber and Wen (1981) extended the model to admit stiffness and/or strength degradation and applied it to analyze multi-degree-of-freedom structures. Baber and Noori (1986) added pinching capability. The Bouc-Wen model has been studied and used by various researchers (e.g., Ang and Wen 1982, Casciati 1987, Maldonado et al. 1987, Sues et al. 1988 and Maldonado 1992 among others) to study various engineering problems. Detailed properties of this model will be discussed in the next chapter.

2.4.2 Current Models for Wood Systems

Ewing et al. (1980) developed a hysteresis model for wood diaphragms to perform seismic analysis of wood diaphragms in masonry buildings. The model follows the backbone curve shown in Fig. 2.7a. [A *backbone*, or *skeleton* or *load envelope*, curve is the locus of extremities of the hysteresis loops (Roberts and Spanos 1990).] Based on observations of hysteresis data from Medearis and Young (1964), they used a trilinear path from the maximum deflection on the positive backbone curve to the maximum deflection on the negative backbone curve (Fig. 2.7b). The unloading slope and the residual force are specified to match experimental data.

Since wood joints govern the overall dynamic behavior of wood structures (Dowrick 1986; Stewart 1987; Dolan 1989; Polensek and Schimel 1991), many researchers used data obtained from tests of wood joints to develop hysteresis models for wood structures. Kivell et al. (1981) derived an idealized hysteresis model for moment resisting

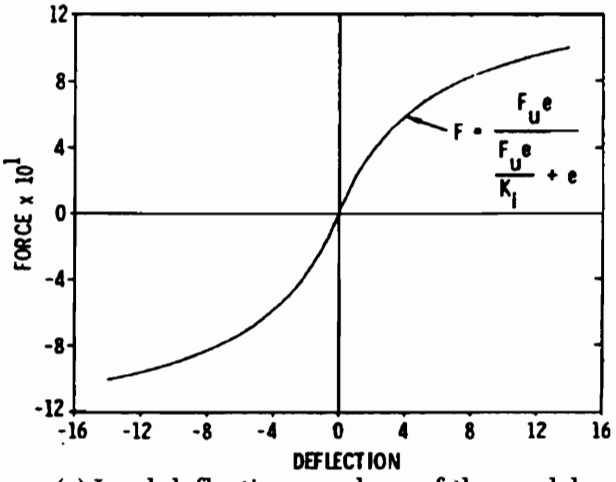

(a) Load-deflection envelope of the model

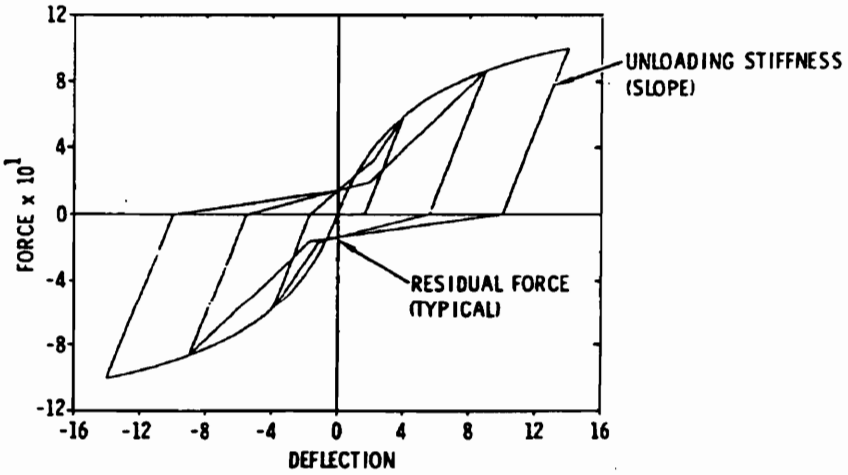

(b) Typical hysteresis loop produced by the model

Figure 2.7: Hysteresis model proposed by Ewing et al. (1980) for wood diaphragms

nailed timber joints (Fig. 2.8a) based on a modification of the Takeda model shown in Fig. 2.6e. The model follows a simple bi-linear backbone curve. Similar to the model by Ewing et al., a trilinear path connects maximum deflections in each half cycle. Kivell et al., however, defined the end points of the lines by a cubic function that passes through the maximum deflections. They used the model to perform dynamic analyses of two simple timber portal frames with nailed beam-to-column connections . The model displays some pinching but does not incorporate stiffness and strength degradation.

Lee (1987) used the hysteresis model earlier proposed by Polensek and Laursen (1984) for nailed plywood-to-wood connections to perform dynamic analyses of wood wall and floor systems using the finite element method. The model follows a trilinear backbone curve. Similar to earlier models, the hysteresis trace between maximum deflections in each half cycle follows a trilinear path. The control points are, however, obtained using a statistical fit of test data. The model relies heavily on the type and size of the nail and the material properties of the side members. The regression equations used to define the control points have a very limited use.

Chou (1987) tested nailed plywood-to-wood connections under cyclic loading and investigated the experimental hysteresis shapes. He used a system of nonlinear Kelvin models in series and in parallel to model the hysteresis loops of the joint. Nail behavior was studied using a modification of the beam-on-elastic-foundation analysis. Nonlinear response was approximated by a linear step-by-step approach; that is, nonlinear response was considered as the sum of different linear responses under small increments of load. It is, however, unclear how Chou's model can be used for dynamic analysis of wood structural systems.

Stewart (1987) and Dolan (1989) modeled hysteresis in nailed sheathing-to-lumber connections. Stewart (1987) idealized pinching and stiffness degradation using a set of force-history rules to obtain the hysteresis shape shown in Fig. 2.9a. A key feature of Stewart's model is the option to include an initial slackness in the first loading

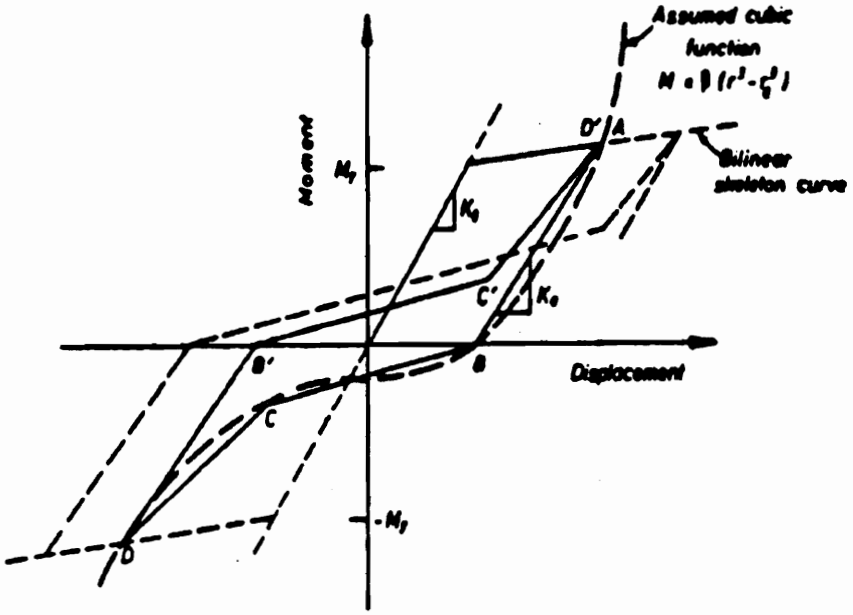

Figure 2.8: Hysteresis model proposed by Kivell et al. (1981) for moment resisting nailed timber joints

cycle. Dean et al. (1989) noted the presence of initial slackness in tests of subassemblies caused by shrinkage clearances at bolt holes or deformation at supports. Dolan (1989) divided a hysteresis loop into four segments, each one defined by an exponential equation with four boundary conditions (Fig. 2.9b). This model was incorporated in a dynamic finite element model that predicts shear wall response to earthquakes.

Ceccotti and Vignoli (1990) developed a hysteresis model for moment-resisting semi-rigid wood joints that are normally used in glulam portal frames in Europe. It also models pinching and stiffness degradation (Fig. 2.10). A set of subroutines were written to define the new hysteretic element and were incorporated into the commercial nonlinear dynamic analysis program DRAIN-2D.

In Japan, several models have been used in dynamic analysis of Japanese wood houses. Sakamoto and Ohashi (1988) proposed two hysteresis models for conventional Japanese wood houses. The first model consists of a parallel combination of a bilinear element and a slip element and the second model follows a trilinear path from the maximum deflection on the positive backbone curve to the maximum deflection on the negative backbone curve. The three control points were obtained from racking tests of shear walls (Fig. 2.11a). Kamiya (1988) proposed the model shown in Fig. 2.11b, which was developed from pseudo-dynamic tests of wood-sheathed shear walls. The model in Fig. 2.11c was proposed by Miyazawa (1990) for Japanese wood-framed construction.

For trussed-frame wood systems, Gavrilović and Gramatikov (1991) used a simple bilinear hysteresis model. The hysteresis trace between maximum deflections in each half cycle also follows a bilinear path.

Foschi and his associates proposed a new hysteresis model for a single dowel-type fastener (Fig. 2.12). The analysis considered the fastener as an elasto-plastic beam on a nonlinear foundation (the wood support), and keeps track of the gap which forms between the beam and the support during cyclic loading (UBC 1993). The model was verified by cyclic testing of nails driven into spruce wood. Hysteresis parameters are obtained from basic characteristics of joint materials, namely, modulus of elasticity

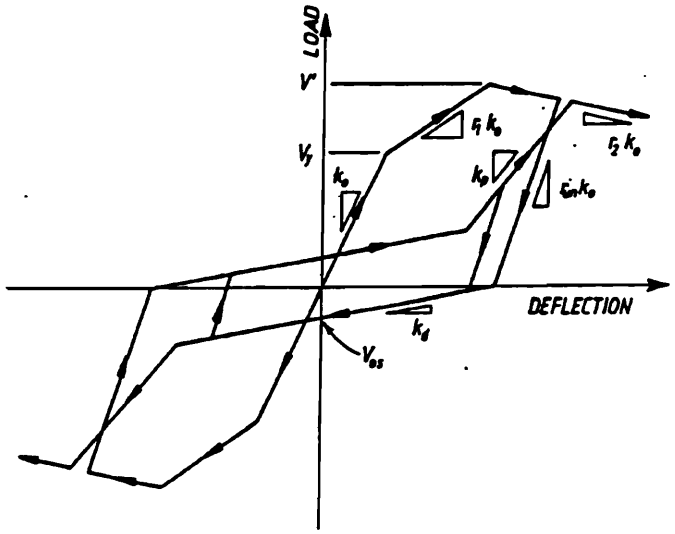

(a) from Stewart (1987)

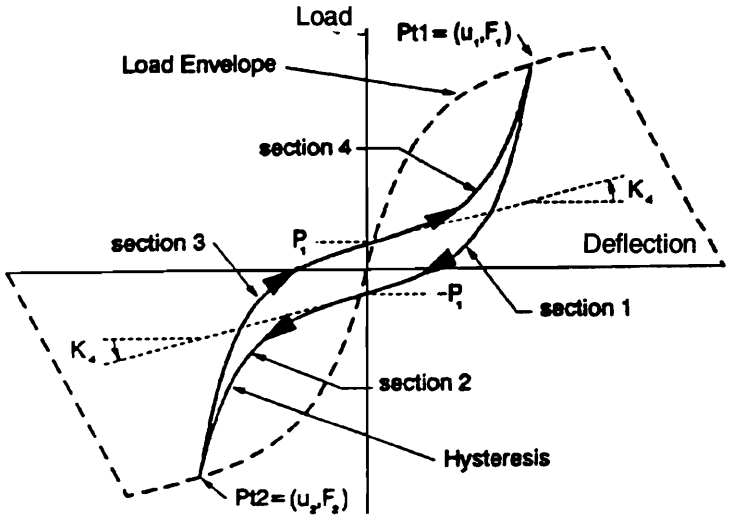

(b) from Dolan (1989)

Figure 2.9: Hysteresis models proposed for nailed sheathing-to-frame connections

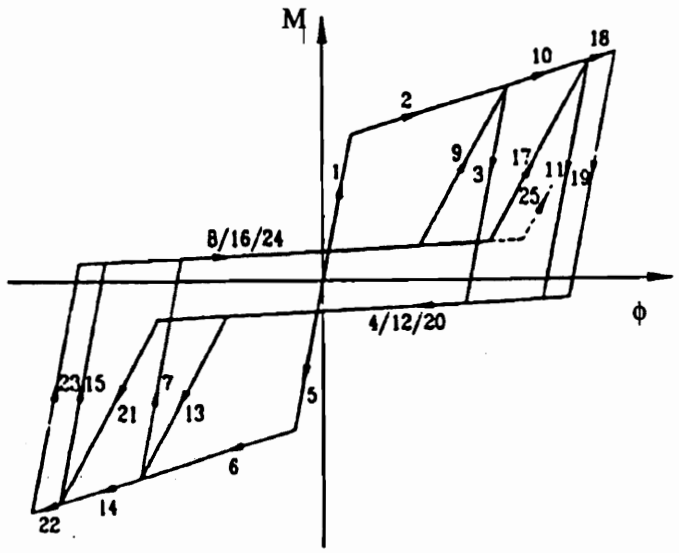

Figure 2.10: Hysteresis model proposed by Ceccotti and Vignoli (1990) for moment resisting semi-rigid wood joints

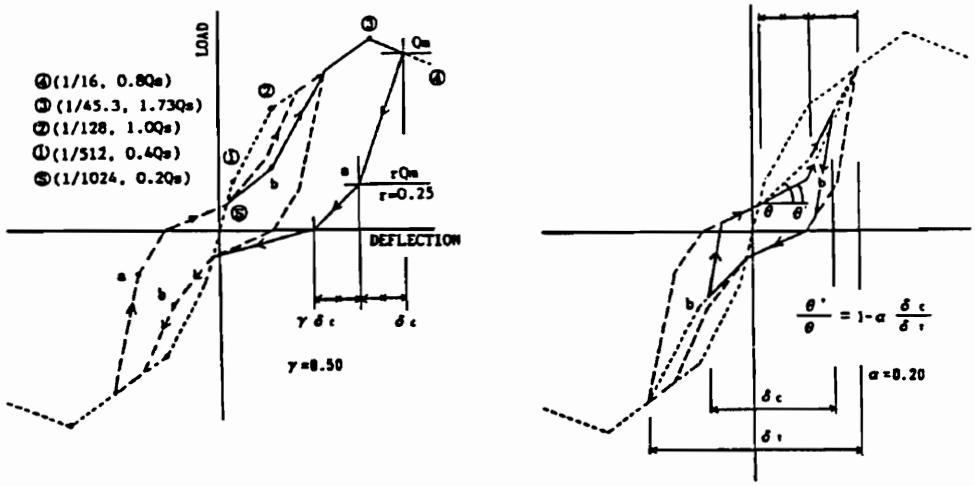

(a) from Sakamoto and Ohashi (1988)

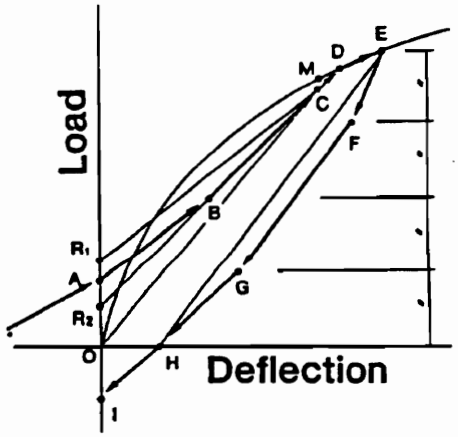

(b) from Kamiya (1988)

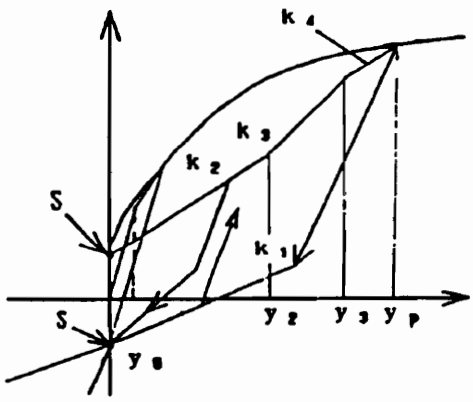

(c) from Miyazawa (1990)

Figure 2.11: Hysteresis models proposed by Japanese researchers

and yield point of the fastener and embedment properties of the side members.

2.4.3 Comments

The available models for wood systems use either a complex set of force-history rules or limited empirical relations. While the current models satisfied some of the specific features of the joints or structural systems that they meant to model, they may be inappropriate for joints or systems with different configurations and material components. Since (*1*) there are hundreds of combinations of materials and joint configurations in wood systems, and (*2*) wood-based products, fasteners and use of wood-based products continue to evolve, a general model is preferred over models derived from specific configurations. A completely empirical model will not only be expensive to obtain but may also be of limited use in dynamic analysis. A mathematical model, meeting all the criteria given in section 2.3.2, is preferred. Model parameters may be estimated from tests of representative wood joints or assemblies.

2.5 Summary

Basic terms and concepts used in structural modeling and dynamic analysis were presented to provide the necessary background for the present work. Cyclic tests on wood subassemblies and wood joints were reviewed. It was pointed out that the hysteresis trace of a wood subsystem or subassembly is governed by the hysterestic characteristics of its primary connection. Thus, we only need to characterize the hysteretic behavior of wood joints to characterize the behavior of wood structures and structural systems. Dowrick (1986) classified the hysteresis loops for timber structures, based on their shape characteristics, into joints with: (*1*) yielding plate, (*2*) yielding nails, and (*3*) yielding bolts. Based on experimental hysteresis, any hysteresis or constitutive model for timber structures should incorporate experimentally observed characteristics such as: (*1*) nonlinear, inelastic load-displacement relationship without a distinct

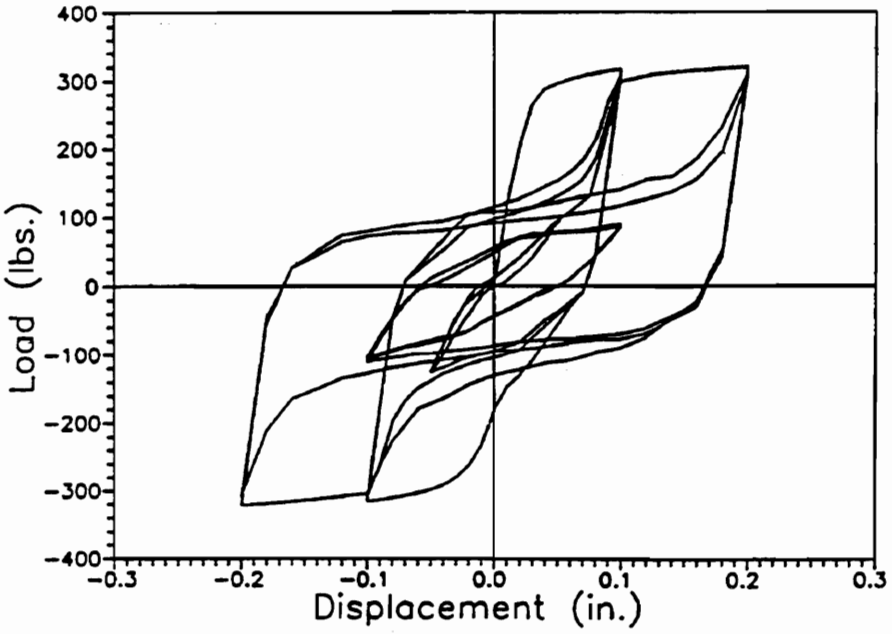

Figure 2.12: Hysteresis model proposed by Foschi and his associates (UBC 1993) for wood joints with dowel-type fasteners

yield point, (*2*) stiffness degradation, (*3*) strength degradation, (*4*) pinching, and (*5*) memory. Incorporating memory means that the model should be capable of predicting response at a given time based not only on instantaneous displacement but also on its past history (i.e., the input and response at earlier times).

Hysteresis models proposed for steel, concrete and wood structures were reviewed. The models for wood were derived from specific joint or system configurations and were expressed using either a complex set of force-history rules or limited empirical relations. It was apparent that there is a need for a general hysteresis model that incorporates all the features given above. Such a model would permit response computations of a wide variety of wood structural systems under arbitrary dynamic loading and help in investigating the safety and performance of engineered wood structures under natural hazards using random vibration analysis.

Chapter 3

Hysteresis Modeling

3.1 General

Analytical modeling of an inelastic structure under seismic loading requires a force-displacement relation that can produce the true behavior of the structure at all displacement levels and strain rates. This is a very stringent requirement considering that numerous factors contribute to the hysteresis behavior of different structural systems (Sozen 1974). Besides, most structural systems, especially wood systems, have hysteretic restoring forces that are difficult to compute because the response depends not only on instantaneous displacement but also on its past history (referred to earlier as memory). The hysteresis model should take this into account while simulating other characteristic features of wood systems that have been identified in the previous chapter. It is important to incorporate strength and/or stiffness degradation and pinching to more accurately represent actual system behavior because degradation might lead to progressive weakening and total failure of structures.

A general hysteresis model for wood joints and structural systems that incorporates the hysteretic features that have been identified in the previous chapter will be presented. The smoothly varying Bouc-Wen hysteresis model and its extensions will be examined. A pinching, degrading model modified to more accurately model the hysteretic behavior of wood joints will be described.

3.2 Approach to Modeling

Generally, there are two possible approaches in obtaining a hysteresis model for wood systems: *(1)* by empirically fitting experimental data from cyclic tests of particular wood joints, or *(2)* by describing system behavior using an approximate mathematical model. Since (*1*) there are hundreds of combinations of materials and joint configurations in wood systems, and (*2*) wood-based products, fasteners and use of wood-based products continue to evolve, a general model is preferred over models derived from specific configurations. A completely empirical model will not only be expensive to obtain but may also be of limited use in dynamic analysis. A mathematical model, meeting the criteria given in section 2.3.2, is preferred. Model parameters may be estimated from tests of representative wood joints or assemblies.

3.3 Mechanical Model

In the previous chapter, a simple single-degree-of-freedom (SDF) mechanical model with system mass, m, a dashpot with viscous damping coefficient, c, and a spring with stiffness, k, was introduced. A brief background was also given on damping and energy dissipation. Here, the mechanical model for nonlinear wood systems is presented.

A nonlinear system can be represented by a dynamic mechanical model with: *(1)* linear spring and nonlinear damping- Coulomb type or aerodynamic type alone or in combination with viscous damping (Fig. 3.1a); *(2)* nonlinear spring and linear viscous damping (Fig. 3.1b); *(3)* nonlinear spring and nonlinear damping (Fig. 3.1c); *(4)* linear spring, linear viscous damping and nonlinear hysteretic element (Fig. 3.1d), or; *(5)* various combinations of *(1)* to *(4)*. The choice of an appropriate mechanical model depends on the complexity of the mathematical expression that describes the model and its compatibility with known solution techniques.

An efficient way to treat a nonlinear hysteretic system is to separate the source of nonlinearity in the system from any linear components. This results in a mechanical

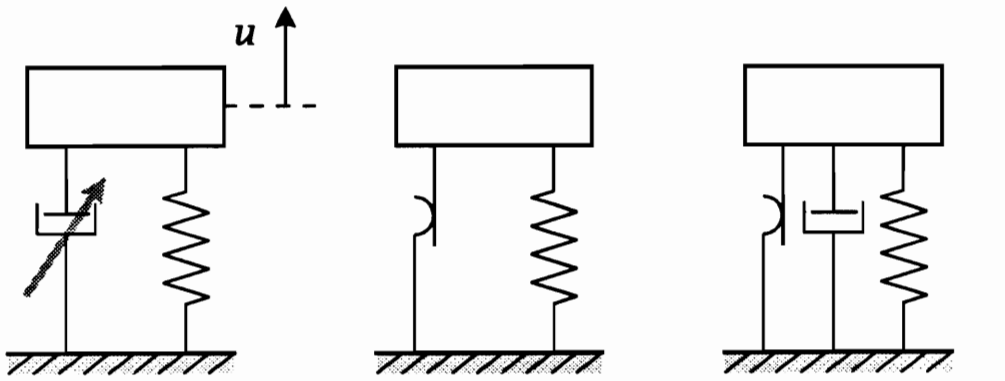

aerodynamic damping Coulomb damping Coulomb & viscous damping

(a) linear spring and nonlinear damping

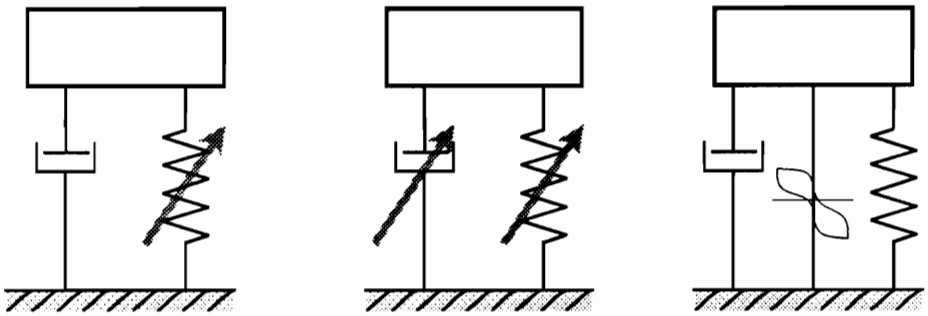

(b) nonlinear spring and linear viscous damping

(c) nonlinear spring and nonlinear damping

(d) linear spring, linear damping and hysteretic element

Figure 3.1: Typical mechanical models for nonlinear systems

model with three parallel elements: *(1)* a linear viscous damping, *(2)* a linear spring and *(3)* a hysteretic element (Fig. 3.2a). This achieves two things: *(1)* analytical difficulty in treating the different sources of energy dissipation in the system is avoided since the non-viscous types are lumped together into the hysteresis element, and *(2)* standard values for the viscous damping ratio of linear wood systems can be used for analysis. Once the parameters of the hysteresis model are identified, dissipated hysteretic energy can be obtained from the hysteresis trace of the response.

3.4 The Bouc-Wen-Baber-Noori Model

3.4.1 Background

Bouc (1967) suggested a versatile, smoothly varying hysteresis model for a SDF mechanical system under forced vibration. With the mechanical model shown in Fig. 3.2a, Wen (1976; 1980) generalized Bouc's hysteretic constitutive law and developed an approximate solution procedure for random vibration analysis based on the method of equivalent (or statistical) linearization. Baber and Wen (1981) extended the model to admit stiffness and/or strength degradation as a function of hysteretic energy dissipation and applied it to a multi-degree-of-freedom system. Later on, Baber and Noori (1986) further extended the modified Bouc model by incorporating pinching while maintaining it in a form compatible with Wen and Baber and Wen's statistical linearization solution. Response statistics obtained by the statistical linearization technique were shown to reasonably approximate those obtained by Monte Carlo Simulation. The final model will be called the Bouc-Wen-Baber-Noori (BWBN) model in the present work.

Many researchers have used the early form of the modified Bouc model in random vibration investigations of hysteretic systems. With the features added by Baber and Wen (1981) and Baber and Noori (1986), it has more closely approximated the hysteretic behavior of wood joints and structural systems. However, it needs further modification to be applicable in modeling general wood system behavior.

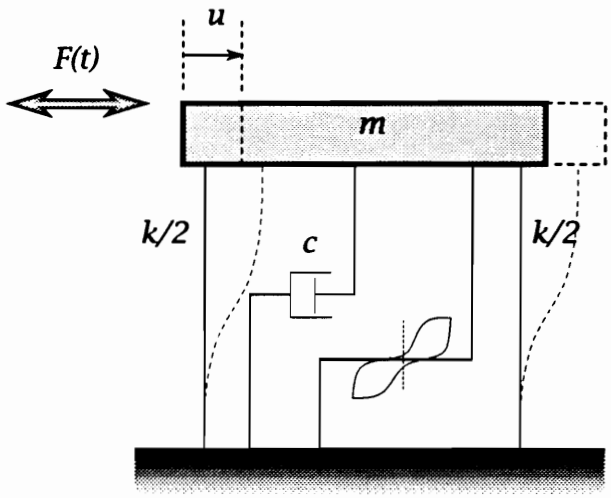

(a) schematic model

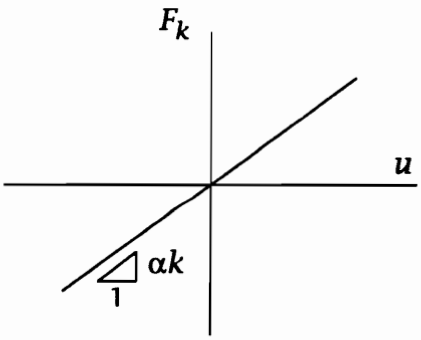

(b) non-damping linear restoring force component

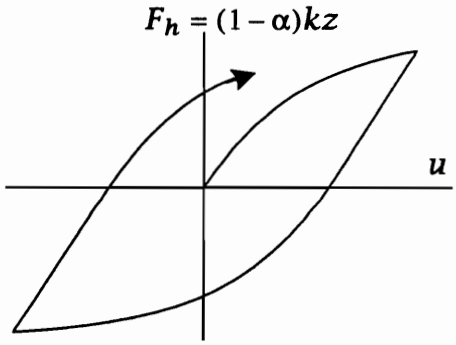

(c) hysteretic restoring force component

Figure 3.2: Hysteretic SDF system for wood structural systems

3.4.2 Equation of Motion and Constitutive Relations

Considering the SDF hysteretic system in Fig. 3.2a, the equation of motion may be generally written as

$$m\ddot{u} + c\dot{u} + R[u(t), z(t); t] = F(t) \tag{3.1}$$

where dots designate time derivatives; $F(t)$ is the forcing function; the damping restoring force, $c\dot{u}$, is assumed linear and $R[u(t), z(t); t]$ is the non-damping restoring force consisting of the linear restoring force $\alpha k u$ and the hysteretic restoring force $(1-\alpha)kz$ (Figs. 3.2b and c). Dividing both sides of Eq. (3.1) by m, the following standard form is obtained:

$$\ddot{u} + 2\xi_o\omega_o\dot{u} + \alpha\omega_o^2 u + (1-\alpha)\omega_o^2 z = f(t) \tag{3.2}$$

where the hysteretic displacement z is a function of the time history of u; it is related to u through the following first-order nonlinear differential equation,

$$\dot{z} = h(z)\left\{\frac{A\dot{u} - \nu(\beta|\dot{u}||z|^{n-1}z + \gamma\dot{u}|z|^n)}{\eta}\right\} \tag{3.3}$$

where,

$f(t)$ = mass-normalized forcing function,

ω_o = preyield natural frequency of the system ($\sqrt{k_i/m}$); k_i is initial stiffness,

ξ_o = linear damping ratio ($c/2\sqrt{k_i m}$),

α = a weighting constant representing the relative participations of the linear and nonlinear terms ($0 < \alpha < 1$); also called "rigidity ratio",

A = parameter that regulates the tangent stiffness and ultimate hysteretic strength,

β, γ, n = hysteresis shape parameters,

ν, η = strength and stiffness degradation parameters, respectively; if $\nu = \eta = 1.0$, the model does not degrade,

$h(z)$ = the pinching function introduced by Baber and Noori (1986); if $h(z) = 1.0$, the model does not pinch.

The hysteretic restoring force F_h is given by the fourth term in Eq. (3.2) as $F_h = (1 - \alpha)\omega_o^2 z$. Since $[(1 - \alpha)\omega_o^2]$ is a time-invariant system property, the hysteretic restoring force will also be referred to as z from hereon.

Equation (3.3) defines the constitutive law, based on a modified "endochronic" model of the force-displacement relations. The hereditary restoring force model satisfies the requirement that the response depends not only on instantaneous displacement but also on its past history (referred to earlier as memory).

3.4.3 Hysteresis Shape Properties

Baber (1980) and Maldonado et al. (1987) examined in great detail the properties of the Bouc-Wen or Modified-Bouc model (i.e., the non-degrading, $\nu = \eta = 1.0$, and non-pinching, $h(z)$=1, model). To understand the effects of the model parameters on hysteresis shape, let us examine the parameters α, A, β, γ and n.

3.4.3.1 Parameters A and α

From Eq. (3.1), the total non-damping restoring force F_T is expressed as

$$F_T = k[\alpha u + (1 - \alpha)z] \,. \tag{3.4}$$

Recall that $\alpha k u$ is the linear restoring force (due to the spring element) and $(1 - \alpha)kz$ is the the hysteretic restoring force (due to the hysteretic element). The tangent stiffness to the nonlinear restoring force is obtained by differentiating F_T with respect to displacement u:

$$\frac{dF_T}{du} = k\left[\alpha + (1 - \alpha)\frac{dz}{du}\right] \tag{3.5}$$

where $\frac{dz}{du}$ is the tangent to the nonlinear path in the z-u plane. This is obtained by dividing both sides of Eq. (3.3) by $\dot{u}$ (or $\frac{du}{dt}$),

$$\frac{dz}{du} = h(z)\left\{\frac{A - \nu(\beta\,\mathrm{sgn}(\dot{u})\,|z|^{n-1}z + \gamma|z|^n)}{\eta}\right\} \tag{3.6}$$

where sgn(·) = the signum function (i.e., sgn(a) gives -1, 0 or 1 depending on whether a is negative, zero or positive, respectively). The ultimate value of z, or z_u, is obtained by setting $\frac{dz}{du}$ to zero and solving it for z to get

$$z_u = \left[\frac{A}{\nu\,(\beta+\gamma)}\right]^{1/n}. \tag{3.7}$$

Assuming that ν, β, γ and n do not change, this shows that A regulates the ultimate hysteretic strength, z_u.

To investigate the effect of A on the tangent stiffness in the z-u plane, set $\nu = \eta =$ 1.0 and $h(z)$=1, and rewrite Eq. (3.6) as

$$\frac{dz}{du} = A - (\beta\,\mathrm{sgn}(\dot{u})\,|z|^{n-1}z + \gamma|z|^n) \tag{3.8}$$

At the limit $z \to u \to 0$,

$$\left.\frac{dz}{du}\right|_{z=u=0} = A \tag{3.9}$$

This means that A sets the initial tangent stiffness. Eqs. (3.7) and (3.9), thus, show that increasing the value of A increases both the ultimate hysteretic strength, z_u, and the initial tangent stiffness, $\frac{dz}{du}$ at $z = u = 0$.

In the special case where A=1, a physical interpretation of the parameter α may be obtained. Substitute Eq. (3.9) into (3.5) to obtain the initial tangent stiffness, k_i, in the F_T-u plane,

$$k_i = \left.\frac{dF_T}{du}\right|_{z=u=0} = k\,[\alpha + (1-\alpha)\cdot 1] \tag{3.10}$$

which gives

$$k_i = k\,. \tag{3.11}$$

At z_u, $\frac{dz}{du}$=0 and the final tangent stiffness, k_f, is

$$k_f = \left.\frac{dF_T}{du}\right|_{z=z_u} = k\alpha\,. \tag{3.12}$$

From Eqs. (3.11) and (3.12),

$$\alpha = \frac{k_f}{k_i}. \tag{3.13}$$

Thus, α is the ratio of the final tangent stiffness to the initial stiffness, when A=1.

The preceding discussion may also be extended to provide some insight into the relationship of hystereses in the F_T-u and the z-u planes. For illustration purpose, we will keep A=1. First, consider a half cycle in the z-u plane. After plotting the tangent stiffness lines at z=0, Eq. (3.9), and $z = z_u$, the hysteresis may be plotted as shown in Fig. 3.3a. When A=1, the "yield" displacement, u_y, corresponding to the intersection of the initial and final tangent stiffness lines, is numerically equal to z_u.

In the F_T-u plane, the yield force is

$$F_{Ty} = k[\alpha u_y + (1 - \alpha) z_u] \tag{3.14}$$

or

$$u_y = z_u = \frac{F_{Ty}}{k} . \tag{3.15}$$

As seen in Fig. 3.3b, F_{Ty} corresponds to the intersection of the initial and final tangent stiffness lines and not to the actual force in the hysteresis curve corresponding to u_y. Fig. 3.3 shows that the hysteresis may be plotted in either plane, since it can be easily mapped from one to the other. The present work will focus mainly on the hysteresis in the z-u plane.

3.4.3.2 Parameters β and γ

Focusing on the non-degrading, non-pinching BWBN model, the constitutive relations may be broken into four segments. Eq. (3.8) is expressed as four differential equations,

$$\frac{dz}{du} = A - (\beta + \gamma) z^n \qquad z \geq 0, \dot{u} \geq 0 \tag{3.16}$$

$$\frac{dz}{du} = A - (\gamma - \beta) z^n \qquad z \geq 0, \dot{u} < 0 \tag{3.17}$$

$$\frac{dz}{du} = A + (-1)^{n+1} (\beta + \gamma) z^n \qquad z < 0, \dot{u} < 0 \tag{3.18}$$

$$\frac{dz}{du} = A + (-1)^{n+1} (\gamma - \beta) z^n \qquad z \leq 0, \dot{u} \geq 0 \tag{3.19}$$

Considering the simple case where $n = 1$, solutions to the above equations are plotted in Fig. 3.4, where u_o is the displacement at z=0, a quantity which varies from cycle to

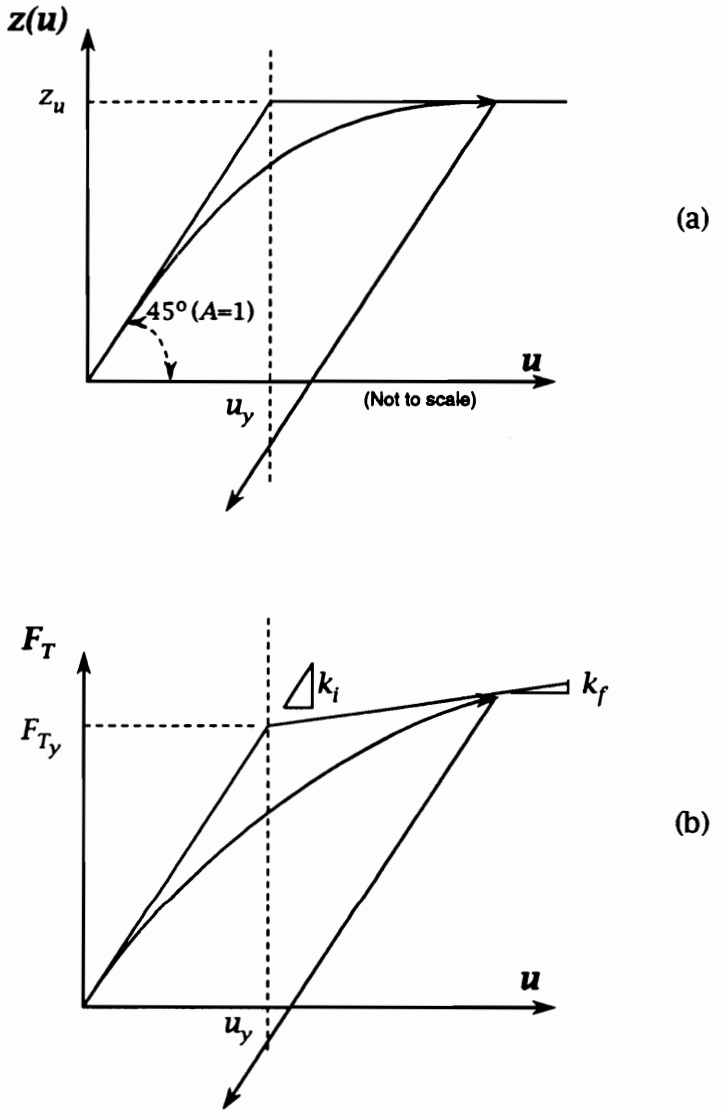

Figure 3.3: Nondegrading and non-pinching BWBN model: (a) z-u plane, (b) F_T-u plane

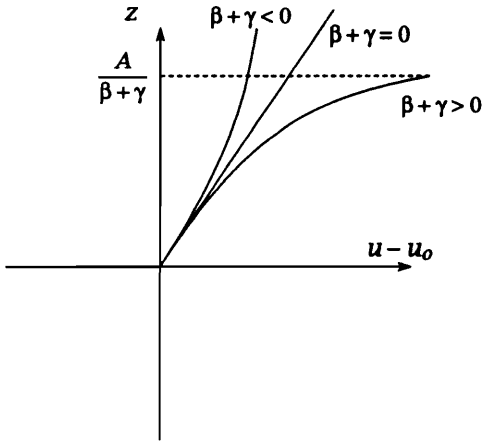

(a) loading

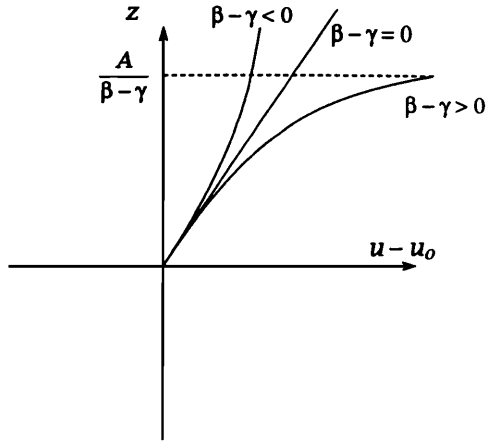

(b) unloading

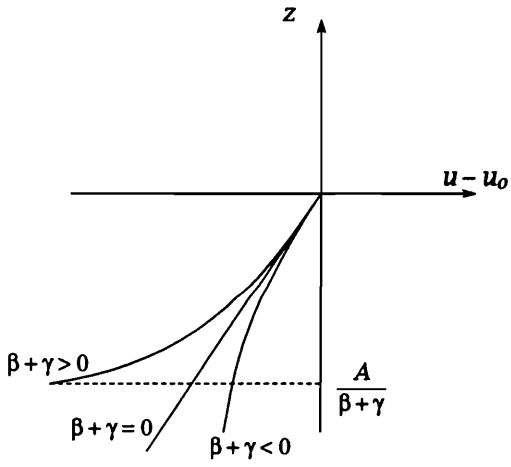

(c) loading

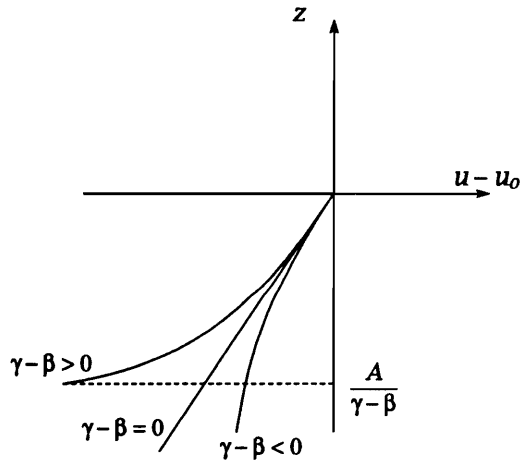

(d) unloading

Figure 3.4: Hysteresis loop behavior for n=1

cycle. Eqs. (3.16) and (3.18) (Figs. 3.4a and c) are the *loading*, or outward, paths and Eqs. (3.17) and (3.19) (Figs. 3.4b and d) are the *unloading*, or inward, paths.

The equations for the loading paths may be combined and rewritten as

$$\frac{dz}{du} = A - (\beta + \gamma)|z|^n \qquad z\dot{u} > 0 \tag{3.20}$$

Similarly, for the unloading paths,

$$\frac{dz}{du} = A - (\gamma - \beta)|z|^n \qquad z\dot{u} < 0 \tag{3.21}$$

With these equations, it can be readily seen that when β=0, the two equations are the same and the loading and unloading paths coalesce into a single path. Although the path may remain nonlinear (when n >1), it is nonhysteretic.

Examining the positive loading (Fig. 3.4a) and unloading (Fig. 3.4b) paths, it is observed that a variety of hysteresis shapes may be obtained by varying the values of A, β and γ. When β <0, a negative dissipation energy is obtained. Since this cannot be physically realized, β should therefore always be positive, regardless of the value of γ. With this restriction, hysteresis shapes resulting from possible combinations of β and γ are shown in Fig. 3.5.

Depending on γ, a softening or hardening model may be obtained. A softening characteristic is obtained when the slope of the hysteresis path decreases with increasing $|z|$. A hardening model is obtained when the slope of the hysteresis path increases with increasing $|z|$. As seen in Fig. 3.5, positive γ tends to cause softening and negative γ tends to cause hardening, but the limiting behavior will remain softening unless $|\gamma| > |\beta|$ and $\gamma < 0$. To obtain a linear unloading path, set $\gamma = \beta$.

3.4.3.3 Parameter n

The effect of n on the skeleton curves of the hysteresis will be investigated in this section. In Fig. 3.6, the skeleton curves for n=1,3,6 and 12 are shown for the case A=1, $\beta = \gamma = 0.5$. It can be seen that as n increases, the model approaches the elasto-plastic behavior. This can be shown analytically by examining the softening model, $(\beta+\gamma)> 0$.

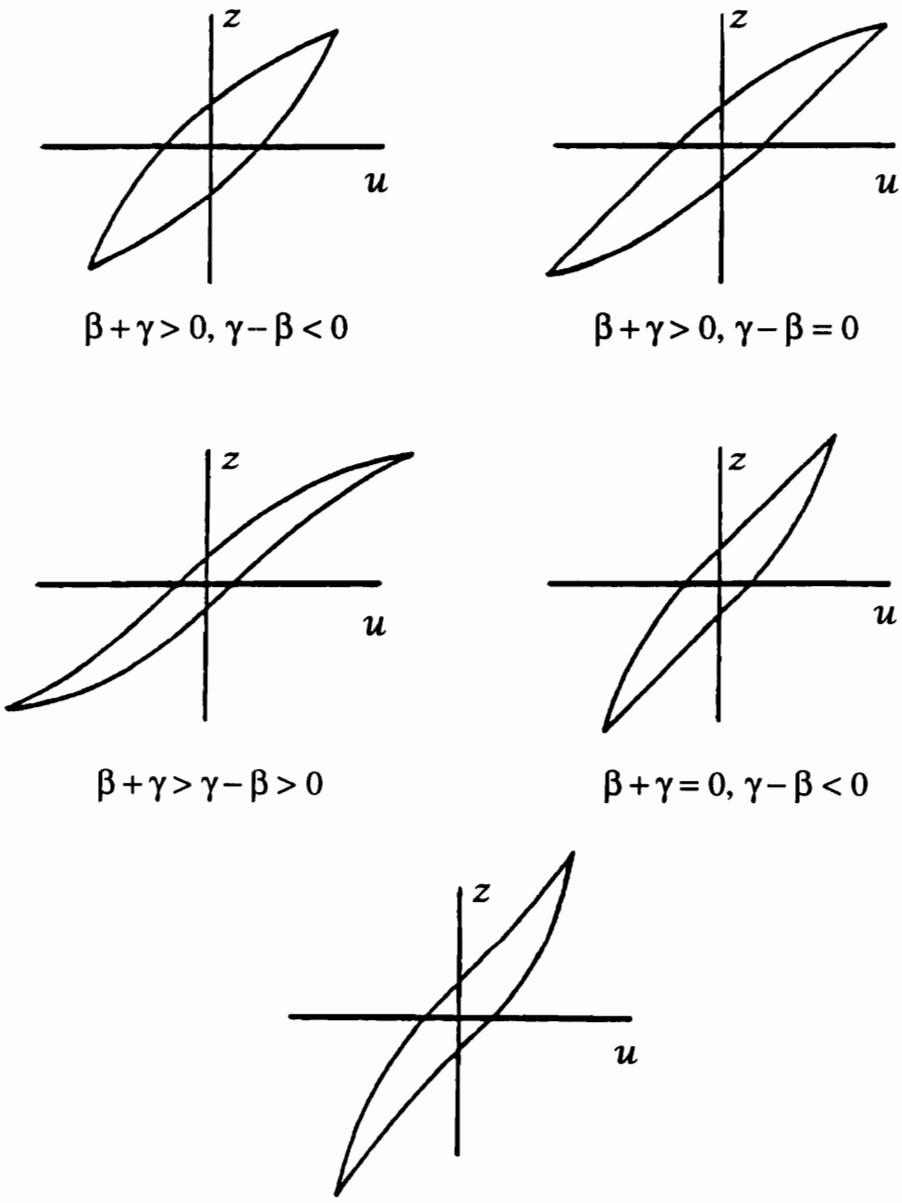

Figure 3.5: Possible hysteresis shapes, n=1 (from Baber 1980)

The loading path is given by Eq. (3.20). Considering the non-degrading case, ν=1, and substituting for $(\beta + \gamma)$ from Eq. (3.7) into (3.20), we get

$$\frac{dz}{du} = A - A\left(\frac{z}{z_u}\right)^n . \tag{3.22}$$

When $z < z_u$, as $n \to \infty$, $(z/z_u)^n = 0$ and $\frac{dz}{du} = A$. Thus, the loading path for $0 < z < z_u$ is linear. When $z = z_u$, $\frac{dz}{du} = 0$ as before. This is a horizontal line.

The unloading path when $z > 0$ is defined by Eq. (3.21) and may be expressed as

$$\frac{dz}{du} = A - \left[A\left(\frac{\gamma - \beta}{\gamma + \beta}\right)\right]\left(\frac{z}{z_u}\right)^n \tag{3.23}$$

after some manipulation of Eq. (3.7) and substitution into (3.21). Again, as $n \to \infty$, the slope approaches a constant value A, which is the same as that for the loading path.

The foregoing shows that as $n \to \infty$, the hysteresis in the z-u plane produces an elasto-plastic model. Following Fig. 3.3, this would produce a true bilinear hysteresis in the F_T-u plane, with $\alpha > 0$, and a true elasto-plastic hysteresis, with $\alpha \approx 0$.

3.4.4 Strength and Stiffness Degradation and Pinching

Degradation is controlled by defining the parameters ν and η as functions of the dissipated hysteretic energy given by

$$\varepsilon = \int_{u_o}^{u_f} F_h \cdot du \;\; = (1-\alpha)\omega_o^2 \int_{u_o}^{u_f} z\, du \;\; = (1-\alpha)\omega_o^2 \int_{t_o}^{t_f} z\dot{u}\, dt \tag{3.24}$$

Then, A, ν and η may be written as

$$\begin{aligned} A(\varepsilon) &= A_o - \delta_A\, \varepsilon \\ \nu(\varepsilon) &= 1.0 + \delta_\nu\, \varepsilon \\ \eta(\varepsilon) &= 1.0 + \delta_\eta\, \varepsilon \end{aligned} \tag{3.25}$$

where A_o is the initial value of A and the δ's are constants specified for the desired rate of degradation. A value of $\delta = 0$ means no degradation. If A decreases (i.e., $\delta_A > 0$), both strength and stiffness degrade (Fig. 3.7). If ν increases (i.e., $\delta_\nu > 0$), strength

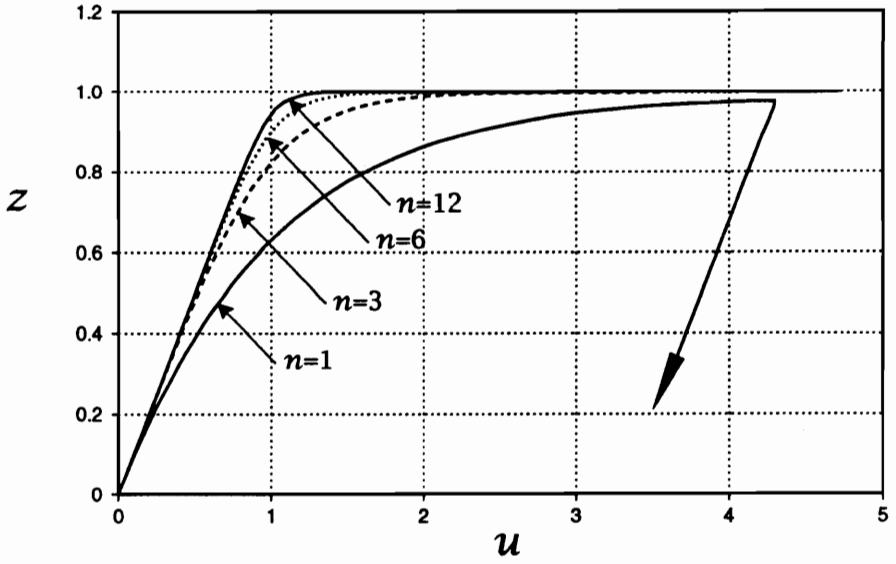

Figure 3.6: Skeleton curves with varying n

alone degrades (Fig. 3.8). If η increases (i.e., $\delta_\eta > 0$), stiffness alone degrades (Fig. 3.9). Figures 3.10a, b and c show the effect of changing values of A, ν and η, respectively, using the stiffness, dz/du, vs. z/z_u plot. Note that each plot shows the positive z loading case only.

Sues et al. (1988) suggested an alternative stiffness degradation scheme similar to that of Clough for reinforced concrete elements (see Fig. 2.6c). The stiffness degradation parameter, η, is defined such that the value of A (which controls the initial loading slope of each hysteresis cycle) reflects the maximum deformation reached in the previous cycle. The desired displacement dependent stiffness degradation is achieved by

$$\eta_i = A_o \frac{(u_{p_i} - u_{p_{i-1}})}{(z_{p_i} - z_{p_{i-1}})} \tag{3.26}$$

where,

η_i = value of η during the i^{th} half cycle ,

u_{p_i} = peak displacement in i^{th} half cycle,

z_{p_i} = peak z value in i^{th} half cycle

$u_{p_{i-1}}$ = peak displacement in $(i-1)^{th}$ half cycle (note that this is the peak opposite and immediately before that in the i^{th} half cycle),

$z_{p_{i-1}}$ = peak z value in $(i-1)^{th}$ half cycle.

Sues et al. (1988) found Eq. (3.26) to adequately model the stiffness degradation observed in scale model tests of a reinforced concrete building and a reinforced concrete frame. Incorporating Eq. (3.26) with pinching (like the one that will be described next), the author, however, found that the rate of degradation increases too fast and out of control. The resulting model is practically useless. Thus, for a Bouc-Wen model that incorporates pinching, the energy-based stiffness degradation originally proposed by Baber and Wen (1981), and given in Eq. (3.25), is preferred.

The pinching function, $h(z)$, originally proposed by Baber and Noori (1986), allows

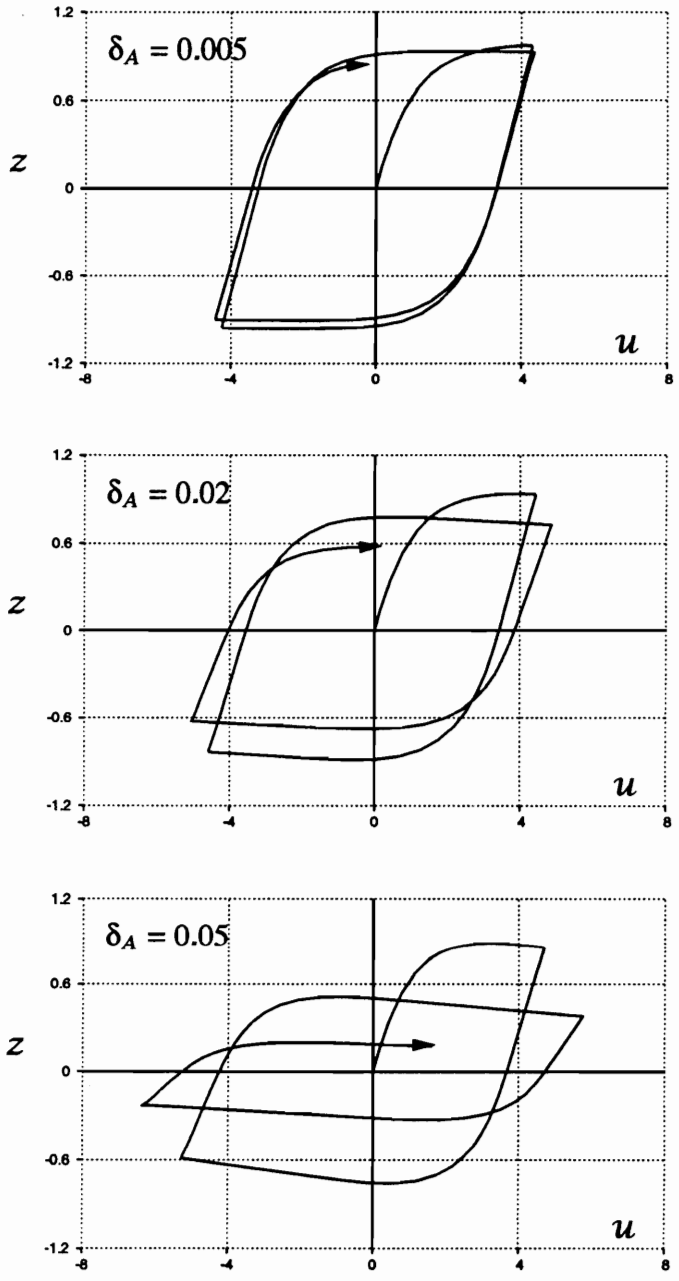

Figure 3.7: Strength and stiffness degradation- effect of varying A

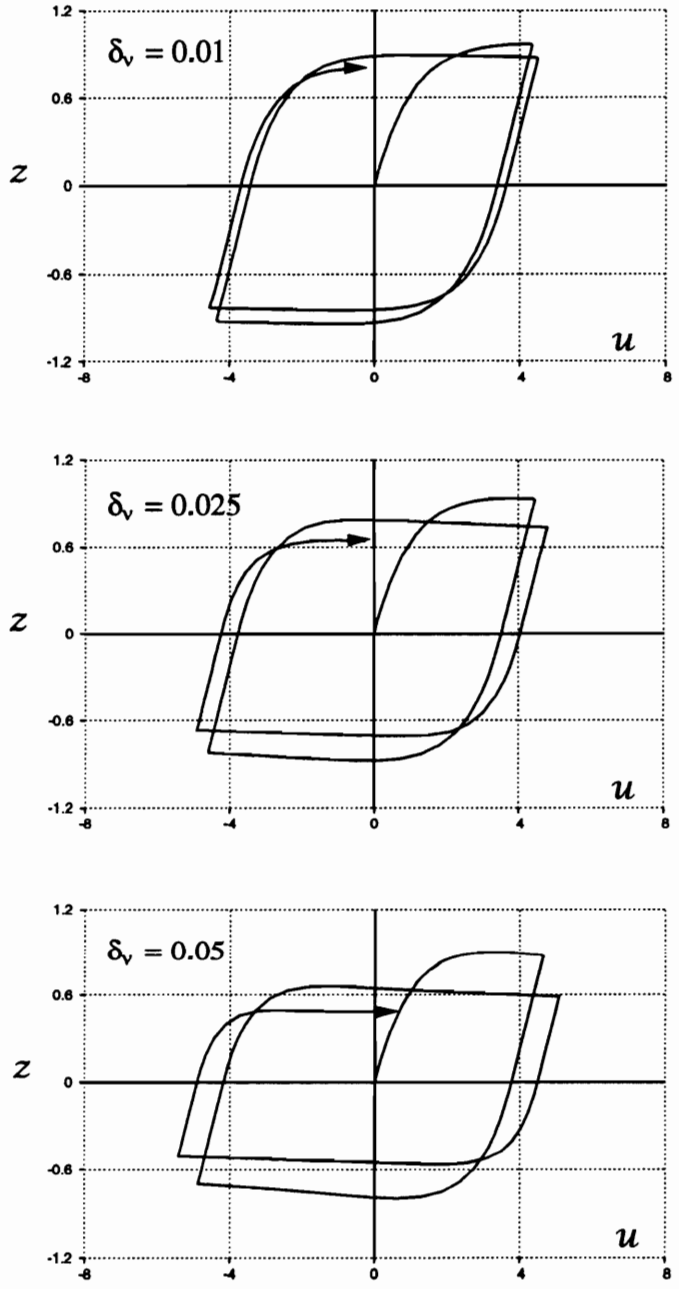

Figure 3.8: Strength degradation- effect of varying ν

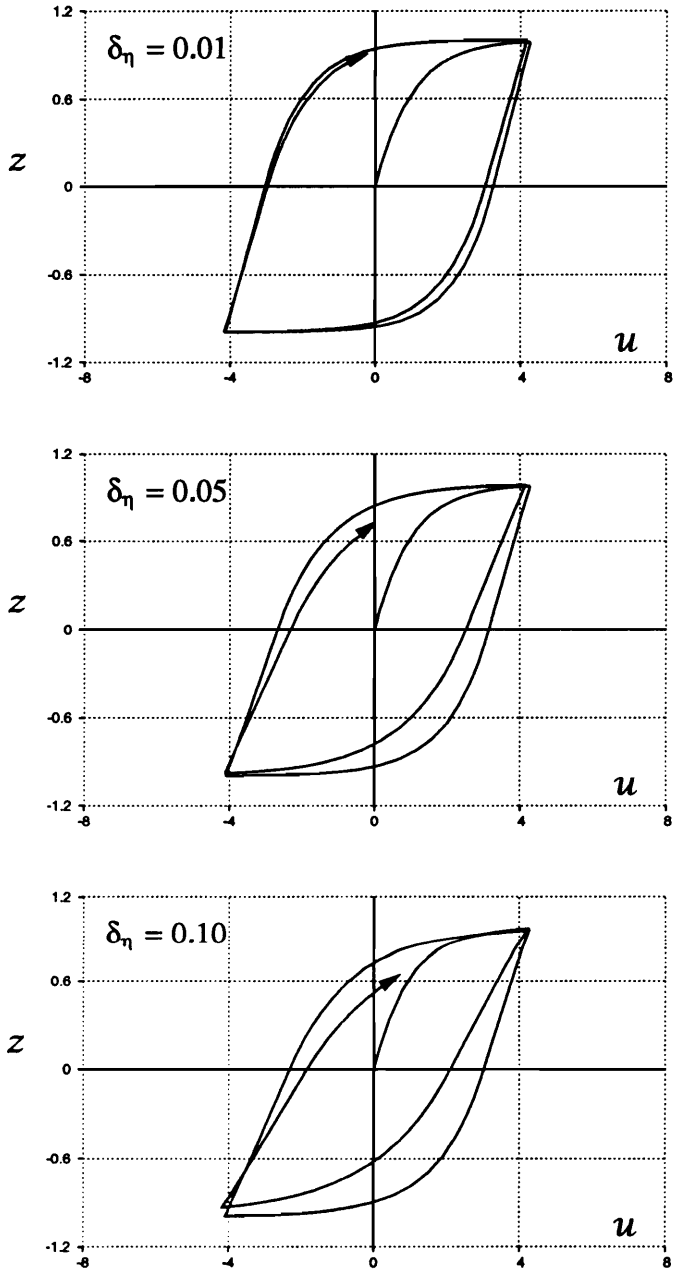

Figure 3.9: Stiffness degradation- effect of varying η

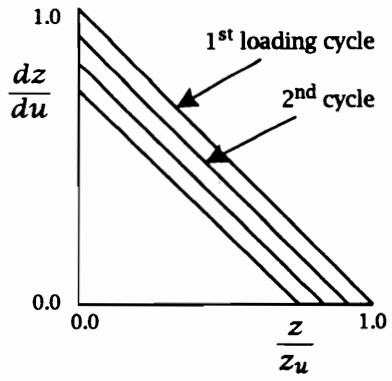

(a) only A is degrading

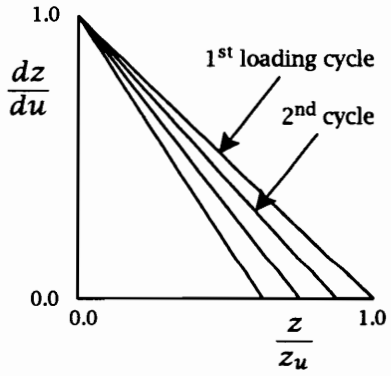

(b) only ν is degrading

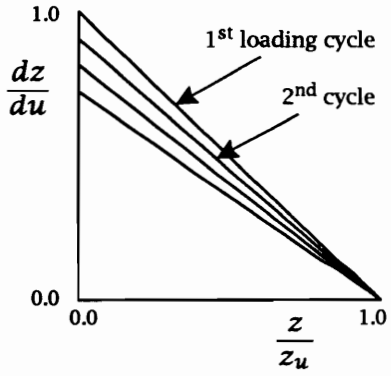

(c) only η is degrading

Figure 3.10: Degradation effect using dz/du vs. z/z_u plot

control of pinching severity and sharpness as functions of ε. It is defined by the following expressions (Baber and Noori 1986):

$$h(z) = 1.0 - \zeta_1 \, e^{(-z^2/\zeta_2^2)} \tag{3.27}$$

$$\zeta_1(\varepsilon) = \zeta_{1_o} \, [1.0 - e^{(-p\varepsilon)}] \tag{3.28}$$

$$\zeta_2(\varepsilon) = (\psi_o + \delta_\psi \varepsilon) \, (\lambda + \zeta_1) \tag{3.29}$$

where,

ζ_1 = controls the magnitude of initial drop in slope, dz/du; ($\zeta_1 < 1.0$) ,

ζ_2 = controls the rate of change of the slope, dz/du,

ψ_o = parameter that contributes to the amount of pinching,

δ_ψ = parameter specified for the desired rate of change of ζ_2 based on ε,

p = constant that controls the rate of initial drop in slope,

ζ_{1_o} = measure of total slip,

λ = small parameter that controls the rate of change of ζ_2 as ζ_1 changes.

The pinching function effect can be seen from the plot of stiffness, dz/du, against z/z_u in the absence of degradation (Fig. 3.11). Fig. 3.11a shows that when ζ_1 varies while ζ_2 is kept constant, dz/du drops at the start of the second and successive loading cycles. Pinching is induced by forcing minimum tangent stiffness when z=0. Then, the stiffness increases relatively rapidly as z increases, slowing down as the original slope is approached. When ζ_2 is kept constant, the original slope is reached at the same level of z in all cycles. When ζ_2 is varied and ζ_1 is kept constant, the level of drop at the start of the second and successive loading cycles remains the same but the original slope is reached at increasing levels of z. Thus, it may be stated that ζ_1 controls the severity of pinching while ζ_2 controls the rate of pinching. Fig. 3.11c shows the pinching function effect when both ζ_1 and ζ_2 vary.

While Baber and Noori's pinching function improved the versatility and capability of the BWBN model, most wood joints and structural systems, that show pinching behavior, do not pinch at z=0 (e.g., Fig. 2.4). Thus, the pinching function should be

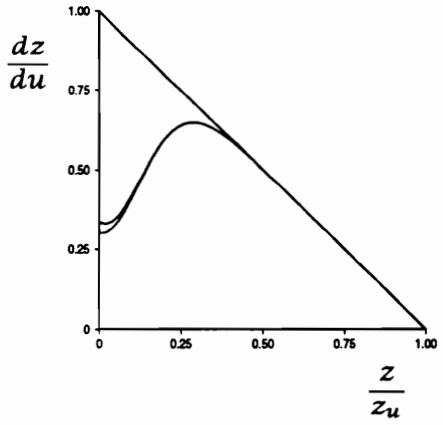

(a) only ζ_1 varies (ζ_2 is constant)

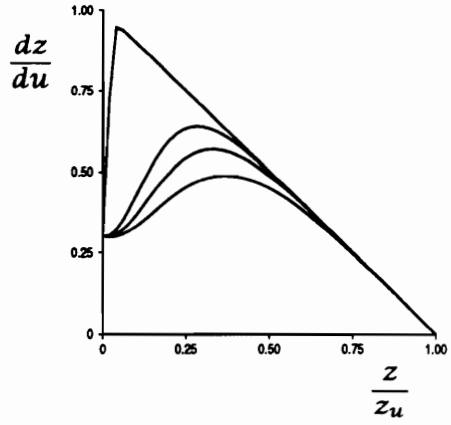

(b) only ζ_2 varies (ζ_1 is constant)

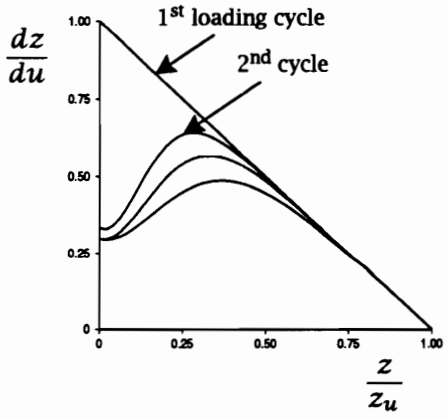

(c) both ζ_1 and ζ_2 vary

Figure 3.11: Baber and Noori's (1986) pinching function effect (dz/du vs. z/z_u)

modified. Section 3.5 will discuss the pinching behavior of wood systems and the development of an appropriate pinching function.

3.4.5 Model Limitation

Maldonado et al. (1987) and Casciati (1987) observed that the most serious drawback in the original Bouc-Wen model (i.e., the nondegrading, nonpinching type) was its inability to form a small loop during partial loading-unloading (see Fig. 3.12). Instead, the model softens during reloading without stress reversal. Most materials, including wood, demonstrate hysteresis loops in loading situations without stress reversal. This unwanted model behavior, however, is of relatively minor consequence in seismic analysis because seismic ground motions induce stress reversals on structures. Seismic ground action is often treated as a zero mean random process. For other loadings (e.g., wind) where this mechanical behavior needs to be modeled properly for analysis, a modification to the Bouc-Wen model was proposed by Casciati (1987). Two terms are added in the hysteretic constitutive equation so that the stiffness at the beginning of reloading, when there is no stress reversal, is greater than the one at the end of unloading. These terms disappear during unloading.

Casciati's modification of the Bouc-Wen model will not be considered in the present work. Dynamic analysis will be limited, for now, to wood structural systems under earthquake loading.

3.5 Pinching of Wood Systems

3.5.1 Experimental Observations

A closer examination of the pinching behavior of wood subassemblies in Fig. 2.4 and the nailed sheathing joint in Fig. 2.5c shows that the pinching function should have the following features (illustrated in Fig. 3.13):

- In initial loading (starting from rest), no pinching occurs.

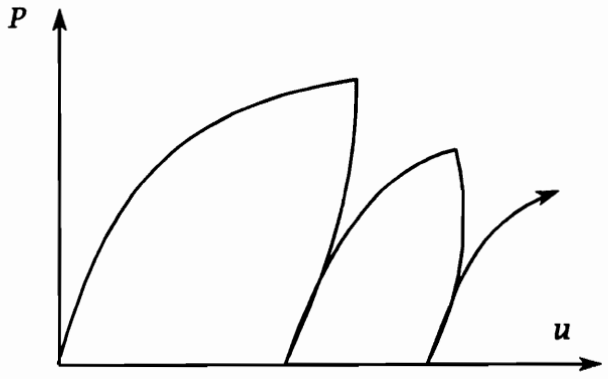

(a) Bouc-Wen hysteresis behavior

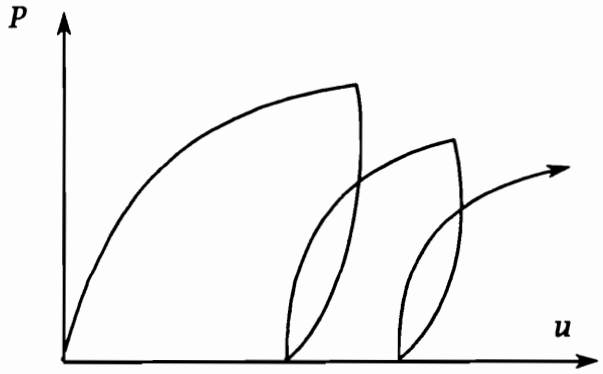

(b) behavior of most materials (including wood)

Figure 3.12: Hysteresis during partial loading-unloading

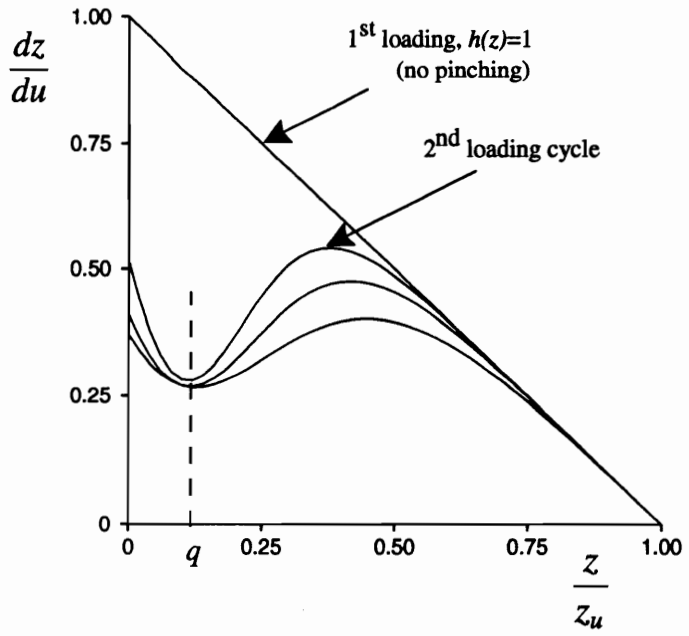

Figure 3.13: Pinching of wood systems (dz/du vs. z/z_u)

- In the second loading cycle, pinching starts: dz/du drops at z=0 and continues to decrease until it reaches a minimum at z = some fraction of z_u, or qz_u. Then the stiffness increases relatively rapidly as z increases, slowing down as the original slope is approached. As z finally approaches the ultimate value, the slope sharply decreases and reaches zero at z_u.
- In the third and successive cycles, the drop of dz/du at z=0 slows down but the stiffness reaches a minimum at qz_u again. Medearis and Young (1964) first noticed this on cyclic tests of plywood shear walls and called qz_u the *invariant point.* Others call it the *residual force.*

3.5.2 Pinching Function Development

Baber and Noori (1986) introduced the use of dz/du vs. z curves to develop hysteresis models. Here, the object is to obtain mathematical functions that would provide the dz/du behavior shown in Fig. 3.13 and listed in section 3.5.1. To do this, the tangent stiffness function, given earlier in Eq. 3.6 as

$$\frac{dz}{du} = h(z)\left\{\frac{1-\nu(\beta\,\mathrm{sgn}(\dot{u})\,|z|^{n-1}z+\gamma|z|^{n})}{\eta}\right\}, \tag{3.30}$$

is examined.

To get the desired pinching, the pinching function, $h(z)$, should be a small value at z=0 and reach a minimum at $z = qz_u$; this makes dz/du minimum at this level as well. As z increases, $h(z)$ should approach 1 to allow dz/du to return to the original stiffness path. During unloading, $h(z)$ should not cause pinching even at $z = qz_u$. Thus, pinching should be induced during loading only, that is, when $z\dot{u} > 0$ or $\mathrm{sgn}(z)\cdot\mathrm{sgn}(\dot{u})$ is positive [see Eq. (3.20)].

Several modifications of Baber and Noori's (1986) original function, defined by Eqs. (3.27), (3.28) and (3.29), were investigated. One that meets the foregoing requirements with the least modification of Baber and Noori's function is

$$h(z) = 1.0 - \zeta_1\, e^{[-(z\,\mathrm{sgn}(\dot{u})-qz_u)^2/\zeta_2^2]} \tag{3.31}$$

where q is a constant that sets a fraction of z_u as the pinching level and all other parameters are as previously defined. Eq. (3.31) is a generalization of Baber and Noori's pinching function; that is, when q=0, the model reverts back to Baber and Noori's original function. It is desired that as little modification as possible is introduced to Baber and Noori's equation in the hope that the new model will maintain the original form's compatibility with closed-form statistical linearization during random vibration analysis.

Figure 3.14 shows $h(z)$ as a function of z and sgn($\dot{u}$), where ζ_1=0.85, ζ_2=0.02, q=0.15 and z_u=1.0. Its effect on dz/du satisfies the pinching requirements for wood systems and produces a dz/du vs. z/z_u plot similar to that in Fig. 3.13.

3.6 Summary

The Bouc-Wen-Baber-Noori (BWBN) hysteresis model was used as the basis of a general model for wood joints and structural systems. The mechanical model consisted of three parallel elements: *(1)* a linear viscous damping, *(2)* a linear spring and *(3)* a hysteretic element. The hysteretic element was defined by a nonlinear first-order differential equation with a form similar to that in the endochronic theory of plasticity. The hereditary nature of the constitutive relations satisfied the requirement that the response depends not only on instantaneous displacement but also on its past history (or memory).

The form and properties of the original Bouc-Wen model and its extensions were presented. The pinching capability of the BWBN model was modified so that it would represent pinching in dowel-type wood joints more accurately. The generalized pinching capability enhanced the model's versatility. The modified BWBN model is, in fact, applicable to structures made of other materials, such as steel and reinforced concrete, that exhibit pinching similar to that observed in dowel-type wood joints and plywood shear walls. In summary, the modified BWBN hysteresis model incorporates all the experimentally observed characteristics of timber structures that were identified in

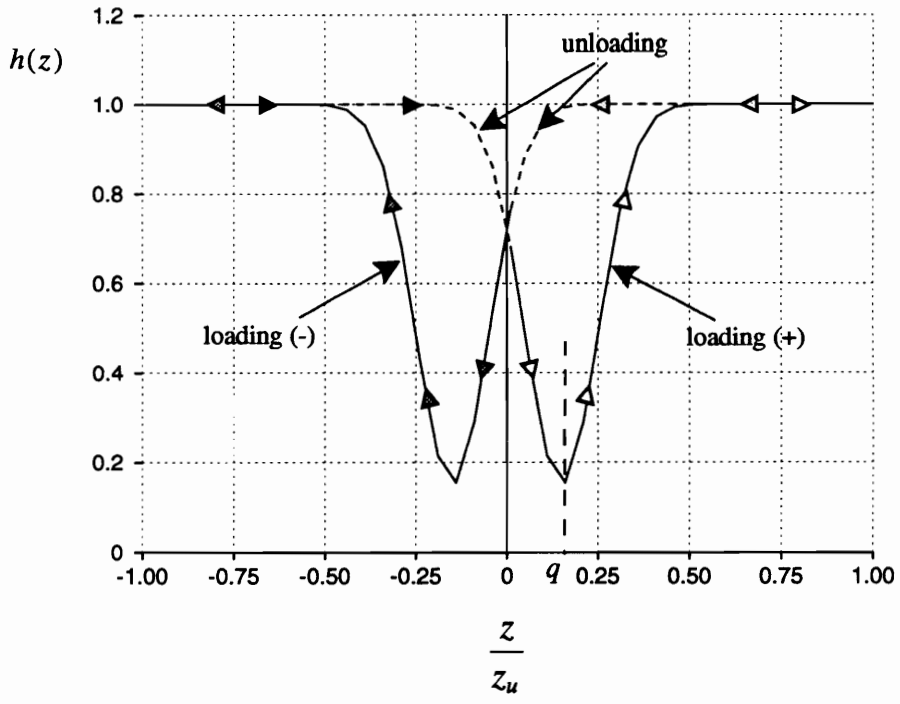

Figure 3.14: Behavior of the proposed pinching function for wood systems

the previous chapter. It has: (*1*) a nonlinear, inelastic load-displacement relationship without a distinct yield point, (*2*) stiffness degradation, (*3*) strength degradation, (*4*) pinching, and (*5*) memory.

Chapter 4

Structural Modeling and Nonlinear Dynamic Analysis

4.1 General

General purpose dynamic analysis programs have long been used in the analysis and design of reinforced concrete and steel structures. These programs have, however, seen very limited use in the analysis of wood structures because the available material models and finite elements are inadequate to model wood system response. It was not until the start of the 1980's that hysteresis models specifically derived for wood systems surfaced in the literature (see the review in section 2.4.2). (Note that all the models for wood have only been proposed in the past 13 years.) The models for wood have been incorporated into either existing commercial programs (e.g., DRAIN-2D) or new programs written to solve a specific problem. The availability of various types of hysteresis models for wood structures allowed researchers and engineers to perform dynamic analyses of wood structures and structural systems. The problems considered and the types of analysis so far employed can be found in Gupta and Moss (1991). It is clear, however, that a wide gap between advances in general structural dynamics and the dynamic analysis of wood structures remains.

The basis, form and properties of a general hysteresis model for wood joints and structural systems were presented in the previous chapter. This chapter consists of three major parts. In the first part, the complete form of the modified Bouc-Wen-Baber-Noori (BWBN) model for single-degree-of-freedom (SDF) wood systems is summarized

and a model for multi-degree-of-freedom (MDF) systems is derived. The second part deals with model validation. It provides a brief introduction to parameter estimation methods and compares model behavior with a selected number of experimental hysteresis results. In the last part, the model is used to obtain the response of SDF wood systems under deterministic or prescribed dynamic loading.

4.2 Proposed Model for Wood Structural Systems

Structures are continuous systems and as such have an infinite number of degrees-of-freedom. For analytical purposes, the structure is simplified by means of *spatial discretization* of the continuum. The following discretization methods can be used in the dynamic modeling of structures (Clough and Penzien 1993): (*1*) concentrated mass method, (*2*) generalized displacements method, and (*3*) finite element method. Use of any of these methods results in a discretized structural model with a finite number of degrees-of-freedom. The present work will concentrate on the concentrated mass method only.

4.2.1 Model for SDF Systems

While few real structures are accurately modeled by SDF models, such models may still be used for preliminary dynamic analyses of many types of structures. In some cases, a SDF model is sufficient to obtain a basic understanding of the dynamic behavior of the structural system. Fig. 4.1 shows a SDF dynamic model idealization of a trussed wood-frame and a wood shear wall. The structural mass is assumed to be concentrated in the direction of the displacement. Stewart (1987) and Kamiya (1988) performed time history analyses of wood-sheathed shear walls using a SDF model that incorporates their hysteresis models presented in section 2.4.2. Stewart obtained hysteresis parameters from full-scale cyclic tests of the walls, while Kamiya obtained model parameters from pseudo-dynamic tests. Gavrilović and Gramatikov (1991) also used a

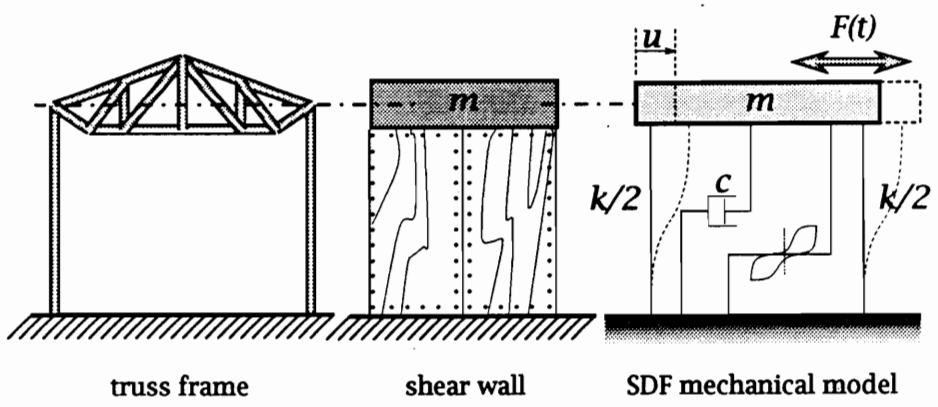

Figure 4.1: SDF idealization of wood structural systems

SDF model to compute the dynamic response of a trussed-frame wood structure.

The hysteresis model developed and described in the previous chapter will now be summarized for SDF wood systems. The equation of motion is

$$\ddot{u} + 2\xi_o\omega_o\dot{u} + \alpha\omega_o^2 u + (1-\alpha)\omega_o^2 z = f(t)\,. \tag{4.1}$$

So that α is the ratio of the final tangent stiffness to the initial stiffness (see section 3.4.3.1), A will be set to unity (A=1) in the hysteretic constitutive relations. Then, the constitutive law, Eq. (3.3), becomes

$$\dot{z} = h(z)\left\{\frac{\dot{u} - \nu(\beta|\dot{u}||z|^{n-1}z + \gamma\dot{u}|z|^n)}{\eta}\right\} \tag{4.2}$$

with pinching function

$$h(z) = 1.0 - \zeta_1\, e^{[-(z\,\mathrm{sgn}(\dot{u}) - qz_u)^2/\zeta_2^2]} \tag{4.3}$$

where

$$\zeta_1(\varepsilon) = \zeta_{1_o}\,[1.0 - e^{(-p\varepsilon)}] \tag{4.4}$$

$$\zeta_2(\varepsilon) = (\psi_o + \delta_\psi\varepsilon)\,(\lambda + \zeta_1)\,. \tag{4.5}$$

Strength and stiffness degradation are modeled, respectively, by

$$\nu(\varepsilon) = 1.0 + \delta_\nu\,\varepsilon \tag{4.6}$$

$$\eta(\varepsilon) = 1.0 + \delta_\eta\,\varepsilon\,.$$

Note that parameter A is now treated as a constant (in this case A=1). Pinching, and strength and stiffness degradation are controlled by the hysteretic energy dissipation

$$\varepsilon = (1-\alpha)\omega_o^2 \int_{t_o}^{t_f} z\dot{u}\,dt\,. \tag{4.7}$$

A summary of hysteresis model parameters is given in Table 4.1.

The foregoing model satisfies all the experimentally observed features of hysteretic behavior of wood joints and structural systems, namely, (*1*) nonlinear hysteresis, (*2*) stiffness degradation, (*3*) strength degradation, (*4*) pinching and (*5*) memory (see section 2.3.2).

Table 4.1: Tabulated summary of hysteresis model parameters

Parameter	Definition
System properties and hysteresis parameters	
ω_o (rad/sec)	natural frequency of the structural system
ξ_o	damping ratio of the structural system
α	rigidity ratio; a weighting constant representing the relative participations of the linear and nonlinear terms ($0< \alpha <1$)
β, γ	parameters that control the basic hysteresis shape ($\beta > 0$)
n	parameter that controls hysteresis curve smoothness
Degradation parameters	
δ_ν	parameter that controls strength degradation
δ_η	parameter that controls stiffness degradation
Pinching parameters	
ζ_1	parameter that controls the severity of pinching; depends on the values of ζ_{1o} and p
ζ_2	parameter that controls the rate of pinching; depends on the values of ζ_1, ψ_o, δ_ψ and λ
ζ_{1o}	measure of total slip (e.g., ζ_{1o}= 0.98 means a high pinching system and ζ_{1o}= 0.70 means a low pinching system)
q	percentage of ultimate restoring force z_u where pinching (or slipping) occurs
p	parameter that controls the rate of initial drop in slope
ψ_o	parameter that contributes to the amount of pinching
δ_ψ	parameter specified for the desired rate of change of ζ_2 based on ε
λ	parameter that controls the rate of change of ζ_2 as ζ_1 changes

4.2.2 Model for MDF Systems

Multi-storey buildings have been commonly treated as "shear-beam" or, simply, shear buildings in most earthquake engineering studies. A shear building model, the simplest MDF model possible, is based on the following assumptions (Paz 1991): (*1*) the total mass of the structure is concentrated at the levels of the floors (or the roof, at the top floor), (*2*) the girders on the floors are infinitely rigid as compared to the columns, and (*3*) the deformation of the structure is independent of the axial forces present in the columns. The structure will now only have as many degrees-of-freedom as it has lumped masses at the floor levels. With the second assumption, rotation at the girder-to-column joint is suppressed. The third assumption means that the rigid girders remain horizontal during ground motion.

While many wood structures may not be ideal candidates as shear building models, these models may still provide enhancements that make them more preferable than alternative SDF models. A two-storey wood building shown in Fig. 4.2a, for example, may be better represented by a three-degree-of-freedom shear building than by a SDF model. The first mass, m_1, is assumed to be concentrated at the floor of the first storey. Corresponding hysteretic properties are obtained from the floor-to-foundation connections. The second mass, m_2, is concentrated on the second-storey floor. Corresponding hysteretic properties are obtained from the columns (or walls) connecting the first and second storey floor systems. The trussed-roof structure carries m_3, with corresponding hysteretic properties obtained from the columns (or walls) connecting the second storey floor system and the roof system. Sakamoto and Ohashi (1988) used the shear building model to compute the seismic response of one-, two- and three-storey conventional Japanese wood houses. Fig. 4.3 shows the lumped mass model that they used.

Generally, a shear building model may have up to r lumped masses and, thus, r degrees-of-freedom. Considering the shear building model in Fig. 4.2b, the relative displacement of the i^{th} mass with respect to the ground displacement is indicated

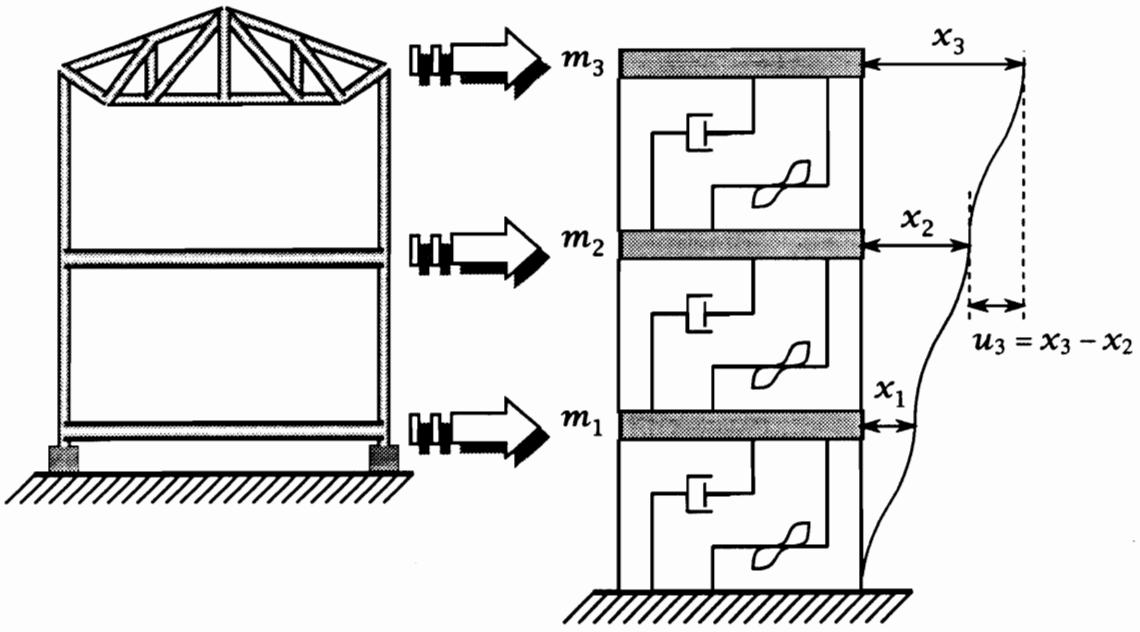

(a) two-storey wood building

(b) shear building model

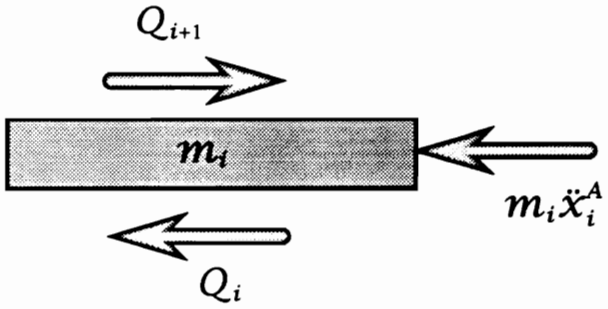

(c) forces acting on i^{th} mass

Figure 4.2: MDF idealization of multi-storey wood buildings

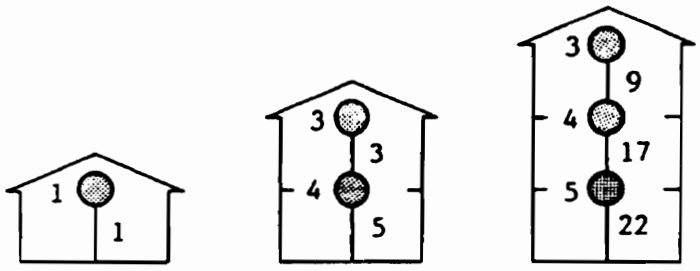

Figure 4.3: Sakamoto and Ohashi's (1988) MDF idealization of multi-storey conventional Japanese houses

by x_i. Interstorey drift, or the relative displacement between floors, is denoted by $u_i = x_i - x_{i-1}$. When dynamically loaded, the i^{th} mass is acted upon by the forces shown in Fig. 4.2c, where $\ddot{x}_i^A$ is the absolute acceleration, $\ddot{x}_i^A = \ddot{x}_i + \ddot{x}_g$, and Q_i is the total restoring force of the i^{th} mass given as

$$Q_i = c_i(\dot{x}_i - \dot{x}_{i-1}) + \alpha_i k_i(x_i - x_{i-1}) + (1 - \alpha_i)k_i z_i \tag{4.8}$$

or, in terms of u_i,

$$Q_i = c_i\dot{u}_i + \alpha_i k_i u_i + (1 - \alpha_i)k_i z_i \,. \tag{4.9}$$

Using D'Alembert's principle, the equation of motion is obtained as

$$m_i\ddot{x}_i^A + Q_i - Q_{i+1} = 0 \tag{4.10}$$

or, after substituting $\ddot{x}_i^A$ and Eq. (4.8) and rearranging,

$$\begin{aligned} m_i\ddot{x}_i - c_i\dot{x}_{i-1} + (c_i - c_{i+1})\dot{x}_i + c_{i+1}\dot{x}_{i+1} - \\ \alpha_i k_i x_{i-1} + (\alpha_i k_i - \alpha_{i+1}k_{i+1})x_i + \alpha_{i+1}k_{i+1}x_{i+1} + \\ (1 - \alpha_i)k_i z_i - (1 - \alpha_{i+1})k_{i+1}z_{i+1} \;=\; -m_i\ddot{x}_g \end{aligned} \tag{4.11}$$

where $i = 1, 2, \ldots, r$. The assemblage of equations of motion for all r masses gives the following matrix equation:

$$[M]\{\ddot{X}\} + [C]\{\dot{X}\} + [K^\alpha]\{X\} + [H^\alpha]\{Z\} = -[M]\{\mathcal{I}\}\ddot{x}_g \tag{4.12}$$

where $\{X\}$ is the relative displacement vector, $\{Z\}$ is the vector for the hysteretic component of the displacement and $\{\mathcal{I}\}$ is the influence vector (all entries are 1, in this case).

The hysteretic displacement, z_i, of the i^{th} mass is related to the relative displacement between floors, u_i, through the following first-order nonlinear differential equation:

$$\dot{z}_i = h(z_i)\left\{\frac{\dot{u}_i - \nu_i(\beta_i|\dot{u}_i||z_i|^{n_i-1}z_i + \gamma_i\dot{u}_i|z_i|^{n_i})}{\eta_i}\right\} \tag{4.13}$$

where the parameters are the same as in the SDF model except that they are now defined for each element. That is,

$$h(z_i) = 1.0 - \zeta_{1_i} e^{[-(z_i \operatorname{sgn}(\dot{u}_i) - q_i z_{u_i})^2 / \zeta_{2_i}^2]} \tag{4.14}$$

$$\zeta_{1_i}(\varepsilon_i) = \zeta_{1_{oi}} [1.0 - e^{(-p_i \varepsilon_i)}] \tag{4.15}$$

$$\zeta_{2_i}(\varepsilon_i) = (\psi_{o_i} + \delta_{\psi_i} \varepsilon_i)(\lambda_i + \zeta_{1_i}) \tag{4.16}$$

$$\nu_i(\varepsilon_i) = 1.0 + \delta_{\nu_i} \varepsilon_i \tag{4.17}$$

$$\eta_i(\varepsilon_i) = 1.0 + \delta_{\eta_i} \varepsilon_i \tag{4.18}$$

$$\varepsilon_i = (1 - \alpha_i)\omega_{o_i}^2 \int_{t_o}^{t_f} z_i \dot{u}_i \, dt \, . \tag{4.19}$$

Note that $u_i = x_i - x_{i-1}$ and $i = 1, 2, \ldots, r$.

All the matrices in Eq. (4.12) have dimension $(r \times r)$. $[M]$ is the diagonal mass matrix. $[C]$ is the damping matrix with the following nonzero entries:

$$[C] = \begin{bmatrix} (c_1 + c_2) & -c_2 & & & \\ -c_2 & (c_2 + c_3) & -c_3 & & \\ & \ddots & \ddots & \ddots & \\ & & c_{n-1} & (c_{n-1} + c_n) & -c_n \\ & & & -c_n & c_n \end{bmatrix} . \tag{4.20}$$

The linear part of the stiffness matrix, $[K^\alpha]$, has the following nonzero entries:

$$[K^\alpha] = \begin{bmatrix} (k_1^\alpha + k_2^\alpha) & -k_2^\alpha & & & \\ -k_2^\alpha & (k_2^\alpha + k_3^\alpha) & -k_3^\alpha & & \\ & \ddots & \ddots & \ddots & \\ & & k_{n-1}^\alpha & (k_{n-1}^\alpha + k_n^\alpha) & -k_n^\alpha \\ & & & -k_n^\alpha & k_n^\alpha \end{bmatrix} \tag{4.21}$$

where $k_i^\alpha = \alpha_i k_i$. Matrix $[H^\alpha]$ contains the hysteretic elements with the following

nonzero entries:

$$[H^{\alpha}]=\begin{bmatrix} h_1^{\alpha} & -h_2^{\alpha} & & & \\ & h_2^{\alpha} & -h_3^{\alpha} & & \\ & & \ddots & \ddots & \\ & & & h_{n-1}^{\alpha} & -h_n^{\alpha} \\ & & & & h_n^{\alpha} \end{bmatrix} \tag{4.22}$$

where $h_i^{\alpha} = (1 - \alpha_i)k_i$.

The model for MDF shear buildings is now complete and is described by Eqs. (4.12) to (4.22). There are a total of $2r$ unknowns: r unknowns in vector $\{X\}$ plus r unknowns in $\{Z\}$. There are r equations in (4.12) and another r equations to define the constitutive relations of each deforming element, Eqs. (4.13) to (4.19). If we are interested in the behavior and performance of the i^{th} mass, its hysteresis may be plotted in the z_i-u_i plane. Note that u_i is the interstorey drift, or the relative displacement between floors, calculated as $(x_i - x_{i-1})$.

If it is desired to obtain u_i directly, the equations of motion should be formulated in terms of u_i. Substituting $\ddot{x}_i^A = \ddot{x}_i + \ddot{x}_g = \sum_{j=1}^{i} \ddot{u}_j + \ddot{x}_g$ into Eq. (4.10) and dividing by m_i,

$$\sum_{j=1}^{i} \ddot{u}_j + \ddot{x}_g + \frac{Q_i}{m_i} - \frac{Q_{i+1}}{m_i} = 0 \tag{4.23}$$

The relative accelerations are decoupled by subtracting the $(i-1)^{th}$ equation from the i^{th} equation (except when $i = 1$) to obtain

$$\ddot{u}_i - (1 - \delta_{i1})\frac{Q_{i-1}}{m_{i-1}} + \left[1 + (1 - \delta_{i1})\frac{m_i}{m_{i-1}}\right]\frac{Q_i}{m_i} - (1 - \delta_{ir})\frac{Q_{i+1}}{m_{i+1}}\frac{m_{i+1}}{m_i} = -\delta_{i1}\ddot{x}_g \tag{4.24}$$

where δ_{i1}, δ_{ir} are Kronecker deltas (i.e., $\delta_{ir} = 1$ when $i = r$, 0 otherwise); they are introduced so that the equation will be valid for the first mass ($i = 1$) and last mass ($i = r$), as well as all the intermediate masses. The complete model is now described by Eqs. (4.24) and (4.13) to (4.19).

Other structural models may be used instead of the simple shear building model

given above. Related work will be cited but no other model that specifically incorporates the modified BWBN hysteresis model will be formulated.

Takizawa (1975) proposed a structural modeling technique that considers the interaction of inelastic storey drifts. His approach required that the structural mechanism producing the inelastic response deformations be known or assumed. The post-yield degrees-of-freedom are then based on the frame yield mechanism, with the pre-yield stiffness based upon the natural frequency. His approach sometimes leads to a SDF system. Baber (1980) reviewed other modeling techniques and chose the discrete hinge concept, normally used in deterministic analysis of yielding structures, to model plane frame structures. Yielding was confined to discrete hinge regions that incorporate the non-pinching BWBN constitutive relations. Baber (1980; 1986a; 1986b) performed zero and non-zero mean random vibration analyses of hysteretic frames using this approach. Fig. 4.4 shows a typical discrete hinge model of a planar frame. Maldonado (1992) used a similar approach in developing a response spectrum method for plane frames with potential plastic hinges modeled by the non-pinching non-deteriorating BWBN constitutive law.

Previous work have, thus, shown that incorporation of the BWBN hysteresis model into analytical MDF structural models is not limited to shear type buildings. If desired, it can be used with other structural modeling techniques.

4.3 Model Validation

4.3.1 Parameter Estimation

There are typically two steps in constructing a mathematical model from measured data (Ljung and Söderström 1983): *(1)* selecting a family of candidate models that represents the general behavior of the physical system, and *(2)* choosing a particular member of this family that best describes the observed data. A general hysteresis model has just been proposed for wood structural systems. The model then needs

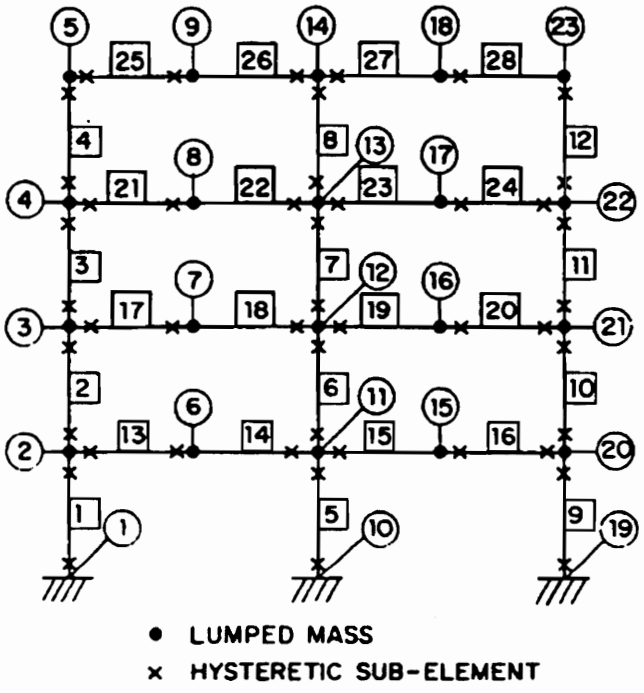

Figure 4.4: Hysteresis frame discrete hinge model (from Baber 1986b)

to be explicitly defined for a particular set of system materials and configurations. This is specifically known as a *parameter estimation* problem, or generally as a *system identification* problem.

System identification is defined as "a process for constructing a mathematical description or model of a physical system when both the input to the system and the corresponding output are known" (Yao 1985). The general topic of system identification originated from mechanical control theory and electrical engineering but has since been used in many branches of science and engineering. For structural engineering applications, the input is usually a forcing function and the output is displacement, velocity, or acceleration response of the structure to this force. Thus, the particular model obtained from the identification process should produce a response that closely matches the system output, given the same input (Yao 1985).

Ideally, one should use system identification techniques such as Newton's iterative algorithm, Gauss method, or Extended Kalman Filtering technique to systematically determine the hysteresis model parameters from experimental data (e.g., Sues et al. 1988; Maruyama et al. 1989). But this is a major project by itself and is beyond the scope of the present work. For the purpose of this dissertation, a practical, albeit nonsystematic, approach will be used.

Properties needed in the equation of motion are estimated from the physical system. The system's natural frequency, ω_o, is computed as $\sqrt{k_i/m}$, where m is the estimated mass of the system and k_i is its initial stiffness. From the system's experimental hysteresis, the nonlinear weighting constant, α, is computed as the ratio of the final tangent stiffness, k_f, to initial stiffness, k_i. Since system nonlinearity, hysteretic damping, and the non-viscous energy dissipation property are modeled by the hysteretic element, the value of the *linear* damping ratio, ξ_o, is not critical and may be arbitrarily chosen within the range 0.01 and 0.05 (Yeh et al. 1971; Chui and Smith 1989) for all wood systems.

Hysteresis shape parameter values for β and γ should be chosen such that

$$\beta + \gamma > 0 \text{ and } \gamma - \beta \leq 0.$$

Note that, to obtain positive energy dissipation, β should be positive. The pinching level constant, q, is determined from the experimental hysteresis as the ratio of the residual force (at invariant point) to the maximum restoring force. The pinching and degradation parameters, p, ζ_{1_o}, λ, ψ_o, δ_ψ, δ_ν and δ_η, are obtained by experimentation. That is, they are assigned certain values, the response is computed using the computer program that is described in section 4.4 and the model hysteresis is plotted and compared with experimental hysteresis. This is repeated until the basic hysteresis shape is satisfactorily reproduced.

4.3.2 Comparison With Experimental Hysteresis

Model parameters of three common wood joints, to represent the major hysteresis types for timber structures that Dowrick (1986) identified (see section 2.3.1), were estimated. Figures 4.5a, b and c show the hysteresis shapes produced by the model.

For a SDF wood system, with ω_o=9.425 rad/s, ξ_o=0.05, α=0.25, whose behavior is governed by joints with yielding plates, the hysteresis parameters are: β=0.5, γ = 0.5, n=1, q=0, $h(z)$=1.0, δ_ν=0 and δ_η = 0 (Fig. 4.5a). Model parameters for a system, with ω_o=6.283 rad/s, ξ_o=0.05, α=0.10 and joints with yielding nails, are: β=1.5, γ = −0.5, n=1, q=0.10, ζ_{1_o}=0.97, λ=0.10, p=1, ψ_o=0.20, δ_ψ=0.002, δ_ν=0.005 and δ_η = 0.05 (Fig. 4.5b). For a wood structural system, with bolted joints and ω_o=3.0 rad/s, ξ_o=0.05, α=0.35, the model parameters are: β=2.0, γ = −1.0, n=1, q=0, ζ_{1_o}=0.98, λ=0.10, p=2.0, ψ_o=0.20, δ_ψ=0.004, δ_ν=0.0 and δ_η = 0.025 (Fig. 4.5c). Note that to get the exact hysteresis shapes and response values as shown in Fig. 2.5, complete information about connection materials, test set-up and the forcing function that was used for testing are needed. Since most of these are not known, the focus should only be on modeling the basic hysteresis shape of the joints in Fig. 2.5; thus, no specific force and displacement units are considered.

(a) model for joint with yielding plate

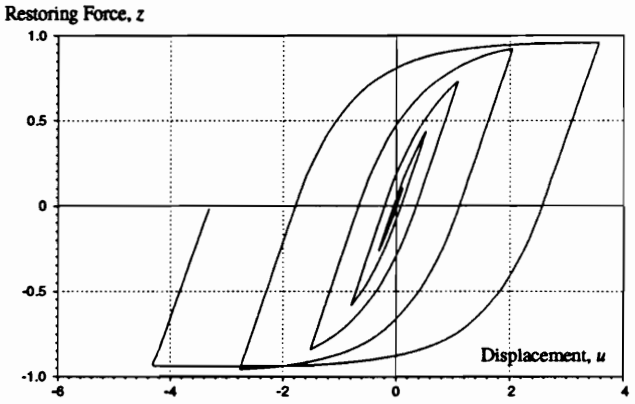

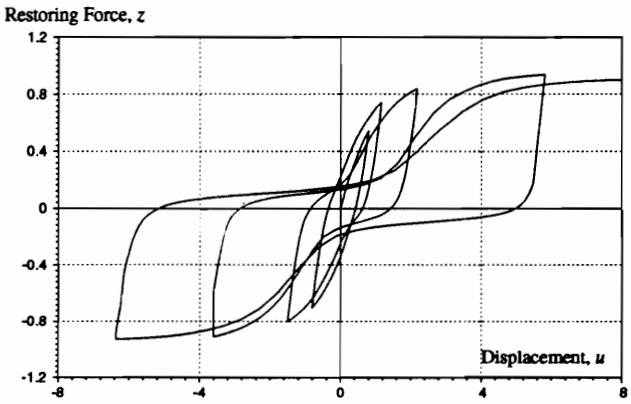

(b) model for joint with yielding nail

(c) model for joint with yielding bolt

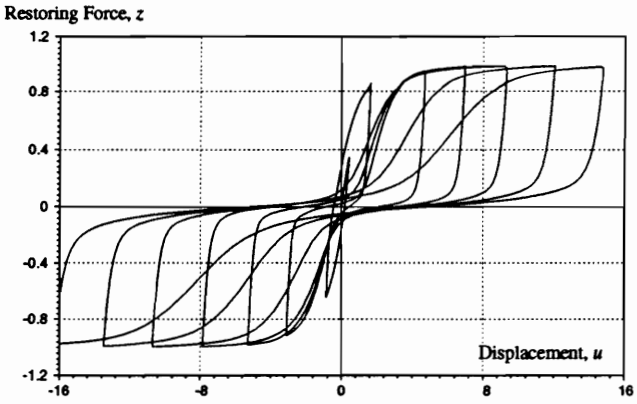

Figure 4.5: Hysteresis loops produced by the modified BWBN model

Comparison of model hysteresis (Fig. 4.5) with experimental hysteresis (Fig. 2.5) shows that the proposed model reasonably mimics the basic hysteresis shape of test data. The slight discrepancy in the hysteresis shapes of the yielding bolt joints (Fig. 2.5c vs. Fig. 4.5c) may be largely attributed to different forcing functions used in the test and the analysis. Even then, the basic behavior of the actual bolt joint can be observed in the model hysteresis.

The model is very flexible and can actually produce a wide variety of hysteresis shapes if the parameters are varied.

4.3.3 Potential

Although some practical guidance has been presented to obtain hysteresis parameters for any wood system, it is ideal that system identification techniques be used to estimate the parameters of the proposed model. This will allow us to: *(1)* systematically obtain a system model from laboratory or field data for predicting the structural response of similar real-world systems under adverse environmental loadings such as earthquakes or winds, and *(2)* estimate the existing conditions of structures for the assessment of damage and deterioration. The latter may be used to obtain an "improved" or "updated" mathematical model that better represents the characteristics of the existing structure. The updated model may then be used to assess safety and reliability of the existing structure. Maruyama et al. (1989) have performed system identification of the non-pinching BWBN model using the Extended Kalman Filter algorithm. Loh and Chung (1993) applied a three-stage identification approach for hysteretic systems with non-deteriorating, non-pinching BWBN model. In the first stage, a sequential regression analysis was used to identify whether the structure is in elastic or inelastic response. Either a time domain least-squares or the Gauss-Newton method was used to form a second stage identification. Finally, the Extended Kalman Filtering technique was used to identify the noise-corrupt input-output data. If the same or similar techniques can be successfully applied to the proposed model, hysteresis parameters of

any system configuration and material combination can be systematically estimated as long as hysteresis data are available.

4.4 Nonlinear Time History Analysis

4.4.1 Preliminary Considerations

4.4.1.1 Governing Equations

The complete set of equations that governs the dynamic behavior of a SDF wood system were given in section 4.2.1. The equation of motion and constitutive law are given by Eqs. 4.1 and 4.2, respectively. From Eq. 4.7, the rate of change of the hysteretic energy dissipation may be written as

$$\dot{\varepsilon} = (1 - \alpha)\omega_o^2 z\dot{u} \,. \tag{4.25}$$

All parameters are as previously defined.

4.4.1.2 Overview of Numerical Solution Methods

The governing equations may be solved using any of the available algorithms for nonlinear structural dynamics. Time derivatives are usually approximated by difference equations involving one or more increments of time. (A *differential equation* involves functions and their derivatives defined on some continuous interval, while a *difference equation* involves functions and their differences defined at discrete points.) Discrete systems of difference equations are solved using step by step methods, which may be classified as either *single step* or *multistep* . A single step method requires information about the solution (i.e., displacement, velocity or acceleration) from a single preceding step to obtain the solution at the current point in time. A multistep method requires information from several preceding steps.

If a given step formula expresses the response at time t only in terms of the previously obtained solution at times before t, it is called an *explicit* method. If the response

at time t depends also on the solution at time t, then the method is *implicit.*

When at least two equations, in a set of difference equations, have very different scales of the independent variable on which the dependent variables are changing, the set of equations is said to be *stiff.* This is often encountered in many physically important situations or systems. When this occurs, one is "required to follow the variation in the solution of the shortest length scale to maintain stability of the integration, even though accuracy requirements allow a much larger stepsize" (Press et al. 1992). Special algorithms addressing this issue should be used to solve a stiff set of equations.

Adeli et al. (1978) evaluated several commonly used explicit and implicit numerical integration techniques in nonlinear structural dynamics and compared their accuracy, stability and efficiency as applied to a plane stress problem. They concluded that, among the explicit methods they considered, the central difference predictor is better than the two-cycle iteration with the trapezoidal rule and the fourth-order Runge-Kutta method. Among the implicit methods, the Park stiffly-stable method was rated better than the Newmark-Beta method and Houbolt's procedure. Comparing the Park stiffly-stable method to the central difference method, they found that the Park method is better for elastoplastic analysis, especially when there are geometric nonlinearities. Park's method is based on a class of time integrators originally proposed by Gear (1971).

Several new solution algorithms have been proposed for structural dynamic problems since Adeli et al.'s study. An excellent review of the new methods can be found in Allahabadi (1987). He chose the constant average acceleration (CAA) method, a special case of the Newmark-Beta method, with some enhancements as the solution algorithm for DRAIN-2DX. Detailed properties of the Newmark method, including five other traditional methods for nonlinear dynamic analysis, are given in Barbat and Canet (1989).

4.4.1.3 Solution Approach

Let us consider a vector **y** defined as

$$\mathbf{y} = \begin{Bmatrix} y_1 \\ y_2 \\ y_3 \\ y_4 \end{Bmatrix} = \begin{Bmatrix} u \\ \dot{u} \\ z \\ \varepsilon \end{Bmatrix} \tag{4.26}$$

Then, Eqs. (4.1), (4.2) and (4.25) may be rearranged into a set of 4 first-order nonlinear ordinary differential equations,

$$\dot{y}_1 = y_2 \tag{4.27}$$

$$\dot{y}_2 = -\alpha\omega_o^2 y_1 - 2\xi_o\omega_o y_2 - (1-\alpha)\omega_o^2 y_3 + f(t) \tag{4.28}$$

$$\dot{y}_3 = h(z)\left\{\frac{y_2 - \nu(\beta|y_2||y_3|^{n-1}y_3 - \gamma y_2|y_3|^n)}{\eta}\right\} \tag{4.29}$$

$$\dot{y}_4 = (1-\alpha)\omega_o^2\, y_2 y_3 \tag{4.30}$$

This arrangement results in a stiff set of equations. Thus, a stiffly-stable method, known as Gear's Backward Differentiation Formula (BDF) (Gear 1971; IMSL 1987), was used to solve for **y**. Gear's BDF method is an implicit multistep method. A simple computer program, incorporating the IMSL subroutine for Gear's BDF method, was written to compute the response time histories of SDF wood systems subjected to arbitrary dynamic loading.

4.4.2 Response to General Cyclic Loading

The computer program accepts the following types of loading: (*1*) a single sinusoidal function of the form $f(t) = (a_1 + a_2 t)\sin(\omega t)$, where the a_i's are specified constants, (Fig. 4.6a); (*2*) a series of sinusoidal functions as shown in Fig. 4.6b where $f_i(t) = a_i \sin(\omega_i t)$ for each region, $t_{i-1} < t < t_i$, $i = 1, 2, \ldots, 5$ and where amplitude a_i and frequency ω_i for each region are specified independently; and (*3*) an arbitrary acceleration input such as the ground acceleration record shown in Fig. 4.6c.

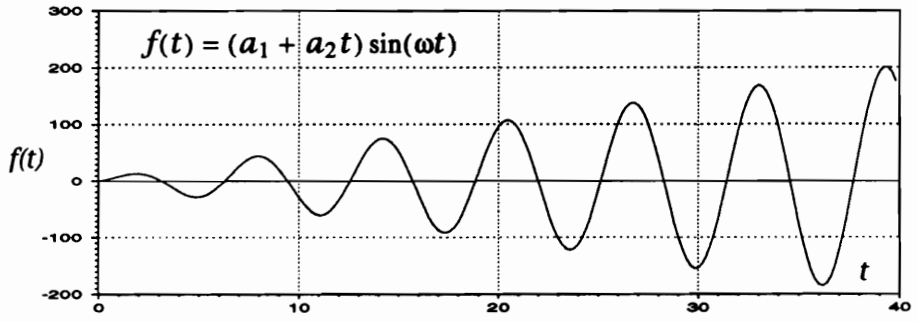

(a) Load type *1* : increasing amplitude sinusoidal load

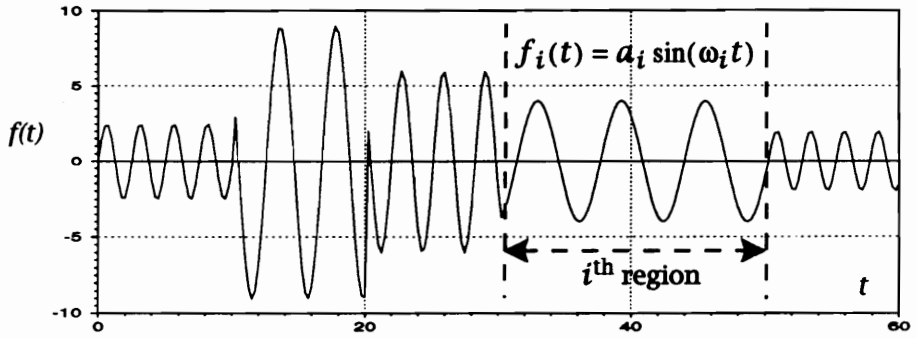

(b) Load type *2* : general cyclic load

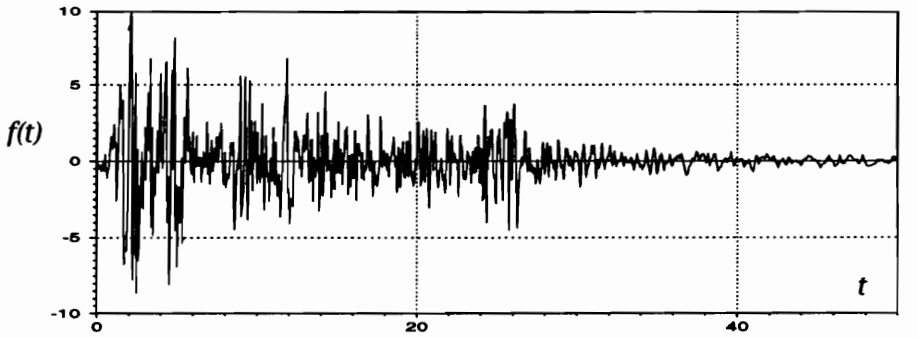

(c) Load type *3* : arbitrary dynamic load

Figure 4.6: Loading types handled by the computer program

Loading types (*1*) and (*2*) are used to verify the program and check the basic capability of the proposed hysteresis model. They are also used to compare model hysteresis with experimental hysteresis (e.g., section 4.3.2). Most available hysteresis data of wood joints and systems have been obtained from static cyclic load tests, where the test specimen is subjected to a predetermined number of displacement controlled loading cycles. The displacement pattern is normally increasing as shown in Fig. 4.7a. Since the experimental hysteresis loops in Fig. 2.5 were obtained in this manner, the hysteretic response of common wood joints in Fig. 4.5 using the proposed model were obtained, using the dynamic analysis program, with input defined by loading type (*1*) shown in Fig. 4.6a.

The use of tests with increasing amplitude pattern alone to model hysteresis behavior of wood systems has been criticized (Moss 1991; Reyer and Oji 1991), however, and a test procedure with increasing-decreasing-increasing loading pattern, producing hysteresis inner loops from the smaller amplitude loading, is currently being proposed in ASTM (Fig. 4.7b). Current hysteresis models proposed for wood, with the exception of that proposed by the UBC researchers shown in Fig. 2.12, did not consider the hysteresis inner loops produced from the smaller amplitude loading cycles. Fig. 4.8 shows that the modified BWBN model produces small hysteresis loops similar to the behavior of dowel-type fasteners, modeled by the UBC model, when subjected to a loading pattern similar to loading type (*2*). The hysteresis plots were obtained with load histories having different combinations of amplitude and frequency for each region as shown in the side plots in Fig. 4.8. The SDF system used in all hysteresis plots has the following properties: ω_o=3.0 rad/s, ξ_o=0.05, α=0.10, β=1.5, $\gamma = -0.5$, n=1, q=0.10, ζ_{1_o}=0.97, λ=0.10, p=1, ψ_o=0.20, δ_ψ=0.002, δ_ν=0.005 and $\delta_\eta = 0.05$.

Including loading type (*2*) as an option for load input in the program, therefore, allowed investigation of model response to general cyclic loading. This will assume greater importance if the ASTM test procedure proposal is passed and adopted. If desired, a specialized loading pattern based on the proposed standard may be added

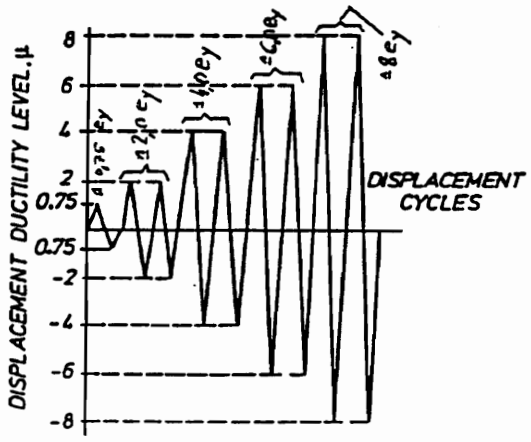

(a) displacement-controlled loading cycles
(increasing amplitude pattern)

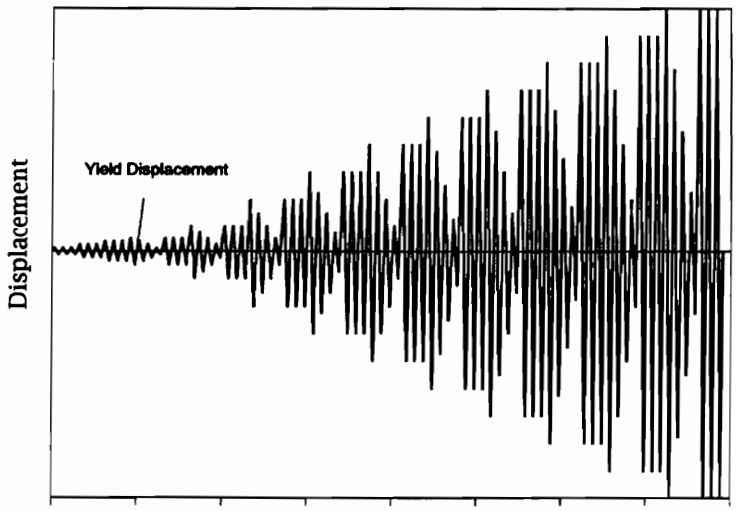

(b) amplitude pattern proposed in ASTM

Figure 4.7: Cyclic loading patterns for tests of wood joints and structural systems

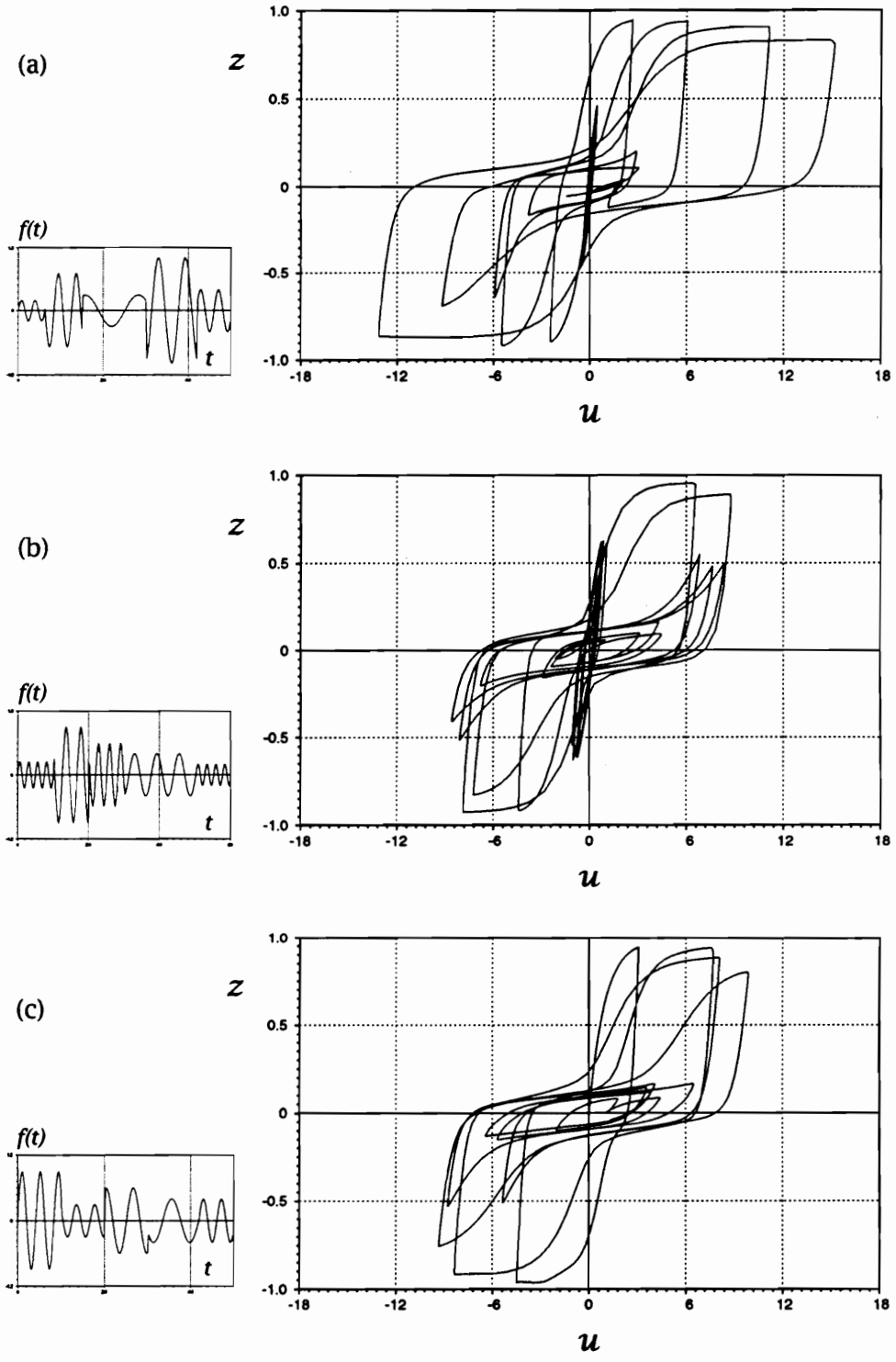

Figure 4.8: Modified BWBN response to general cyclic load

as another load input option to the program.

After the model was verified and validated (in section 4.3.2), loading type (*3*) was added as a load input option. Response of SDF wood systems under a prescribed arbitrary dynamic loading is discussed next.

4.4.3 Response to Seismic Loading

4.4.3.1 Introduction

Since we are primarily interested in the seismic response of wood structures and structural systems, earthquake accelerogram data will be used for $f(t)$ in time history analysis. For illustration purpose, only the Loma Prieta accelerogram record will be used (Fig. 4.9a). It is the ground acceleration record of the earthquake that occurred in the San Francisco Bay Area in California in October 17, 1989. The epicenter of the 7.1 Richter scale earthquake was located at the Loma Prieta peak in the Santa Cruz Mountains, about 60 miles (97 km) southeast of San Francisco. The accelerogram was recorded in Eureka, California and has a peak horizontal acceleration of $0.63g$, where g is the acceleration of gravity. It was estimated that a ground acceleration of about $0.3g$ occurred in the bay mud area (Turner et al. 1990).

The relative velocity and pseudo acceleration spectra of the Loma Prieta earthquake are shown in Figs. 4.9b and c, respectively.

Consider three hypothetical simple wooden buildings in Eureka, CA at the time of the Loma Prieta earthquake. How would they have behaved if the ground where they stand moved horizontally with acceleration shown in Fig. 4.9a?

Modeling the buildings as SDF systems, to simplify the analysis, and using the proposed hysteresis model for wood structures to represent the three buildings, their global response time history (i.e., solution of $\mathbf{y}$ for the entire time duration under consideration) can be computed as described earlier. As an illustration of response computations, no specific units of force, displacement, velocity and energy are considered. Additionally, the hysteresis parameter values used in response computations should

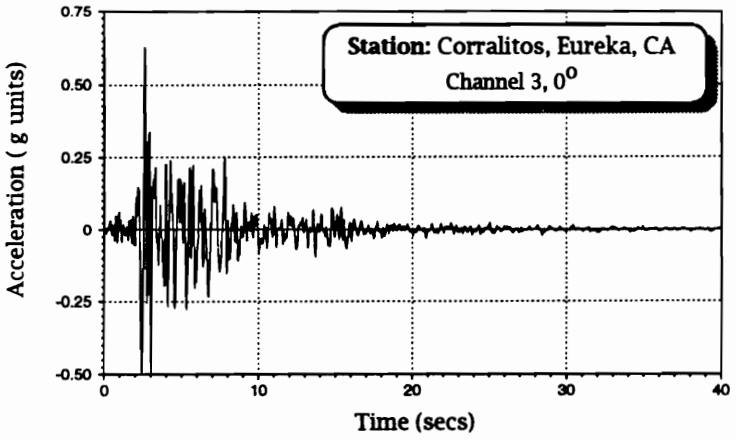

(a) acceleration record

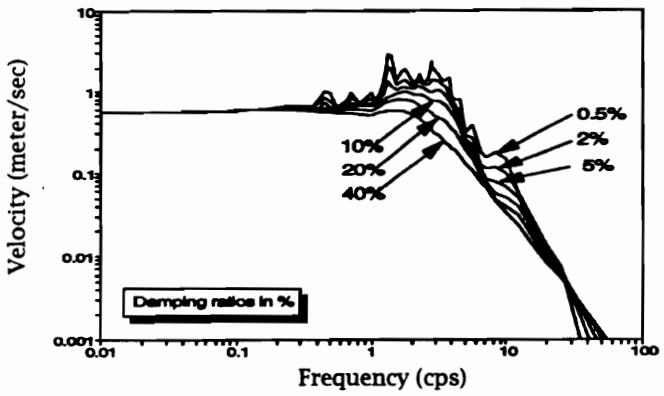

(b) relative velocity spectra

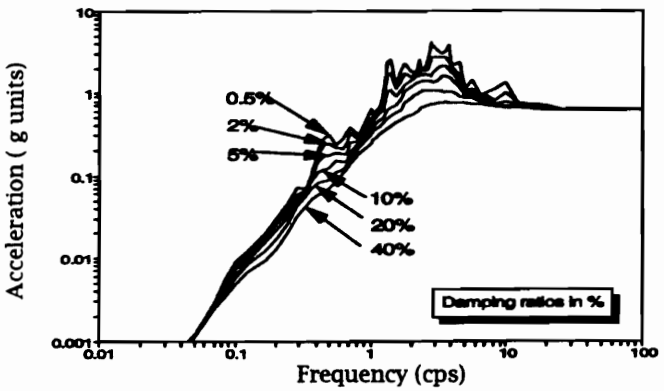

(c) pseudo acceleration spectra

Figure 4.9: The Loma Prieta earthquake ground acceleration

not be viewed as realistic representation of any physical system.

4.4.3.2 Trussed-frame Building

The first building is a trussed-frame structure whose behavior was primarily governed by metal plate connections that have hysteresis behavior given by that in Fig. 4.5a. The SDF system model was assumed to have the following properties (these were taken to be the same as those in section 4.3.2 and Fig. 4.5a): ω_o=9.425 rad/s, ξ_o=0.05, α=0.25; the hysteresis parameters are: β=0.5, γ = 0.5, n=1, q=0, $h(z)$=1.0, δ_ν=0 and δ_η = 0.

The hysteresis response of this trussed-frame building to the Loma Prieta accelerogram is given in Fig. 4.10. Response time histories are shown in Fig. 4.11.

4.4.3.3 Building with Plywood Shear Walls

The other building had plywood shear walls to resist lateral loads. The shear walls governed the building behavior and have hysteresis loops given by that in Fig. 4.5b for nailed sheathing joints. The model parameters for the system are assumed as: ω_o=6.283 rad/s, ξ_o=0.05, α=0.10, β=1.5, γ = −0.5, n=1, q=0.10, ζ_{1_o}=0.97, λ=0.10, p=1, ψ_o=0.20, δ_ψ=0.002, δ_ν=0.005 and δ_η = 0.05.

The building governed by plywood shear walls would respond to the Loma Prieta accelerogram as shown in Figs. 4.12 and 4.13.

4.4.3.4 Heavy Timber Building

The third building is of heavy timber construction. The members are primary held together by bolted joints that behave like the one in Fig. 4.5c. The SDF system properties are assumed as: ω_o=3.0 rad/s, ξ_o=0.05, α=0.35, β=2.0, γ = −1.0, n=1, q=0, ζ_{1_o}=0.98, λ=0.10, p=2.0, ψ_o=0.20, δ_ψ=0.004, δ_ν=0.0 and δ_η = 0.025.

This building would have a hysteretic behavior due to the Loma Prieta accelerogram as shown in Fig. 4.14. The response time histories are shown in Fig. 4.15.

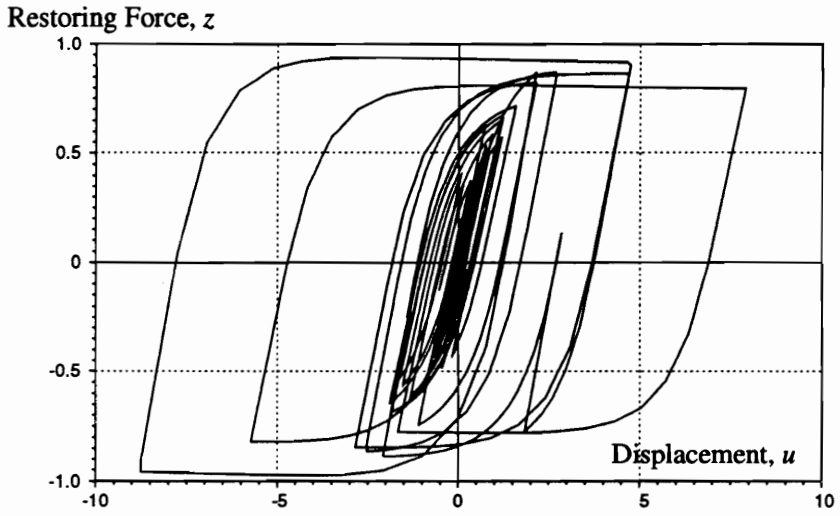

Figure 4.10: Hysteresis response of a trussed-frame building to the Loma Prieta accelerogram

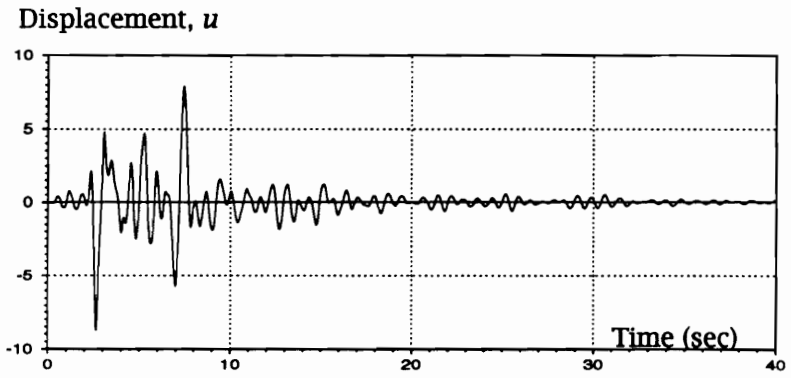

(a) displacement time history

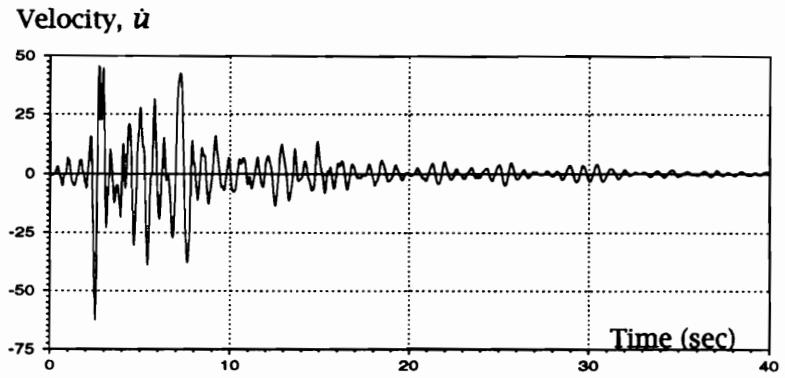

(b) velocity time history

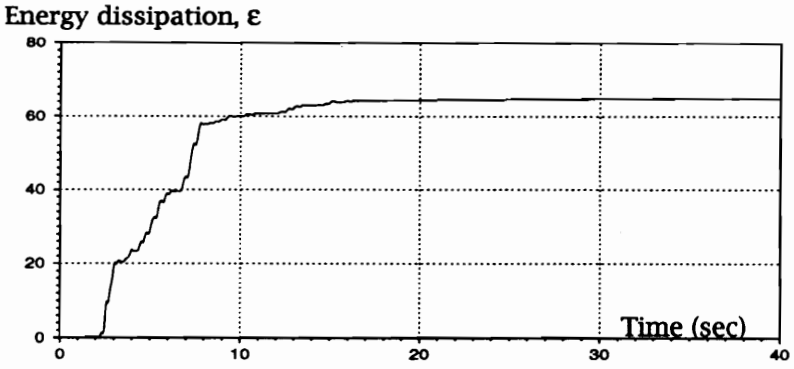

(c) hysteretic energy dissipation time history

Figure 4.11: Response time histories of a trussed-frame building to the Loma Prieta accelerogram

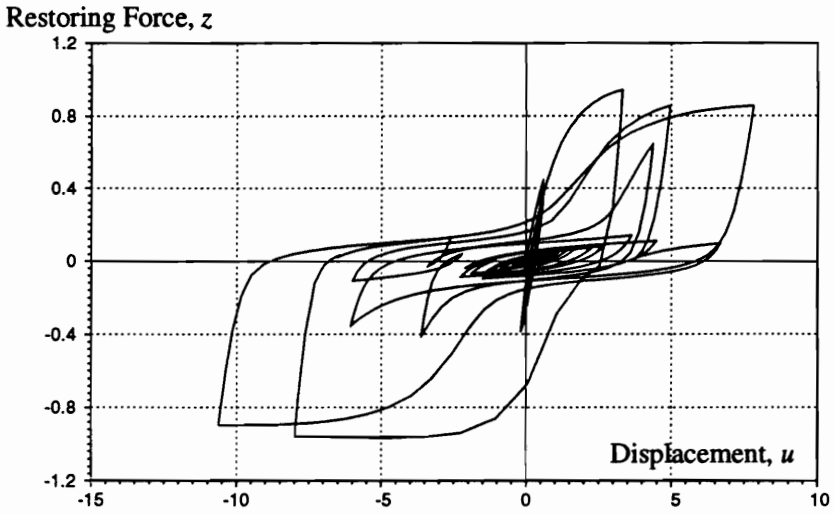

Figure 4.12: Hysteresis response of a building with plywood shear walls to the Loma Prieta accelerogram

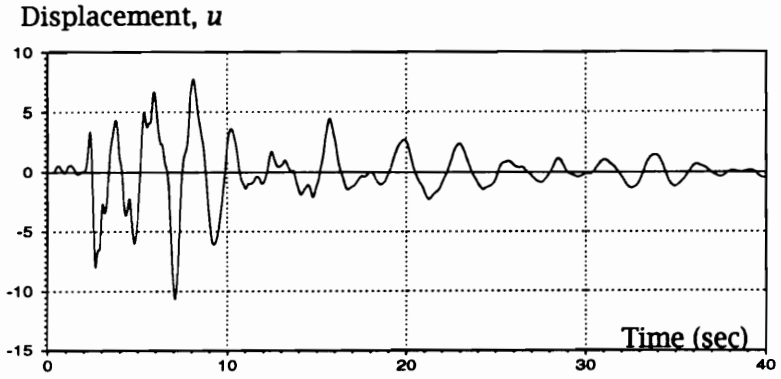

(a) displacement time history

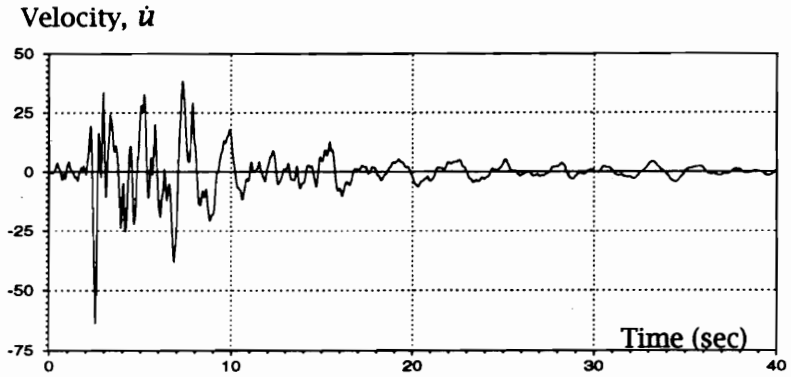

(b) velocity time history

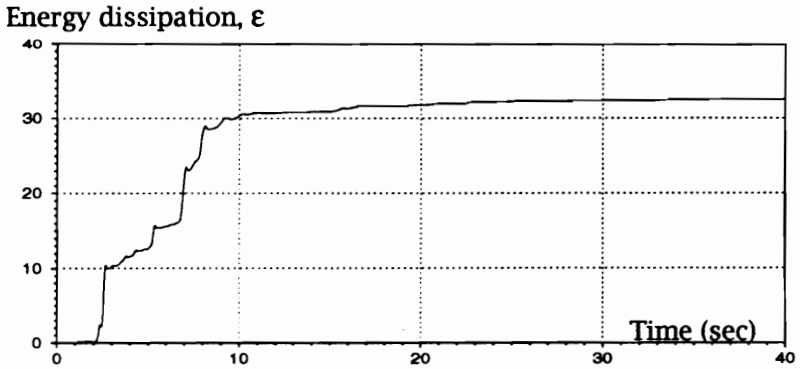

(c) hysteretic energy dissipation time history

Figure 4.13: Response time histories of a building with plywood shear walls to the Loma Prieta accelerogram

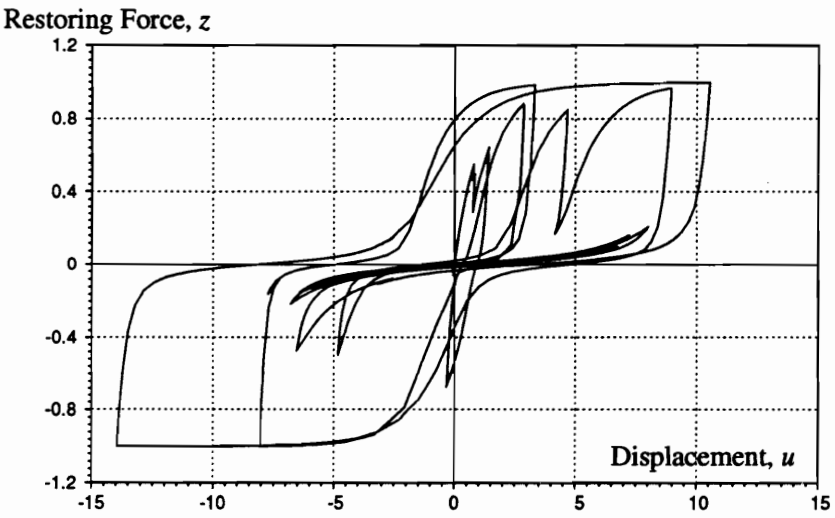

Figure 4.14: Hysteresis response of a heavy timber building to the Loma Prieta accelerogram

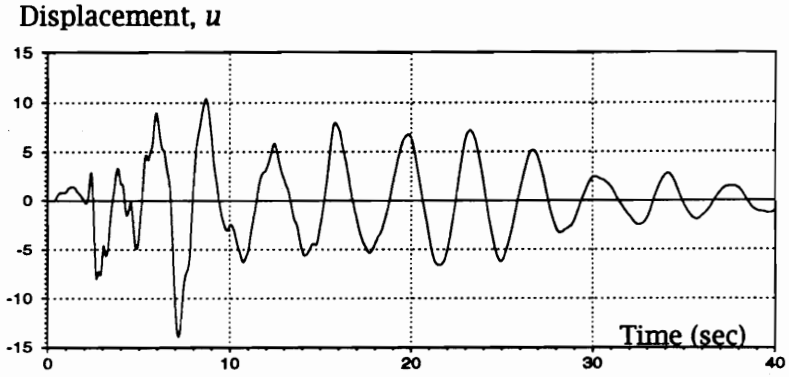

(a) displacement time history

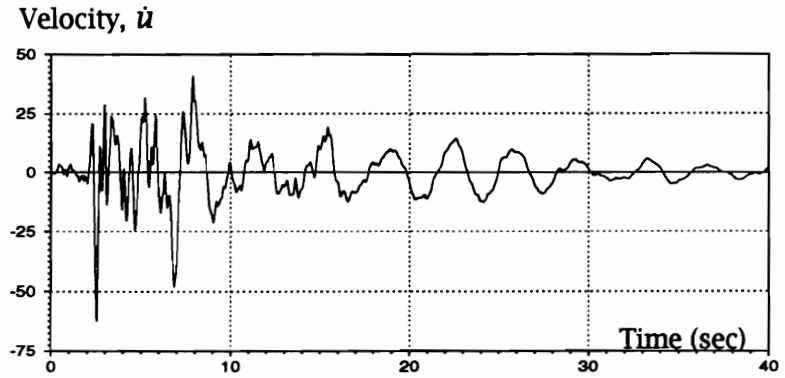

(b) velocity time history

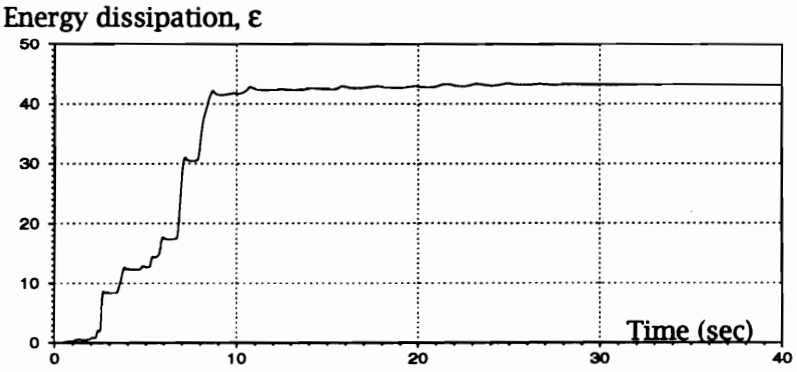

(c) hysteretic energy dissipation time history

Figure 4.15: Response time histories of a heavy timber building to the Loma Prieta accelerogram

4.4.4 Comments

Recall that the purpose of performing time history analyses of the hypothetical wooden buildings is to demonstrate the analytical capability of the proposed modified BWBN model under deterministic or prescribed dynamic loading. If the SDF system properties were obtained from actual tests using an appropriate system identification method, we can comment on seismic performance and safety of these buildings based on the computed response. Key dynamic properties, including ductility, can be obtained from hysteresis plots similar to those shown in Figs. 4.10, 4.12 and 4.14. Various types of sensitivity and parametric studies, like those mentioned by Stalnaker and Gramatikov (1991), can be performed using the model, without the need for additional physical testing. Model parameters that critically affect the ductility, serviceability and safety of the wood structure under study can be identified.

The present analysis has been limited to SDF systems. For a more refined analysis, MDF models can be constructed to represent various types of wood structures and structural systems, where each degree-of-freedom is modeled by the hysteretic behavior of its governing connection. (See section 4.2.2 for the formulation for shear building models.) The proposed hysteresis model can be included as an alternative subroutine to existing nonlinear dynamic analysis programs. It can also be incorporated into finite element models in dynamic analysis.

With currently available hysteresis models for wood joints and structural systems, one subroutine for each connection type, that defines its hysteretic behavior, has to be implemented. Incorporating a new model for a specific connection set-up into a commercial dynamic analysis program, such as DRAIN-2D or its latest version DRAIN-2DX, is a major undertaking (Dowrick 1986). Thus, analytical study of a wood structural system that requires several models of hysteresis behavior is very laborious. Because of the general nature of the proposed model, however, only one subroutine for hysteretic constitutive relations needs to be written for the whole gamut of wood products, fastener types and configurations that are currently used in construction. Only the model

parameters have to be changed for the desired hysteresis shape. Thus, with the proposed general hysteresis model, analytical study of MDF wood structural systems that need to be modeled by several different hysteresis shapes is simplified.

4.5 Summary

The complete form of the modified Bouc-Wen-Baber-Noori (BWBN) model proposed for SDF wood systems was summarized. A model for MDF shear buildings was formulated and alternative models for planar frames were reviewed. The topic of system identification and parameter estimation was introduced. A general set of rules for identifying hysteresis model parameters for wood systems was given. Comparison of model hysteresis with experimental hysteresis showed that the proposed model reasonably mimics the basic hysteresis shape of test data.

The proposed hysteresis model was implemented in a nonlinear dynamic analysis computer program for SDF systems. Incorporation of the model into the program was relatively straightforward. System response from arbitrary dynamic loading, such as cyclic or earthquake-type loadings, can be computed. Three SDF wood systems were subjected to the Loma Prieta accelerogram to obtain their hysteresis loops and response time histories. Advantages of using the proposed model over currently available models in nonlinear dynamic analysis of more complex wood structural systems were identified.

The computer program allows response computations of a wide variety of wood structures and structural systems that can be modeled as SDF systems, as long as hysteresis parameters for these systems are known. The program may be extended to handle dynamic analysis of MDF systems.

Chapter 5

Random Vibration Analysis

5.1 General

There are two different approaches in evaluating structural response to dynamic loads: (*1*) deterministic, and (*2*) non-deterministic or stochastic or random. The type of loading considered in the analysis determines the kind of approach to use. When the loading is assumed as a known function of time (i.e., its time variation is completely known at each time instant, also called deterministic dynamic loading), the method of analysis used to evaluate the response is called *deterministic dynamic analysis.* When the loading is not completely known *a priori* but can be defined in a statistical sense (also called random loading or excitation), the corresponding analysis is defined as *non-deterministic* or *stochastic dynamic analysis.* It is most popularly referred to as *random vibration analysis* in the literature.

The previous chapters were concerned with deterministic analysis. Herein, random vibration analysis of single-degree-of-freedom (SDF) wood structural systems, modeled by the modified Bouc-Wen-Baber-Noori (BWBN) restoring force model, will be presented. The present work will focus on earthquake-type loadings modeled as a random process. The objective of the analysis is to obtain response statistics that can be used in designing structural systems based on accepted levels of safety, measured in terms of probability of failure. Some basic concepts of random vibration analysis related to the present work will be reviewed under appropriate sections.

5.2 Brief Historical Background

Random vibration has become an important subject in the analysis and design of a wide variety of problems encountered in aerospace, mechanical and civil engineering. It involves a combination of concepts found in system dynamics, probability and stochastic processes.

In the mid 1950's, studies on the vibration of aircraft fuselage panels showed that the excitation involved and the corresponding panel response were not repeatable, highly irregular and complex (Roberts and Spanos 1990). Classical methods of dynamic analysis (i.e., deterministic) proved inadequate in evaluating the responses of interest. Advances in high speed flight created similar problems in various aspects of aircraft design and analysis. It had become apparent that a theory capable of analyzing dynamic response due to randomly fluctuating loadings needed to be developed. Fortunately, it was soon discovered that much previous work in statistical communication theory, especially by Rice (1944), could be easily adapted in formulating a response analysis methodology for linear systems under random excitation. Furthermore, a huge body of literature on stochastic processes tracing back to Brownian movement physics (Einstein 1905) already provide a well-established mathematical foundation for its complete development. Random vibration theory was, therefore, "developed through an adaptation of existing knowledge" (Roberts and Spanos 1990). [Vanmarcke (1983) and Roberts and Spanos (1990) provide an excellent historical development of random vibration theory.] Today, it is a rapidly growing branch of engineering mechanics, with applications encompassing a wide variety of engineering disciplines.

5.3 Basic Requirements

Response analysis of nonlinear dynamical systems subjected to stochastic excitations basically involve three elements: *(1)* a mathematical constitutive model that best represents system behavior under loading, *(2)* a stochastic process model that

simulates natural hazard loadings, and *(3)* a solution technique that allows practical estimates of response of the structural system, modeled by *(1)*, subjected to stochastic excitations, modeled by *(2)*. In this section, several stochastic excitation models suggested to simulate seismic ground motion will be briefly introduced and various solution techniques that have been used to solve nonlinear random vibration problems will be presented.

5.3.1 Hysteresis Models

In Chapter 2, hysteresis models used to represent the behavior of various structures, with special emphasis on wood, under cyclic loading were reviewed and discussed. In Chapters 3 and 4, a modification of the hysteresis model based on Bouc (1967), Wen (1976;1980), Baber and Wen (1981) and Baber and Noori (1986), and referred to as the modified Bouc-Wen-Baber-Noori (BWBN) model, was proposed for dynamic analysis of wood structures. The same model for SDF systems, summarized in section 4.2.1 [Eqs. (4.1) to (4.7)], will now be used in random vibration analysis. The parent forms of the modified BWBN model have been successfully used in random vibration analysis using statistical linearization (Wen 1980; Baber and Wen 1981; Baber and Noori 1986). Because of their versatility and stability in obtaining convergence, the non-degrading and non-pinching models have been extensively used in random vibration analysis of a wide variety of engineering problems [e.g., dynamic analyses of concrete and steel structures (Sues et al. 1988), liquefaction of sand deposits under earthquake loadings (Pires et al. 1983), base isolated structures with hysteretic dampers (Constantinou and Tadjbakhsh 1985), hysteretic systems under bidirectional ground motions (Park et al. 1985), seismic damage in unreinforced masonry buildings (Kwok 1987) and dynamic analysis of large structural systems (Casciati 1987), among others].

While the special form of the differential equation that represents the constitutive relations in the modified BWBN model makes it especially suited in random vibration analysis using statistical linearization, any nonlinear relations as used in deterministic

analysis (like those reviewed in section 2.4) and verified by experiments can also be used in random vibration analysis, as shown by Pradlwarter and Schuëller (1992). They have presented a general statitistical linearization approach to obtain the response statistics of nonlinear multi-degree-of-freedom (MDF) systems.

5.3.2 Stochastic Models of Ground Motion

Earthquake ground motions are generated through numerous random phenomena and are essentially random in nature. Thus, they may be modeled as random processes. A random process is a parametered random variable. A random process, say $X(t)$, represents an infinite set of possible time functions, none of which are exactly alike. A particular realization (or time history) of this process is a *sample* function of the underlying random process; an *ensemble* of the process is a collection or family of such sample functions (Ang 1974) as shown in Figure (5.1).

A random process is normally described by its probabilistic nature which is normally limited to the "two point" probability law, i.e. probabilistic information based on a pair of random variables $X(t_1)$ and $X(t_2)$ at any two time instants t_1 and t_2. These descriptors are further limited to the *mean value function* $\mu_X(t) = E[X(t)]$ and the *autocorrelation function* $R_{XX}(t_1, t_2) = E[X(t_1)X(t_2)]$, where $E[.]$ is the expected value. A *stationary* random process has an autocorrelation function that depends only on time lag $\tau = t_2 - t_1$ and not on actual time instants t_1 and t_2. Its mean remains constant with time.

For a stationary Gaussian random process, the mean value and autocorrelation functions are sufficient to completely describe the process. Since earthquake motions are usually assumed as a zero mean Gaussian process, the information about the autocorrelation function is adequate. In seismic analysis, the use of the *Power Spectral Density* (PSD) function, a representation of the same random process in the frequency domain, rather than the autocorrelation function is preferred. PSD function, $\Phi_X(\omega)$,

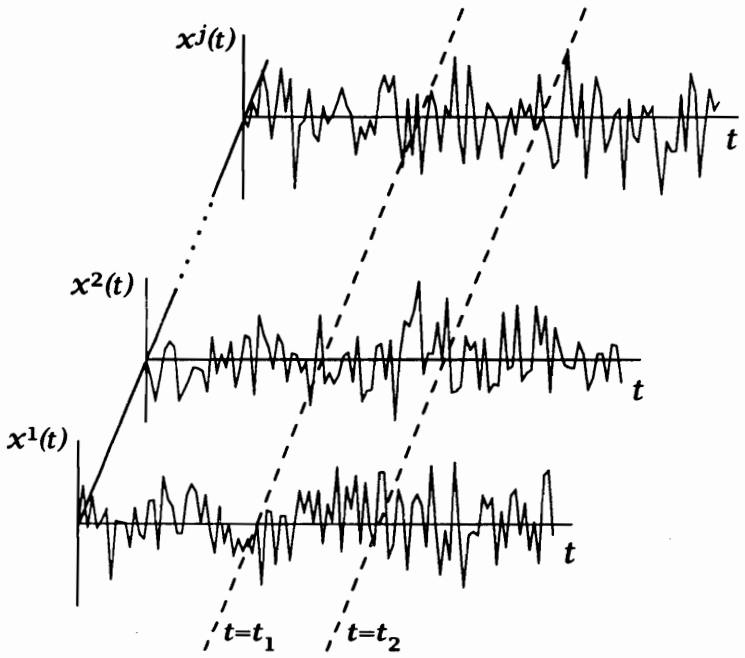

Figure 5.1: Ensemble of a random process, $X(t)$

and autocorrelation function, $R_{XX}(\tau)$, are Fourier transform pairs:

$$\begin{aligned} R_{XX}(\tau) &= \int_{-\infty}^{\infty} \Phi_X(\omega)\, e^{i\omega\tau}\, d\omega \\ \Phi_X(\omega) &= \frac{1}{2\pi}\int_{-\infty}^{\infty} R_{XX}(\tau)\, e^{-i\omega\tau}\, d\tau \end{aligned} \tag{5.1}$$

where ω is the frequency of the random process $X(t)$ (here, the seismic ground motion).

For simplicity, a stationary Gaussian process, with PSD and autocorrelation functions shown in Figure 5.2, will be used to model seismic ground motions. This is also known as *white noise*, and has the following characteristics:

$$\begin{aligned} \Phi_X(\omega) &= S_o \\ R_{XX}(\tau) &= 2\pi S_o \delta(\tau) \end{aligned} \tag{5.2}$$

where δ is the Dirac delta function, giving a sharp impulse at $\tau = 0$, as shown in Figure 5.2b. Although actual earthquakes are nonstationary and do not have a flat power spectrum, it may be satisfactory for wide band excitation (i.e., when the excitation spectrum varies slowly in the vicinity of the structures's natural frequency). Filtering and modulation of the input excitation can be easily incorporated in the model [e.g., Baber (1980) and Baber and Wen (1981)].

The most common filter transfer function for stationary filtered white noise excitation is that proposed by Kanai (1957) and Tajimi (1960). Application of this filter gives the following Kanai-Tajimi power spectral density:

$$\Phi(\omega) = S_o \frac{1 + \left[2\xi_g \frac{\omega}{\omega_g}\right]^2}{\left[1 - \left(\frac{\omega}{\omega_g}\right)^2\right]^2 + \left[2\xi_g \frac{\omega}{\omega_g}\right]^2} \tag{5.3}$$

where ω_g and ξ_g are the dominant frequency and damping, respectively, of the ground through which the seismic wave propagates. This gives a better approximation of the spectral power distributions in actual earthquakes. To obtain a nonstationary filtered white noise random process, the stationary filtered white noise may be multiplied by a specified time varying function [e.g., Amin and Ang (1968), Shinozuka and Sato (1967), among others].

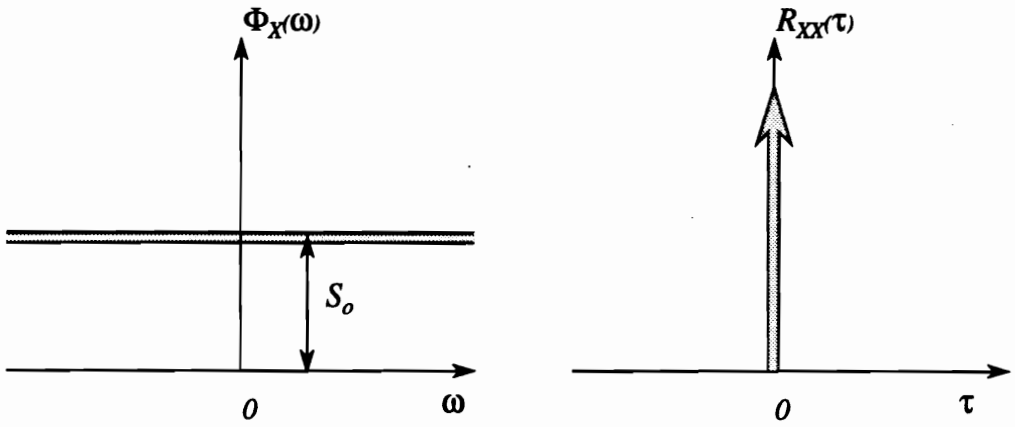

a) Power Spectral Density (PSD) function

b) Autocorrelation function

Figure 5.2: Probabilistic description of a Gaussian white noise

A number of other stochastic models for artificial ground acceleration has been developed and successfully applied to a variety of structural dynamics problems. Noori (1984), Shinozuka and Deodatis (1988) and Kozin (1988) provide extensive reviews of currently available models, including those based on: *(1)* filtered white noise processes, *(2)* filtered Poisson processes, *(3)* spectral representation of stochastic processes, *(4)* stochastic wave theory, and *(5)* auto-regressive moving average (ARMA) models. Shinozuka and Deodatis (1988) provided the mathematical expressions for the first four models along with comments on their usefulness, advantages and disadvantages while Kozin (1988) discussed the features and current developments in ARMA model procedures for earthquake engineering applications.

5.3.3 Methods for Nonlinear Random Vibrations

An analytical solution of differential equations, representing nonlinear dynamic systems, is difficult. The powerful methods of linear system theory, such as the normal mode approach and the convolution integral, cannot be applied because the principle of superposition does not apply to nonlinear problems (Nigam 1983). Hysteretic sysytems, which have multivalued functions in the equations of motion, make an exact solution even more difficult to obtain. Thus, many researchers used either solution methods specific to the particular problem or approximate solutions. Methods of analysis fall into the following broad categories (Branstetter et. al. 1988; Roberts and Spanos 1990):

1. *Markov methods*- These are based on the theory of continuous Markov processes, also known as "diffusion processes". Either the Fokker-Planck-Kolmogorov (FPK) equation or Ito's stochastic differential equation is used to obtain the exact solution. An approximate analytical technique, called "stochastic averaging", has been used for lightly damped oscillators with wide-band random excitation. In this method, the governing FPK equations for two-dimensional Markov process is reduced to a one-dimensional Markov process. Other approximate solutions

of the FPK equation have been used [see Nigam (1983)]. Solutions based on this method, however, are limited by the requirement that actual excitation be assumed as white noise or filtered white noise [see Roberts (1981a), for a detailed review].

2. *Perturbation and functional series methods*- Both methods are valid only if the system nonlinearities are small (Roberts 1981b). The basic idea in the perturbation approach is to solve differental equations that contain a small paramater, say ϵ, by considering an approximate solution expressed as a power series in this parameter. The first term in the expansion is the linear response (i.e., response when all the system nonlinearities are removed). The subsequent terms express the influence of nonlinearity (Roberts and Spanos 1990).

   Functional series methods, on the other hand, are based on either the generalization of the convolution integral, known as the Voltera series expression (Roberts 1981b) or expansions based on the Wiener-Hermite procedure (Orabi and Ahmadi 1987).

3. *Moment closure*- From the equations of motion, equations for the moments of the response such as the mean and mean square are derived. Then estimates of the probability distribution of the response are obtained by using a variety of analytical expansions of the Gaussian distribution. With nonlinear systems, a "closure approximation" is used to replace a hierarchy of coupled equations to obtain a soluble set of equations.

4. *Statistical linearization*- This is also known as "equivalent linearization" or "stochastic linearization". The basic idea is to replace the governing set of nonlinear equations by an equivalent set of linear equations, minimizing the difference between the sets in a statistical sense. This may be based on either stochastic averaging of slowly varying response parameters (Caughey 1971) or a single-valued first order differential representation of hysteretic restoring force, by adding to the size of

the response-measures state vector [e.g., Wen (1980) and Baber and Wen (1981)]. A new extension to this approach, called *statistical quadratization*, has been proposed (Donley and Spanos 1990). In this approach, the nonlinearity is replaced with equivalent polynomials up to quadratic order and then solved by the Volterra series method.

5. *Equivalent nonlinear equations*- A generalization of the basic statistical linearization concept has been proposed by Caughey (1986). The original set of nonlinear equations is replaced by an equivalent set of nonlinear equations that belong to a class of problems which can be solved exactly. The application of this method, however, is very limited at present.

6. *Simulation methods*- Sample functions of the excitation process are digitally simulated, then sample functions of the response are computed using the excitation samples. Simulation methods can be applied to the response and performance analyses of any systems subjected to random excitations, as long as computer algorithms to obtain the response to deterministic excitations are available. The most common type is the Monte Carlo simulation (MCS). Since each individual computation is deterministic, a large number of calculations are performed to infer about response statistics.

Other methods, e.g., associate linear system approach (Bhartia and Vanmarcke 1991), decomposition method of Adomian (Branstetter et al. 1988), etc., have been proposed, but the statistical linearization technique is "the one that has been most extensively used and is probably the most useful from an engineering point of view" (Roberts 1981b). This technique gives reasonably good results for even strongly nonlinear systems, be it of the geometric or material source, and is easily extended into the analysis of MDF systems (Wen 1988; Spanos and Lutes 1986). These make statistical linearization the clear choice over other approximate methods, discussed above, in random vibration analysis of complex MDF systems. The other methods tend to involve

severe analytical difficulty and/or excessive computational requirements in dealing with these types of problem.

Thus, the statistical linearization method will be used to solve a SDF hysteretic wood system, modeled by the modified BWBN model, subjected to a Gaussian white noise excitation. The approximate solution will be verified with MCS results as benchmark.

5.4 Statistical Linearization

5.4.1 Role of Statistical Linearization

Roberts and Spanos (1990) wrote,

> In designing structures and machines to withstand complex environmental loads there are usually two basic stages. In the first, a systematic study is undertaken of the influence of various disposable system parameters on the overall level of response. For example, one is often interested in how a variety of possible structural modifications can affect the system's response level. On the basis of such a study an optimization of the system, with regard to certain parameters, is often the ultimate objective. For this purpose a detailed knowledge of the probability distribution of the response is not required. It is sufficient to use simple response level indices, such as the mean and mean-square characteristics of the response. In the second stage, once an optimal design configuration for the system has been established, a reliability study is carried out in which statistics relating to the system's safety are estimated, for a class of random excitations which are likely to be encountered during the system's lifetime.

What makes statistical linearization a very versatile and flexible method is the fact that estimates of the first and second moments of the response (e.g., mean, mean square and power spectrum) are easily obtained, even for highly nonlinear, complex MDF systems under nonstationary random excitations. Thus, it is *highly suited* in the

first phase of design, as discussed above . Since a detailed knowledge of the probability of response is not required at this stage, the inherent assumption of Gaussian response in this technique does not influence the choice of an optimum system. For this same reason, however, statistical linearization is *not ideal* in the second design stage, where knowledge of the precise shape of the probablity distribution of the response in its extreme "tails" is required. In most cases, MCS is the only available recourse to obtain reliable estimates of the system's safety. In estimating nonstationary response statistics, five hundred response samples are normally required (Spanos 1980). For typical engineering applications involving SDF systems, Spanos (1981) has estimated that the computational efficiency of the statistical linearization method is of the order of one hundred (10^2) to one thousand (10^3) times greater than that of the approach based on MCS. The significance of the computational superiority of statistical linearization increases with (*1*) increasing number of response samples generated for the Monte Carlo study, (*2*) decreasing values of the damping, and (*3*) increasing dimension of the structural system.

Thus, successful application of the statistical linearization method in the initial design stage could save a substantial amount of time, money and effort. This is one of the main reasons for its popularity among designers of complex, critical systems.

5.4.2 General Procedure

Wen (1988) reviewed the theoretical background and applications of the statistical linearization technique in earthquake engineering, especially to inelastic and hysteretic systems. Roberts and Spanos's (1990) book provides an excellent and very comprehensive discussion of the method. Before we proceed in the linearization of the modified BWBN model, a brief overview of the general procedure is given first.

The equation of motion of a general SDF nonlinear system may be written as

$$g(\ddot{x}, \dot{x}, x) = f(t) \tag{5.4}$$

where x is the system displacement response, $g(\cdot)$ represents the total internal force

acting on the system and $f(t)$ is a zero-mean Gaussian white noise.

Equation (5.4) is replaced by an equivalent linear system with the following equation of motion

$$m\ddot{x} + c\dot{x} + kx = f(t) \tag{5.5}$$

where m, c and k are determined by the requirement that the mean square error $E[e^2]$ is minimized, where

$$e = g(\ddot{x}, \dot{x}, x) - (m\ddot{x} + c\dot{x} + kx) \ . \tag{5.6}$$

This error is a random process. If the mean square error is minimized, we obtain

$$\begin{aligned} \frac{\partial}{\partial m} E[e^2] &= 0 \\ \frac{\partial}{\partial c} E[e^2] &= 0 \\ \frac{\partial}{\partial k} E[e^2] &= 0 \ . \end{aligned} \tag{5.7}$$

By substituting Eq. (5.6) into Eq. (5.7), the coefficients of the equivalent linear system can be solved. Since m, c and k are functions of the response statistics, an iterative procedure is generally required to solve Eq. (5.5). The iterative process is repeated until a desired convergence is achieved.

5.4.3 Linearization of the Modified BWBN Model

Consider the SDF model, with the modified BWBN restoring force model, in section 4.2.1, Eqs. (4.1) to (4.7). Only Eq. (4.2), representing the constitutive relations, needs to be linearized. First, let us introduce a vector $\mathbf{y}$ defined as

$$\mathbf{y} = \begin{Bmatrix} y_1 \\ y_2 \\ y_3 \end{Bmatrix} = \begin{Bmatrix} u \\ \dot{u} \\ z \end{Bmatrix} \ . \tag{5.8}$$

Then, the governing equations, (4.1) and (4.2), may be rearranged in the form $\dot{\mathbf{y}} = g(\mathbf{y}) + \mathbf{f}$, where

$$\dot{y}_1 = y_2 \tag{5.9}$$

$$\dot{y}_2 = -\alpha\omega_o^2 y_1 - 2\xi_o\omega_o y_2 - (1-\alpha)\omega_o^2 y_3 + f(t) \tag{5.10}$$

$$\dot{y}_3 = \left\{1.0 - \zeta_1\, e^{[-(z\,\mathrm{sgn}(\dot{u})-qz_u)^2/\zeta_2^2]}\right\} \times \left\{\frac{y_2 - \nu(\beta|y_2||y_3|^{n-1}y_3 - \gamma y_2|y_3|^n)}{\eta}\right\} . \tag{5.11}$$

Equation (5.11) may be replaced by the linearized form,

$$\dot{y}_3 = C_{e3}\, y_2 + K_{e3}\, y_3 \tag{5.12}$$

where the coefficients C_{e3} and K_{e3} are obtained such that the mean square error $E[e^2]$ is minimized, where

$$e = g_3(y_2, y_3) - C_{e3}\, y_2 - K_{e3}\, y_3 \tag{5.13}$$

and $g_3(y_2, y_3)$, or $g_3(\mathbf{y})$, is the right-hand side of Eq. (5.11). Assuming that responses y_2 and y_3 are jointly Gaussian, Atalik and Utku (1976) have shown that the linearization coefficients may be obtained as

$$C_{e3} = E\left[\frac{\partial g_3(\mathbf{y})}{\partial y_2}\right] \qquad K_{e3} = E\left[\frac{\partial g_3(\mathbf{y})}{\partial y_3}\right] \tag{5.14}$$

where $E[\cdot]$ is the expected value. (See Appendix A for details.) Thus,

$$C_{e3} = E\left[\frac{\partial}{\partial y_2}\left\{\left[1.0 - \zeta_1\, e^{[-(z\,\mathrm{sgn}(\dot{u})-qz_u)^2/\zeta_2^2]}\right] \times \left[\frac{y_2 - \nu(\beta|y_2||y_3|^{n-1}y_3 - \gamma y_2|y_3|^n)}{\eta}\right]\right\}\right] \tag{5.15}$$

$$K_{e3} = E\left[\frac{\partial}{\partial y_3}\left\{\left[1.0 - \zeta_1\, e^{[-(z\,\mathrm{sgn}(\dot{u})-qz_u)^2/\zeta_2^2]}\right] \times \left[\frac{y_2 - \nu(\beta|y_2||y_3|^{n-1}y_3 - \gamma y_2|y_3|^n)}{\eta}\right]\right\}\right] . \tag{5.16}$$

Since the degradation and pinching parameters ν, η, ζ_1 and ζ_2 are functions of y_2 and y_3 [Eqs. (4.4) to (4.7)], exact evaluation of the expected values is extremely difficult. Realizing, however, that these parameters are slowly varying, it can be assumed that partial derivatives involving ν, η, ζ_1 and ζ_2 in Eqs. (5.15) and (5.16) may be neglected

and, by first order approximation, the parameters may be replaced by μ_ν, μ_η, μ_{ζ_1} and μ_{ζ_2}, respectively, where

$$\begin{aligned} \mu_\nu &= 1.0 + \delta_\nu \mu_\varepsilon \\ \mu_\eta &= 1.0 + \delta_\eta \mu_\varepsilon \\ \mu_{\zeta_1} &= \zeta_{1_o} [1.0 - e^{(-p\mu_\varepsilon)}] \\ \mu_{\zeta_2} &= (\psi_o + \delta_\psi \mu_\varepsilon)(\lambda + \mu_{\zeta_1}) \end{aligned} \tag{5.17}$$

and

$$\mu_\varepsilon = (1 - \alpha)\omega_o^2 \int_{t_o}^{t_f} E[y_2 y_3]\, dt\,. \tag{5.18}$$

Then, partial differentiation of Eqs. (5.15) and (5.16) yields

$$C_{e3} = \frac{1}{\mu_\eta} - \frac{\mu_\nu}{\mu_\eta}(\beta C_1 + \gamma C_2) - \frac{\mu_{\zeta_1}}{\mu_\eta} C_3 + \frac{\mu_{\zeta_1}\mu_\nu}{\mu_\eta}(\beta C_4 + \gamma C_5) \tag{5.19}$$

and

$$\begin{aligned} K_{e3} &= -\frac{\mu_\nu}{\mu_\eta}(\beta K_1 + \gamma K_2) + 2\frac{\mu_{\zeta_1}}{\mu_\eta \mu_{\zeta_2}^2}(K_3 - q z_u K_4) \\ &\quad + \frac{\mu_{\zeta_1}\mu_\nu}{\mu_\eta \mu_{\zeta_2}^2} 2 q z_u (\beta K_5 + \gamma K_6) - 2\frac{\mu_{\zeta_1}\mu_\nu}{\mu_\eta \mu_{\zeta_2}^2}(\beta K_7 + \gamma K_8) \\ &\quad + n\frac{\mu_{\zeta_1}\mu_\nu}{\mu_\eta}(\beta K_9 + \gamma K_{10}) \end{aligned} \tag{5.20}$$

where

$$C_1 = E[\mathrm{sgn}(y_2)|y_3|^{n-1} y_3] \tag{5.21}$$

$$C_2 = E[|y_3|^n] \tag{5.22}$$

$$C_3 = E[e^{-(y_3 \mathrm{sgn}(y_2) - q z_u)^2/\zeta_2^2}] \tag{5.23}$$

$$C_4 = E[\mathrm{sgn}(y_2)|y_3|^{n-1} y_3\ e^{-(y_3 \mathrm{sgn}(y_2) - q z_u)^2/\zeta_2^2}] \tag{5.24}$$

$$C_5 = E[|y_3|^n\ e^{-(y_3 \mathrm{sgn}(y_2) - q z_u)^2/\zeta_2^2}] \tag{5.25}$$

$$K_1 = E[n|y_2||y_3|^{n-1}] \tag{5.26}$$

$$K_2 = E[n y_2 |y_3|^{n-2} y_3] \tag{5.27}$$

$$K_3 = E[y_2 y_3\ e^{-(y_3 \mathrm{sgn}(y_2) - q z_u)^2/\zeta_2^2}] \tag{5.28}$$

$$K_4 = E[|y_2| e^{-(y_3 \mathrm{sgn}(y_2) - q z_u)^2/\zeta_2^2}] \tag{5.29}$$

$$K_5 = E[y_2 |y_3|^{n-1} y_3 \; e^{-(y_3 \mathrm{sgn}(y_2) - q z_u)^2/\zeta_2^2}] \tag{5.30}$$

$$K_6 = E[|y_2| |y_3|^n \; e^{-(y_3 \mathrm{sgn}(y_2) - q z_u)^2/\zeta_2^2}] \tag{5.31}$$

$$K_7 = E[|y_2| |y_3|^{n-1} y_3^2 \; e^{-(y_3 \mathrm{sgn}(y_2) - q z_u)^2/\zeta_2^2}] \tag{5.32}$$

$$K_8 = E[y_2 |y_3|^n y_3 \; e^{-(y_3 \mathrm{sgn}(y_2) - q z_u)^2/\zeta_2^2}] \tag{5.33}$$

$$K_9 = E[|y_2| |y_3|^{n-1} \; e^{-(y_3 \mathrm{sgn}(y_2) - q z_u)^2/\zeta_2^2}] \tag{5.34}$$

$$K_{10} = E[y_2 |y_3|^{n-2} y_3 \; e^{-(y_3 \mathrm{sgn}(y_2) - q z_u)^2/\zeta_2^2}] \; . \tag{5.35}$$

The foregoing expectations are solved by substituting the zero-mean joint Gaussian probability density function for y_2 and y_3, given by

$$f_{Y_2 Y_3}(y_2, y_3) = \frac{1}{2\pi \sigma_2 \sigma_3 \sqrt{1 - \rho_{23}^2}} \exp\left\{ -\frac{1}{2(1 - \rho_{23}^2)} \left[\frac{y_2^2}{\sigma_2^2} - 2\rho_{23} \frac{y_2}{\sigma_2} \frac{y_3}{\sigma_3} + \frac{y_3^2}{\sigma_3^2} \right] \right\} \tag{5.36}$$

(where σ_2 and σ_3 are the respective root mean square values of y_2 and y_3, and ρ_{23} is their correlation coefficient) into the following definition of the expected value of a function $h(y_2, y_3)$:

$$E[h(y_2, y_3)] = \int_{-\infty}^{\infty} \int_{-\infty}^{\infty} h(y_2, y_3) \, f_{Y_2 Y_3}(y_2, y_3) \, dy_2 dy_3 \; . \tag{5.37}$$

The resulting integrals are then evaluated to obtain

$$C_1 = \frac{1}{\pi} (2)^{n/2} \; \sigma_3^n \; \Gamma\left(\frac{n+2}{2} \right) I_{sn} \tag{5.38}$$

$$C_2 = \frac{1}{\sqrt{\pi}} (2)^{n/2} \; \sigma_3^n \; \Gamma\left(\frac{n+1}{2} \right) \tag{5.39}$$

$$C_3 = \frac{\mu_{\zeta_2}}{\sqrt{2\sigma_3^2 + \mu_{\zeta_2}^2}} \, e^{-\Delta_1} \, \mathrm{erfc}\left(\frac{-\Delta_3}{\sqrt{2}} \right) \tag{5.40}$$

$$C_4 = \frac{1}{\sqrt{2\pi} \, \sigma_3} \, e^{-\Delta_1} \, [I_{GL}(1, n) - I_{GL}(-1, n)] \tag{5.41}$$

$$C_5 = \frac{1}{\sqrt{2\pi} \, \sigma_3} \, e^{-\Delta_1} \, [I_{GL}(1, n) + I_{GL}(-1, n)] \tag{5.42}$$

$$K_1 = \frac{n}{\pi} (2)^{n/2} \; \sigma_2 \sigma_3^{n-1} \; \Gamma\left(\frac{n+2}{2} \right) \left[\frac{2}{n} (1 - \rho_{23}^2)^{(n+1)/2} + \rho_{23} \, I_{sn} \right] \tag{5.43}$$

$$K_2 = \frac{n}{\sqrt{\pi}} (2)^{n/2} \; \rho_{23} \sigma_2 \sigma_3^{n-1} \; \Gamma\left(\frac{n+1}{2} \right) \tag{5.44}$$

$$K_3 = \frac{\mu_{\zeta_2}}{\sqrt{2\sigma_3^2 + \mu_{\zeta_2}^2}} \frac{\sigma_2}{\sigma_3} e^{-\Delta_1} \times \left[\rho_{23}(\mu_{1*}^2 + \sigma_{1*}^2)\text{erfc}\left(\frac{-\Delta_3}{\sqrt{2}}\right) + \sqrt{\frac{2}{\pi}}\mu_{1*}\Delta_2 e^{-\Delta_3^2/2} \right] \quad (5.45)$$

$$K_4 = \frac{\mu_{\zeta_2}}{\sqrt{2\sigma_3^2 + \mu_{\zeta_2}^2}} \frac{\sigma_2}{\sigma_3} e^{-\Delta_1} \times \left[\rho_{23}\mu_{1*}\,\text{erfc}\left(\frac{-\Delta_3}{\sqrt{2}}\right) + \sqrt{\frac{2}{\pi}}\Delta_2 e^{-\Delta_3^2/2} \right] \quad (5.46)$$

$$K_5 = \frac{1}{\pi}\frac{\sigma_2}{\sigma_3} e^{-\Delta_1} \left\{ \sqrt{1-\rho_{23}^2}\,[I_{sum}(1,n) - I_{sum}(-1,n)] + \sqrt{\frac{\pi}{2}}\frac{\rho_{23}}{\sigma_3}[I_{GL}(1,n+1) + I_{GL}(-1,n+1)] \right\} \quad (5.47)$$

$$K_6 = \frac{1}{\pi}\frac{\sigma_2}{\sigma_3} e^{-\Delta_1} \left\{ \sqrt{1-\rho_{23}^2}\,[I_{sum}(1,n) + I_{sum}(-1,n)] + \sqrt{\frac{\pi}{2}}\frac{\rho_{23}}{\sigma_3}[I_{GL}(1,n+1) - I_{GL}(-1,n+1)] \right\} \quad (5.48)$$

$$K_7 = \frac{1}{\pi}\frac{\sigma_2}{\sigma_3} e^{-\Delta_1} \left\{ \sqrt{1-\rho_{23}^2}\,[I_{sum}(1,n+1) + I_{sum}(-1,n+1)] + \sqrt{\frac{\pi}{2}}\frac{\rho_{23}}{\sigma_3}[I_{GL}(1,n+2) - I_{GL}(-1,n+2)] \right\} \quad (5.49)$$

$$K_8 = \frac{1}{\pi}\frac{\sigma_2}{\sigma_3} e^{-\Delta_1} \left\{ \sqrt{1-\rho_{23}^2}\,[I_{sum}(1,n+1) - I_{sum}(-1,n+1)] + \sqrt{\frac{\pi}{2}}\frac{\rho_{23}}{\sigma_3}[I_{GL}(1,n+2) + I_{GL}(-1,n+2)] \right\} \quad (5.50)$$

$$K_9 = \frac{1}{\pi}\frac{\sigma_2}{\sigma_3} e^{-\Delta_1} \left\{ \sqrt{1-\rho_{23}^2}\,[I_{sum}(1,n-1) + I_{sum}(-1,n-1)] + \sqrt{\frac{\pi}{2}}\frac{\rho_{23}}{\sigma_3}[I_{GL}(1,n) - I_{GL}(-1,n)] \right\} \quad (5.51)$$

$$K_{10} = \frac{1}{\pi}\frac{\sigma_2}{\sigma_3} e^{-\Delta_1} \left\{ \sqrt{1-\rho_{23}^2}\,[I_{sum}(1,n-1) - I_{sum}(-1,n-1)] + \sqrt{\frac{\pi}{2}}\frac{\rho_{23}}{\sigma_3}[I_{GL}(1,n) + I_{GL}(-1,n)] \right\} \quad (5.52)$$

where I_{sn} is given by

$$I_{sn} = 2\,\text{sgn}(\rho_{23}) \int_{\theta_o}^{\pi/2} \sin^n\theta \; d\theta \quad (5.53)$$

$$\theta_o = \tan^{-1}\left(\frac{\sqrt{1-\rho_{23}^2}}{\rho_{23}}\right) \;;$$

I_{GL} is a Gauss-Laguerre quadrature:

$$I_{GL}(f_i, m) = \int_0^\infty \exp\left[-\frac{1}{2}\left(\frac{y_3 - f_i\,\mu_{1*}}{\sigma_{1*}}\right)^2 + y_3\right] \times \left[1 + f_i \operatorname{erf}\left(\frac{\rho_{23} y_3}{\sqrt{2}\sigma_3\sqrt{1-\rho_{23}^2}}\right)\right] y_3^m \, e^{-y_3}\, dy_3 \quad ; \tag{5.54}$$

I_{sum} is a standard summation:

$$I_{sum}(f_i, m) = \sigma_{2*}\, e^{-\Delta_3^2/2} \sum_{k=0}^{m} \binom{m}{k} (\mu_{2*})^{m-k}\, \sigma_{2*}^k\, (2)^{(k-1)/2} \times f_{sgn}\left[\gamma\left(\frac{k+1}{2}, \frac{\mu_{2*}^2}{2\sigma_{2*}^2}\right) - \Gamma\left(\frac{k+1}{2}\right)\right] \tag{5.55}$$

$$f_{sgn} = \begin{cases} (-1)^k & \text{if } f_i = 1 \\ (-1)^{m-k-1} & \text{if } f_i = -1 \end{cases} \quad ;$$

the constants are:

$$\Delta_1 = \frac{q^2 z_u^2}{2\sigma_3^2 + \mu_{\zeta_2}^2} \tag{5.56}$$

$$\Delta_2 = \sqrt{\sigma_3^2(1-\rho_{23}^2) + \rho_{23}^2\sigma_{1*}^2} \tag{5.57}$$

$$\Delta_3 = \frac{\rho_{23}\mu_{1*}}{\Delta_2} \tag{5.58}$$

$$\mu_{1*} = \frac{2qz_u\sigma_3^2}{2\sigma_3^2 + \mu_{\zeta_2}^2} \tag{5.59}$$

$$\sigma_{1*} = \frac{\mu_{\zeta_2}\sigma_3}{\sqrt{2\sigma_3^2 + \mu_{\zeta_2}^2}} \tag{5.60}$$

$$\mu_{2*} = \frac{\mu_{1*}\sigma_3^2(1-\rho_{23}^2)}{\Delta_2^2} \tag{5.61}$$

$$\sigma_{2*} = \frac{\sigma_{1*}\sigma_3\sqrt{1-\rho_{23}^2}}{\Delta_2} \quad ; \tag{5.62}$$

erf(·) is the error function, erfc(·) is the complementary error function, Γ(·) is the Gamma function and $\gamma(a, b)$ is the incomplete Gamma function, a is the regular Gamma function argument and b is the upper limit of the Gamma function integral (see Appendix B). Details of expectation derivations are given in Appendix C.

Note that several researchers have previously obtained solutions for C_1, C_2, K_1 and K_2 (Baber and Wen 1981; Chang et al. 1986; Casciati 1987; Maldonado 1992). Chang et

al. and Casciati obtained the same form for I_{sn} in C_1 and K_1, but it does not agree with that originally proposed by Baber and Wen (Maldonado's form, given in summation form and valid only for odd values of n, does not contain I_{sn}). The derivation of K_1, presented in Appendix C, shows that the solution given in Eq. (5.43) is valid for the full range of possible values of ρ_{23} (i.e., $-1 \leq \rho_{23} \leq 1$). The same is true for C_1 given in Eq. (5.38). Comparison with previously proposed forms of I_{sn} shows that Baber and Wen's form is valid only for $\rho_{23} < 0$, while Chang et al.'s form is valid only for $\rho_{23} > 0$.

5.4.4 Response Evaluation

The governing equations, Eqs. (5.9), (5.10) and (5.12), are now a set of first order linear differential equations. They may be rewritten in matrix form as

$$\dot{\mathbf{y}} = \mathbf{G}\mathbf{y} + \mathbf{f} \tag{5.63}$$

where

$$\mathbf{G} = \begin{bmatrix} 0 & 1 & 0 \\ -\alpha\omega_o^2 & -2\xi_o\omega_o & -(1-\alpha)\omega_o^2 \\ 0 & C_{e3} & K_{e3} \end{bmatrix} \tag{5.64}$$

and

$$\mathbf{f} = \begin{Bmatrix} 0 \\ f(t) \\ 0 \end{Bmatrix} . \tag{5.65}$$

When Eq. (5.63) is post-multiplied by $\mathbf{y}^T$, the expectation operators are applied and the resulting equation is added unto its transpose, the covariance equation

$$\dot{\mathbf{S}} = \mathbf{G}\mathbf{S} + \mathbf{S}\mathbf{G}^T + \mathbf{B} \tag{5.66}$$

for the zero mean time lag covariance matrix $\mathbf{S} = E[\mathbf{y}\mathbf{y}^T]$ is derived,

$$\mathbf{S} = \begin{bmatrix} E[y_1^2] & E[y_1y_2] & E[y_1y_3] \\ & E[y_2^2] & E[y_2y_3] \\ \text{sym} & & E[y_3^2] \end{bmatrix} . \tag{5.67}$$

In Eq. (5.66), **B** is a matrix of the expected values of the products of the forcing functions and the reponse vectors,

$$\mathbf{B} = E[\mathbf{f}\mathbf{y}^{\mathrm{T}} + \mathbf{y}\mathbf{f}^{\mathrm{T}}] \ . \tag{5.68}$$

When $f(t)$ is a zero mean Gaussian white noise with constant power spectral density S_o, then **B** has only one nonzero term and can be written as

$$B_{ij} = \delta_{i2}\delta_{2j}\, 2\pi S_o \tag{5.69}$$

where δ_{ij} is the Kronecker delta.

The desired response statistics are elements of the zero mean time lag covariance matrix **S** obtained by numerical integration of Eq. (5.66). For example, the mean square responses (or in our case, the variances) are obtained from Eq. (5.67) as

$$\begin{aligned} \sigma_u^2 &= \sigma_1^2 = E[y_1^2] \\ \sigma_{\dot{u}}^2 &= \sigma_2^2 = E[y_2^2] \\ \sigma_z^2 &= \sigma_3^2 = E[y_3^2] \ . \end{aligned} \tag{5.70}$$

The correlation coefficient ρ_{23} needed to compute the linearization coefficients C_{e3} and K_{e3} at each time step are also obtained from Eq. (5.67) as

$$\rho_{23} = \frac{E[y_2 y_3]}{\sigma_2\, \sigma_3} = \frac{S_{23}}{\sigma_2\, \sigma_3} \ . \tag{5.71}$$

The pinching function $h(z)$ and degradation parameters $\nu(\varepsilon)$ and $\eta(\varepsilon)$ are updated at each time step by replacing ε in the approximate equations by its expected value μ_ε. This is obtained by integrating

$$\dot{\mu_\varepsilon} = (1 - \alpha)\omega_o^2\, S_{23} \tag{5.72}$$

parallel with Eq. (5.66) to allow updating the deterioration and pinching parameters, and to complete the evaluation of the **G** matrix. Numerical integration of Eqs. (5.66) and (5.72) yields the *nonstationary solution*. Any general purpose routines in ordinary differential equation software packages can be used. For the *stationary solution*,

Eq. (5.66) is solved with $\dot{\mathbf{S}} = 0$. The resulting equation is the well known Liapunov matrix equation:

$$\mathbf{G}\,\mathbf{S} + \mathbf{S}\,\mathbf{G}^{\mathrm{T}} + \mathbf{B} = 0 \ . \tag{5.73}$$

Efficient iterative solution algorithms, such as that proposed by Bartels and Stewart (1972), are available to solve this equation. Alternatively, Eq. (5.73) can be recast into a standard matrix inversion problem, as shown by Roberts and Spanos (1990).

Note that the procedure discussed above dispenses with the assumption of slowly varying response parameters (known as the Krylov-Bogoliubov, KB, assumption) that is normally invoked in statistical linearization (Caughey 1971). This is ideal because this assumption (*1*) is equivalent to assuming a narrow band process (i.e., a random process with significant power spectral density values over a narrow frequency band around a central frequency) "while it is known that the response of hysteretic systems is wide band" (Baber and Wen 1981), (*2*) prohibits drifts in the system, and (*3*) may seriously underestimate the root mean square (RMS) response (Wen 1988). Except for any inaccuracy introduced in numerical calculation, the solution obtained using the scheme discussed in this section "is that of the system with is the best linear approximation of the original nonlinear system, i.e., it gives the least mean square error" (Wen 1986). A potential limitation of the current procedure, however, is the fact that the number of unknowns in the covariance matrix **S** increases according to $3n_{df}(3n_{df} + 1)/2$, where n_{df}= number of degrees of freedom of the system (Wen 1986), limiting this method to systems with medium to small number of degrees of freedom, depending on the available computing power.

5.4.5 Comment on the Linearized Model

The linearized model, completely described by Eqs. (5.9), (5.10) and (5.12), can be related to the generalized Maxwell model shown in Fig. 5.3 (Chang et al. 1986). First, let us write the equation of motion of the linearized model in the following general form:

$$m\ddot{y}_1 + c\dot{y}_1 + ky_1 + hy_3 = F(t) \ , \tag{5.74}$$

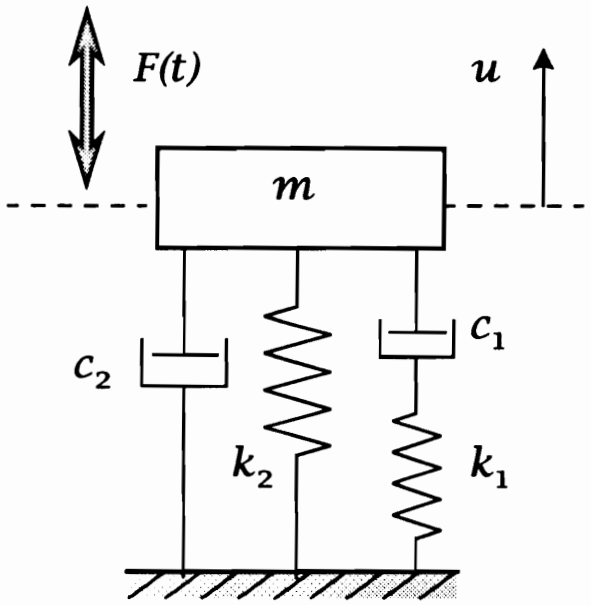

Figure 5.3: A SDF generalized Maxwell model

with the constitutive relations given by

$$\dot{y}_3 = C_{e3}\,\dot{y}_1 + K_{e3}\,y_3 \ . \tag{5.75}$$

[Note that $h = (1 - \alpha)\,k$.] Let us eliminate y_3 from Eqs. (5.74) and (5.75) to obtain the following third-order differential equation of motion:

$$\frac{m}{h}\,\dddot{y}_1 + \left(\frac{c}{h} - \frac{K_{e3}}{h}m\right)\ddot{y}_1 + \left(-\frac{K_{e3}}{h}c + C_{e3} + \frac{k}{h}\right)\dot{y}_1 - \frac{K_{e3}k}{h}y_1 = \frac{1}{h}\dot{F} - \frac{K_{e3}}{h}F \ . \tag{5.76}$$

Now, if we consider the equation of motion of the mass supported by a generalized Maxwell model consisting of three parallel elements as shown in Fig. 5.3 and compare it with Eq. (5.76), it can be shown that, if

$$h = k_1 \ , \quad k = k_2 \ , \quad c = c_2 \ , \quad C_{e3} = 1 \ , \quad \text{and} \quad K_{e3} = -\frac{k_1}{c_1} \ , \tag{5.77}$$

then the linearized model is equivalent to the linear viscoelastic model shown in Fig. 5.3 (Chang et al. 1986). (Note that $y_1 = u$.) This comparison also means that for the linearized model to be physically realizable, C_{e3} must be positive and K_{e3} must be negative. This is actually the case as results of numerical studies showed. Other results will be discussed next.

5.5 Numerical Studies

5.5.1 Introduction

There are basically two methods that can be used to evaluate the accuracy of approximate solutions, such as statistical linearization, to nonlinear random vibration problems: (*1*) comparison with exact theoretical solution, and (*2*) comparison with Monte Carlo simulation (MCS) results (Shinozuka 1972; Spanos and Mignolet 1989). The first approach is based on the solution of pertinent FPK equation (see section 5.3.3). Unfortunately, this is often inapplicable since exact solutions of the FPK equation have only been obtained for a very limited case of problems (i.e., linear SDF systems and nonlinear SDF systems with nonhysteretic stiffness and displacement dependent

damping). Furthermore, this approach assumes that the response is a Markov process. "This is a serious limitation since it effectively restricts consideration to those cases where the excitation processes can be modeled adequately in terms of white noise processes" (Roberts and Spanos 1990). Thus, MCS is normally the only available method to check the accuracy of approximate solutions to nonlinear random vibration problems of practical engineering interest.

In the absence of applicable exact solution to a system with a modified BWBN hysteresis model, MCS results will be used to evaluate the accuracy of the procedure presented in the previous section. Response statistics obtained in both MCS and linearization analyses will be plotted together and compared graphically. Visual inspection is a standard method of evaluating the accuracy of linearization results (Roberts and Spanos 1990). Theoretical bounds on the errors of response statistics obtained by approximate methods have not been completely established yet (Roberts and Spanos 1990).

The nonstationary (or transient) response of a SDF system will be obtained by numerical integration of Eqs. (5.66) and (5.72). The concept of stationary response is not applicable in the present problem since system degradation and pinching are time-dependent phenomena.

It has been mentioned earlier that about five hundred simulation samples are required to obtain nonstationary response statistics. Fig. 5.4 shows, however, that cutting the sample size to two hundred, thereby cutting computing time by about sixty percent, causes a negligible loss in accuracy. Thus, all simulation results will be obtained from two hundred response samples. Fig. 5.5 shows hysteresis plots of two SDF systems under a sample white noise excitation (S_o = 1.0). The first system (Fig. 5.5a) is a nondegrading (i.e., $\delta_\eta = \delta_\nu = 0.0$), low pinching system with the following properties: ω_o=2.0 rad/s, ξ_o=0.05, α=0.10, β=1.5, $\gamma = -0.5$, n=1, q=0.10, ζ_{1_o}=0.85, λ=0.05, p=1, ψ_o=0.20 and δ_ψ=0.002. The second (Fig. 5.5b) is a degrading, high pinching system with: ω_o=2.0 rad/s, ξ_o=0.05, α=0.10, β=1.5, $\gamma = -0.5$, n=1, q=0.10, ζ_{1_o}=0.97, λ=0.05,

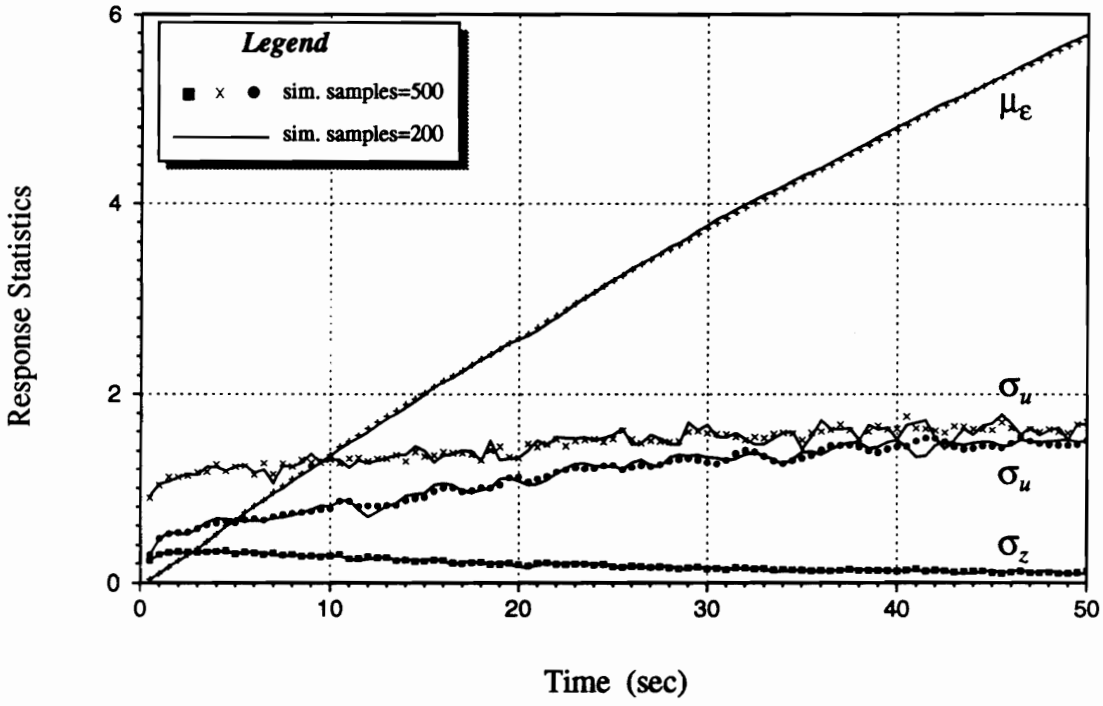

Figure 5.4: Comparison of response statistics using different simulation sample sizes

p=1, ψ_o=0.20, δ_ψ=0.002, δ_ν=0.005 and δ_η = 0.05.

With about a dozen model parameters and a wide range of possible parameter values, there is a danger of spending limitless time performing numerical studies. To avoid this problem, the present analysis will focus on verifying the applicability of the approximate solution scheme to the proposed hysteresis model for wood structural systems, for a range of practical cases. Linearization solutions to the parent forms of the modified BWBN model have been extensively studied and verified using MCS (Baber 1980; Baber and Wen 1981; Noori 1984) and will not be repeated here. Any limitations to the new model and/or the approximate solution will be identified and, if, possible explained.

5.5.2 Base System: Building With Plywood Shear Walls

Let us consider a SDF wood building whose response is governed by plywood shear walls and with hysteresis similar to that in Fig. 4.5b. For our base system, the following properties are considered: ω_o=4.7124 rad/s, ξ_o=0.10, α=0.10, β=1.5, γ = −0.5, n=1, q=0.10, ζ_{1_o}=0.96, λ=0.10, p=1, ψ_o=0.20, δ_ψ=0.01, δ_ν=0.005 and δ_η = 0.05. (The effect of changing these parameter values on the accuracy of response statistics obtained by statistical linearization will be considered in the following sections.) Three levels of white noise excitation (S_o = 0.1, 0.5 and 1.0; see Table 5.1) are used to obtain the zero time lag covariance matrix response, starting with zero initial conditions. Figures 5.6 to 5.10 show comparisons of simulation and linearization results.

Figure 5.6 shows that linearization results generally agree with simulation results. The former, however, tends to slightly underestimate root mean square (RMS) displacements, σ_u, from time t=15 to 45 seconds at high excitation level (S_o = 1.0). On the other hand, RMS velocities, $\sigma_{\dot{u}}$, RMS restoring forces, σ_z, and mean dissipated energy, μ_ε, are estimated very closely at all excitation levels as shown in Figs 5.7 to 5.9.

The variations of correlation coefficients $\rho_{u\dot{u}}$ and $\rho_{\dot{u}z}$ during transient response of the system are plotted in Figs. 5.10a and b, respectively. In both cases, linearization

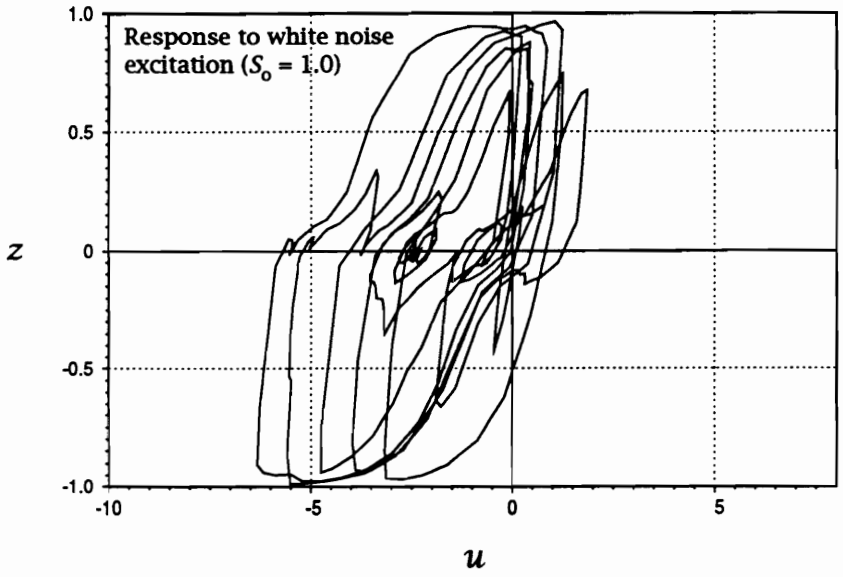

(a) nondegrading, low pinching system

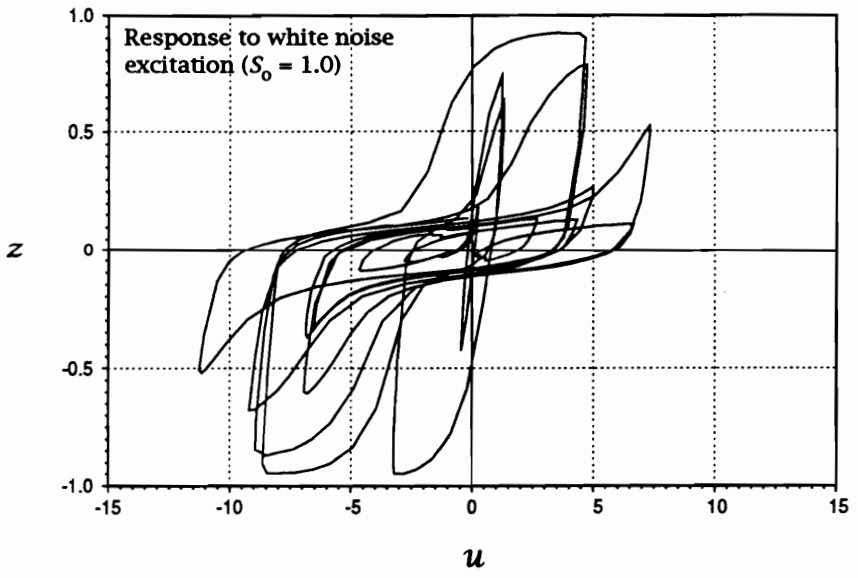

(b) degrading, high pinching system

Figure 5.5: Sample hysteresis plots of SDF systems under white noise excitation

Table 5.1: White noise excitation intensity levels [g = acceleration of gravity (32.2 ft/s^2); 1 ft = 0.305 m]

White Noise Level S_o	**Average Peak Acceleration** (Based on 500 simulation samples)
1.0	0.96 g
0.5	0.68 g
0.1	0.31 g

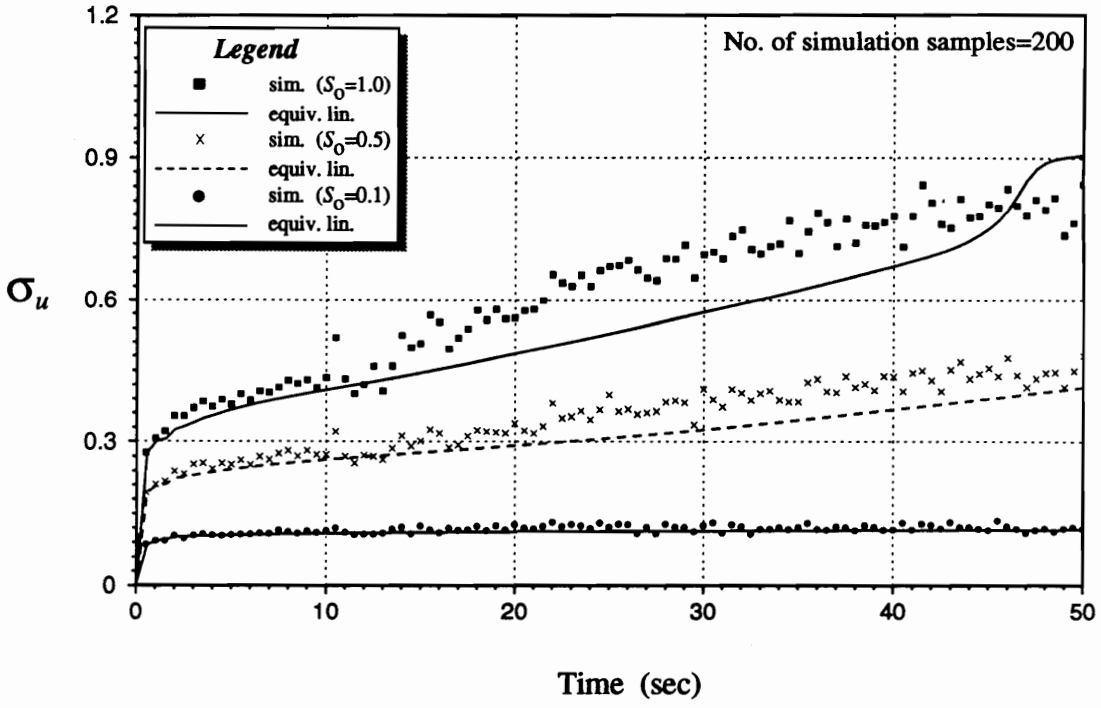

Figure 5.6: Nonstationary root mean square (RMS) displacement response of a SDF system under stationary white noise input

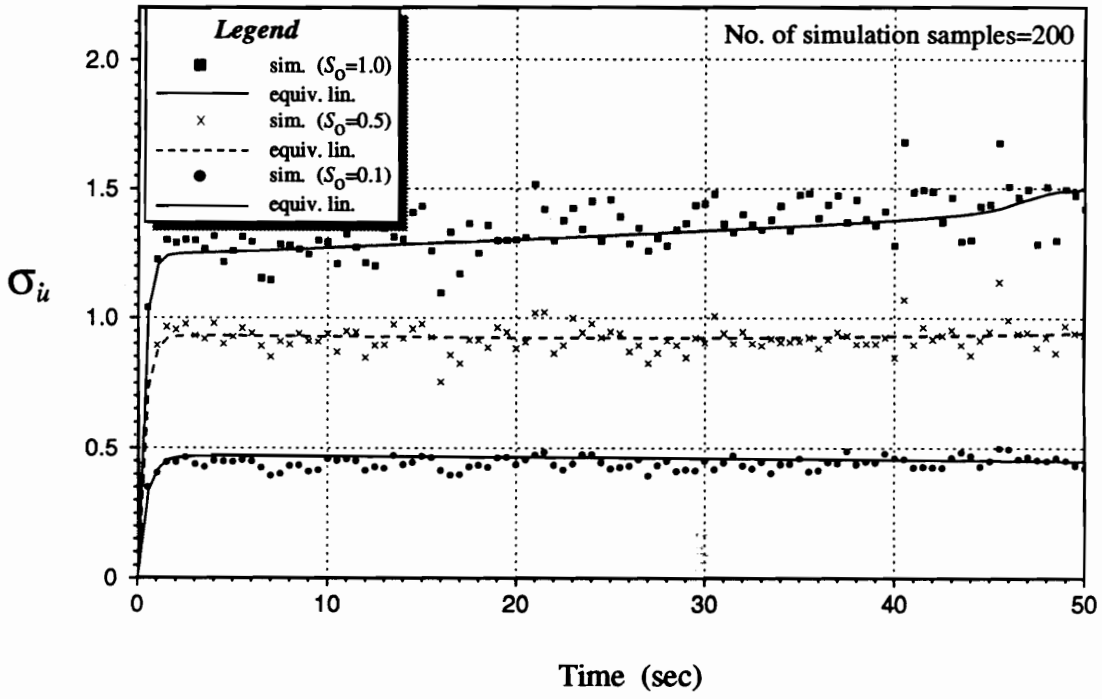

Figure 5.7: Nonstationary RMS velocity response of a SDF system under stationary white noise input

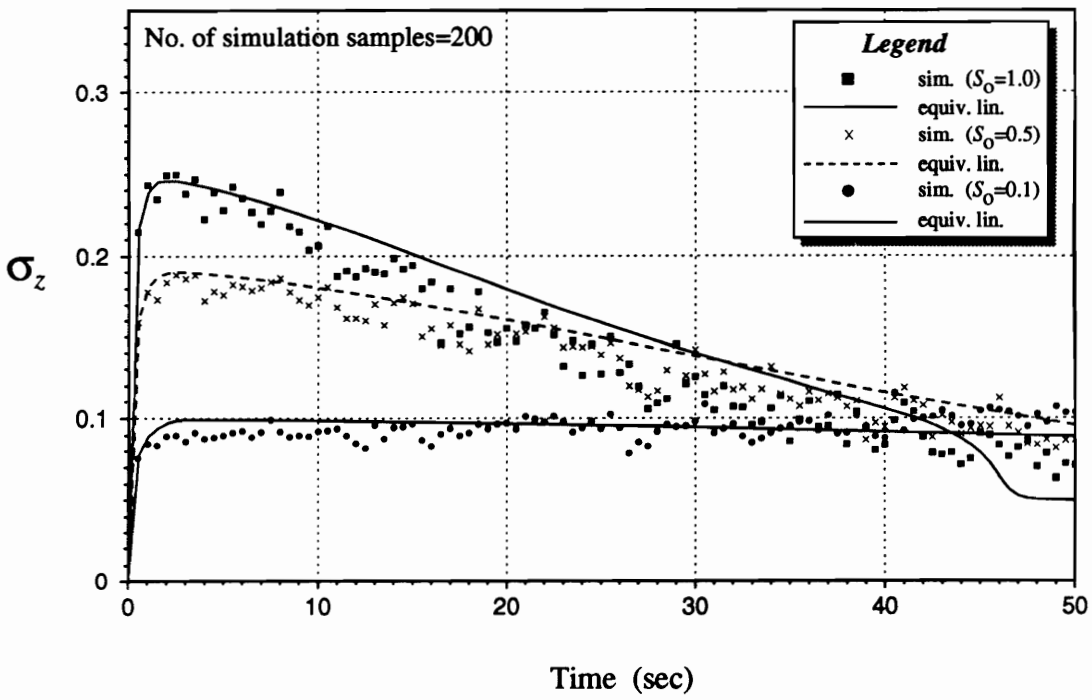

Figure 5.8: Nonstationary RMS restoring force of a SDF system under stationary white noise input

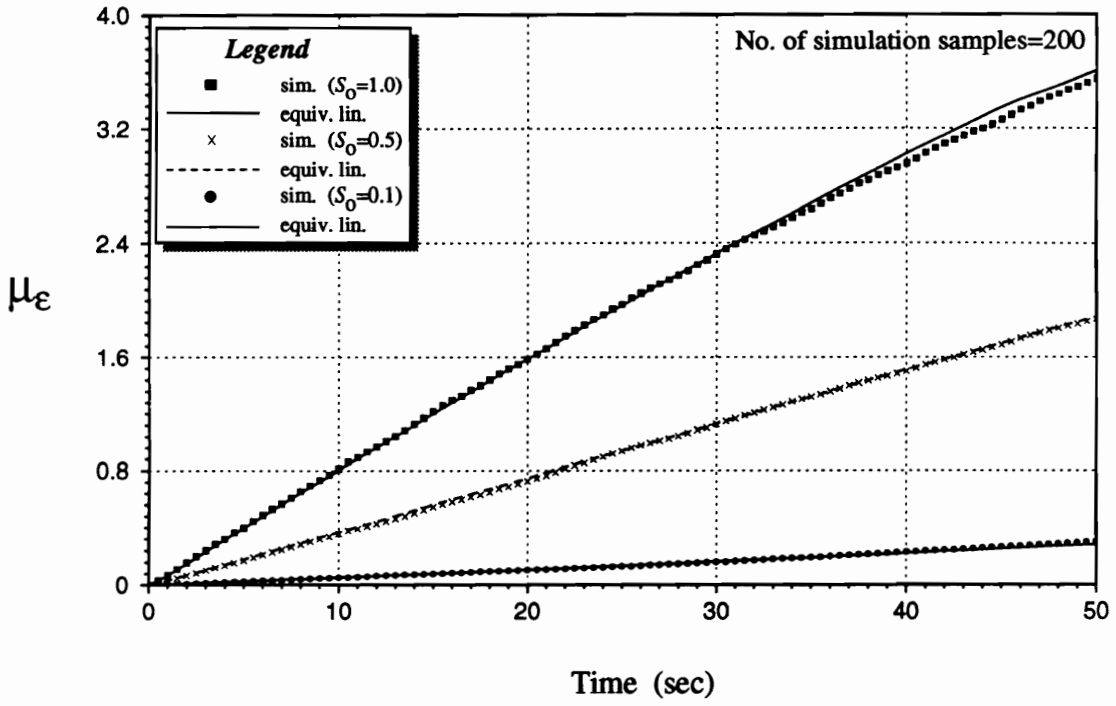

Figure 5.9: Variation of mean energy dissipation for a SDF system under stationary white noise input

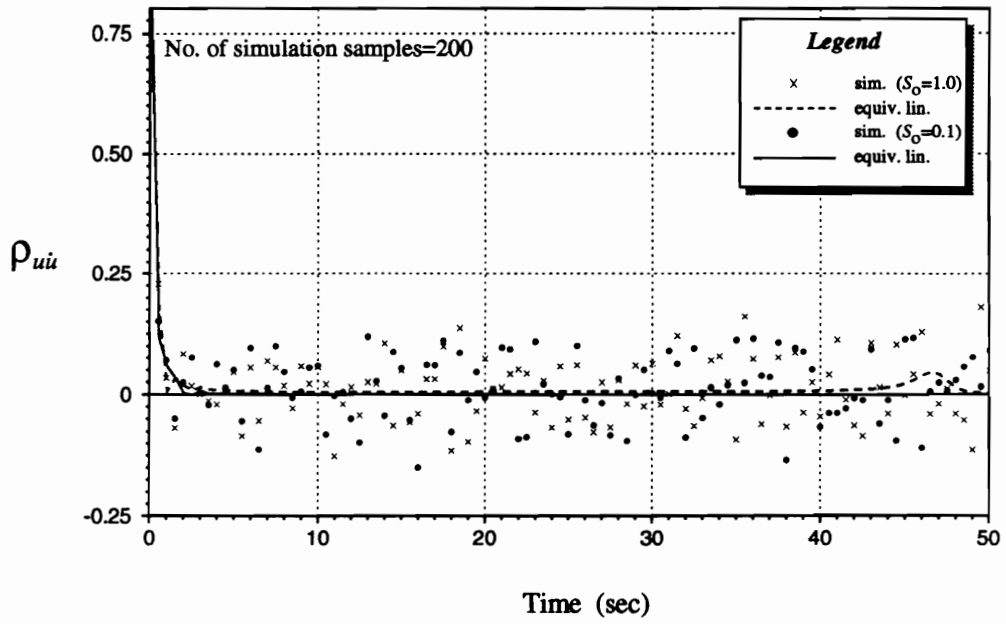

(a) corelation coefficient for displacement and velocity

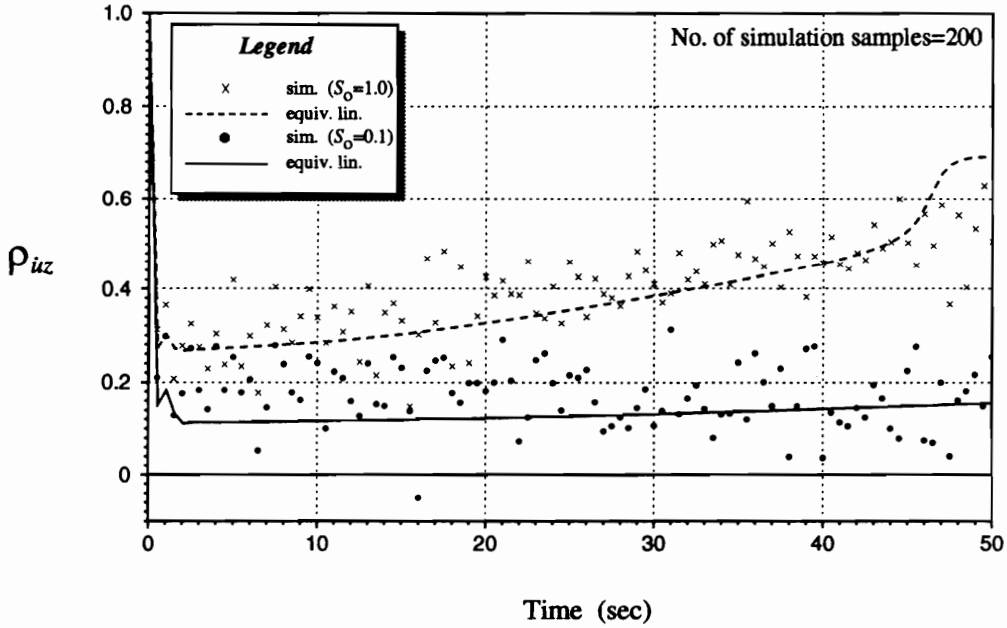

(b) corelation coefficient for velocity and restoring force

Figure 5.10: Variation of correlation coefficients during transient response of a SDF system under stationary white noise input

results estimate the general trend very well. Greater scatter in the simulation results here than in those for RMS predictions means that a larger ensemble sample is needed to obtain better estimates of correlation coefficients. The current two hundred sample ensemble is, however, sufficient for the present work since we are primarily interested in RMS estimates.

The effect of changing model parameter values on the accuracy of response statistics obtained by statistical linearization will be considered next. The parameters of the base system will be changed one at a time. For example, to evaluate the effect of system frequency on the accuracy of linearization results, all the parameters of the base system, except for the frequency, will be fixed. The frequency values given in Table 5.2 will be used for analysis and the linearization and MCS results for each frequency level will be compared. The process is repeated until all the parameters listed in Table 5.2 are studied. Thus, all systems to be studied, from hereon, will assume the base properties given earlier in this section unless otherwise stated. Response statistics will be obtained only for white noise excitation level S_o=0.5, corresponding to an average peak acceleration of $0.681g$ (see Table 5.1).

5.5.3 Effect of System Properties and Model Parameters

In this section, the effect of varying system properties (frequency, ω_o, and damping ratio, ξ_o) and hysteresis parameters (α and n) on the accuracy of response statistics obtained by statistical linearization will be studied. Since initial studies seemed to indicate that the response statistics are most affected by changes in system frequency, three frequency levels will be considered (see Table 5.2). Figures 5.11 to 5.14 show comparisons of simulation and linearization results.

Figures 5.11 and 5.12 show that linearization solutions of RMS displacement and RMS velocity, respectively, agree very well with simulation results. RMS displacements when ω_o=2.0 rad/sec are only slightly underestimated from t >15 seconds. Figure 5.13

Table 5.2: Parameter values considered in numerical studies

Parameter	**Range of Values** min		max
System properties and hysteresis parameters			
ω_o (rad/sec)	0.80	2.00	6.50
ξ_o	0.01		0.10
α	0.05		0.50
n	1.00		12.00
Degradation parameters			
δ_ν	0.00		0.20
δ_η	0.00		0.20
Pinching parameters			
ζ_{1o}	0.70		0.98
q	0.00		0.20
p	1.00		2.00
ψ_o	0.01		0.50
δ_ψ	0.00		0.20
λ	0.01		0.60

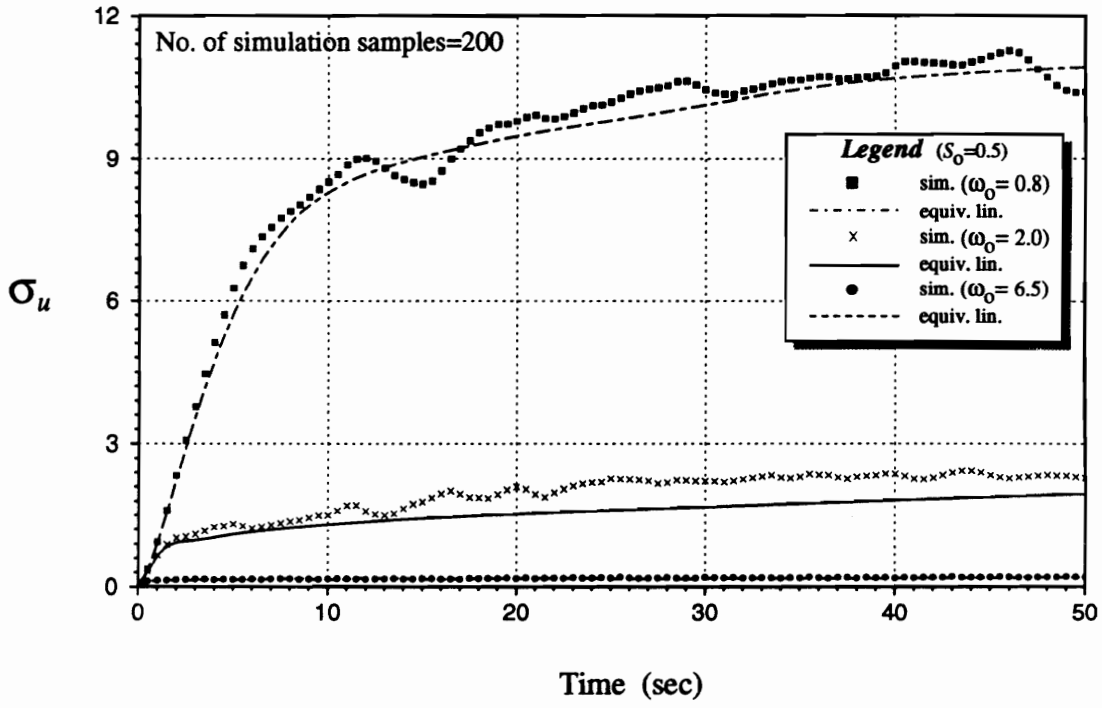

Figure 5.11: Nonstationary RMS displacement response of a SDF system under stationary white noise input- effect of system frequency (ω_o)

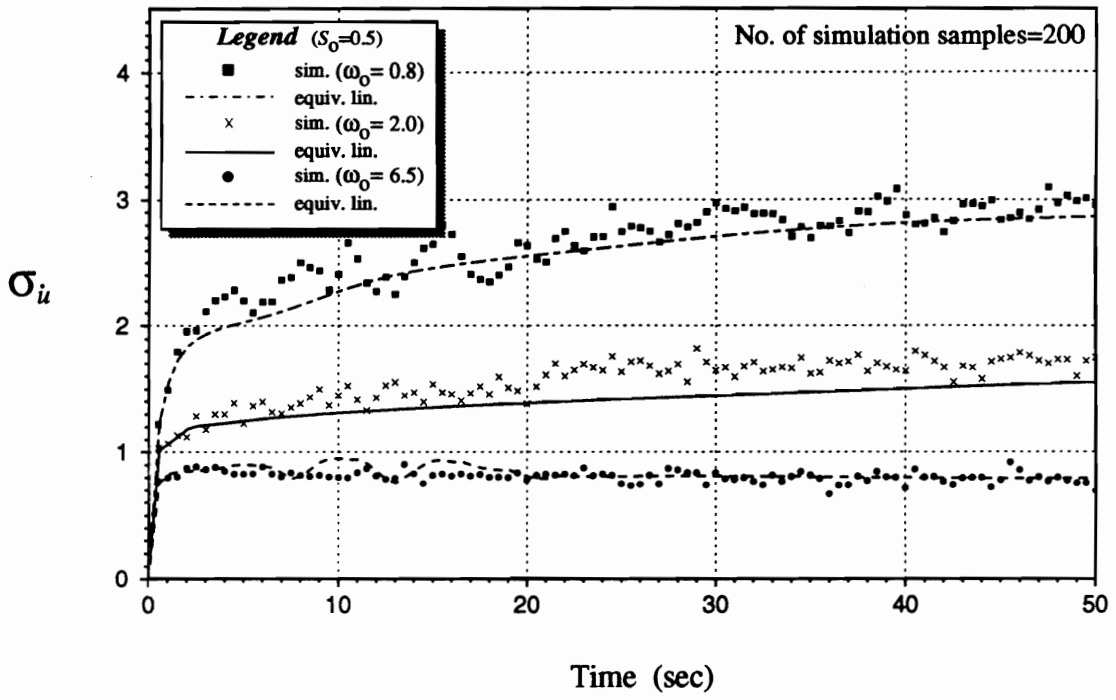

Figure 5.12: Nonstationary RMS velocity response of a SDF system under stationary white noise input- effect of system frequency (ω_o)

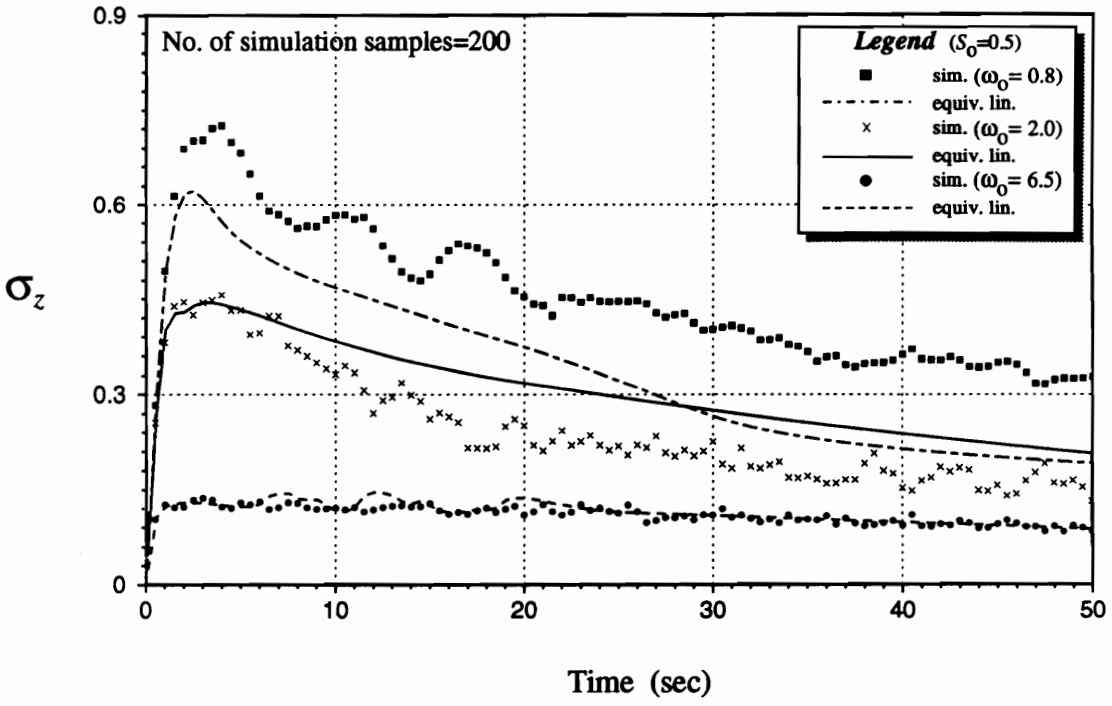

Figure 5.13: Nonstationary RMS restoring force of a SDF system under stationary white noise input- effect of system frequency (ω_o)

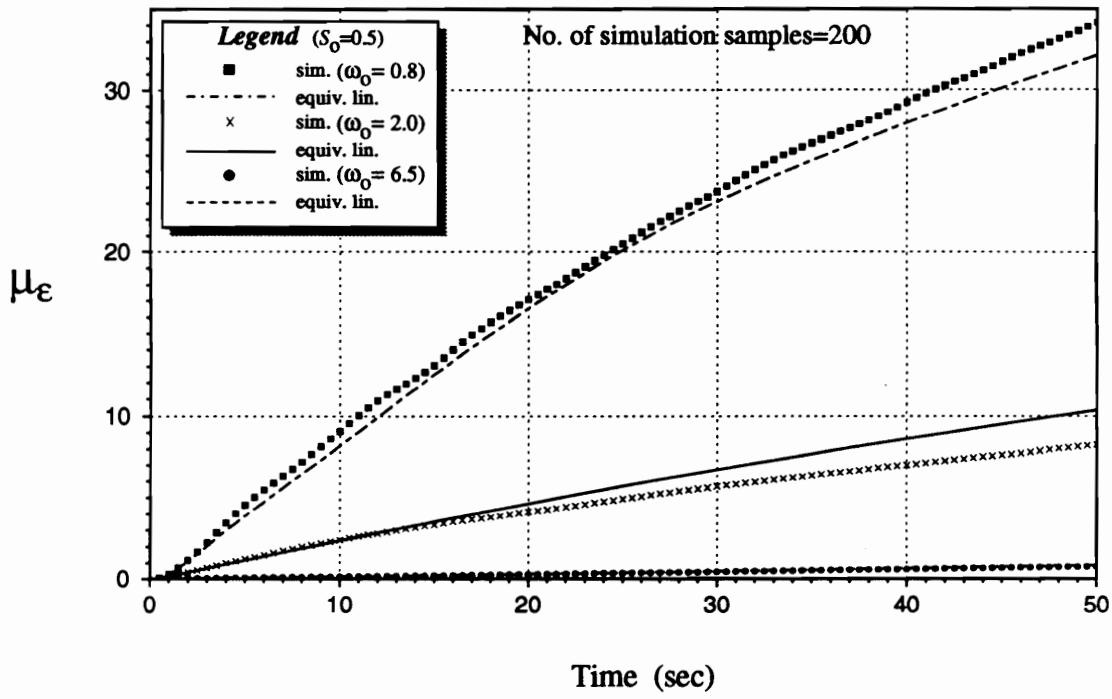

Figure 5.14: Variation of mean energy dissipation for a SDF system under stationary white noise input- effect of system frequency (ω_o)

shows that RMS forces are estimated very well when ω_o=0.8 rad/sec , but are overestimated when ω_o=2.0 rad/sec and underestimated when ω_o=6.5 rad/sec. Mean energy dissipation is reasonably estimated at all frequency levels (Fig. 5.14).

The foregoing shows that the accuracy of response statistics obtained by statistical linearization is heavily influenced by system frequency. This is significant since most wood structural systems tend to loosen at the joints after heavy shaking, resulting in a decreased system frequency (or longer natural period). Thus, in studying the influence of other model parameters on the accuracy of response statistics obtained by linearization, two frequency levels will be considered (the base system frequency, ω_o=4.7124 rad/sec, and a low frequency system, ω_o=0.8 rad/sec). To save space, response comparisons, from hereon, will be limited to RMS displacement σ_u and RMS restoring force σ_z. Structural design is typically based on displacement response limits.

The effect of damping ratio (ξ_o) on the accuracy of response statistics obtained by statistical linearization is demonstrated in Figs. 5.15 and 5.16. RMS displacements are estimated extremely well at both levels of ξ_o, when ω_o=0.8 rad/sec (Fig. 5.15a), but are underestimated, slightly when ξ_o=0.10 and more seriously when ξ_o=0.01, when ω_o=4.7124 rad/sec (Fig. 5.15b). The opposite is observed in Fig. 5.16. RMS forces are underestimated at both levels of ξ_o, when ω_o=0.8 rad/sec, but are estimated satisfactorily when ω_o=4.7124 rad/sec.

With two levels of rigidity ratio (α=0.05 and 0.50), linearization results agree very closely with MCS results except (*1*) when α=0.05 and ω_o=4.7124 rad/sec, where the RMS displacement is underestimated from $t \geq$15 seconds (Fig. 5.17b), and (*2*) when α=0.05 and ω_o=0.8 rad/sec, where the RMS force is underestimated (Fig. 5.18a). The general response trends are, however, preserved by the linearization solution.

Two levels of n (1 and 12) are considered to determine its effect on the accuracy of linearization results. Recall that the case of n=12 corresponds to a nearly elasto-plastic case in the z-u plane as shown in Fig. 3.6. Figure 5.19 shows that linearization results compare generally well with MCS RMS displacements. The RMS displacement is only

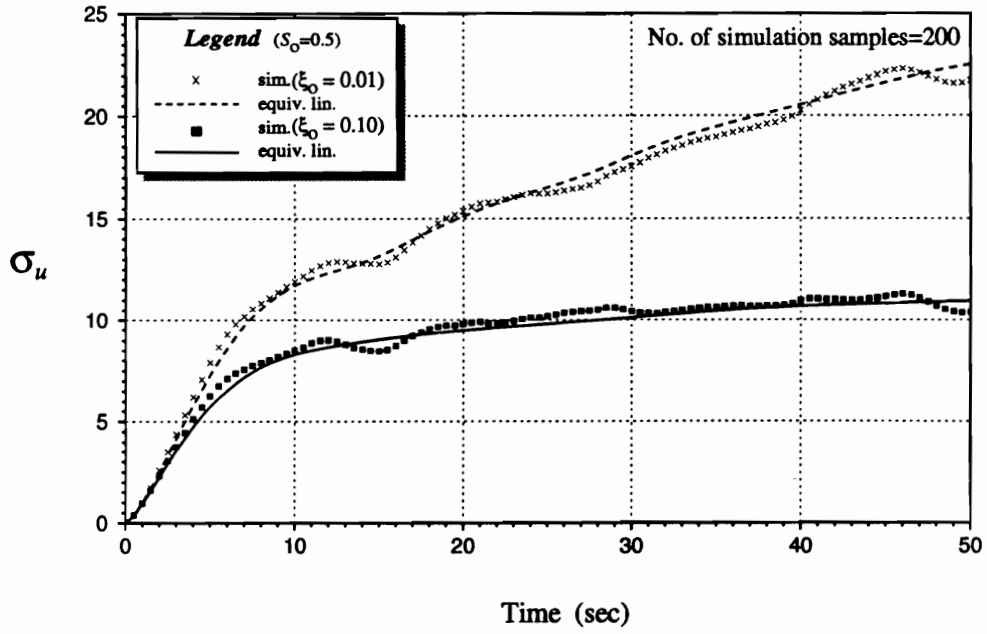

(a) system with ω_0=0.8 rad/sec

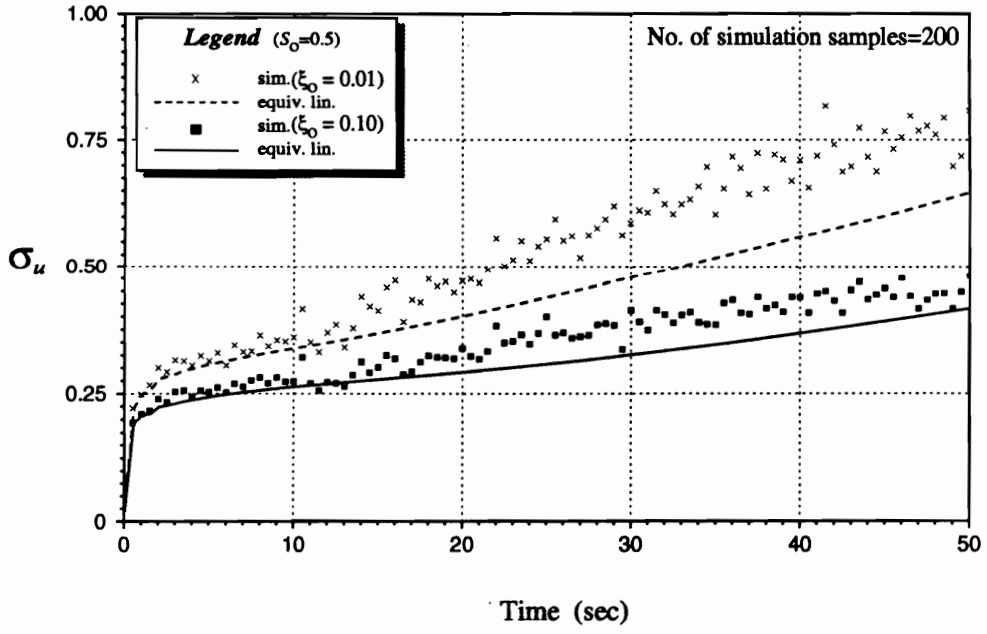

(b) system with ω_0=4.7124 rad/sec

Figure 5.15: Nonstationary RMS displacement response of a SDF system under stationary white noise input- effect of damping ratio (ξ_o)

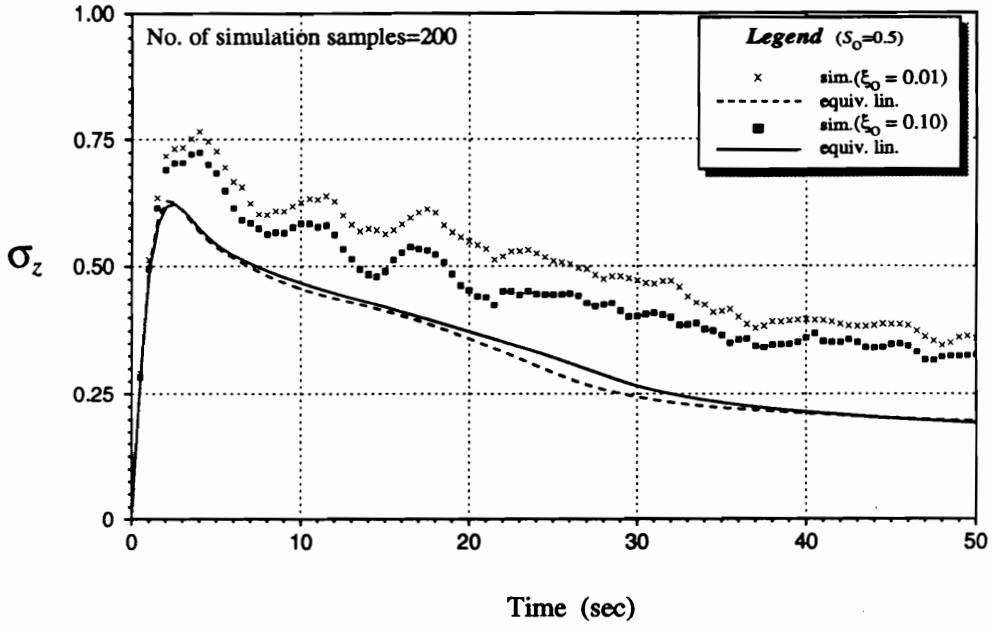

(a) system with ω_o=0.8 rad/sec

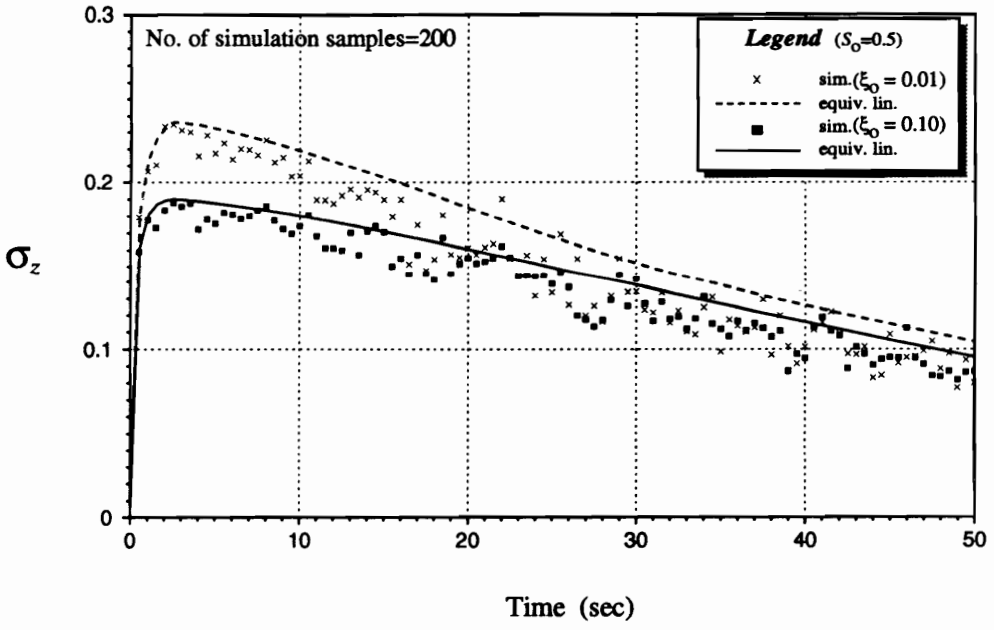

(b) system with ω_o=4.7124 rad/sec

Figure 5.16: Nonstationary RMS restoring force of a SDF system under stationary white noise input- effect of damping ratio (ξ_o)

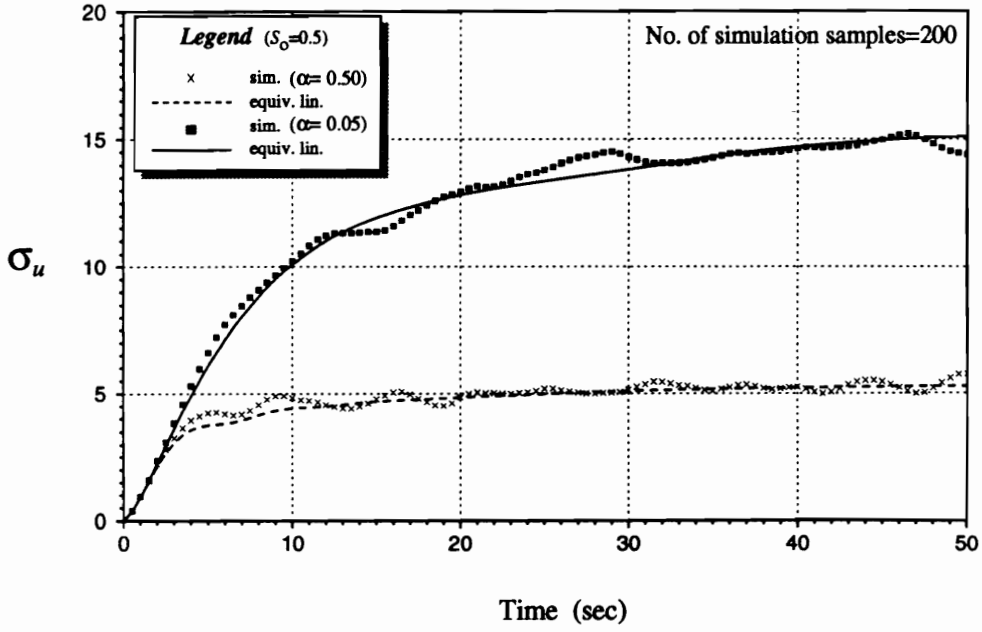

(a) system with ω_0=0.8 rad/sec

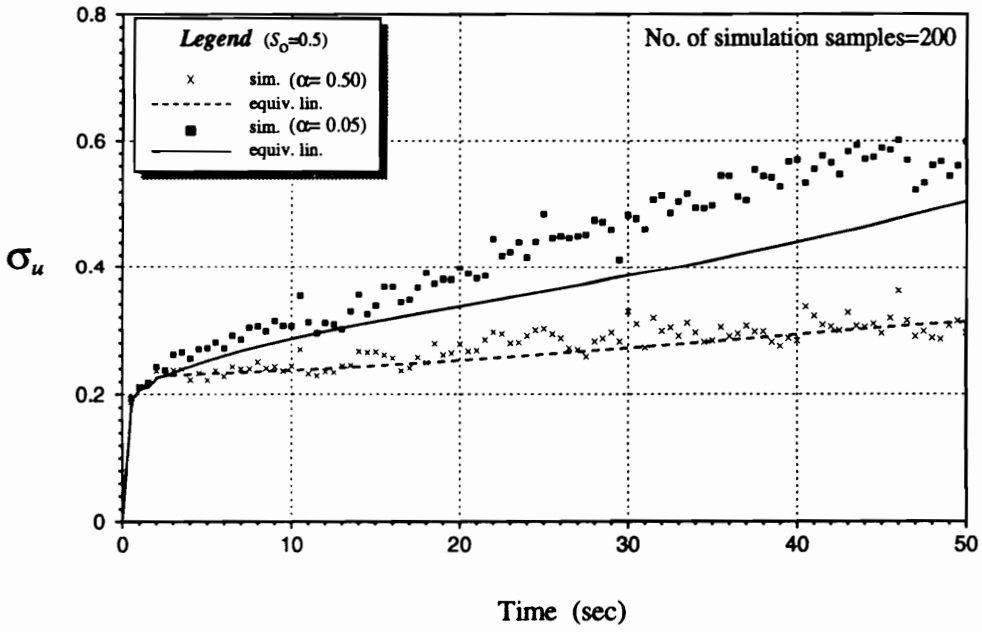

(b) system with ω_0=4.7124 rad/sec

Figure 5.17: Nonstationary RMS displacement response of a SDF system under stationary white noise input- effect of α

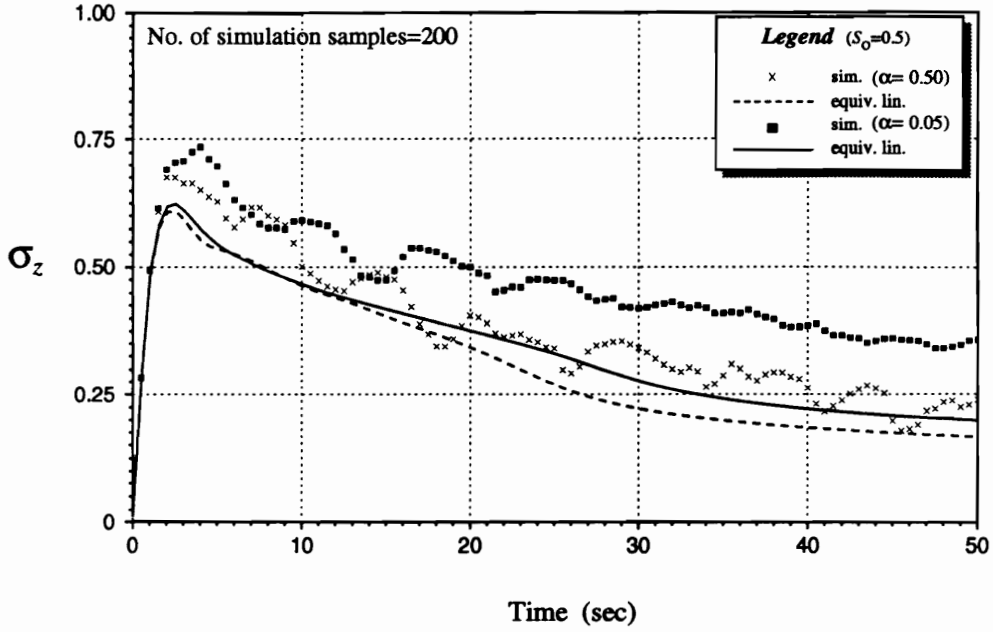

(a) system with ω_o=0.8 rad/sec

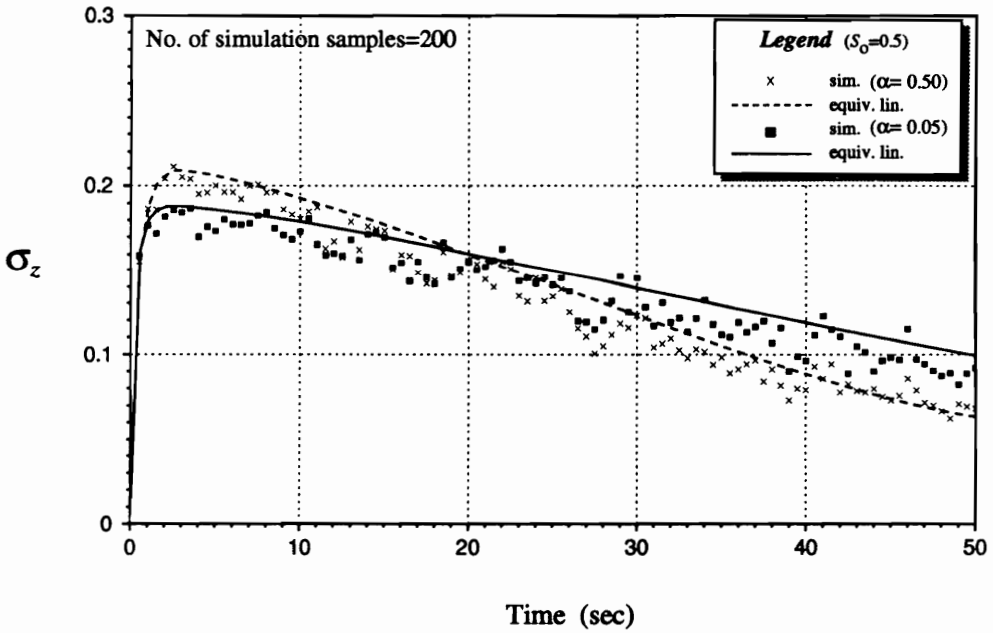

(b) system with ω_o=4.7124 rad/sec

Figure 5.18: Nonstationary RMS restoring force of a SDF system under stationary white noise input- effect of α

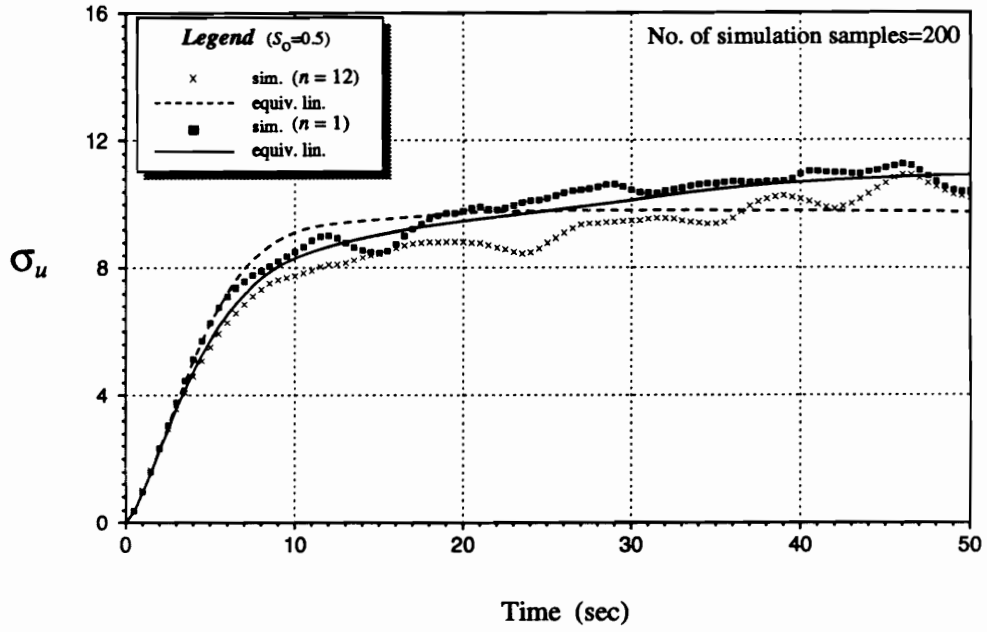

(a) system with ω_o=0.8 rad/sec

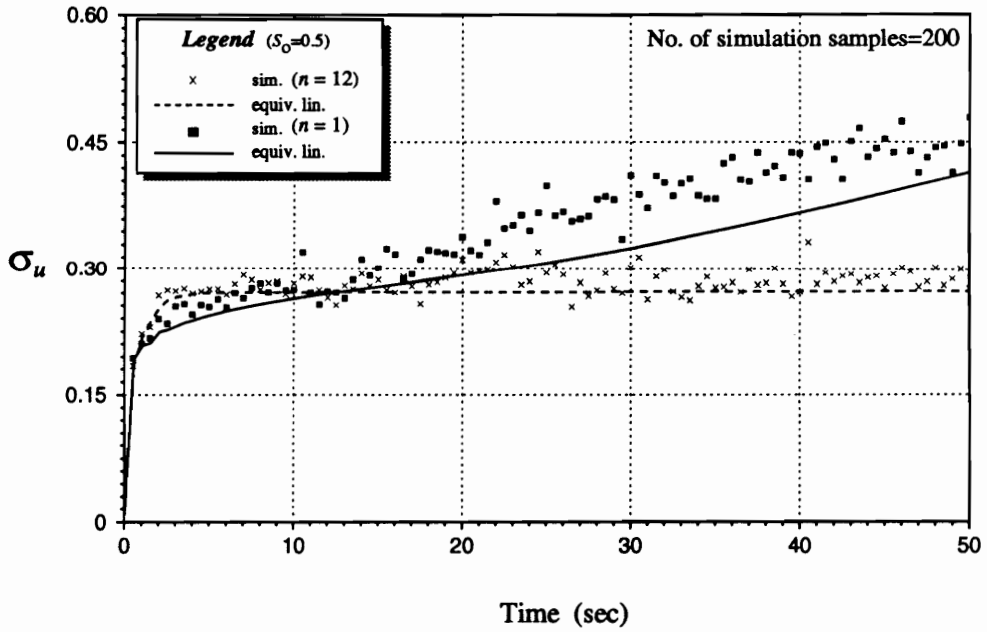

(b) system with ω_o=4.7124 rad/sec

Figure 5.19: Nonstationary RMS displacement response of a SDF system under stationary white noise input- effect of n

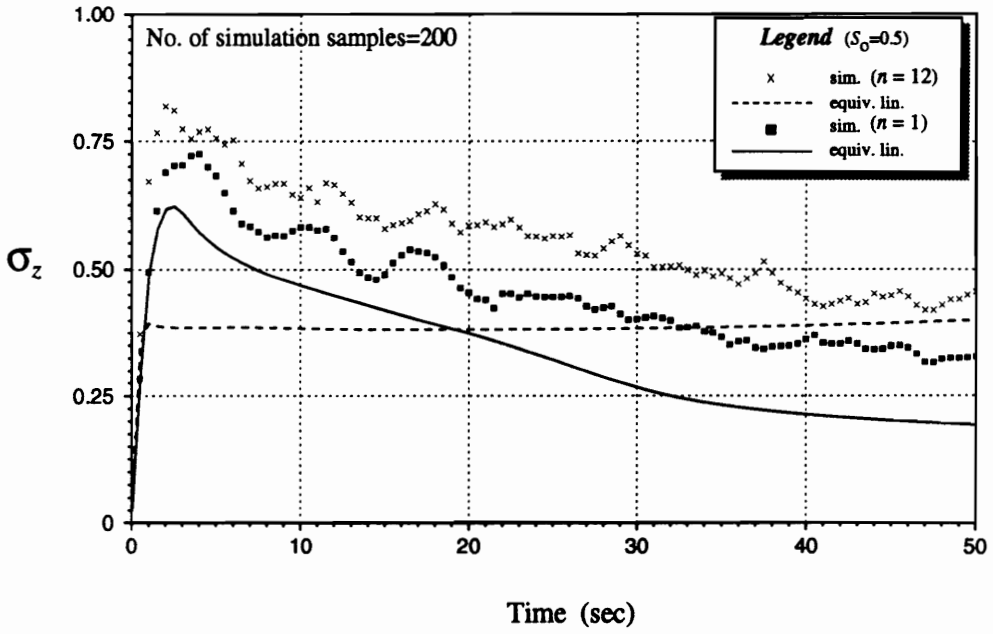

(a) system with ω_o=0.8 rad/sec

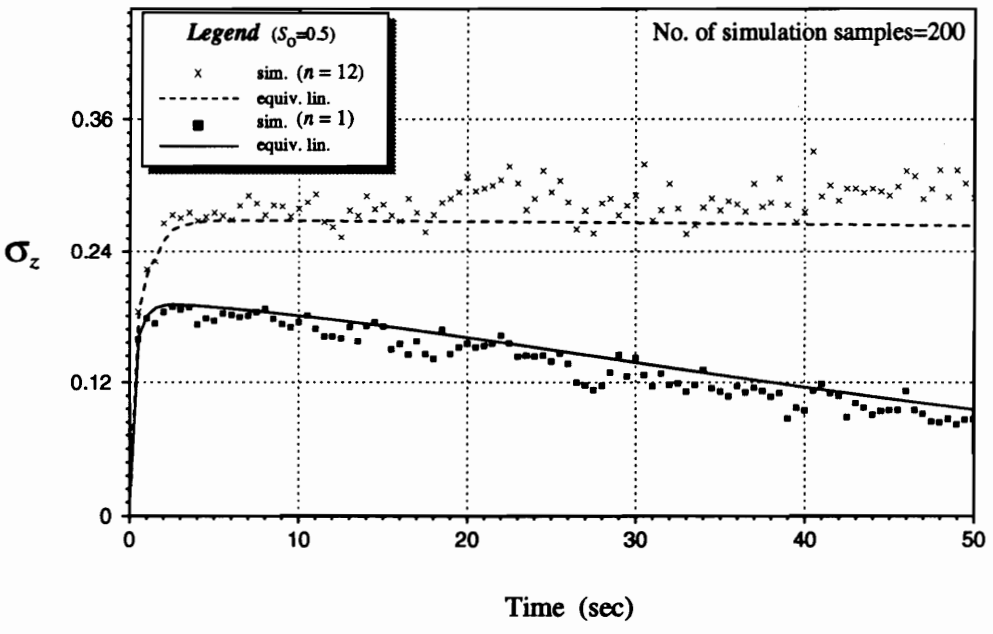

(b) system with ω_o=4.7124 rad/sec

Figure 5.20: Nonstationary RMS restoring force of a SDF system under stationary white noise input- effect of n

slightly underestimated when n=1, ω_o=4.7124 rad/sec, at $t \geq$20 seconds. The RMS forces are somewhat underestimated when n=1 and severely so when n=12 [ω_o=0.8 rad/sec; Fig. 5.20a]. Not only do linearization estimates miss the peak force but the solution also misses the response trend in the latter. Fig. 5.20b (ω_o=4.7124 rad/sec), on the other hand, shows excellent agreement between linearization and MCS results at both levels of n.

5.5.4 Effect of Degradation Parameters

While Baber (1980) has extensively studied the effect of varying the stiffness and strength degradation parameters on the accuracy of response statistics obtained by statistical linearization, their influence on systems with general pinching behavior, as proposed in the present work, has not been investigated yet. We will, therefore, look into this effect in this section.

Two cases of strength degradation are analyzed: (*1*) no degradation (δ_ν=0), and (*2*) severe degradation (δ_ν=0.2). Figure 5.21 shows that linearization results compare adequately with MCS results in estimating RMS displacements. There is only slight underestimation at both levels of δ_ν when ω_o=4.7124 rad/sec and t >20 seconds. Figure 5.22a (ω_o=0.8 rad/sec) shows that linearization results underestimate the peak restoring force when there is no degradation. It also severely underestimates RMS forces from $t \geq$ 38 seconds. This may not be of any practical importance, however, since peak RMS force is typically reached within the first ten seconds of response. Figure 5.22b (ω_o=4.7124 rad/sec), on the other hand, shows that RMS forces are estimated very well by the linearization solution at both levels of δ_ν.

Similarly, two cases of stiffness degradation are analyzed: (*1*) no degradation (δ_η=0), and (*2*) severe degradation (δ_η=0.2). Figure 5.23 shows that linearization results compare satisfactorily with MCS results in estimating RMS displacements. There is only slight underestimation at both levels of δ_η, when ω_o=4.7124 rad/sec and t >20 seconds. Figure 5.24 shows that linearization results underestimate the RMS restoring

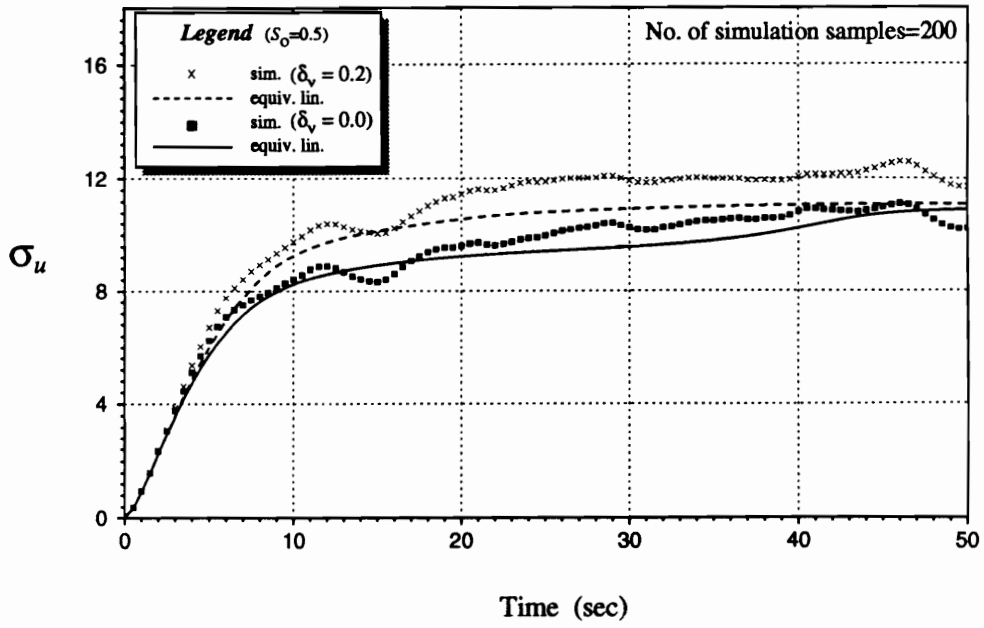

(a) system with ω_o=0.8 rad/sec

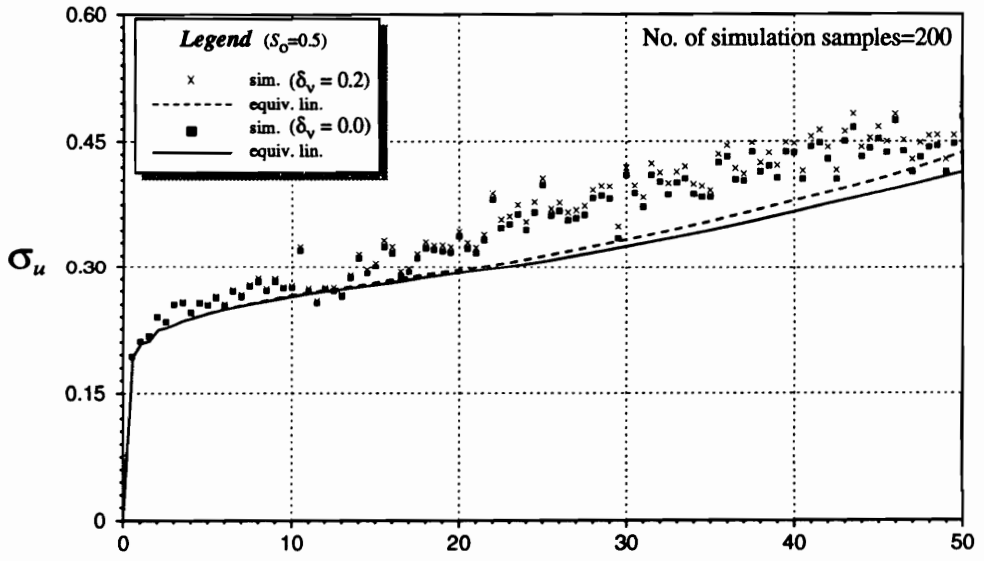

(b) system with ω_o=4.7124 rad/sec

Figure 5.21: Nonstationary RMS displacement response of a SDF system under stationary white noise input- effect of δ_v

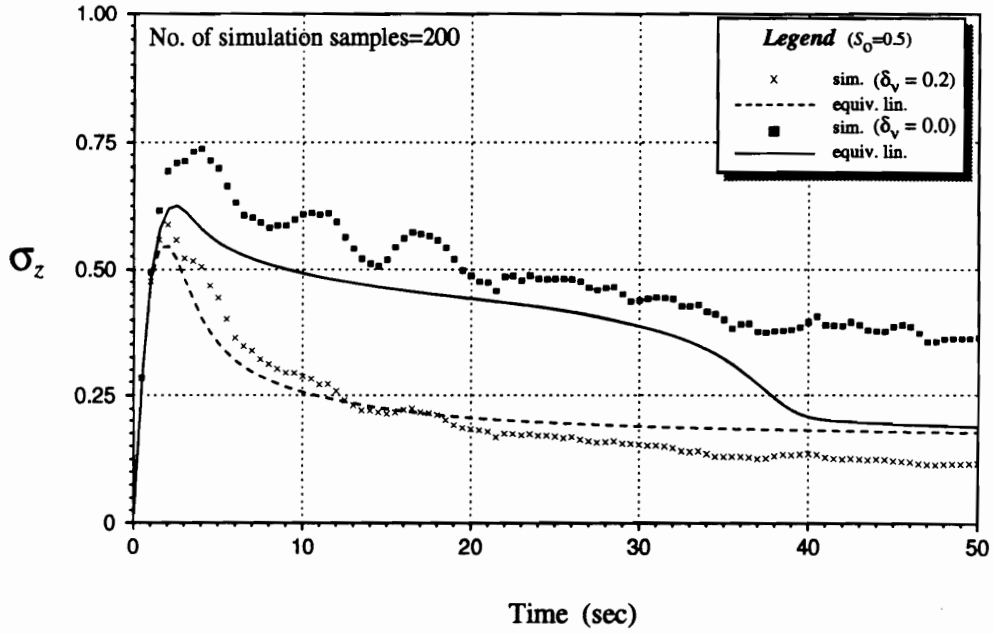

(a) system with ω_o=0.8 rad/sec

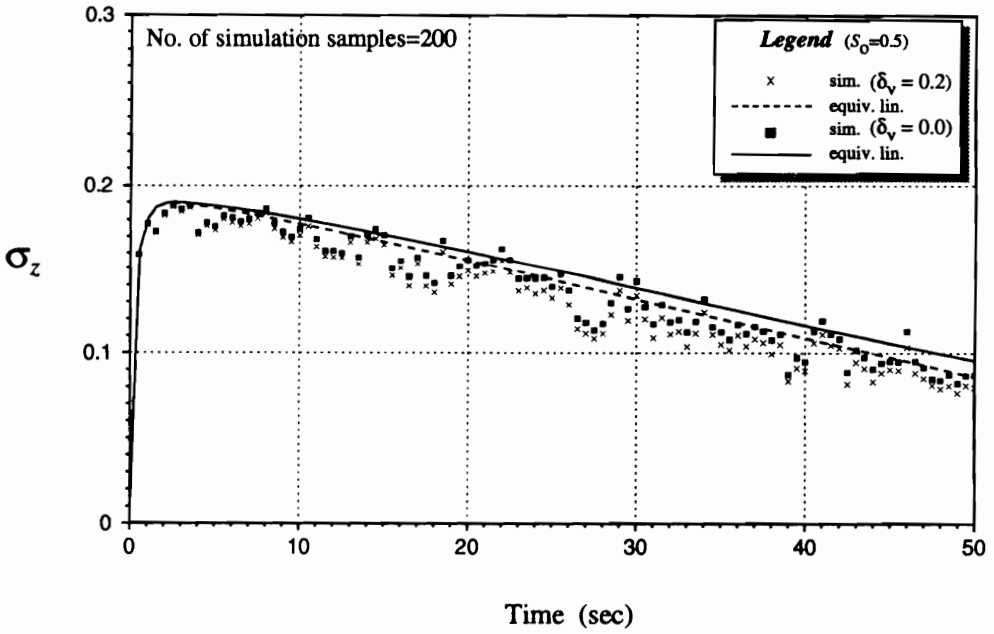

(b) system with ω_o=4.7124 rad/sec

Figure 5.22: Nonstationary RMS restoring force of a SDF system under stationary white noise input- effect of δ_v

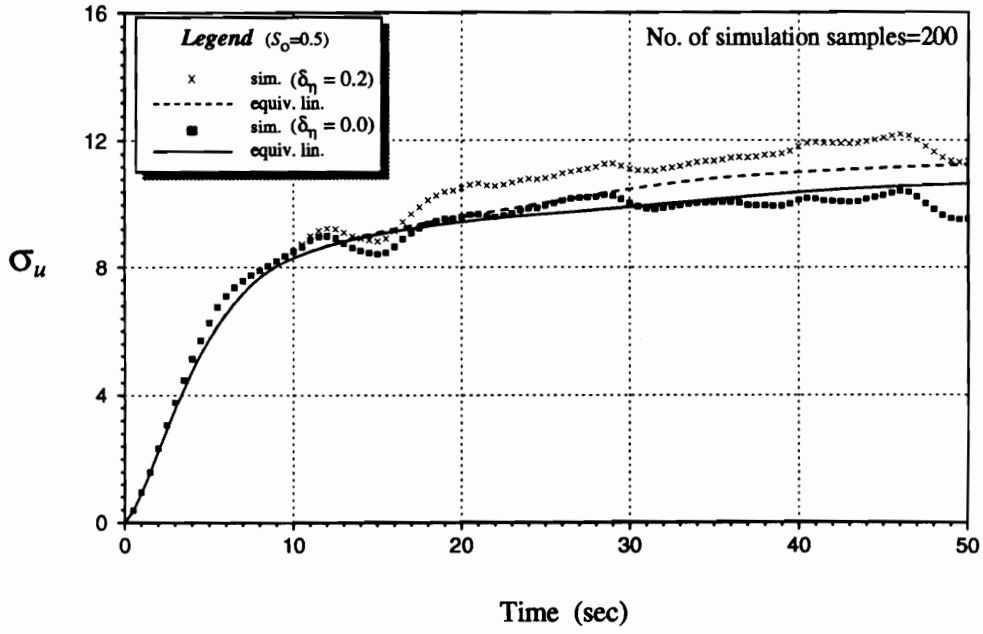

(a) system with ω_o=0.8 rad/sec

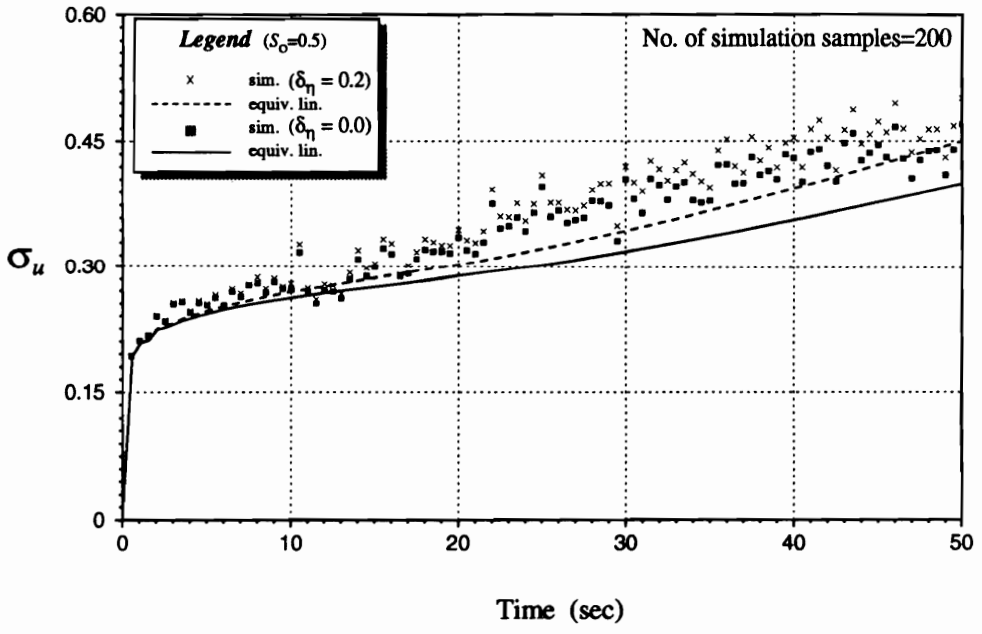

(b) system with ω_o=4.7124 rad/sec

Figure 5.23: Nonstationary RMS displacement response of a SDF system under stationary white noise input- effect of δ_η

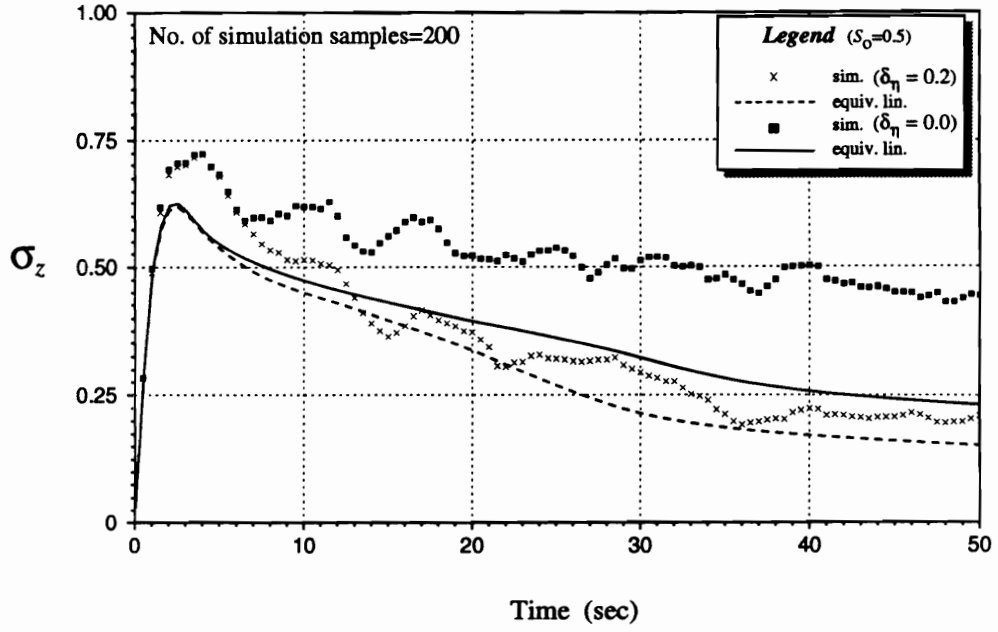

(a) system with ω_o=0.8 rad/sec

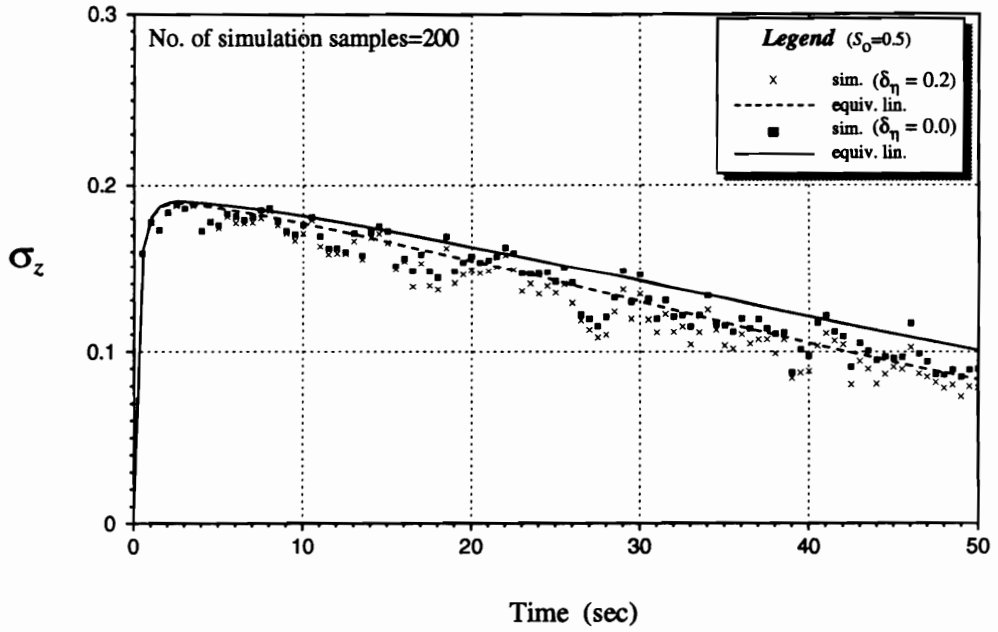

(b) system with ω_o=4.7124 rad/sec

Figure 5.24: Nonstationary RMS restoring force of a SDF system under stationary white noise input- effect of δ_η

forces when there is no degradation and ω_o=0.8 rad/sec. In all other cases, RMS forces are reasonably estimated.

5.5.5 Effect of Pinching Parameters

In this section, the effect of varying pinching parameters (ζ_{1o}, q, p, ψ_o, δ_ψ and λ) on the accuracy of response statistics obtained by statistical linearization will be studied. First, a low pinching system (ζ_{1o}=0.7) is compared with a high pinching system (ζ_{1o}=0.98). Figure 5.25 shows that the linearization solutions are reasonably good in all cases. In Fig. 5.26a (ω_o=0.8 rad/sec), it is seen that although linearization results follow the general trend of RMS forces from MCS, the former underestimates the latter. When ω_o=4.7124 rad/sec (Fig. 5.26b), however, the linearization and MCS results are in excellent agreement at both levels of ζ_{1o}.

Two pinching levels are considered (q=0 and 0.2). Recall that when q=0, the original BWBN model is obtained. Fig. 5.27 shows that, except for a slight underestimation when ω_o=4.7124 rad/sec, $t \geq$20 seconds, linearization results estimate the RMS displacements sufficiently well. Fig. 5.28a (ω_o=0.8 rad/sec) shows that linearization results underestimate the RMS restoring forces. In Fig. 5.28b (ω_o=4.7124 rad/sec), however, generally good agreement between the two solution methods are seen at both levels of pinching.

The influence of p (1.0 and 2.0), a constant that controls the rate of initial drop in slope, on the accuracy of response statistics obtained by statistical linearization is shown in Figs. 5.29 and 5.30. Linearization solutions of RMS displacement compare favorably with those obtained by simulation for both levels of p and both levels of system frequency (Fig. 5.29). Linearization solutions of RMS restoring force, when ω_o=0.8 rad/sec, underestimate those by simulation (Fig. 5.30a). When ω_o=4.7124 rad/sec, linearization results agree very well with simulation results at both levels of p (Fig. 5.30b). Note that when ω_o=0.8 rad/sec, the change of p from 1.0 to 2.0 does not significantly

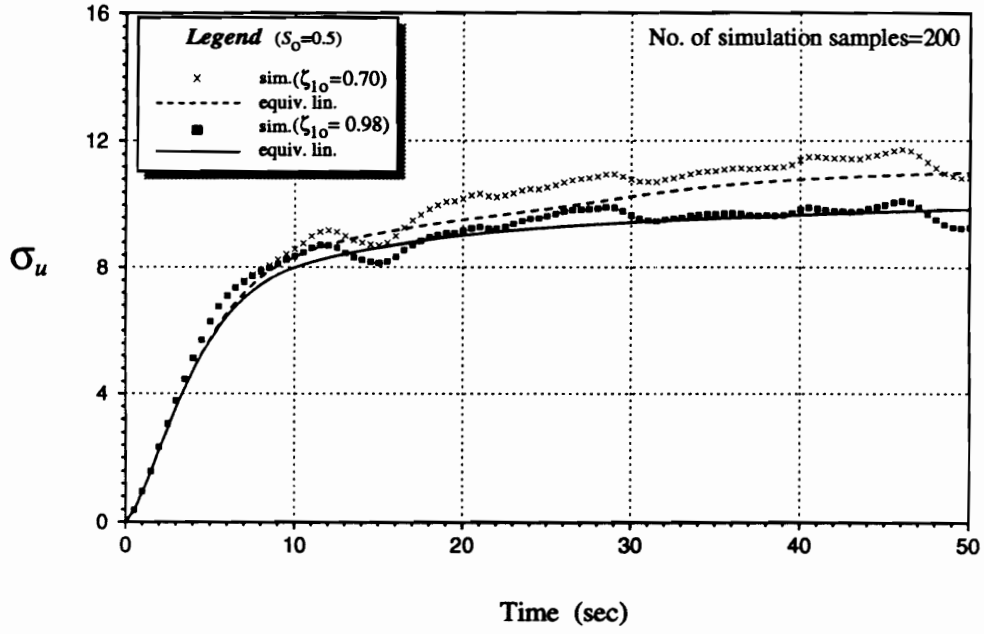

(a) system with ω_o=0.8 rad/sec

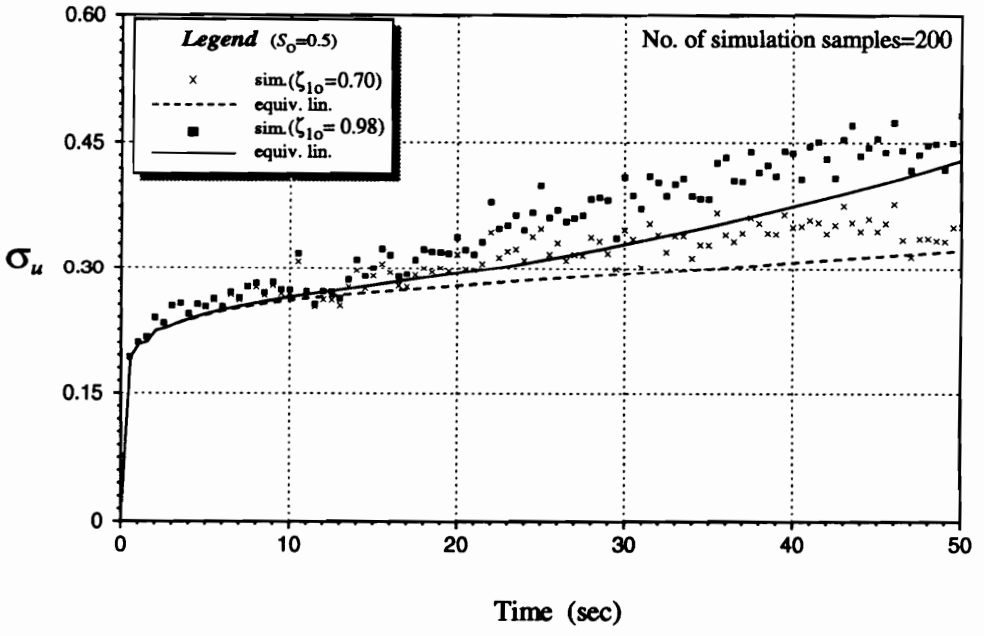

(b) system with ω_o=4.7124 rad/sec

Figure 5.25: Nonstationary RMS displacement response of a SDF system under stationary white noise input- effect of ζ_{1o}

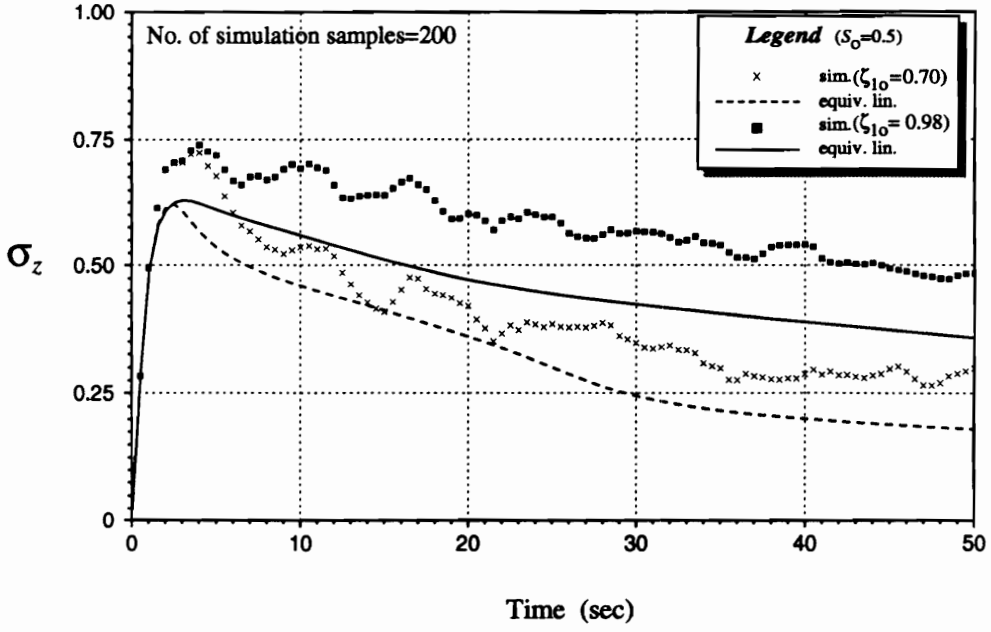

(a) system with ω_o=0.8 rad/sec

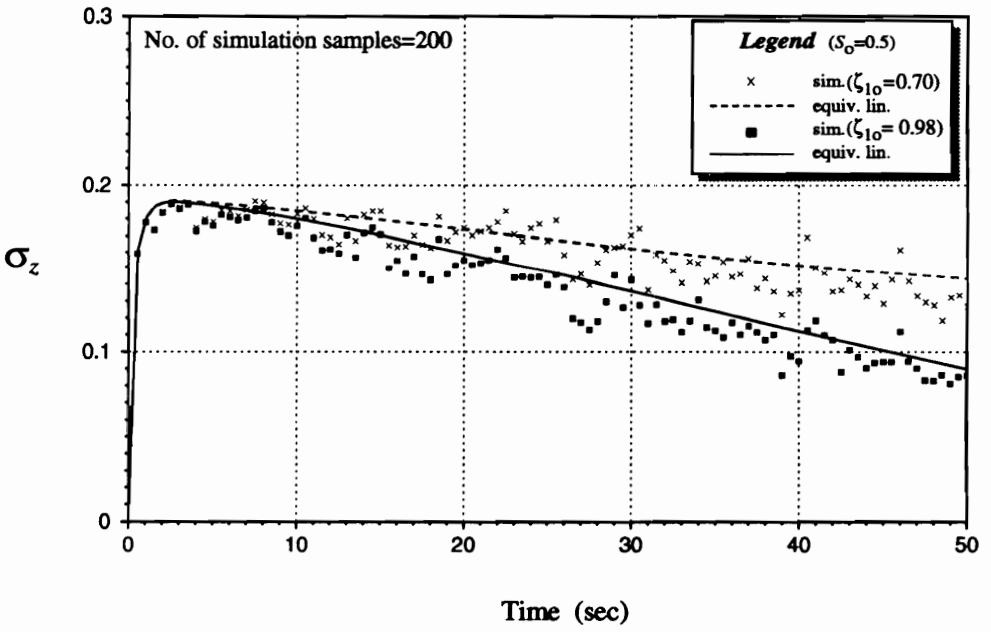

(b) system with ω_o=4.7124 rad/sec

Figure 5.26: Nonstationary RMS restoring force of a SDF system under stationary white noise input- effect of ζ_{1o}

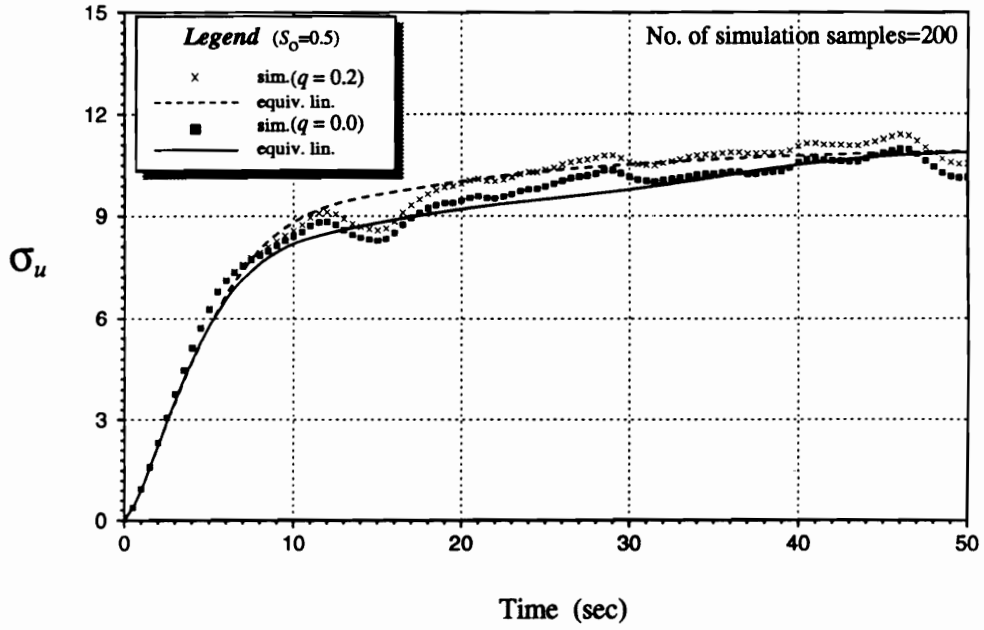

(a) system with ω_o=0.8 rad/sec

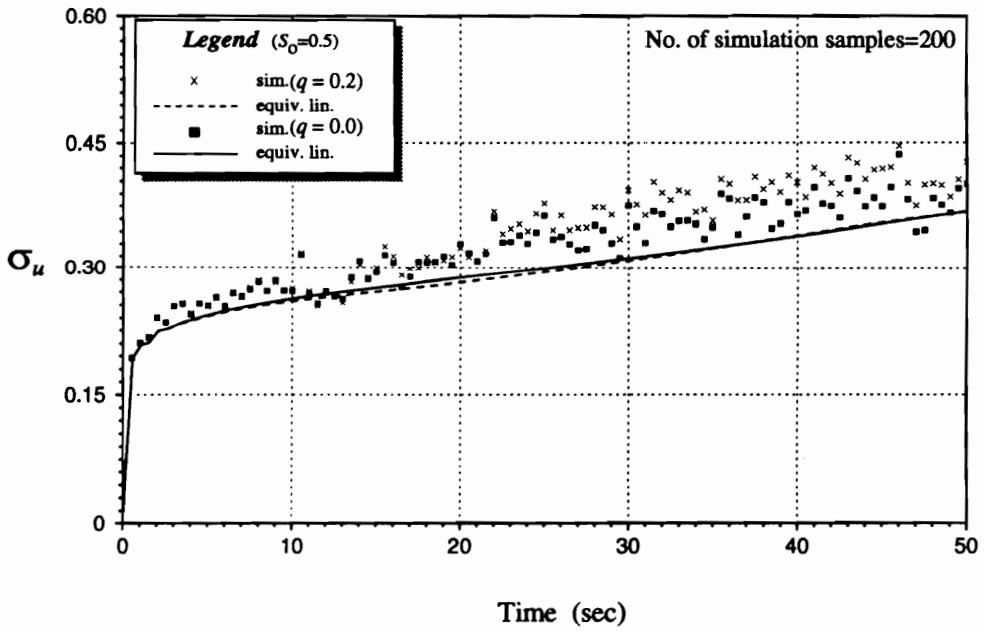

(b) system with ω_o=4.7124 rad/sec

Figure 5.27: Nonstationary RMS displacement response of a SDF system under stationary white noise input- effect of q

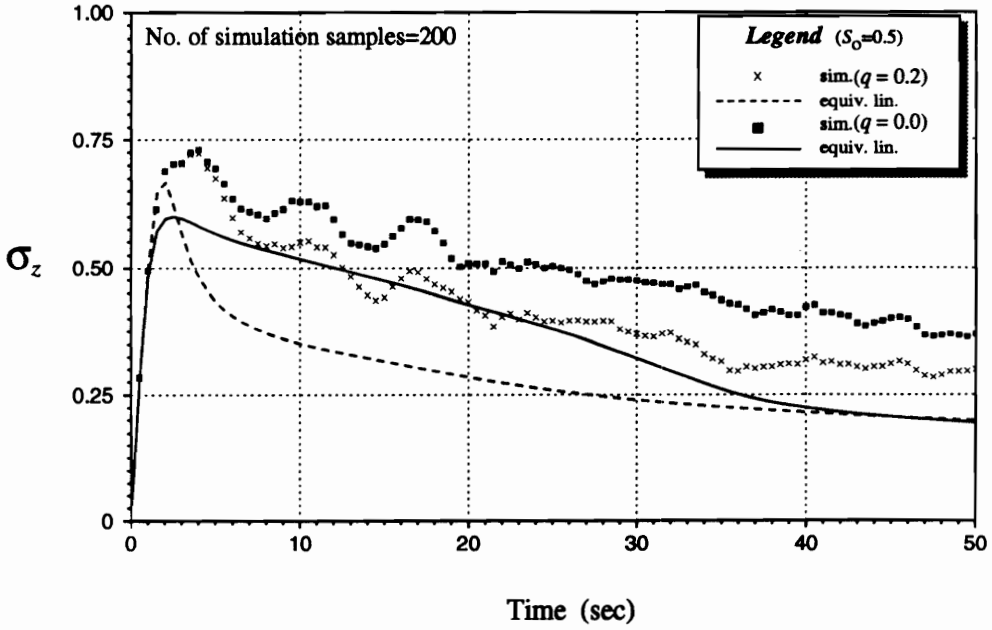

(a) system with ω_o=0.8 rad/sec

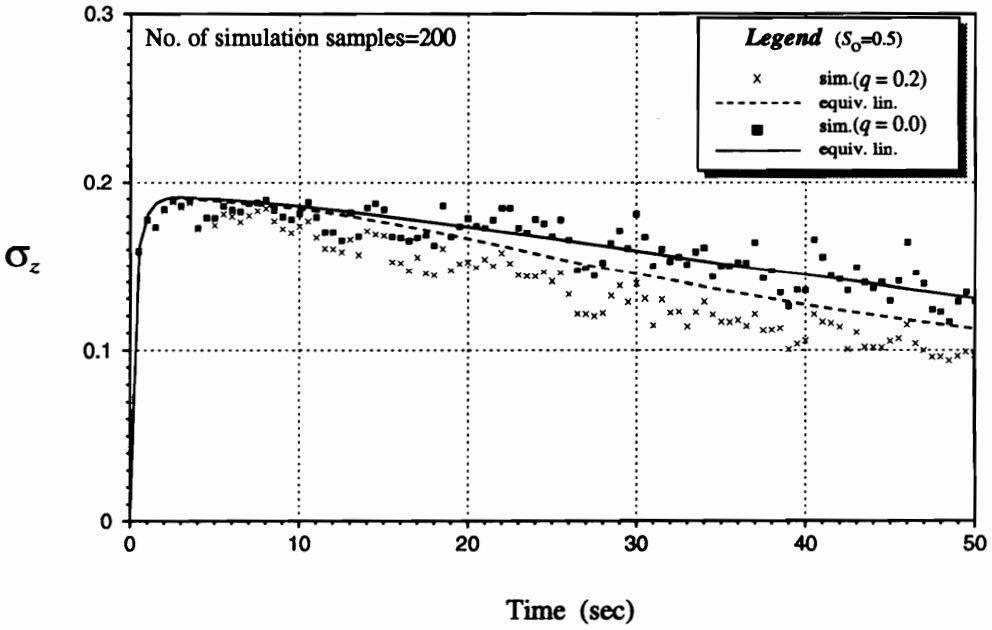

(b) system with ω_o=4.7124 rad/sec

Figure 5.28: Nonstationary RMS restoring force of a SDF system under stationary white noise input- effect of q

affect the response statistics obtained by either the linearization technique or the simulation method (Figs. 5.29a and 5.30a).

Two levels of ψ_o (0.01 and 0.50), a parameter that contributes to the amount of pinching, will be considered. Linearization solutions of RMS displacement compare very well with those by simulation (Fig. 5.31). With RMS restoring force, linearization solutions miss the peak force at both levels of ψ_o when ω_o=0.8 rad/sec; also, linearization solutions underestimate those by simulation when ψ_o=0.50 (Fig. 5.32a). When ω_o=4.7124 rad/sec (Fig. 5.32b), linearization and simulation estimates agree at both levels of ψ_o.

The influence of δ_ψ (0 and 0.2) on the accuracy of response statistics obtained by statistical linearization will be studied. Figure 5.33 shows that linearization estimates of RMS displacements are slightly lower than those of MCS when ω_o=0.8 rad/sec, δ_ψ=0.2 and $t \geq 18$ seconds and when ω_o=4.7124 rad/sec , δ_ψ=0 and $t \geq 18$ seconds. With RMS restoring forces (Fig. 5.34), linearization results compare satisfactorily with MCS results except when δ_ψ=0 and ω_o=0.8 rad/sec.

Finally, linearization and MCS results are compared when λ=0.01 and 0.60. Figure 5.35 shows that this parameter has a minor influence on the RMS displacement response. Linearization results underestimate RMS displacement slightly when ω_o=4.7124 rad/sec, but are generally good, otherwise. In Fig. 5.36a (ω_o=0.8 rad/sec), linearization results underestimate the RMS restoring forces, but preserve the response trend. Good agreement between linearization and MCS results are obtained, however, when ω_o=4.7124 rad/sec (Fig. 5.36b).

5.5.6 Comments

Considering the range of cases studied in the preceding sections (and summarized in Table 5.2), it can be generally stated that statistical linearization gives reasonably good estimates of response statistics. Although plots of variations of RMS velocities and mean energy dissipation of the response with time were not included, they show

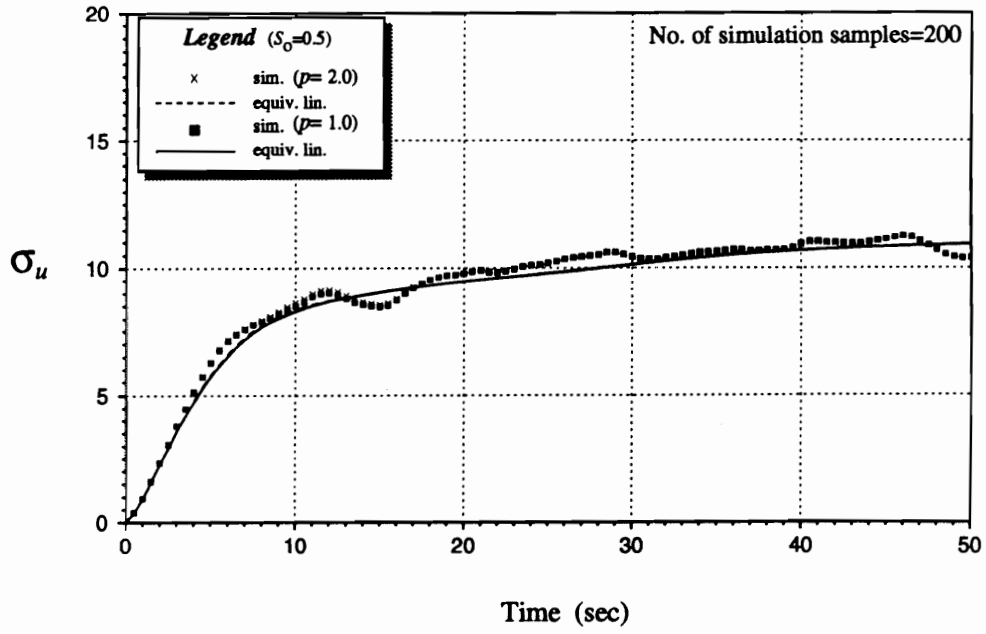

(a) system with ω_o=0.8 rad/sec

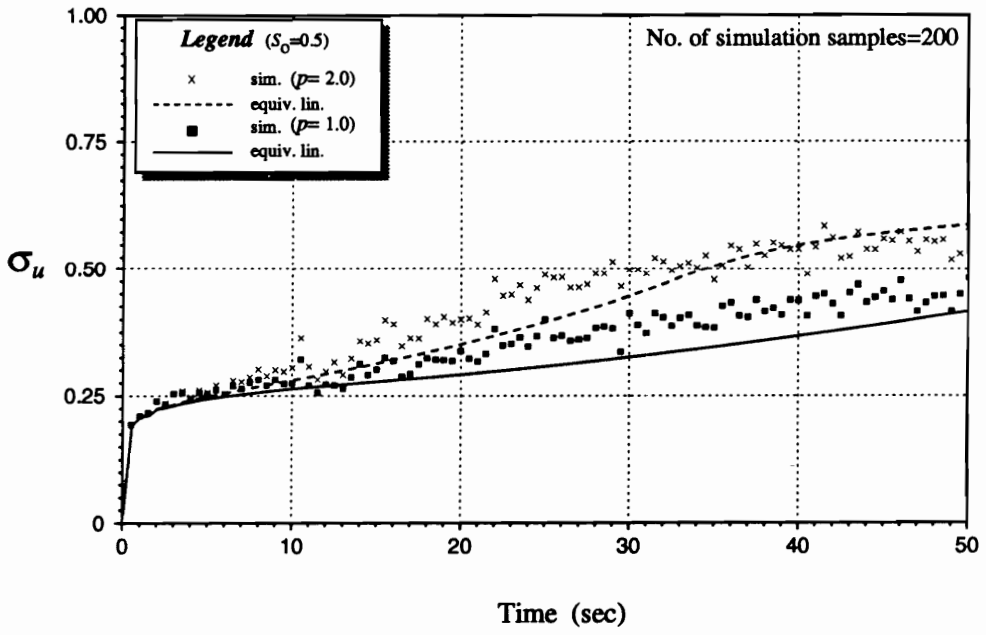

(b) system with ω_o=4.7124 rad/sec

Figure 5.29: Nonstationary RMS displacement response of a SDF system under stationary white noise input- effect of p

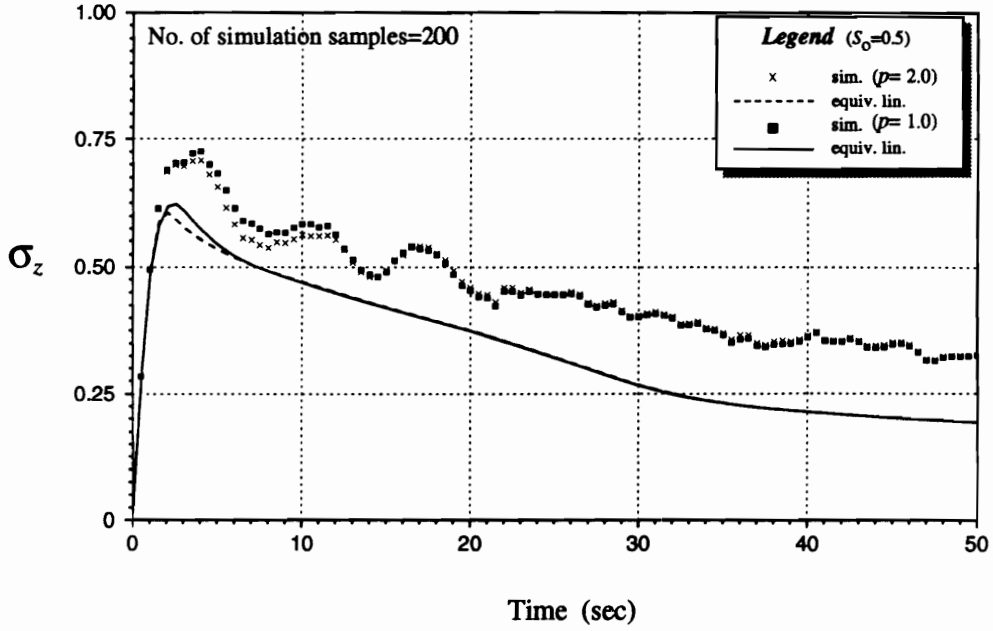

(a) system with ω_o=0.8 rad/sec

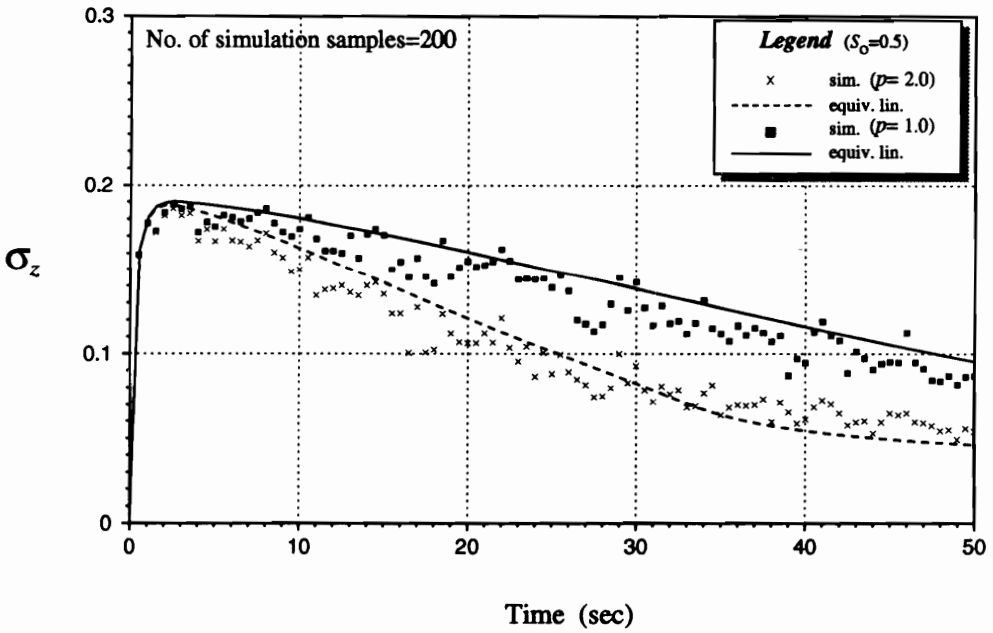

(b) system with ω_o=4.7124 rad/sec

Figure 5.30: Nonstationary RMS restoring force of a SDF system under stationary white noise input- effect of p

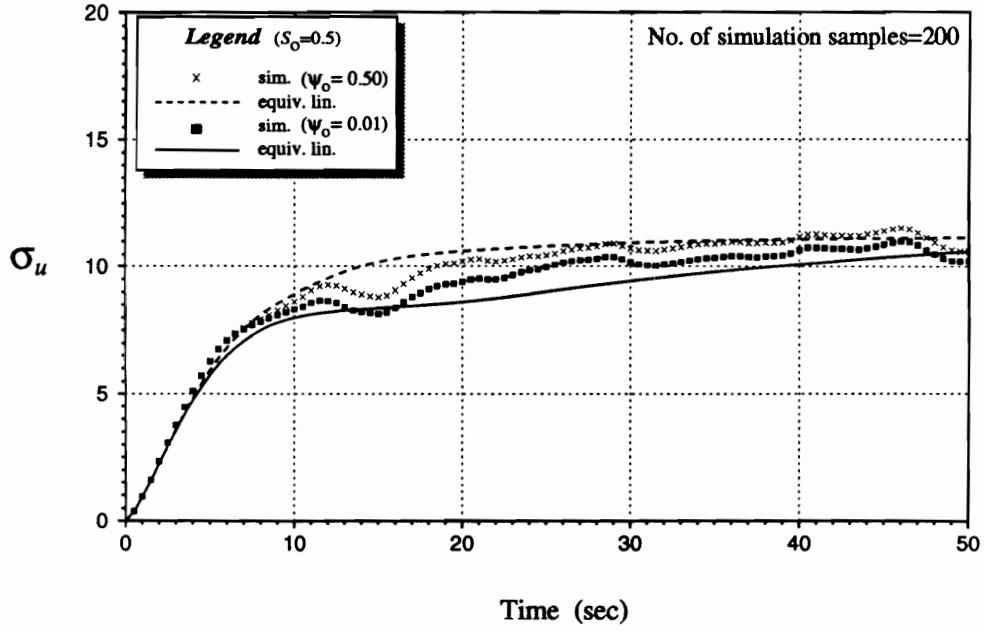

(a) system with ω_0=0.8 rad/sec

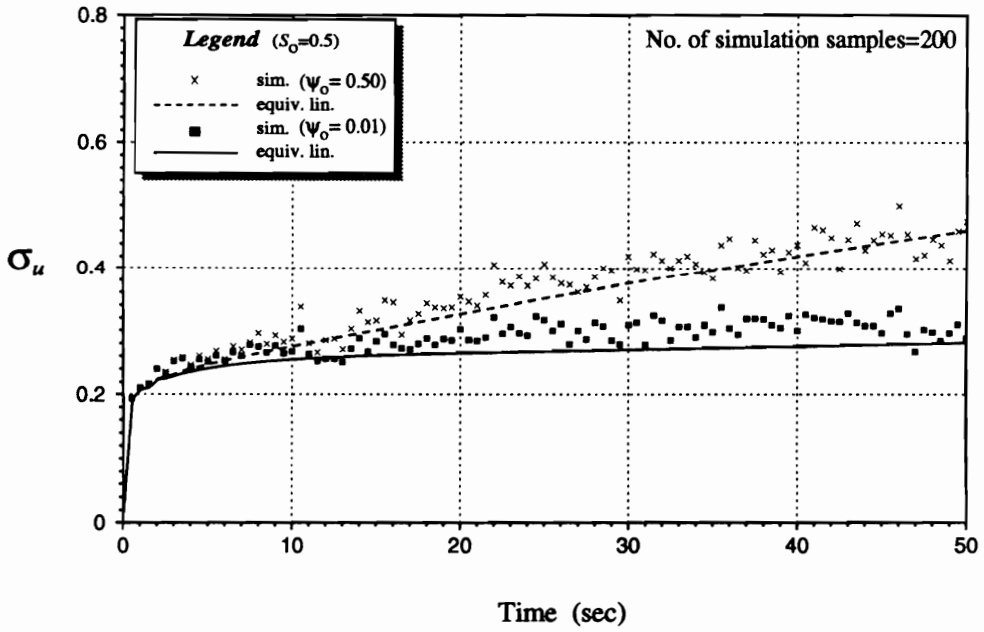

(b) system with ω_0=4.7124 rad/sec

Figure 5.31: Nonstationary RMS displacement response of a SDF system under stationary white noise input- effect of ψ_o

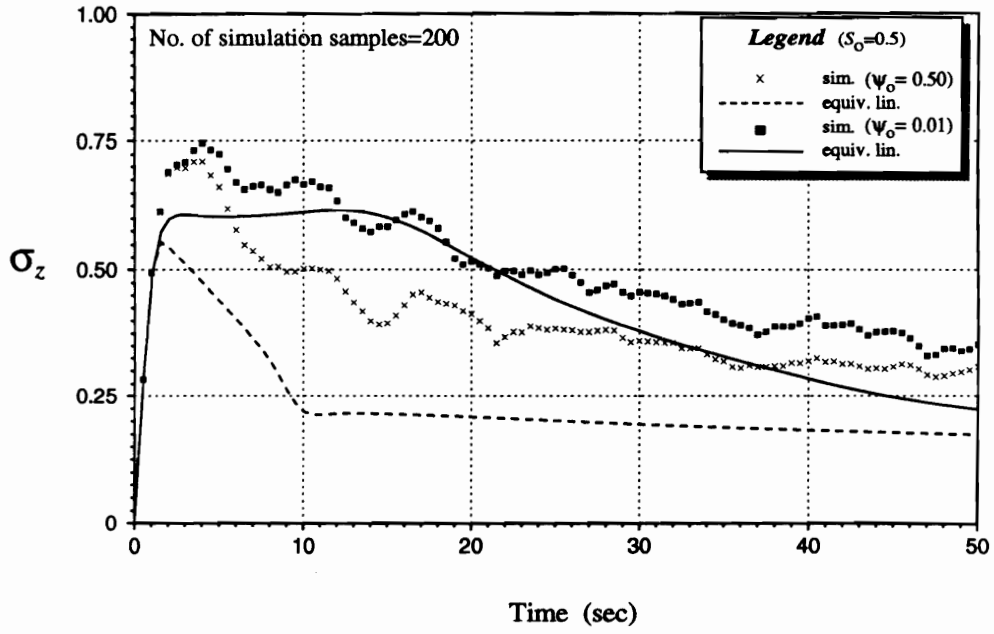

(a) system with ω_o=0.8 rad/sec

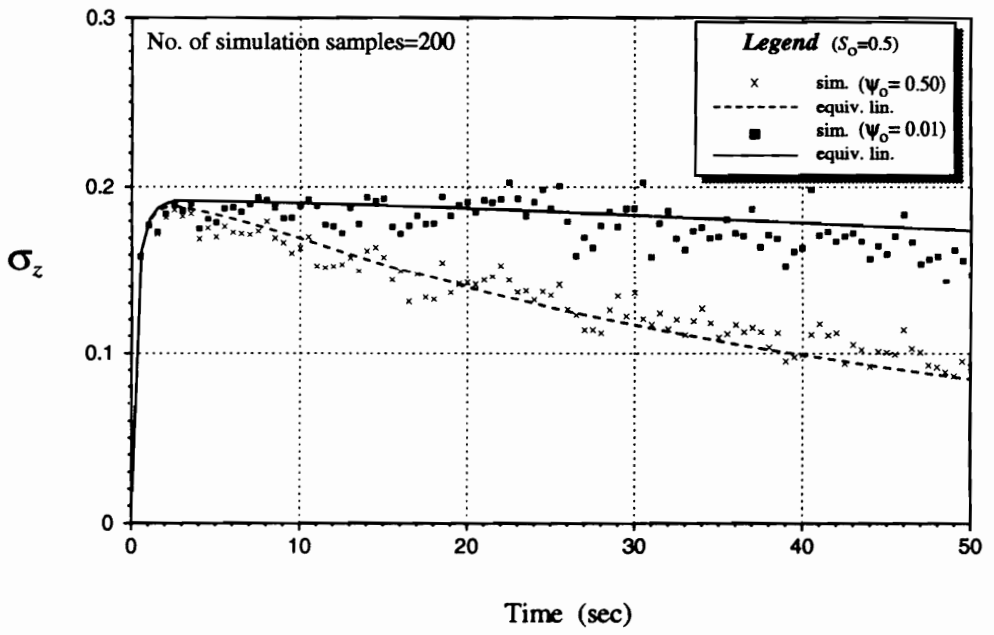

(b) system with ω_o=4.7124 rad/sec

Figure 5.32: Nonstationary RMS restoring force of a SDF system under stationary white noise input- effect of ψ_o

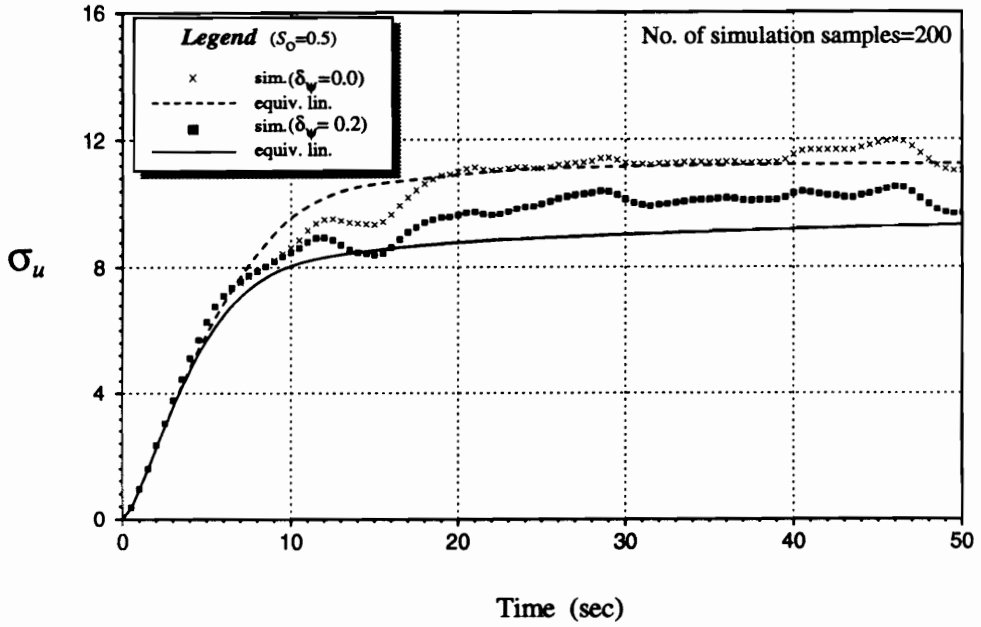

(a) system with ω_o=0.8 rad/sec

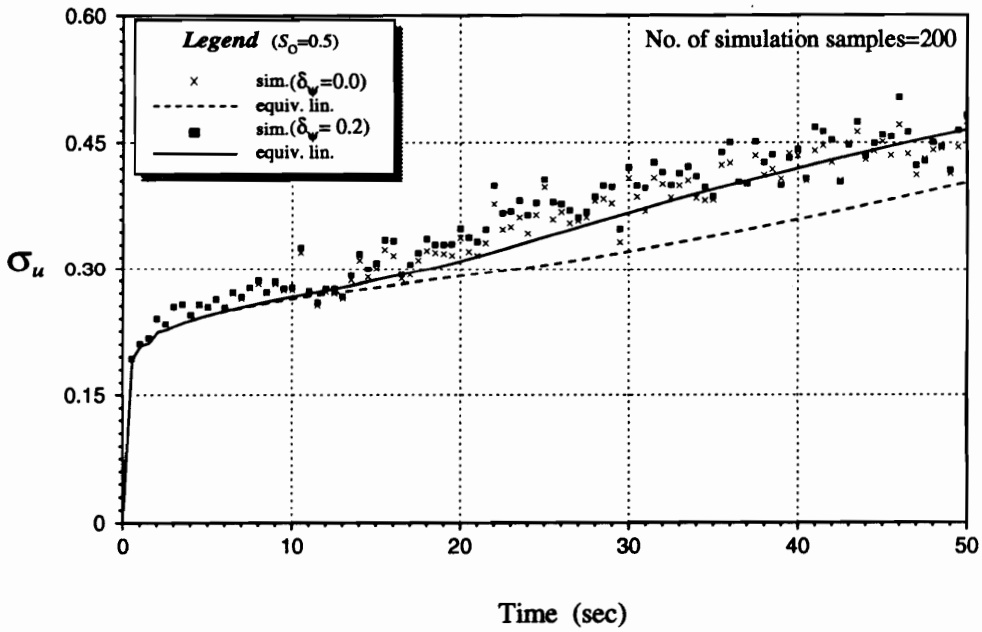

(b) system with ω_o=4.7124 rad/sec

Figure 5.33: Nonstationary RMS displacement response of a SDF system under stationary white noise input- effect of δ_ψ

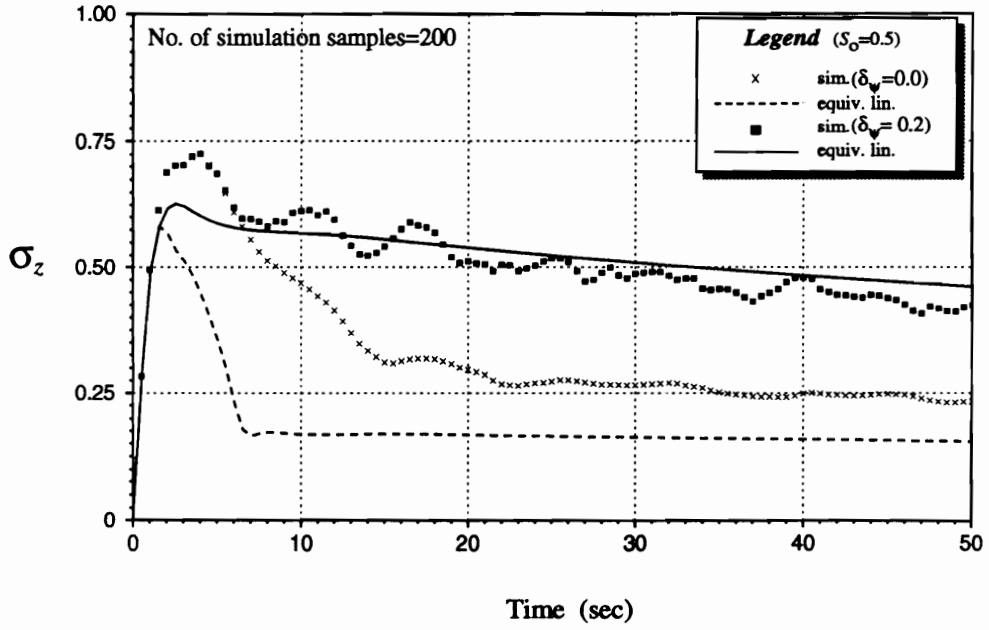

(a) system with ω_o=0.8 rad/sec

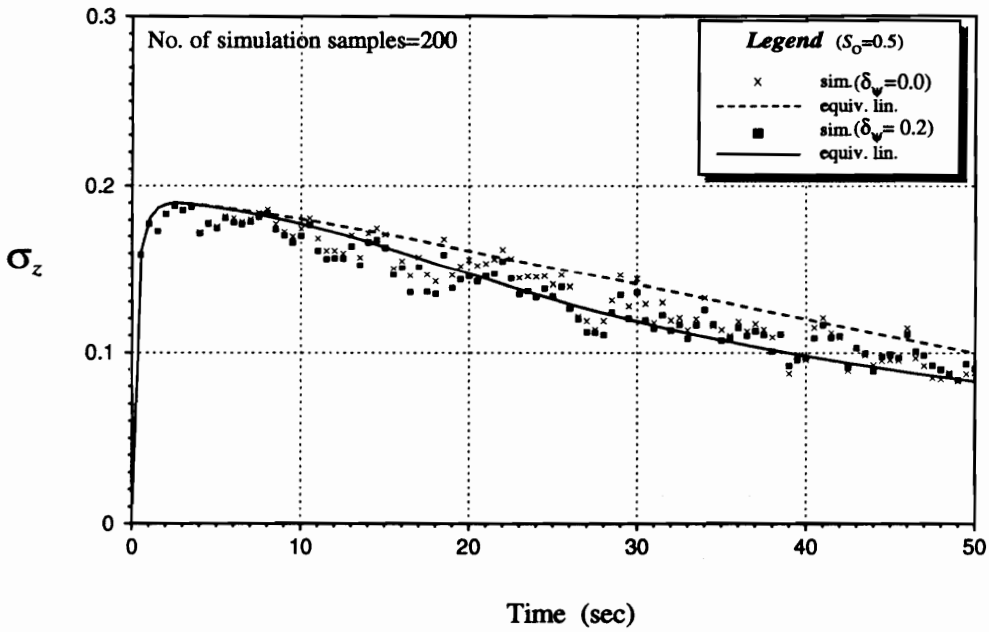

(b) system with ω_o=4.7124 rad/sec

Figure 5.34: Nonstationary RMS restoring force of a SDF system under stationary white noise input- effect of δ_ψ

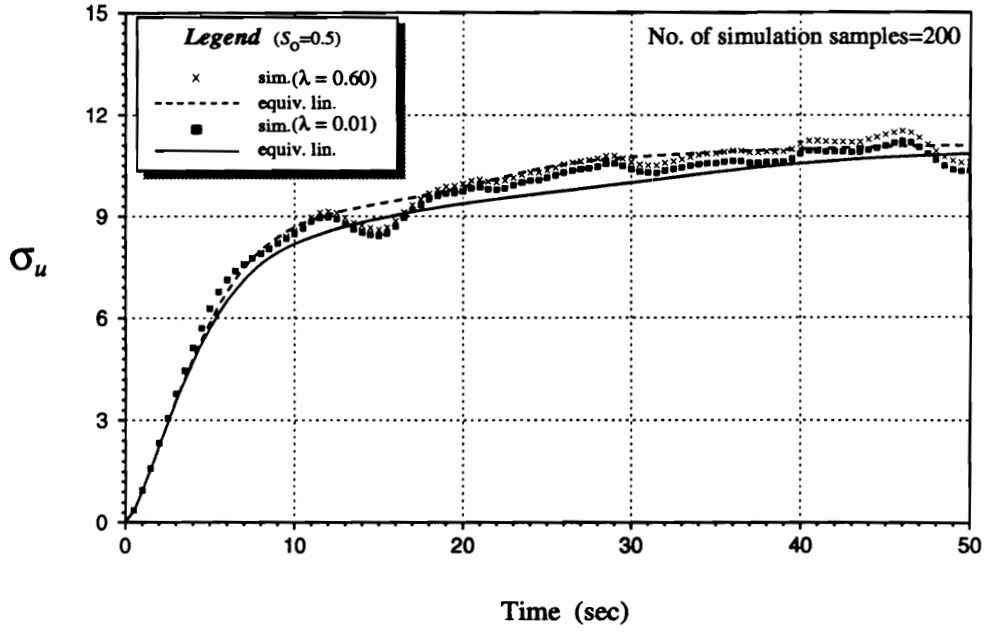

(a) system with ω_o=0.8 rad/sec

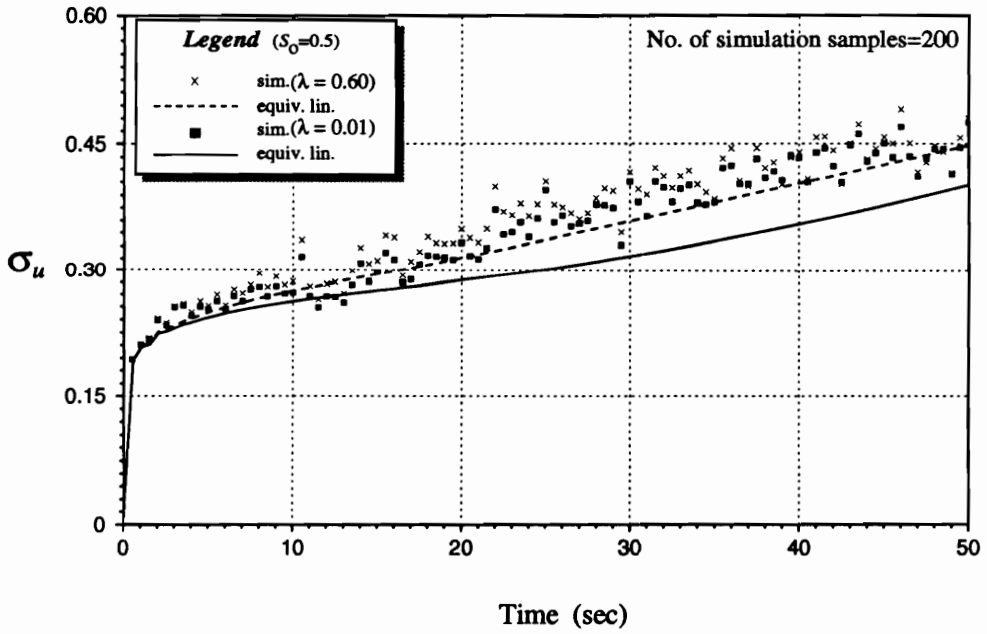

(b) system with ω_o=4.7124 rad/sec

Figure 5.35: Nonstationary RMS displacement response of a SDF system under stationary white noise input- effect of λ

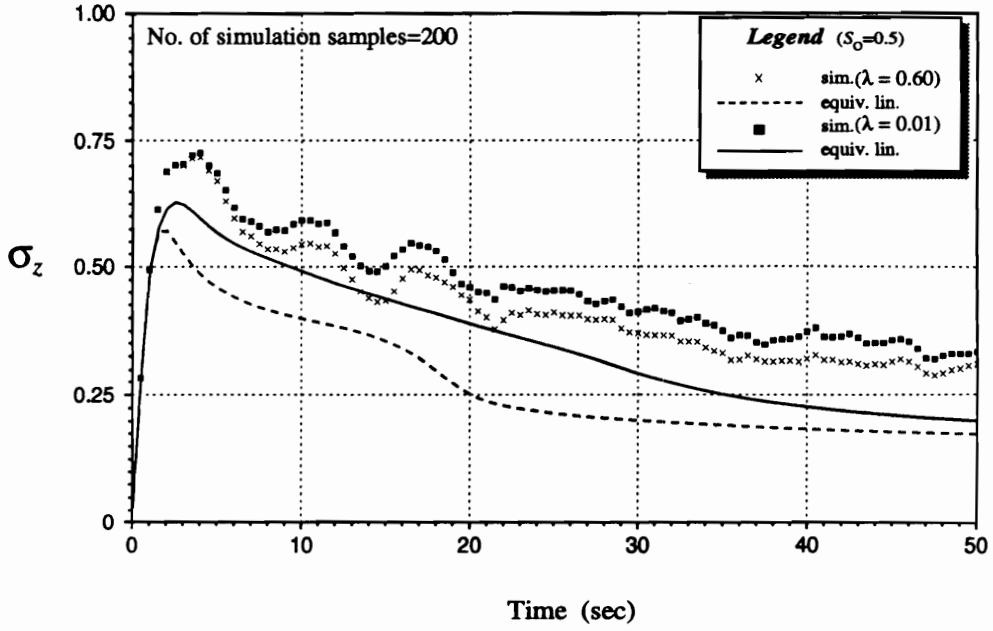

(a) system with ω_0=0.8 rad/sec

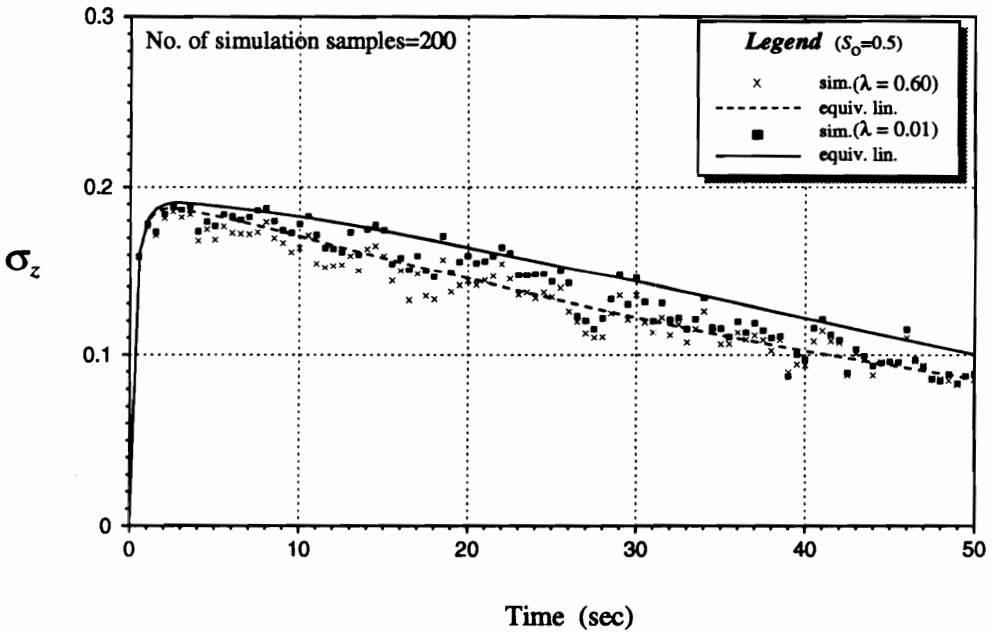

(b) system with ω_0=4.7124 rad/sec

Figure 5.36: Nonstationary RMS restoring force of a SDF system under stationary white noise input- effect of λ

better accuracy of linearization estimates than that seen for RMS displacements and restoring forces in Figs. 5.15 to 5.36. Results of numerical studies have shown that, for structures with low system natural frequency (e.g., ω_o=0.8 rad/sec), pinching parameters p and λ do not significantly affect mean-square response statistics, and may, thus, be set to some constant value.

A general trend that can be clearly observed from the plots in Figs. 5.15 to 5.36 is the relatively poorer linearization estimates for RMS restoring forces when ω_o=0.8 rad/sec. In most cases, however, relative errors between the linearization and the MCS estimates are within the range 0 to 20 percent found to be representative of linearization solutions (Spanos 1981; Branstetter et al. 1988; Roberts and Spanos 1990). The linearization solutions tend to be on the nonconservative side, underestimating the exact RMS responses most of the time. This tendency is consistent with that found in previous studies (Spanos 1981; Wen 1986; Branstetter et al. 1988; Roberts and Spanos 1990) and has been "attributed to the fact that the linearized system response follows a Gaussian probability law whereas the response of the original nonlinear system may deviate significantly from a Gaussian law at the extreme tail" (Wen 1986). And since the linearization is based on the minimization of the mean-square errors, prediction of statistical moments of the response (covariance matrix) are typically good, as shown here, while prediction of extreme value and autocorrelation function may not be as good.

Successful application of the method of statistical linearization in random vibration analyses of degrading hysteretic systems with general pinching behavior reinforce the claim of flexibility, efficiency and reasonable acccuracy of this method. A word of caution, however, is in order; quoting Roberts and Spanos (1990),

> Generally, the extensively documented accuracy of the statistical linearization technique for estimating the statistical moments for system response, for a broad class of nonlinear problems of engineering practice, should be deemed as a reasonable basis for attempting to use the method for a new

problem of interest. Nevertheless, indiscriminate dependence on the results of the method is inadvisable. A more logical approach could involve the prior verification of a representative set of response statistics derived by the method of statistical linearization by comparisons with Monte Carlo simulations. Then, the method can be used repeatedly as the basis of critical technical estimations regarding a particular problem of interest.

As the comparisons of MCS and linearization results showed, there may be a few cases, especially at low natural frequency, where statistical linearization solutions severely underestimate the mean-square response of a SDF system with the modified BWBN restoring force model. This section provides an example verification procedure that can be used in applying the method to specific engineering problems. The solution method presented herein is general and can be applied not only in random vibration analysis of wood structural systems but also in the analysis of a wide variety of hysteretic systems with pinching behavior, including reinforced concrete structures, braced steel frames and laterally loaded piles.

5.6 Potential Applications in System Performance Evaluation

Potential practical applications of the analysis method discussed in the previous section and of the response statistics obtained from the analysis will be presented here. No additional work will be performed.

5.6.1 Design Response Value Calculation

Although the method of statistical linearization is best suited in the first stage of design (i.e., finding an optimum system configuraton) as discussed in section 5.4.1, there are situations when the precise shape of the probability distribution of the response in its extreme tails is not available and the cost of MCS studies is prohibitive. Response analysis results using statistical linearization may still be used in designing

for maximum response. In this case, the approximate percentile values of design responses of interest, such as displacement of a point, member forces, floor acceleration, etc., are obtained by: (*1*) calculating the response standard deviations, σ or RMS, and (*2*) amplifying the standard deviations by a peak factor, F_p. The method of statistical linearization was shown to reasonably estimate RMS responses of SDF wood systems in the previous section. Here, two common methods of obtaining a maximum design response value are presented. The concepts involved are related to the first-passage time problem of probability theory. It should be emphasized that the computed design response represents the probable maximum response of the system from an ensemble of possible ground motion histories.

Let us consider mass displacement, u, of the SDF wood system as the response of interest. If we assume a maximum response level, U_{max}, in either direction and allow a small probability, p_o, of exceeding this value in time t_d (Fig. 5.37), we can obtain U_{max} as

$$U_{max} = F_{p_1}\, \sigma_u \tag{5.78}$$

where F_{p_1} is the peak factor, given by

$$F_{p_1} = \left\{ 2 \ln \left[-\frac{1}{\pi} \frac{\sigma_{\dot{u}}}{\sigma_u} \frac{t_d}{\ln(1 - p_o)} \right] \right\}^{1/2} , \tag{5.79}$$

if the excursions are assumed as a Poisson process.

Examination of Eq. (5.79) shows that it varies mildly with changes in t_d, $\sigma_{\dot{u}}/\sigma_u$ or the natural frequency of the system ω_o. Thus, F_{p_1} is normally assumed constant; a value of 3 to 5 may be satisfactory. For $F_{p_1} = 3$, the design response value is 3 standard deviations higher than the mean.

If, on the other hand, the mean of the maximum response U_{max} is needed, Davenport (1964) proposed the following peak factor formula:

$$F_{p_2} = \sqrt{2 \ln \left(\frac{\sigma_{\dot{u}} t_d}{\sigma_u \pi} \right)} + \frac{0.5772}{\sqrt{2 \ln \left(\frac{\sigma_{\dot{u}} t_d}{\sigma_u \pi} \right)}} . \tag{5.80}$$

Then, the mean of the maximum response may be computed as

$$\mu_{U_{max}} = F_{p_2}\, \sigma_u . \tag{5.81}$$

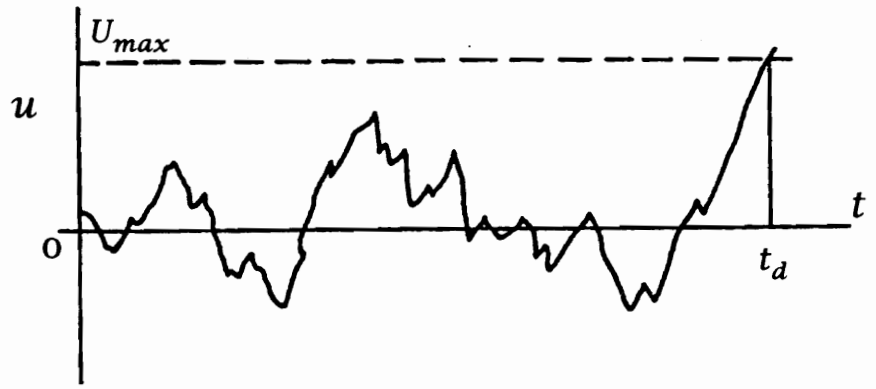

Figure 5.37: First crossing of maximum response U_{max}

The foregoing shows that, in certain cases, response statistics obtained by statistical linearization can be used directly in design. Use of the equations given above is straightforward and will not be demonstrated.

5.6.2 Dynamic Reliability Analysis

The response statistics obtained in random vibration analysis can also be used in structural reliability analysis. The following discussion is based on the work of Shinozuka (1964) and Shinozuka et al. (1968). Other approaches may be used [see, for example, Baber (1980)]. Again considering the displacement u, its upper and lower bounds can be determined for the probability $P(u, U_{max})$ that the absolute value of u will exceed a threshold value U_{max} (> 0) in an arbitrary time interval. The upper bound $P_u(u, U_{max})$ is given by

$$P_u(u, U_{max}) = \int_0^\infty [h_1(t) + h_2(t)]\, dt \tag{5.82}$$

where $h_1(t)$ is the rate of u crossing the threshold U_{max} from below and $h_2(t)$ is the rate of u crossing $-U_{max}$ from above. They are given by

$$h_1(t) = \int_0^\infty \dot{u}\, f_{U\dot{U}}(U_{max}, \dot{u})\, d\dot{u} \tag{5.83}$$

$$h_2(t) = \int_{-\infty}^0 |\dot{u}|\, f_{U\dot{U}}(-U_{max}, \dot{u})\, d\dot{u} \tag{5.84}$$

where $f_{U\dot{U}}(u, \dot{u})$ is the joint probability density function of u and $\dot{u}$. Assuming a zero-mean Gaussian response process, as in random vibration analysis, $f_{U\dot{U}}(u, \dot{u})$ is given in the form of Eq. (5.36). The lower bound $P_l(u, U_{max})$, on the other hand, is given by

$$P_l(u, U_{max}) = \max_{0<t<\infty} [P\{u > U_{max}\} + P\{u < -U_{max}\}] \tag{5.85}$$

With the aid of the equations given above, Shinozuka et al. (1968) showed that the upper bound $P_u(u, U_{max})$ is computed as

$$P_u(u, U_{max}) = \frac{1}{\pi}\frac{\sigma_{\dot{u}}}{\sigma_u} \int_0^\infty \left\{ \sqrt{1-\rho_{u\dot{u}}^2} \exp\left[-\frac{1}{2(1-\rho_{u\dot{u}}^2)} \left(\frac{U_{max}}{\sigma_u}\right)^2 \right] + H(\rho_{u\dot{u}}) \sqrt{2\pi\rho_{u\dot{u}}} \frac{U_{max}}{\sigma_u} \exp\left[-\frac{1}{2}\left(\frac{U_{max}}{\sigma_u}\right)^2 \right] \right\} dt \tag{5.86}$$

where $H(\cdot)$ is the Heaviside function, $\bar{\sigma}_u$ is the maximum standard deviation of u that occurs at $t = \bar{t}$ (i.e., $\bar{\sigma}_u = E[u^2(\bar{t})]$). The lower bound $P_l(u, U_{max})$ is given by either

$$P_l(u, U_{max}) = 2\left[1 - \Phi\left(\frac{U_{max}}{\bar{\sigma}_u}\right)\right], \tag{5.87}$$

in terms of the standardized normal cumulative distribution function $\Phi(\cdot)$, or

$$P_l(u, U_{max}) = 1 + \text{erf}\left(-\frac{U_{max}}{\bar{\sigma}_u\sqrt{2}}\right), \tag{5.88}$$

in terms of the error function $\text{erf}(\cdot)$ (see Appendix B).

Structural reliability analyses can now be performed using Eqs. (5.86) and either (5.87) or (5.88). The threshold value U_{max} should be specified from the system's lateral resisting capacity.

5.6.3 Seismic Damage Analysis

The underlying concept in most seismic design codes does not allow damage during low magnitude earthquakes, allows some damage during moderate or intermediate tremors and prevents collapse during severe earthquakes. Limiting the potential damage to some tolerable level is, however, only implied in most design codes because they are based largely on qualitative engineering judgment. Thus, Ang (1988) and his associates used the Bouc-Wen model (or the non-degrading, non-pinching BWBN model) to develop a reliability-based damage-limiting seismic design procedure for reinforced concrete buildings. A similar approach was used to perform seismic damage analysis of unreinforced masonry buildings (Kwok 1987). Structural damage was quantified using a damage index expressed as a combination of maximum displacement and hysteretic energy dissipation. Both quantities can also be obtained from random vibration analysis of hysteretic wood systems using the proposed model. Following Ang's work, random vibration analysis of wood structural systems using the proposed hysteresis model could provide a method for *(1)* cumulative damage model development for, and *(2)* safety and damage assessment of, wood structures subjected to dynamic loading.

Following DiPasquale et al. (1990), structural damage can be generally described as a function, $f : \mathbf{R}^n \rightarrow \mathbf{R}^n$. The function, f, is defined on the volume (Ω) occupied by the structure and normally takes values in the interval (0,1). It describes the loss of resistance in the neighborhood of a given point. The global damage state can thus be defined as a functional of f,

$$D_T = \int_\Omega w(\mathbf{x})\, f(\mathbf{x})\, d(\mathbf{x}) \tag{5.89}$$

where $w(\mathbf{x})$ is an appropriate weighting function.

For practicality, the damaged state is reduced to a finite number of dimensions, by lumping procedures, in order to solve the problem of damage assessment for a real structure. The structure is modeled as an assemblage of elements and joints, for each of which a damage index is computed from the history of loading during the earthquake (DiPasquale et al. 1990). The global damage index may then be expressed as a weighted average of the damage indices for the single elements (Park et al. 1985). In a MDF shear-beam model, for example, the storey damage, D_i, is weighted by the energy absorbing contribution factor, ϕ_i. Then, the overall damage index is obtained by

$$D_T = \sum_i \phi_i D_i \tag{5.90}$$

where

$$\phi_i = \frac{E_{a_i}}{\sum_i E_{a_i}}$$

in which E_{a_i} is the total absorbed energy (including the potential energy) of the ith storey.

The foregoing implies that we need only to determine a damage function that reasonably represents the governing damage process at an element to obtain a global measure of building damage. In timber structures, an appropriate damage function for connections need to be determined.

Consistent with the damage process in wood connections, the form of the proposed

damage function by Park and Ang (1985), given as

$$D = \frac{\delta_m}{\delta_u} + \frac{\kappa}{Q_y \delta_u} \int dE \tag{5.91}$$

where

δ_m = maximum deformation under earthquake,

δ_u = ultimate deformation under monotonic loading,

Q_y = calculated joint yield strength,

dE = incremental absorbed hysteretic energy,

κ = non-negative parameter,

or its variations can be used. With this function, damage may be caused by a single severe (stress) excursion as well as by repeated stress reversals. Energy dissipation is a good measure of cumulative damage under stress reversals because it mirrors the loading history and parallels the process of damage evolution (Ang and Wen 1988). Furthermore, the form of Eq. (5.91) has already been successfully used to model damage in reinforced concrete and unreinforced masonry buildings (Park and Ang 1985; Park et al. 1987; Kwok 1987; Ang and Wen 1988).

5.7 Summary

Basic concepts of random vibration theory, related to the present work, were reviewed. Nonlinear random vibration analysis of single-degree-of-freedom (SDF) wood structural systems, modeled by the modified Bouc-Wen-Baber-Noori (BWBN) restoring force model, was presented. A stationary Gaussian white noise process was used to model the random characteristics of earthquakes. Nonstationary response statistics of SDF wood systems were obtained by Monte Carlo simulation and statistical linearization. It was shown that, for a range of practical system and model parameter values, the statistical linearization solutions give reasonably good estimates of response statistics. This technique is sufficient in obtaining relevant response statistics that can be used

in finding an optimum system configuration for design and, in some cases, in calculating design response values. An example verification procedure that can be used in applying the method to new engineeering problems was presented. The response analysis technique is general and can be applied not only in random vibration analysis of wood structural systems but also in the analysis of a wide variety of hysteretic systems with general pinching behavior, including reinforced concrete structures, braced steel frames and laterally loaded piles. It can also be applied to multi-degree-of-freedom systems, as long as appropriate structural models are available and appropriate hysteresis model parameters for these systems are known.

Potential practical applications of the analysis method and of the response statistics obtained from the analysis were presented. Successful application of the method of statistical linearization in random vibration analysis of wood structural systems opens up future research opportunities, in the league of those in other structural materials, in the area of analysis and design of timber structures against natural hazards. This could help narrow the gap between advances in general structural dynamics and those in wood engineering and, thus, improve the competitiveness of engineered wood systems.

Chapter 6

Summary, Conclusions and Recommendations

6.1 Summary and Conclusions

A general hysteresis model for wood joints and structural systems was developed and used to obtain the nonstationary response statistics of wood structural systems under earthquake-type loadings, modeled as a random process. The new restoring force model is a modification of the Bouc-Wen-Baber-Noori (BWBN) model. The hysteretic constitutive law, based on the endochronic theory of plasticity and characterized by a single mathematical form, produces a versatile, smoothly varying hysteresis that models previously observed behavior of wood joints and structural systems, namely, (*1*) nonlinear, inelastic behavior, (*2*) stiffness degradation, (*3*) strength degradation, (*4*) pinching, and (*5*) memory. The constitutive law takes into account the experimentally observed dependence of wood joints' response to their past history (i.e., the input and response at earlier times, or memory).

Practical guidelines to estimate the hysteresis parameters of any wood joint or structural system were given. Hysteresis shapes produced by the proposed model were shown to compare reasonably well with experimental hysteresis of wood joints with: (*1*) yielding plates, (*2*) yielding nails, and (*3*) yielding bolts.

The model is versatile and can actually model a wide variety of hysteresis shapes, degradations, and pinching behavior to cover a whole gamut of possible combinations of materials and joint configurations in wood systems. Continued evolution of wood-based products, fasteners, and use of wood-based products need not be a problem, as long as hysteresis data from tests of representative wood joints or structural systems

are available, from which model parameters can be estimated.

The proposed model was verified using a nonlinear dynamic analysis program for single-degree-of-freedom (SDF) systems. Three SDF wood systems were subjected to the Loma Prieta accelerogram to obtain their response time histories. Advantages of using the proposed model over currently available models in nonlinear dynamic analysis of more complex systems were identified. A multi-degree-of-freedom (MDF) shear building model incorporating the proposed hysteresis model was formulated but not implemented on a computer.

For more realistic loadings, the random characteristics of earthquakes were modeled as a stochastic or random process. Nonlinear response statistics of SDF wood systems were obtained by Monte Carlo simulation and statistical linearization. It was shown that, for a range of practical system and model parameter values, the statistical linearization solutions give reasonably good estimates of mean-square response. An example verification procedure that can be used in applying the method to practical engineering problems was presented. The response analysis technique is general and can be applied not only in random vibration analysis of wood structural systems but also in the analysis of a wide variety of hysteretic systems with general pinching behavior, including reinforced concrete structures, braced steel frames and laterally loaded piles. It can also be applied to MDF systems, as long as appropriate structural models are available and appropriate hysteresis model parameters for these systems are known.

Potential practical applications of the analysis method and of the response statistics obtained from the analysis were presented. The present work is the first known attempt to use random vibration techniques in studying the response of wood structures under natural hazard loadings. Successful application of the method of statistical linearization in random vibration analysis of wood structural systems opens up future research opportunities, in the league of those in other structural materials, in the area

of analysis and design of timber structures against natural hazards. These opportunities will be discussed next.

6.2 Recommendations for Future Work

Research on dynamic analysis of wood structures has lagged behind advances in general structural dynamics mainly because of (*1*) many factors affecting the collection of test data and (*2*) difficulties in characterizing the dynamic behavior of wood joints and structural systems. The latter hindered investigations into their performance under dynamic loading. The present work attempted to address this problem and succeeded in (*1*) deriving a general hysteresis model for wood structures, and (*2*) using the model to obtain the nonstationary response statistics of wood structural systems under earthquake-type loadings, modeled as a random process. It is clear, however, that this is just the first step. Much work remains to be done. The following topics are recommended for future work:

1. *System Identification* - although some practical guidance has been presented to obtain hysteresis parameters for any wood system, it is ideal that system identification techniques be used to estimate the parameters of the proposed model (section 4.3). This will allow us to: (*a*) systematically obtain a system model from laboratory or field data for predicting the structural response of similar real-world systems during earthquake or wind events, and (*b*) estimate the existing conditions of structures for the assessment of damage and deterioration. If successful, hysteresis parameters of any system configuration and material combination can be systematically estimated as long as hysteresis data are available. Furthermore, various types of sensitivity and parametric studies, like those mentioned by Stalnaker and Gramatikov (1991), can be performed using the model, without the need for additional physical testing. Model parameters that critically affect the

ductility, serviceability and safety of the wood structure under study can be identified.

2. *Multi-degree-of-freedom Systems* - the model for MDF shear buildings that was formulated in the present work (section 4.2.2) should be implemented numerically for random vibration analyses (both Monte Carlo simulation and statistical linearization) [e.g., Baber (1980) and Baber and Wen (1981)]. The proposed hysteresis model should also be incorporated in the formulation of discrete hinge and finite element models for wood structural systems. Incorporation of the hysteresis model to commercial dynamic analysis programs should also be explored. The modified BWBN model is, in fact, applicable to structures made of other materials, such as steel and reinforced concrete, and may also be used for deterministic dynamic and random vibration analyses of these structures.

3. *Dynamic Reliability Analysis and First-Passage Studies* - the present random vibration analysis yielded the zero time lag covariance matrix with estimates of the system's mean-square statistics. While these are useful quantities, there are many cases, especially in seismic design, where accurate statistics of maximum response, instead of mean-square response, are needed. Studies of maximum response statistics fall under the domain of first-passage time problems. One approach was introduced in section 5.6.2. Other methods may be found in Baber (1980).

4. *Seismic Damage Analysis* - structural damage due to a seismic event may be quantified using a damage index expressed as a combination of maximum displacement and hysteretic energy dissipation (see section 5.6.3). Both quantities can be obtained from random vibration analysis of hysteretic wood systems using the proposed model. Following Ang's (1988) work, random vibration analysis of wood structural systems using the proposed hysteresis model could provide a method for *(a)* cumulative damage model development for, and *(b)* safety and damage

assessment of, wood structures subjected to dynamic loading.

The foregoing list of potential research topics shows that with the proposed hysteresis model for wood structural systems and the successful application of statistical linearization in nonlinear random vibration analysis of these systems, a number of future research opportunities in the area of analysis and design of timber structures against natural hazards have opened up. All this will hopefully help wood engineering research catch up with advances in general structural dynamics and improve the competitiveness of engineered wood systems.

Bibliography

[1] Abramowitz, M. and I.A. Stegun. 1965. *Handbook of Mathematical Functions.* Dover Publications, Inc., New York, NY.

[2] Adeli, H., J.M. Gere and W. Weaver Jr. 1978. "Algorithms for nonlinear structural dynamics." *Journal of the Structural Division ASCE* 104(ST2):263-280.

[3] Allahabadi, R. 1987. "Seismic response and damage assessment for 2D Structures." PhD Thesis, Dept. of Civil Eng., Univ. of California, Berkeley, CA.

[4] Amin, M. and A. H-S. Ang. 1968. "Nonstationary stochastic model of earthquake motions." *Journal of Engineering Mechanics ASCE* 94(EM2): 559-583.

[5] Ang, A. H-S. 1974. "Probabilistic concepts in earthquake engineering." In *Applied Mechanics in Earthquake Engineering*, W.D. Iwan, ed., ASME, New York, NY. pp.225-259.

[6] Ang, A. H-S. 1988. "Seismic damage assessment and basis for damage-limiting design." *Probabilistic Engineering Mechanics* 3(3): 559-583.

[7] Ang, A. H-S. and Y-K. Wen. 1982. "Prediction of structural damage under random earthquake excitations." *Earthquake Ground Motion and Its Effects on Structures ASME*, AMD Vol. 53: 91-107.

[8] Ang, A. H-S. and Y-K. Wen. 1988. "Nonlinear random vibration in structural safety and performance evaluation." In *Nonlinear Stochastic Dynamic Engineering Systems*, F. Ziegler and G.I. Schuëller (Eds.), Springer-Verlag, Berlin, Germany.

[9] Atalik, T.S. and S. Utku. 1976. "Stochastic linearization of multidegree of freedom nonlinear systems." *Earthquake Engineering and Structural Dynamics* 4: 411-420.

[10] Baber, T.T. 1980. "Stochastic equivalent linearization for hysteretic, degrading, multistory structures." PhD Thesis, Dept. of Civil Eng., Univ. of Illinois at Urbana-Champaign, Urbana, IL.

[11] Baber, T.T. 1986a. "Modal analysis for random vibration of hysteretic frames." *Earthquake Engineering and Structural Dynamics* 14:841-859.

[12] Baber, T.T. 1986b. "Nonzero mean random vibration of hysteretic frames." *Computers and Structures* 23:265-277.

[13] Baber, T.T. and M.N. Noori. 1986. "Modeling general hysteresis behavior and random vibration application." *Journal of Vibration, Acoustics, Stress and Reliability in Design ASME* 108: 411-420.

[14] Baber, T.T. and Y-K. Wen. 1981. "Random vibration of hysteretic degrading systems." *Journal of the Engineering Mechanics Division ASCE* 107(EM6):1069-1089.

[15] Barbat, A.H. and J.M. Canet. 1989. *Structural Response Computations in Earthquake Engineering.* Pineridge Press, Swansea, U.K.

[16] Bartels, R.H. and G.W. Stewart. 1972. "Solution of the matrix equation **AX** + **XB** = **C**." *Algorithm 432 in Communications of the ACM*, 15(9).

[17] Bhartia, B.K. and E.H. Vanmarcke. 1991. "Associate linear system approach to nonlinear random vibration." *Journal of Engineering Mechanics ASCE* 117(10):2407-2428.

[18] Bhatti, M.A. and K.S. Pister. 1981. "Transient response analysis of structural systems with nonlinear behavior." *Computers and Structures* 13:181-188.

[19] Bouc, R. 1967. "Forced vibration of mechanical systems with hysteresis", Abstract. Proc. Fourth Conference on Nonlinear Oscillation, Praque, Czechoslovakia.

[20] Branstetter, L.J., G.D. Jeong and J.T.P. Yao. 1988. "Mathematical modelling of structural behaviour during earthquakes." *Probabilistic Engineering Mechanics* 3(3):130-145.

[21] Buchanan, A.H. and J.A. Dean. 1988. "Practical design of timber structures to resist earthquakes." Proc. 1988 International Conference on Timber Engineering, Seattle, WA 1: 813-822.

[22] Casciati, F. 1987. "Nonlinear stochastic dynamics of large structural systems by equivalent linearization." In *Reliability and Risk Analysis in Civil Engineering 2*, N.C. Lind, ed., University of Waterloo, Canada. pp.1165-1172 .

[23] Caughey, T.K. 1971. "Nonlinear theory of random vibrations." *Adv. Applied Mechanics* 11:209-253.

[24] Caughey, T.K. 1986. "On the response of non-linear oscillators to stochastic excitation." *Probabilistic Engineering Mechanics* 1:2-4.

[25] Ceccotti, A. and A. Vignoli. 1990. "Engineered timber structures: An evaluation of their seismic behavior". Proc. 1990 International Timber Engineering Conference, Tokyo, Japan , 946-953.

[26] Chang, T.-P., T. Mochio and E. Samaras. 1986. "Seismic response analysis of nonlinear structures." *Probabilistic Engineering Mechanics* 1(3):157-166.

[27] Cheung, K.C., R.Y. Itani and A. Polensek. 1988. "Characteristics of wood diaphragms: Experimental and parametric studies." *Wood and Fiber Science* 20(4):438-456

[28] Chou, C. 1987. "Modeling of nonlinear stiffness and nonviscous damping in nailed joints betweeen wood and plywood." PhD Thesis, Dept. of Forest Products, Oregon State Univ., Corvallis, OR.

[29] Chui, Y. H. and I. Smith. 1989. Quantifying damping in structural timber components. Proc. Second Pacific Timber Engineering Conference, Auckland, New Zealand .

[30] Clough, R.W. and J. Penzien 1993. *Dynamics of Structures*, Second Edition. McGraw-Hill Book Co., New York, NY.

[31] Conner, H.W., D.S. Gromala, and D.W. Burgess. 1987. "Roof connections in houses: key to wind resistance". *Journal of Structural Engineering ASCE* 113(12):2459-2474.

[32] Constantinou, M.C. and I.G. Tadjbakhsh. 1985. "Hysteretic dampers in base isolation: random approach." *Journal of Structural Engineering ASCE* 111(4):705-721.

[33] Crandall, S.J. 1970. "The role of damping in vibration theory". *Journal of Sound and Vibration* 11(1):3-18.

[34] Davenport, A.G. 1964. "Note on the distribution of the largest value of a random function with application to gust loading." *Proc. Inst. Civ. Eng.* 28:187-196.

[35] Dean, J. A., B. L. Deam, and A. H. Buchanan. 1989. "Earthquake resistance of timber structures". *NZ Journal of Timber Construction* 5(2):12-16.

[36] Diekmann, E.D. 1989. Diaphragms and Shear Walls. in *Wood Engineering and Construction Handbook*, K. Faherty and T. Williamson, eds., McGraw-Hill Pub. Co., New York, NY.

[37] DiPasquale, E., J.W. Ju, A. Askar and A.S. Cakmak. 1990. "Relation between global damage indices and local stiffness degradation". *Journal of Structural Engineering ASCE* 116(5):1140-1456.

[38] Dolan, J.D. 1989. "The dynamic response of timber shear walls". PhD thesis, Dept. of Civil Engineering. Univ. of British Columbia, Vancouver, BC, Canada.

[39] Donley, M.G. and P.D. Spanos. 1990. *Dynamic Analysis of Non-linear Structures by the Method of Statistical Linearization.* Vol. 57 in *Lecture Notes in Engineering*, C.A. Brebbia and S.A. Orszag (Eds.), Springer-Verlag, Berlin, Germany.

[40] Dowrick, D.J. 1986. "Hysteresis loops for timber structures". *Bulletin of New Zealand National Society of Earthquake Engineering* 19(20):143-152.

[41] Einstein, A. 1905. "On the movement of small particles suspended in a stationary liquid demanded by the molecular-kinetic theory of heat." *Ann. Phys.* 17:549-569.

[42] Ewing, R.D., T.J. Healey and M.S. Agbabian. 1980. "Seismic analysis of wood diaphragms in masonry buildings." Proc. Workshop on Design of Horizontal Wood Diaphragms, Applied Technology Council, Berkeley, CA, 253-276.

[43] Falk, R.H. and L.A. Soltis. 1988. "Seismic behavior of low-rise wood framed buildings". *The Shock and Vibration Digest* 20(12):3-7.

[44] Filiatrault, A. and R.O. Foschi. 1991. "Static and dynamic tests of timber shear walls fastened with nails and wood adhesive". *Canadian Journal of Civil Engineering* 18:749-755.

[45] Gavrilović, P. and K. Gramatikov. 1991. "Experimental and theoretical investigations of wooden truss-frame structures under quasi-static and dynamic loads." Proc. Workshop on Full-scale Behavior of Wood-Framed Buildings in Earthquakes and High Winds, Watford, United Kingdom, XXVI-1-37.

[46] Gear, C.W. 1971. *Numerical Initial Value Problems in Ordinary Differential Equations.* Prentice-Hall, Englewood Cliffs, NJ.

[47] Gupta, A.K. and P.J. Moss, eds. 1991. Proc. Workshop on Full-scale Behavior of Wood-Framed Buildings in Earthquakes and High Winds, Watford, United Kingdom.

[48] Hirashima, Y. 1988. "Analysis of observed earthquake response of post-and-beam wood structure." Proc. 1988 International Conference on Timber Engineering, Seattle, WA 2:235-242.

[49] Iemura, H. 1977. "Earthquake response of stationary and deteriorating hysteretic structures." Dept. of Civil Engineering, Kyoto University, Kyoto, Japan.

[50] Iwan, W.D. 1969. "Application of nonlinear analysis techniques." In *Applied Mechanics in Earthquake Engineering*, W.D. Iwan, ed., ASME, New York, NY. pp.135-161.

[51] Iwan, W.D. 1977. "The response of simple stiffness degrading structures." Proc. Sixth World Conf. on Earthquake Engineering, New Delhi, India, Vol. 2:1094-1099.

[52] IMSL. 1987. *User's manual: Math/Library.* International Mathematical and Statistical Library, Inc., Houston, TX.

[53] Jennings, P.C .1965. "Response of yielding structures to stationary generated ground motion." Proc. Third World Conf. on Earthquake Engineering, Auckland, New Zealand, Vol. 2:783-796.

[54] Jensen, H. and W.D. Iwan. 1992. "Response of systems with uncertain parameters to stochastic excitation." *Journal of Engineering Mechanics ASCE* 118(5):1012-1025.

[55] Kaldjian, M.J. and W.R.S. Fan. 1968. "Earthquake response of a Ramberg-Osgood structure". *Journal of the Structural Division ASCE* 94(ST10): 2451-2465.

[56] Kamiya, F. 1988. "Nonlinear earthquake response analysis of sheathed wood walls by a computer-actuator on-line system." Proc. 1988 International Conference on Timber Engineering, Seattle, WA 1:838-847.

[57] Kanai, K. 1967. "Semi-empirical formula for the seismic characteristics of the ground." Bulletin of the Earthquake Research Institute, Univ. of Tokyo, Tokyo,

Japan. Vol. 35, pp.308-325.

[58] Kivell, B.T., P.J. Moss and A.J. Carr. 1981. "Hysteretic modeling of moment resisting nailed timber joints". *Bulletin of New Zealand Nat. Soc. for Earthquake Eng.* 14(4): 233-245.

[59] Kozin, F. 1988. "Autoregressive moving average models of earthquake records." *Probabilistic Engineering Mechanics* 3(2):58-63.

[60] Kwok, Y.H. 1987. "Seismic damage analysis and design of unreinforced masonry buildings." PhD Thesis, Dept. of Civil Eng., Univ. of Illinois at Urbana-Champaign, Urbana, IL.

[61] Lazan, B.J. 1968. *Damping of Materials and Members in Structural Mechanics.* Pergamon Press, London, Great Britain.

[62] Lee, C-S. 1987. "A composite-beam finite element for seismic analysis of wood-framed buildings." PhD Thesis, Dept. of Civil Engineering, Oregon State Univ. Corvallis, OR.

[63] Ljung, L. and T. Söderström. 1983. *Theory and Practice of Recursive Identification.* The MIT Press, Cambridge, MA.

[64] Loh, C. and R. Ho. 1990. "Seismic damage assessment based on different hysteretic rules". *Earthquake Engineering and Structural Dynamics* 19: 753-771.

[65] Loh, C. and S.-T. Chung. 1993. "A three-stage identification approach for hysteretic systems." *Earthquake Engineering and Structural Dynamics* 22: 129-150.

[66] Maldonado, G.O. 1992. "Stochastic and seismic design response of linear and non-linear structures." PhD Dissertation, Dept. of Engineering Science and Mechanics, Virginia Polytechnic Inst. and State Univ., Blacksburg, VA.

[67] Maldonado, G.O., M.P. Singh, F. Casciati and L. Faravelli. 1987. "Stochastic response of single degree of freedom hysteretic oscillators." Technical Report of Research

Supported by the National Science Foundation (Grant CEE-8412830), Dept. of Engineering Science and Mechanics, Virginia Polytechnic Inst. and State Univ., Blacksburg, VA.

[68] Maruyama, O., C-B. Yun, M. Hoshiya and M. Shinozuka. 1989. "Program EXKAL2 for identification of structural dynamic systems." Technical Report NCEER-89-0014, National Center for Earthquake Eng. Research, State Univ. of New York, Buffalo, NY.

[69] Medearis, K. and D.H. Young. 1964. "Energy absorption of structures under cyclic loading." *Journal of the Structural Division ASCE* 90(ST1): 61-91.

[70] Meirovitch, L. 1985. *Introduction to Dynamics and Control.* John Wiley & Sons Inc., New York, NY.

[71] Meirovitch, L. 1986. *Elements of Vibration Analysis.* McGraw-Hill Book Co., New York, NY.

[72] Miyazawa, K. 1990. "Study on nonlinear static and dynamic structural analysis of wooden wall-frame buildings subjected to horizontal force." Proc. Thirteenth Symposium on Computer Technology of Information, Systems and Applications, A.I.J., Japan.

[73] Moss, P.J. 1991. "The performance of low-rise timber buildings in New Zealand when subjected to seismic, wind and snow loads." Proc. Workshop on Full-scale Behavior of Wood-Framed Buildings in Earthquakes and High Winds, Watford, United Kingdom, XVII-1-64.

[74] Newmark, N. and B. Rosenblueth. 1971. *Fundamentals of Earthquake Engineering.* McGraw-Hill Book Co., New York, NY.

[75] Nigam, N.C.1983. *Introduction to Random Vibrations.* The MIT Press, Cambridge, MA.

[76] Noori, M.N. 1984. "Random vibration of degrading systems with general hysteretic behavior." PhD Dissertation, Dept. of Civil Engineering, Univ. of Virginia, Charlottesville, VA.

[77] Orabi, I.I. and G. Ahmadi. 1987. "A functional series expansion method for the response analysis of a Duffing oscillator subjected to white noise excitations." *Int. J. Non-linear Mech.* 22:451-465.

[78] Park, Y.J. and A.H-S. Ang. 1985. "Mechanistic seismic damage model for reinforced concrete." *Journal of Structural Engineering ASCE* 111(4):722-739.

[79] Park, Y.J., A.H-S. Ang and Y-K. Wen. 1985. "Seismic damage analysis of reinforced concrete buildings." *Journal of Structural Engineering ASCE* 111(4):740-757.

[80] Paz, M. 1991. *Structural Dynamics: Theory and Computations*, Third Edition. Van Nostrand Reinhold, New York, NY.

[81] Pires, J.E.A., Y-K. Wen and A.H-S. Ang. 1983. "Stochastic analysis of liquefaction under earthquake loading." Civil Eng. Studies, Structural Research Series No. 504, Univ. of Illinois at Urbana-Champaign, Urbana, IL.

[82] Polensek, A. 1988. "Effects of testing variables on damping and stiffness of nailed wood-to-sheathing joints." ASTM *Journal of Testing and Evaluation* 16(5): 474-480.

[83] Polensek, A. and K.J. Bastendorff. 1987. "Damping in nailed joints of light-frame wood buildings." *Wood and Fiber Science* 19(2): 110-125.

[84] Polensek, A. and H.I. Laursen. 1984. "Seismic behavior of bending components and intercomponent connections of light framed wood buildings." Final Report to the National Science Foundation (Grant CEE-8104626), Dept. of Forest Products, Oregon State Univ., Corvallis, OR.

[85] Polensek, A. and B.D. Schimel. 1991. "Dynamic properties of light-frame wood subsystems". *Journal of Structural Engineering ASCE* 117(4): 1079-1095.

[86] Pradlwarter, H.J. and G.I. Schuëller. 1992. "Equivalent linearization- a suitable tool for analyzing MDOF-systems." *Probabilistic Engineering Mechanics* 8:115-126.

[87] Press, W.H., B.P. Flannery, S.A. Teukolsky and W.T. Vetterling. 1992. *Numerical Recipes in FORTRAN: The Art of Scientific Computing*, Second Edition. Cambridge University Press, Cambridge, United Kingdom.

[88] Reyer, E. and O.A. Oji. 1991. "A testing procedure for phenomenological modeling of timber joints and members under cyclic loading." Proc. Workshop on Full-scale Behavior of Wood-Framed Buildings in Earthquakes and High Winds, Watford, United Kingdom, XIII-1-22.

[89] Rice, S.O. 1944. "Mathematical analysis of random noise," Pages 133-294 in *Selected Papers in Noise and Stochastic Processes*, N. Wax (Ed.), Dover Publications, Inc., New York, NY.

[90] Roberts, J.B. 1981a. "Response of nonlinear mechanical systems to random excitation; Part 1: Markov methods." *The Shock and Vibration Digest* 13(4):17-28.

[91] Roberts, J.B. 1981b. "Response of nonlinear mechanical systems to random excitation; Part 2: Equivalent linearization and other methods." *The Shock and Vibration Digest* 13(5):15-29.

[92] Roberts, J.B. and P.D. Spanos. 1990. *Random Vibration and Statistical Linearization.* John Wiley & Sons Ltd., West Sussex, England.

[93] Sakamoto, I. and Y. Ohashi. 1988. "Seismic response and required lateral strength of wooden dwellings" Proc. 1988 International Conference on Timber Engineering, Seattle, WA 2:243-247.

[94] Shinozuka, M. 1964. "Probability of structural failure under random loading." *Journal of the Engineering Mechanics Division ASCE* 90(EM5):147-170.

[95] Shinozuka, M. 1972. "Monte Carlo solution of structural dynamics." *Computers and Structures* 2:855-874.

[96] Shinozuka, M. and G. Deodatis. 1988. "Stochastic process models for earthquake ground motions." *Probabilistic Engineering Mechanics* 3(3):114-123.

[97] Shinozuka, M., H. Itagaki and M. Hakuno. 1968. "Dynamic safety analysis of multistory buildings." *Journal of the Structural Division ASCE* 94(ST1):309-330.

[98] Shinozuka, M. and Y. Sato. 1967. "Simulation of nonstationary random processes." *Journal of the Engineering Mechanics Division ASCE* 93(EM1):11-40.

[99] Soltis, L.A. 1984. "Low-rise timber buildings subjected to seismic, wind and snow loads." *Journal of Structural Engineering ASCE* 110(4): 744-753.

[100] Soong, T.T. and M. Grigoriu. 1993. *Random Vibration of Mechanical and Structural Systems.* Prentice-Hall, Englewood Cliffs, NJ.

[101] Sozen, M.A. 1974. "Hysteresis in structural elements." In *Applied Mechanics in Earthquake Engineering*, W.D. Iwan, ed., ASME, New York, NY. pp.63-98.

[102] Spanos, P.D. 1980. "Formulation of stochastic linearization for symmetric or asymmetric MDOF nonlinear systems." *Journal of Applied Mechanics ASME* 47:209-211.

[103] Spanos, P.D. 1981. "Stochastic linearization in structural dynamics." *Applied Mechanics Reviews ASME* 34(1):1-8.

[104] Spanos, P.D. and L.D. Lutes. 1986. "A primer of random vibration techniques in structural engineering." *The Shock and Vibration Digest* 18(4):3-10.

[105] Spanos, P.D. and M.D. Mignolet. 1989. "ARMA Monte Carlo simulation in probabilistic structural analysis." *The Shock and Vibration Digest* 21(11):3-14.

[106] Srinivasan, P. 1982. *Mechanical Vibration Analysis.* Tata McGraw-Hill Pub. Co. Ltd., New Delhi, India.

[107] Stalnaker, J. and K.K. Gramatikov. 1991. "Modeling." Proc. Workshop on Full-scale Behavior of Wood-Framed Buildings in Earthquakes and High Winds, Watford, United Kingdom, VI-1-3.

[108] Stewart, W.G. 1987. "The seismic design of plywood-sheathed shear walls". PhD thesis, Univ. of Canterbury, Christchurch, New Zealand.

[109] Sues, R.H., S.T. Mau and Y-K. Wen. 1988. "System identification of degrading hysteretic restoring forces." *Journal of Engineering Mechanics ASCE* 114(5):833-846.

[110] Tajimi, H. 1960. "A statistical method of determining the maximum response of a building structure during an earthquake." Proc. Second World Conf. on Earthquake Engineering, Tokyo and Kyoto, Japan, Vol. 2:781-797.

[111] Takizawa, H. 1975. "Non-linear models for simulating the dynamic damaging process of low-rise reinforced concrete buildings during severe earthquakes." *Earthquake Engineering and Structural Dynamics* 4: 73-94.

[112] Touliatos, P.G. 1989. "Report on Greek experiences." Proc. Workshop on Structural Behavior of Timber Construction in Seismic Zones, Florence, Italy , 267-296.

[113] Turner, L.S., F. Stewart and K.C.K. Cheung. 1990. "Performance of wood structures: Loma Prieta earthquake aftermath." *Wood Design Focus* 1(4):14-16.

[114] Uang, C. and V.V. Bertero. 1990. "Evaluation of seismic energy in structures." *Earthquake Engineering and Structural Dynamics* 19: 77-90.

[115] UBC. 1993. "Timber engineering software." Dept. of Civil Engineering, Univ. of British Columbia, Vancouver, BC, Canada.

[116] Vanmarcke, E. 1983. *Random Fields: Analysis and Synthesis.* The MIT Press, Cambridge, MA.

[117] Wen, Y-K. 1976. "Method for random vibration of hysteretic systems." *Journal of the Engineering Mechanics Division ASCE* 102(EM2):249-263.

[118] Wen, Y-K. 1980. "Equivalent linearization for hysteretic systems under random excitation." *Journal of Applied Mechanics ASME* 47:150-154.

[119] Wen, Y-K. 1986. "Stochastic response and damage analysis of inelastic structures." *Probabilistic Engineering Mechanics* 1(1):49-57.

[120] Wen, Y-K. 1988. "Equivalent linearization methods." Appendix I in Branstetter, L.J., G.D. Jeong and J.T.P. Yao. 1988. "Mathematical modelling of structural behaviour during earthquakes." *Probabilistic Engineering Mechanics* 3(3):130-145.

[121] Weyerhaeuser. 1990. "The lateral resistance of OSB and plywood under cyclic shear loads." Material Testing Services, Weyerhaeuser Company, Tacoma, WA.

[122] Whale, L.R.J. 1988. "Deformation characteristics of nailed or bolted timber joints subjected to irregular short or medium term lateral loading." PhD Thesis, Polytechnic of the South Bank, CNAA, U.K.

[123] Yao, J.T.P. 1985. *Safety and Reliability of Existing Structures.* Pitman Publishing Inc., Boston, MA.

[124] Yasumura, M., I. Nishiyama, T. Murota, and N. Yamaguchi. 1988. "Experiments on a three-storied wooden frame building subjected to horizontal load." Proc. 1988 International Conference on Timber Engineering, Seattle, WA 2: 262-275.

[125] Yeh, T.C., B.J. Hartz and C.B. Brown. 1971. "Damping sources in wood structures." *Journal of Sound and Vibration* 19(4): 411-419.

Appendix A

Derivation of Linearization Coefficient Formulas

The linearization coefficients for the modified Bouc-Wen-Baber-Noori (BWBN) model were computed in section 5.4.3 by Eq. (5.14). This equation was first presented by Atalik and Utku (1976) and will be derived here, renumbered as follows:

$$\begin{aligned} C_{e3} &= E\left[\frac{\partial g_3(\mathbf{y})}{\partial y_2}\right] \\ K_{e3} &= E\left[\frac{\partial g_3(\mathbf{y})}{\partial y_3}\right] . \end{aligned} \tag{A.1}$$

First, let us consider the mean square error $E[e^2]$ to be minimized, where

$$e = g_3(\mathbf{y}) - C_{e3}\, y_2 - K_{e3}\, y_3 . \tag{A.2}$$

Then,

$$\begin{aligned} E[e^2] &= E[g_3^2(\mathbf{y})] - 2C_{e3}E[y_2 g_3^2(\mathbf{y})] - 2K_{e3}E[y_3 g_3^2(\mathbf{y})] \\ &\quad + C_{e3}^2 E[y_2^2] + 2C_{e3}K_{e3}E[y_2 y_3] + K_{e3}^2 E[y_3^2] . \end{aligned} \tag{A.3}$$

Minimization requires that

$$\begin{aligned} \frac{\partial}{\partial C_{e3}} E[e^2] &= 0 \\ \frac{\partial}{\partial K_{e3}} E[e^2] &= 0 . \end{aligned} \tag{A.4}$$

Substitution of Eq. (A.3) into (A.4) yields two simultaneous equations for the coefficients C_{e3} and K_{e3}:

$$\begin{aligned} C_{e3}E[y_2^2] + K_{e3}E[y_2 y_3] &= E[y_2 g_3(\mathbf{y})] \\ C_{e3}E[y_3 y_2] + K_{e3}E[y_3^2] &= E[y_3 g_3(\mathbf{y})] \end{aligned} \tag{A.5}$$

which can be solved for the coefficients as

$$\begin{Bmatrix} C_{e3} \\ K_{e3} \end{Bmatrix} = \mathbf{S}_{Y_2Y_3}^{-1} \begin{Bmatrix} E[y_2 g_3(\mathbf{y})] \\ E[y_3 g_3(\mathbf{y})] \end{Bmatrix} \tag{A.6}$$

where $\mathbf{S}_{Y_2Y_3}$ is the covariance matrix of y_2 and y_3. This equation can be used directly to obtain C_{e3} and K_{e3} if the joint probability density function of y_2 and y_3 are known. We would like to show , however, that the right-hand sides of Eqs. (A.1) and (A.6) are the same. Direct application of partial differentiation and expectation operators to the nonlinear terms to obtain the equivalent linear coefficients in statistical linearization, such as that given by Eq. (A.1), is simpler and, therefore, more appealing than the solution offered by Eq. (A.6).

Before we proceed, let us consider

$$\tilde{\mathbf{y}} = \begin{Bmatrix} y_2 \\ y_3 \end{Bmatrix} \tag{A.7}$$

only, instead of $\mathbf{y}$ defined in Eq. (A.7). [This also means that the function is now defined as $g_3(\tilde{\mathbf{y}})$, instead of $g_3(\mathbf{y})$.] The proof also requires that the following conditions be met (Atalik and Utku 1976):

1. $\tilde{\mathbf{y}}$ is a jointly Gaussian random vector process with zero mean, i.e., its joint probability density function, $f_{Y_2Y_3}(y_2, y_3)$, is Gaussian:

$$f_{Y_2Y_3}(y_2, y_3) = \left[(2\pi)^2 \det(\mathbf{S}_{Y_2Y_3})\right]^{-1/2} \exp\left[-\frac{1}{2}\,\tilde{\mathbf{y}}^{\mathrm{T}}\,\mathbf{S}_{Y_2Y_3}^{-1}\,\tilde{\mathbf{y}}\right] \tag{A.8}$$

2. $g_3(\tilde{\mathbf{y}})$ is sufficiently smooth and differentiable, and

3. $|g_3(\tilde{\mathbf{y}})| < A \exp(y_2^{a_1} + y_3^{a_2})$, $a_i < 2$ and A is arbitratry.

The last two conditions are met by the modified BWBN model. The first condition can be assumed. Let us then evaluate the right-hand side of Eq. (A.1a):

$$E\left[\frac{\partial g_3(\tilde{\mathbf{y}})}{\partial y_2}\right] = \int_{-\infty}^{\infty}\int_{-\infty}^{\infty} \frac{\partial g_3(\tilde{\mathbf{y}})}{\partial y_2}\, f_{Y_2Y_3}(y_2, y_3)\, dy_2 dy_3 \tag{A.9}$$

which, by integration by parts, gives

$$E\left[\frac{\partial g_3(\tilde{\mathbf{y}})}{\partial y_2}\right] = \int_{-\infty}^{\infty}\left[g_3(\tilde{\mathbf{y}}) f_{Y_2Y_3}(y_2,y_3)\Big|_{-\infty}^{\infty} - \int_{-\infty}^{\infty} g_3(\tilde{\mathbf{y}})\,\frac{\partial f_{Y_2Y_3}(y_2,y_3)}{\partial y_2}\,dy_2\right] dy_3 \,. \tag{A.10}$$

Recall that the function $g_3(\tilde{\mathbf{y}})$ is

$$g_3(\tilde{\mathbf{y}}) = h(y_3)\,\left\{\frac{y_2 - \nu(\beta|y_2||y_3|^{n-1}y_3 - \gamma y_2|y_3|^n)}{\eta}\right\} \tag{A.11}$$

which means that the first term in the right-hand side of Eq. (A.10) evaluates to zero at the limits. The derivative of the joint density function, given in Eq. (A.8), is

$$\frac{\partial}{\partial y_2} f_{Y_2Y_3}(y_2,y_3) = -\frac{1}{2} f_{Y_2Y_3}(y_2,y_3)\left[\frac{\partial \tilde{\mathbf{y}}^{\mathrm{T}}}{\partial y_2}\,\mathbf{S}_{Y_2Y_3}^{-1}\,\tilde{\mathbf{y}} + \tilde{\mathbf{y}}^{\mathrm{T}}\,\mathbf{S}_{Y_2Y_3}^{-1}\,\frac{\partial \tilde{\mathbf{y}}}{\partial y_2}\right] \tag{A.12}$$

which simplifies to

$$\frac{\partial}{\partial y_2} f_{Y_2Y_3}(y_2,y_3) = -f_{Y_2Y_3}(y_2,y_3)\begin{Bmatrix}1\\0\end{Bmatrix}^{\mathrm{T}}\mathbf{S}_{Y_2Y_3}^{-1}\begin{Bmatrix}y_2\\y_3\end{Bmatrix} \,. \tag{A.13}$$

Thus, Eq. (A.10) evaluates to

$$E\left[\frac{\partial g_3(\tilde{\mathbf{y}})}{\partial y_2}\right] = \int_{-\infty}^{\infty}\int_{-\infty}^{\infty} g_3(\tilde{\mathbf{y}})\, f_{Y_2Y_3}(y_2,y_3)\begin{Bmatrix}1\\0\end{Bmatrix}^{\mathrm{T}}\mathbf{S}_{Y_2Y_3}^{-1}\begin{Bmatrix}y_2\\y_3\end{Bmatrix} dy_2\, dy_3 \,. \tag{A.14}$$

Similarly,

$$E\left[\frac{\partial g_3(\tilde{\mathbf{y}})}{\partial y_3}\right] = \int_{-\infty}^{\infty}\int_{-\infty}^{\infty} g_3(\tilde{\mathbf{y}})\, f_{Y_2Y_3}(y_2,y_3)\begin{Bmatrix}0\\1\end{Bmatrix}^{\mathrm{T}}\mathbf{S}_{Y_2Y_3}^{-1}\begin{Bmatrix}y_2\\y_3\end{Bmatrix} dy_2\, dy_3 \,. \tag{A.15}$$

Combining Eqs. (A.14) and (A.15), we obtain:

$$\begin{Bmatrix} E\left[\frac{\partial g_3(\tilde{\mathbf{y}})}{\partial y_2}\right] \\ E\left[\frac{\partial g_3(\tilde{\mathbf{y}})}{\partial y_3}\right] \end{Bmatrix} = \mathbf{S}_{Y_2Y_3}^{-1}\int_{-\infty}^{\infty}\int_{-\infty}^{\infty}\begin{Bmatrix}y_2\\y_3\end{Bmatrix} g_3(\tilde{\mathbf{y}})\, f_{Y_2Y_3}(y_2,y_3)\, dy_2\, dy_3 \tag{A.16}$$

which can be rewritten as

$$\begin{Bmatrix} E\left[\frac{\partial g_3(\tilde{\mathbf{y}})}{\partial y_2}\right] \\ E\left[\frac{\partial g_3(\tilde{\mathbf{y}})}{\partial y_3}\right] \end{Bmatrix} = \mathbf{S}_{Y_2Y_3}^{-1}\begin{Bmatrix} E[y_2 g_3(\tilde{\mathbf{y}})] \\ E[y_3 g_3(\tilde{\mathbf{y}})] \end{Bmatrix} \,. \tag{A.17}$$

Finally, equating Eqs. (A.6) and (A.17) gives

$$\left\{ \begin{array}{c} C_{e3} \\ K_{e3} \end{array} \right\} = \left\{ \begin{array}{c} E\left[\frac{\partial g_3(\tilde{\mathbf{y}})}{\partial y_2}\right] \\ E\left[\frac{\partial g_3(\tilde{\mathbf{y}})}{\partial y_3}\right] \end{array} \right\} \tag{A.18}$$

which is the formula given in Eq. (A.1).

Appendix B

Special Functions

The basic form and properties of the special functions used in the present work will be given here. A thorough presentation of their properties may be found in Abramowitz and Stegun (1965).

B.1 Gamma Function and Related Functions

• **Gamma Function**

Euler's Integral:

$$\Gamma(a) = \int_0^\infty t^{a-1} e^{-t}\, dt \qquad ;(\mathrm{Re}\ a > 0) \tag{B.1}$$

Recurrence Formulas:

$$\Gamma(a+1) = a\,\Gamma(a) = a! = a(a-1)! \tag{B.2}$$

$$\begin{aligned} \Gamma(a+n) &= (a+n-1)(a+2-2)\ldots(a+1)\,\Gamma(a+1) \\ &= (a+n-1)! \\ &= (a+n-1)(a+2-2)\ldots(a+1)a! \end{aligned} \tag{B.3}$$

• **Incomplete Gamma Function**

$$\gamma(a,x) = \int_0^x t^{a-1} e^{-t}\, dt \qquad ;(\mathrm{Re}\ a > 0;\ x \geq 0) \tag{B.4}$$

• **Binomial Coefficient**

$$\binom{a}{b} = \frac{a!}{b!\,(a-b)!} = \frac{\Gamma(a+1)}{\Gamma(b+1)\,\Gamma(a-b+1)} \qquad ;(0 \leq b \leq a) \tag{B.5}$$

B.2 Error Function and the Gaussian Distribution

- **Error Function**

$$\mathrm{erf}(x) = \frac{2}{\sqrt{\pi}} \int_0^x \mathrm{e}^{-t^2}\, dt \tag{B.6}$$

- **Complementary Error Function**

$$\mathrm{erfc}(x) = \frac{2}{\sqrt{\pi}} \int_x^\infty \mathrm{e}^{-t^2}\, dt = 1 - \mathrm{erf}(x) \tag{B.7}$$

- **Gaussian Probability Function**

Probability Density Function (pdf):

$$f_X(x) = \frac{1}{\sqrt{2\pi}\,\sigma_x} \int_{-\infty}^{\infty} \exp\left[-\frac{1}{2}\frac{(x-\mu_x)^2}{\sigma_x^2}\right] dx \tag{B.8}$$

Cumulative Distribution Function (cdf):

The cdf of a standard normal or Gaussian random variable (i.e., $\mu_x = 0$, $\sigma_x = 1$) is

$$\begin{aligned} \Phi(x_o) &= \text{Probability}\{X \le x_o\} \\ &= \frac{1}{\sqrt{2\pi}} \int_{-\infty}^{x_o} \mathrm{e}^{(-x^2/2)}\, dx \end{aligned} \tag{B.9}$$

which is related to the complementary error function and the error function as

$$\Phi(x_o) = \frac{1}{2}\,\mathrm{erfc}\left(\frac{-x_o}{\sqrt{2}}\right) \tag{B.10}$$

$$= \frac{1}{2}\left[1 - \mathrm{erf}\left(\frac{-x_o}{\sqrt{2}}\right)\right], \tag{B.11}$$

respectively. These relations are valid for $-\infty \le x_o \le \infty$ since $\mathrm{erf}(-a) = -\mathrm{erf}(a)$.

Appendix C

Calculation of Expected Values

In calculating the expectations, $E[\cdot]$, given in section 5.4.3 [Eqs. (5.21) to (5.35)], they can be divided, according to the derivation approach, into three groups: (*1*) non-exponential forms: C_1, C_2, K_1 and K_2, (*2*) forms without $|y_3|$ and with exponential function: C_3, K_3 and K_4, and (*3*) forms with $|y_3|$ and exponential function: C_4, C_5, K_5 to K_{10}. A representative function from each group, chosen as the most complicated in its group, will be derived in detail. Calculation of the rest of the expectations easily follows any one of these derivations.

In all cases, the zero-mean joint Gaussian probability density function (pdf) for y_2 and y_3 given as

$$f_{Y_2Y_3}(y_2,y_3)=\frac{1}{2\pi\,\sigma_2\sigma_3\sqrt{1-\rho_{23}^2}}\exp\left\{-\frac{1}{2(1-\rho_{23}^2)}\left[\frac{y_2^2}{\sigma_2^2}-2\rho_{23}\frac{y_2}{\sigma_2}\frac{y_3}{\sigma_3}+\frac{y_3^2}{\sigma_3^2}\right]\right\} \quad \text{(C.1)}$$

(where σ_2 and σ_3 are the respective root mean square values of y_2 and y_3 and ρ_{23} is their correlation coefficient, which will be simplified to $\rho = \rho_{23}$ from hereon) will be used in the following definition of the expected value of a function $h(y_2,y_3)$:

$$E[h(y_2,y_3)]=\int_{-\infty}^{\infty}\int_{-\infty}^{\infty}h(y_2,y_3)\,f_{Y_2Y_3}(y_2,y_3)\,dy_2dy_3\ . \quad \text{(C.2)}$$

To facilitate the evaluation of Eq. (C.2), the bivariate Gaussian pdf is expressed in terms of the marginal pdf of either of the variables and the conditional pdf of the other, i.e.,

$$f_{Y_2Y_3}(y_2,y_3)=f_{Y_2}(y_2)\cdot f_{Y_3|Y_2}(y_3|y_2) \quad \text{(C.3)}$$

or

$$f_{Y_2Y_3}(y_2,y_3)=f_{Y_3}(y_3)\cdot f_{Y_2|Y_3}(y_2|y_3) \quad \text{(C.4)}$$

where, in the case of (C.4),

$$f_{Y_3}(y_3) = \frac{1}{\sqrt{2\pi}\,\sigma_3} \int_{-\infty}^{\infty} \exp\left[-\frac{1}{2}\frac{y_3^2}{\sigma_3^2}\right] dy_3 \tag{C.5}$$

and

$$f_{Y_2|Y_3}(y_2|y_3) = \frac{1}{\sqrt{2\pi}\,\sigma_2\sqrt{1-\rho^2}} \int_{-\infty}^{\infty} \exp\left[-\frac{1}{2}\left(\frac{y_2 - \rho\,(\sigma_2/\sigma_3)\,y_3}{\sigma_2\sqrt{1-\rho^2}}\right)^2\right] dy_3 \ . \tag{C.6}$$

These can be shown by completing the squares in the argument of the exponential function in Eq. (C.1) with respect to y_2.

C.1 Non-exponential Form

Expectations for C_2 and K_2 are easily obtained using the integral form of the Gamma function, given in Appendix B. Derivations of C_1 and K_1, on the other hand, are more involved. Fortunately, they share a similar approach. Thus, we will only derive K_1.

The expectation for K_1 is

$$\begin{aligned} K_1 &= E[n|y_2||y_3|^{n-1}] \\ &= n \int_{-\infty}^{\infty}\int_{-\infty}^{\infty} |y_2||y_3|^{n-1} f_{Y_2Y_3}\, dy_2 dy_3 \ . \end{aligned} \tag{C.7}$$

The domain of integration can be divided into four regions ($y_2 < 0$, $y_2 > 0$, $y_3 < 0$ and $y_3 > 0$) resulting in

$$\begin{aligned} K_1 = {} & n \underbrace{\int_{-\infty}^{0}\int_{-\infty}^{0} (-1)^n y_2 y_3^{n-1} f_{Y_2Y_3}\, dy_2 dy_3}_{\mathcal{A}} \\ & + n \underbrace{\int_{-\infty}^{0}\int_{0}^{\infty} (-1)^{n-1} y_2 y_3^{n-1} f_{Y_2Y_3}\, dy_2 dy_3}_{\mathcal{B}} \\ & + n \underbrace{\int_{0}^{\infty}\int_{-\infty}^{0} (-1) y_2 y_3^{n-1} f_{Y_2Y_3}\, dy_2 dy_3}_{\mathcal{C}} + n \underbrace{\int_{0}^{\infty}\int_{0}^{\infty} y_2 y_3^{n-1} f_{Y_2Y_3}\, dy_2 dy_3}_{\mathcal{D}} \ . \end{aligned} \tag{C.8}$$

Since $f_{Y_2Y_3}(-y_2, -y_3) = f_{Y_2Y_3}(y_2, y_3)$, let $u_2 = -y_2$ and $u_3 = -y_3$, substitute into $\mathcal{A}$ and $\mathcal{B}$ in Eq. (C.8) and flip the integrals to obtain

$$\mathcal{A} = \int_{0}^{\infty}\int_{0}^{\infty} (-1)^{2n+4} u_2 u_3^{n-1} f_{U_2U_3}\, du_2 du_3$$

$$= \int_0^\infty \int_0^\infty u_2 u_3^{n-1} f_{U_2U_3}\, du_2 du_3 \equiv \mathcal{D} \tag{C.9}$$

$$\mathcal{B} = \int_0^\infty \int_{-\infty}^0 (-1)^{2n-3} u_2 u_3^{n-1} f_{U_2U_3}\, du_2 du_3$$

$$= \int_0^\infty \int_{-\infty}^0 (-1) u_2 u_3^{n-1} f_{U_2U_3}\, du_2 du_3 \equiv C\ . \tag{C.10}$$

Thus, K_1 simplifies to

$$K_1 = 2n \left(\underbrace{\int_0^\infty \int_0^\infty y_2 y_3^{n-1} f_{Y_2Y_3}\, dy_2 dy_3}_{I} - \underbrace{\int_0^\infty \int_{-\infty}^0 y_2 y_3^{n-1} f_{Y_2Y_3}\, dy_2 dy_3}_{II} \right) . \tag{C.11}$$

The integrals will be evaluated separately and then combined in the end.

- **Consider** I

With Eq. (C.4), I becomes

$$I = \frac{1}{2\pi\, \sigma_2 \sigma_3 \sqrt{1-\rho^2}} \int_0^\infty y_3^{n-1} \exp\left[-\frac{y_3^2}{2\sigma_3^2} \right]$$

$$\times \int_0^\infty y_2 \exp\left[-\frac{1}{2} \left(\frac{y_2 - \rho\, (\sigma_2/\sigma_3)\, y_3}{\sigma_2 \sqrt{1-\rho^2}} \right)^2 \right] dy_2\, dy_3\ . \tag{C.12}$$

Change variables by letting

$$s = \frac{y_3}{\sigma_3} \quad \text{and} \quad \nu = \frac{y_2 - \rho\, (\sigma_2/\sigma_3)\, y_3}{\sigma_2 \sqrt{1-\rho^2}}\ .$$

Substitute into Eq. (C.12) and simplify,

$$I = \frac{\sigma_2\, \sigma_3^{n-1}}{2\pi} \int_0^\infty s^{n-1} \exp\left(-\frac{s^2}{2} \right) \tag{C.13}$$

$$\times \left[\sqrt{1-\rho^2} \int_{\nu_L}^\infty \nu \exp\left(-\frac{\nu^2}{2} \right) d\nu + \rho\, s \int_{\nu_L}^\infty \exp\left(-\frac{\nu^2}{2} \right) d\nu \right] ds$$

where

$$\nu_L = -\frac{\rho\, s}{\sqrt{1-\rho^2}} \qquad ;\ (0 \le \rho \le 1)\ . \tag{C.14}$$

When $\rho > 0$, then $\nu_L < 0$ and when $\rho < 0$, then $\nu_L > 0$. It is clear that both cases should be considered in obtaining I. The new integration domains are plotted in Fig. C.1 in the ν-s plane.

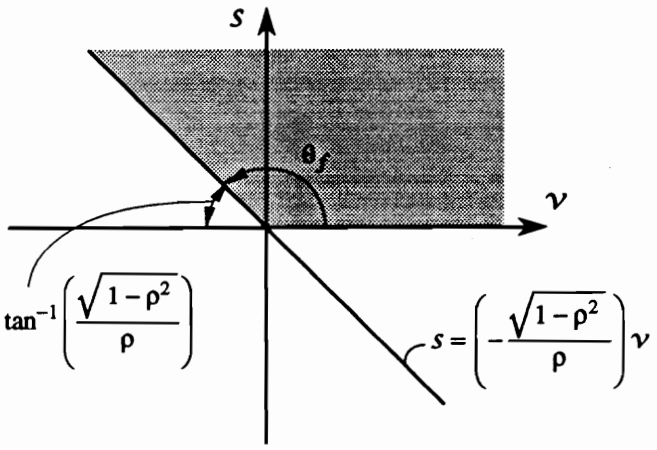

(a) when $\rho > 0$

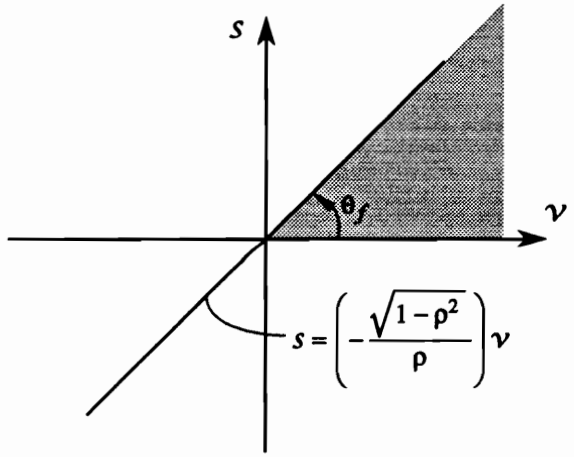

(b) when $\rho < 0$

Figure C.1: Integration domain for K_1's I

The best way to proceed is to change from rectangular coordinates (v,s) to polar coordinates (r,θ). Letting $s = r \sin\theta$ and $v = r \cos\theta$, we obtain $r^2 = s^2 + v^2$ and $dv\,ds = \mathrm{J}\,dr\,d\theta$, where J is the Jacobian of transformation:

$$\mathrm{J} = \begin{vmatrix} \frac{\partial s}{\partial r} & \frac{\partial s}{\partial \theta} \\ \frac{\partial v}{\partial r} & \frac{\partial v}{\partial \theta} \end{vmatrix} = r \ . \tag{C.15}$$

Thus, $dv\,ds = r\,dr\,d\theta$. Substituting the new variables and changing the limits, Eq. (C.13) becomes

$$I = \frac{\sigma_2\,\sigma_3^{n-1}}{2\pi} \underbrace{\int_0^\infty r^{n-1} \exp\left(-\frac{r^2}{2}\right) dr}_{I_a} \tag{C.16}$$

$$\times \left[\sqrt{1-\rho^2} \underbrace{\int_o^{\theta_f} \sin^{n-1}\theta \cos\theta\, d\theta}_{I_b} + \rho \underbrace{\int_0^{\theta_f} \sin^n\theta\, d\theta}_{I_c} \right]$$

where θ_f is obtained graphically from Fig. C.1 as

$$\theta_f = \begin{cases} \pi - \tan^{-1}\left(\frac{\sqrt{1-\rho^2}}{\rho}\right) & \text{if } \rho > 0 \\ -\tan^{-1}\left(\frac{\sqrt{1-\rho^2}}{\rho}\right) & \text{if } \rho < 0 \end{cases} \ . \tag{C.17}$$

It can be shown, using the integral form of the Gamma function [Eq. (B.1)], that

$$I_a = \int_0^\infty r^{n-1} \exp\left(-\frac{r^2}{2}\right) dr = (2)^{n/2}\,\Gamma\left(\frac{n+2}{2}\right) \ . \tag{C.18}$$

Solutions for I_b and I_c are obtained from standard integral tables:

$$I_b = \int_0^{\theta_f} \sin^{n-1}\theta \cos\theta\, d\theta = \frac{1}{n} \sin^n\theta \Big|_0^{\theta_f}$$

$$= \frac{1}{n} \sin^n\theta_f = \frac{(1-\rho^2)^{n/2}}{n} \ , \tag{C.19}$$

and

$$I_c = \int_0^{\theta_f} \sin^n\theta\, d\theta = -\frac{\sin^{n-1}\theta\cos\theta}{n}\Big|_0^{\theta_f} + \frac{n-1}{n} \int_0^{\theta_f} \sin^{n-2}\theta\, d\theta \ . \tag{C.20}$$

Since I_c is solved recursively, we would retain its integral form to preserve generality. Substituting Eqs. (C.18) and (C.19) into (C.16), we finally obtain

$$I = \frac{\sigma_2\,\sigma_3^{n-1}}{2\pi} (2)^{n/2}\,\Gamma\left(\frac{n+2}{2}\right) \left[\frac{(1-\rho^2)^{(n+1)/2}}{n} + \rho \int_0^{\theta_f} \sin^n\theta\, d\theta \right] \ . \tag{C.21}$$

• **Consider *II***

The solution for *II* follows that of *I*. With Eq. (C.4), *II* becomes

$$II = \frac{1}{2\pi\,\sigma_2\sigma_3\sqrt{1-\rho^2}} \int_0^{\infty} y_3^{n-1} \exp\left[-\frac{y_3^2}{2\sigma_3^2}\right] \times \int_{-\infty}^{0} y_2 \exp\left[-\frac{1}{2}\left(\frac{y_2 - \rho\,(\sigma_2/\sigma_3)\,y_3}{\sigma_2\sqrt{1-\rho^2}}\right)^2\right] dy_2\,dy_3 \ . \tag{C.22}$$

Note that the only difference with *I* is the integration limits in y_2. Thus, following the same changes in variables from y_3 to s and y_2 to ν, we obtain

$$II = \frac{\sigma_2\,\sigma_3^{n-1}}{2\pi} \int_0^{\infty} s^{n-1} \exp\left(-\frac{s^2}{2}\right) \times \left[\sqrt{1-\rho^2}\int_{-\infty}^{\nu_U} \nu \exp\left(-\frac{\nu^2}{2}\right) d\nu \ + \ \rho\, s \int_{-\infty}^{\nu_U} \exp\left(-\frac{\nu^2}{2}\right) d\nu\right] ds \tag{C.23}$$

where

$$\nu_U = -\frac{\rho\, s}{\sqrt{1-\rho^2}} \qquad ;\ (0 \le \rho \le 1)\ . \tag{C.24}$$

Again, when $\rho > 0$, then $\nu_U < 0$ and when $\rho < 0$, then $\nu_U > 0$. The new integration domains are plotted in Fig. C.2 in the ν-s plane.

After changing to polar coordinates,

$$II = \frac{\sigma_2\,\sigma_3^{n-1}}{2\pi} \int_0^{\infty} r^{n-1} \exp\left(-\frac{r^2}{2}\right) dr \times \left[\sqrt{1-\rho^2}\int_{\theta_f}^{\pi} \sin^{n-1}\theta\cos\theta\, d\theta \ + \ \rho \int_{\theta_f}^{\pi} \sin^n\theta\, d\theta\right] \ . \tag{C.25}$$

Following the evaluation of integrals in Eqs. (C.18) and (C.19), the final form is obtained as

$$II = \frac{\sigma_2\,\sigma_3^{n-1}}{2\pi}\,(2)^{n/2}\,\Gamma\left(\frac{n+2}{2}\right)\left[-\frac{(1-\rho^2)^{(n+1)/2}}{n} \ + \ \rho \int_{\theta_f}^{\pi} \sin^n\theta\, d\theta\right] \ . \tag{C.26}$$

• **Combine *I* and *II***

Recall that

$$K_1 = 2n\ (I - II)\ .$$

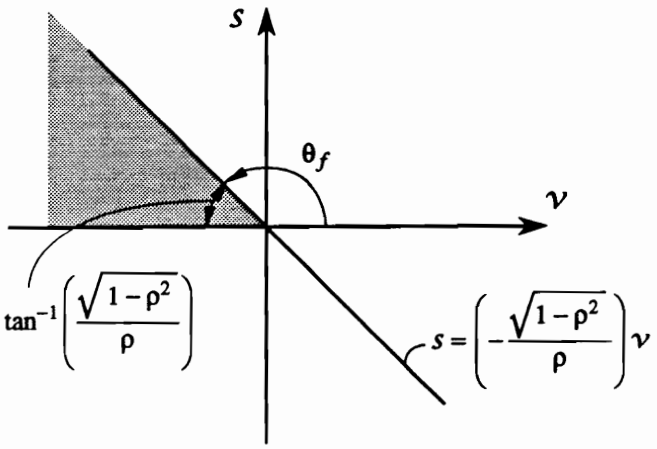

(a) when $\rho > 0$

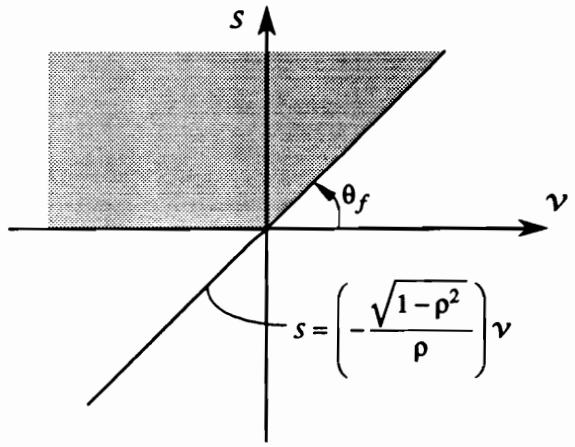

(b) when $\rho < 0$

Figure C.2: Integration domain for K_1's *II*

Thus, substitution of Eqs. (C.21) and (C.26) yields

$$K_1 = \frac{n}{\pi}(2)^{n/2}\,\sigma_2\sigma_3^{n-1}\,\Gamma\left(\frac{n+2}{2}\right)\left[\frac{2}{n}(1-\rho^2)^{(n+1)/2}+\rho\, I_{sn}\right] \tag{C.27}$$

where

$$I_{sn} = \int_0^{\theta_f} \sin^n\theta\; d\theta \;-\; \int_{\theta_f}^{\pi} \sin^n\theta\; d\theta \tag{C.28}$$

which may also be written, for computational efficiency, as

$$\begin{aligned} I_{sn} &= 2\,\mathrm{sgn}(\rho)\int_{\theta_o}^{\pi/2} \sin^n\theta\; d\theta \\ \theta_o &= \tan^{-1}\left(\frac{\sqrt{1-\rho^2}}{\rho}\right) . \end{aligned} \tag{C.29}$$

This completes the derivation of Eq. (5.43).

C.2 Exponential Form Without $|y_3|$

K_3 is selected to represent this group of integrals. Its expectation is

$$\begin{aligned} K_3 &= E[y_2 y_3\; \mathrm{e}^{-(y_3\mathrm{sgn}(y_2)-qz_u)^2/\zeta_2^2}] \\ &= \int_{-\infty}^{\infty}\int_{-\infty}^{\infty} y_2 y_3\; \mathrm{e}^{-(y_3\mathrm{sgn}(y_2)-qz_u)^2/\zeta_2^2}\, f_{Y_2Y_3}\, dy_2 dy_3 . \end{aligned} \tag{C.30}$$

The domain of integration can be divided into two regions ($y_2 < 0$ and $y_2 > 0$) resulting in

$$\begin{aligned} K_1 = &\underbrace{\int_{-\infty}^{\infty}\int_{-\infty}^{0} y_2 y_3\; \mathrm{e}^{-(-y_3-qz_u)^2/\zeta_2^2}\, f_{Y_2Y_3}\, dy_2 dy_3}_{II} \\ &+ \underbrace{\int_{-\infty}^{\infty}\int_{0}^{\infty} y_2 y_3\; \mathrm{e}^{-(y_3-qz_u)^2/\zeta_2^2}\, f_{Y_2Y_3}\, dy_2 dy_3}_{I} . \end{aligned} \tag{C.31}$$

As in section C.1, the integrals will be evaluated separately and then combined in the end.

• **Consider** I

With Eq. (C.4), I becomes

$$I = \frac{1}{2\pi\,\sigma_2\sigma_3\sqrt{1-\rho^2}} \int_{-\infty}^{\infty} y_2 y_3 \exp\underbrace{\left[-\frac{(y_3 - qz_u)^2}{\mu_{\zeta_2}^2} - \frac{y_3^2}{2\sigma_3^2}\right]}_{p_I} \times \int_0^{\infty} y_2 y_3 \exp\left[-\frac{1}{2}\left(\frac{y_2 - \rho\,(\sigma_2/\sigma_3)\,y_3}{\sigma_2\sqrt{1-\rho^2}}\right)^2\right] dy_2\,dy_3 \tag{C.32}$$

where the polynomial p_I after expanding and completing the squares with respect to y_3, can be expresssed as

$$p_I = -\frac{1}{2}\left(\frac{y_3 - \mu_{1*}}{\sigma_{1*}}\right)^2 - \Delta_1 \tag{C.33}$$

$$\mu_{1*} = \frac{2qz_u\sigma_3^2}{2\sigma_3^2 + \mu_{\zeta_2}^2} \tag{C.34}$$

$$\sigma_{1*} = \frac{\mu_{\zeta_2}\sigma_3}{\sqrt{2\sigma_3^2 + \mu_{\zeta_2}^2}} \tag{C.35}$$

$$\Delta_1 = \frac{q^2 z_u^2}{2\sigma_3^2 + \mu_{\zeta_2}^2}\,. \tag{C.36}$$

Substituting back into Eq. (C.32), we obtain

$$I = \frac{e^{-\Delta_1}}{2\pi\,\sigma_2\sigma_3\sqrt{1-\rho^2}} \int_{-\infty}^{\infty} y_3 \exp\left[-\frac{1}{2}\left(\frac{y_3 - \mu_{1*}}{\sigma_{1*}}\right)^2\right] \times \int_0^{\infty} y_2 \exp\left[-\frac{1}{2}\left(\frac{y_2 - \rho\,(\sigma_2/\sigma_3)\,y_3}{\sigma_2\sqrt{1-\rho^2}}\right)^2\right] dy_2\,dy_3\,. \tag{C.37}$$

Then, change variables by letting

$$s = \frac{y_3 - \mu_{1*}}{\sigma_{1*}} \quad \text{and} \quad v = \frac{y_2 - \rho\,(\sigma_2/\sigma_3)\,y_3}{\sigma_2\sqrt{1-\rho^2}}\,.$$

Substitute into Eq. (C.37) and simplify,

$$I = \frac{1}{2\pi}\frac{\sigma_2\sigma_{1*}}{\sigma_3}\,e^{-\Delta_1} \int_{-\infty}^{\infty} (\mu_{1*} + \sigma_{1*}s) \exp\left(-\frac{s^2}{2}\right) \times \int_{v_L}^{\infty} \left[\left(\sqrt{1-\rho^2}\right)v + \left(\frac{\rho\sigma_{1*}}{\sigma_3}\right)s + \frac{\rho\mu_{1*}}{\sigma_3}\right] \exp\left(-\frac{v^2}{2}\right) dv\,ds \tag{C.38}$$

where

$$v_L = -\frac{\rho}{\sigma_3\sqrt{1-\rho^2}}\,(\mu_{1*} + \sigma_{1*}s) \qquad ;\ (0 \le \rho \le 1)\,. \tag{C.39}$$

When $\rho > 0$, then $v_L < 0$ and when $\rho < 0$, then $v_L > 0$. Both cases should be considered in obtaining I as shown in Fig. C.3.

Simple change from rectangular coordinates to polar coordinates is no longer useful since the line defining the lower limit for variable v does not pass through the origin. Here, we would like to rotate the axes counterclockwise by an angle Ω such that the new ordinate, w, is parallel to the line

$$s = -\frac{\mu_{1*}}{\sigma_{1*}} + \left(-\frac{\sigma_3\sqrt{1-\rho^2}}{\rho\sigma_{1*}}\right) v \ . \tag{C.40}$$

The new axes will be called wx-axes (Fig. C.3b) and the new coordinates will be expressed as

$$\begin{aligned} w &= s\cos\Omega - v\sin\Omega \\ x &= s\sin\Omega + v\cos\Omega \end{aligned} \tag{C.41}$$

which leads to the following relations:

$$w^2 + x^2 = s^2 + v^2 \tag{C.42}$$

and

$$dw\,dx = \mathrm{J}\,dv\,ds = dv\,ds \tag{C.43}$$

since

$$\mathrm{J} = \begin{vmatrix} \frac{\partial w}{\partial s} & \frac{\partial w}{\partial v} \\ \frac{\partial x}{\partial s} & \frac{\partial x}{\partial v} \end{vmatrix} = 1 \ . \tag{C.44}$$

To complete the transformation, we need to compute Ω and find the lower limit in x, say x_L. The other limits will not change.

An expression for Ω is obtained by solving for s and v in Eq. (C.41), i.e.,

$$\begin{aligned} s &= w\cos\Omega + x\sin\Omega \\ v &= -w\sin\Omega + x\cos\Omega \end{aligned} \tag{C.45}$$

and substituting them into the equation of the line given by Eq. (C.40) to obtain

$$w\left(\cos\Omega - \frac{\sigma_3\sqrt{1-\rho^2}}{\rho\sigma_{1*}}\sin\Omega\right) + x\left(\sin\Omega + \frac{\sigma_3\sqrt{1-\rho^2}}{\rho\sigma_{1*}}\cos\Omega\right) = -\frac{\mu_{1*}}{\sigma_{1*}} \ . \tag{C.46}$$

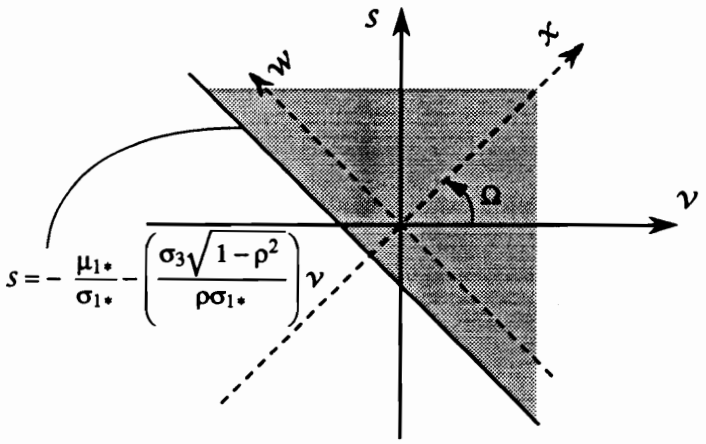

(a) when $\rho > 0$

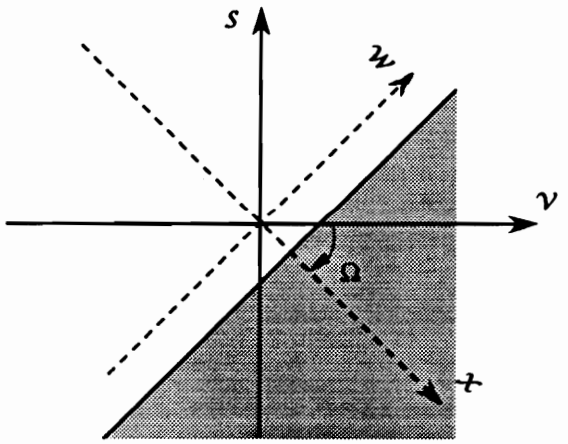

(b) when $\rho < 0$

Figure C.3: Integration domain for K_3's I

The coefficient of w is set to zero to obtain

$$\Omega = \tan^{-1}\left(\frac{\rho\sigma_{1*}}{\sigma_3\sqrt{1-\rho^2}}\right) . \tag{C.47}$$

To find the lower limit in x, set $w = 0$ and solve for x_L in

$$x_L\left(\sin\Omega + \frac{\sigma_3\sqrt{1-\rho^2}}{\rho\sigma_{1*}}\cos\Omega\right) = -\frac{\mu_{1*}}{\sigma_{1*}} \tag{C.48}$$

which gives

$$\begin{aligned} x_L &= -\frac{\mu_{1*}}{\sigma_{1*}}\sin\Omega = -\frac{\mu_{1*}}{\sigma_{1*}}\left(\frac{\rho\sigma_{1*}}{\sqrt{\sigma_3^2(1-\rho^2)+\rho^2\sigma_{1*}^2}}\right) \\ &= -\frac{\rho\mu_{1*}}{\Delta_2} \end{aligned} \tag{C.49}$$

where

$$\Delta_2 = \sqrt{\sigma_3^2(1-\rho^2)+\rho^2\sigma_{1*}^2} . \tag{C.50}$$

The transformation is now complete. Note that the new limit x_L is valid for $-1 \le \rho \le 1$.

Substituting Eqs. (C.42), (C.43), (C.45) and (C.49) into (C.38), we obtain

$$\begin{aligned} I &= \frac{1}{2\pi}\frac{\sigma_2\sigma_{1*}}{\sigma_3}\,\mathrm{e}^{-\Delta_1}\int_{x_L}^{\infty}\int_{-\infty}^{\infty}[\mu_{1*}+\sigma_{1*}(a_2w+a_1x)] \\ &\quad\times\left[\sqrt{1-\rho^2}(-a_1w+a_2x)+\frac{\rho\sigma_{1*}}{\sigma_3}(a_2w+a_1x)+\frac{\rho\mu_{1*}}{\sigma_3}\right] \\ &\quad\times\exp\left[-\frac{1}{2}(w^2+x^2)\right]dw\,dx \end{aligned} \tag{C.51}$$

where

$$a_1 = \sin\Omega = \frac{\rho\sigma_{1*}}{\Delta_2} \tag{C.52}$$

$$a_2 = \cos\Omega = \frac{\sigma_3\sqrt{(1-\rho^2)}}{\Delta_2} . \tag{C.53}$$

The polynomials are then multiplied, similar terms are grouped together and the inner integration in w is carried out to obtain

$$\begin{aligned} I &= \frac{1}{\sqrt{2\pi}}\frac{\sigma_2\sigma_{1*}}{\sigma_3}\,\mathrm{e}^{-\Delta_1} \\ &\quad\times\left(a_3\int_{x_L}^{\infty}x^2\,\mathrm{e}^{-x^2/2}\,dx + a_4\int_{x_L}^{\infty}x\,\mathrm{e}^{-x^2/2}\,dx + a_5\int_{x_L}^{\infty}\mathrm{e}^{-x^2/2}\,dx\right) \end{aligned} \tag{C.54}$$

where

$$a_3 = \frac{\rho\sigma_{1*}}{\sigma_3} \tag{C.55}$$

$$a_4 = \frac{\mu_{1*}}{\sigma_3\,\Delta_1}\,[\sigma_3^2(1-\rho^2)+2\rho^2\sigma_{1*}^2] \tag{C.56}$$

$$a_5 = \frac{\rho\mu_{1*}}{\sigma_3}\,. \tag{C.57}$$

The integrals are evaluated as follows:

$$\int_{x_L}^{\infty} x^2\,\mathrm{e}^{-x^2/2}\,dx = x_L\,\mathrm{e}^{-x_L^2/2} + \sqrt{\frac{\pi}{2}}\left[1+\mathrm{erf}\left(-\frac{x_L}{\sqrt{2}}\right)\right] \tag{C.58}$$

$$\int_{x_L}^{\infty} x\,\mathrm{e}^{-x^2/2}\,dx = \mathrm{e}^{-x_L^2/2} \tag{C.59}$$

$$\int_{x_L}^{\infty} \mathrm{e}^{-x^2/2}\,dx = \sqrt{\frac{\pi}{2}}\left[1+\mathrm{erf}\left(-\frac{x_L}{\sqrt{2}}\right)\right] \tag{C.60}$$

where erf(·) is the error function (see Appendix B, especially for its relation with the Gaussian cumulative distribution function). Substituting these forms back into (C.54), we obtain

$$I = \frac{1}{\sqrt{2\pi}}\frac{\sigma_2\sigma_{1*}}{\sigma_3}\,\mathrm{e}^{-\Delta_1} \times \left\{(a_3+a_5)\sqrt{\frac{\pi}{2}}\left[1+\mathrm{erf}\left(-\frac{x_L}{\sqrt{2}}\right)\right] + (a_3 x_L + a_4)\,\mathrm{e}^{-x_L^2/2}\right\} \tag{C.61}$$

which can also be written as

$$I = \frac{1}{\sqrt{2\pi}}\frac{\sigma_2\sigma_{1*}}{\sigma_3^2}\,\mathrm{e}^{-\Delta_1} \times \left\{\rho\,(\mu_{1*}^2+\sigma_{1*}^2)\sqrt{\frac{\pi}{2}}\left[1+\mathrm{erf}\left(-\frac{x_L}{\sqrt{2}}\right)\right] + (\mu_{1*}\Delta_2)\,\mathrm{e}^{-x_L^2/2}\right\}\,. \tag{C.62}$$

- **Consider *II***

  Similar to *I*,

$$II = \frac{1}{2\pi\,\sigma_2\sigma_3\sqrt{1-\rho^2}}\int_{-\infty}^{\infty} y_2 y_3 \exp\underbrace{\left[-\frac{(-y_3-qz_u)^2}{\mu_{\zeta_2}^2}-\frac{y_3^2}{2\sigma_3^2}\right]}_{p_{II}} \times \int_{-\infty}^{0} y_2 y_3 \exp\left[-\frac{1}{2}\left(\frac{y_2-\rho\,(\sigma_2/\sigma_3)\,y_3}{\sigma_2\sqrt{1-\rho^2}}\right)^2\right] dy_2\,dy_3 \tag{C.63}$$

where the polynomial p_{II} can be expresssed as

$$p_{II} = -\frac{1}{2}\left(\frac{y_3 + \mu_{1*}}{\sigma_{1*}}\right)^2 - \Delta_1 \ . \tag{C.64}$$

Substituting back into Eq. (C.63), we obtain

$$\begin{aligned} II \ = \ & \frac{e^{-\Delta_1}}{2\pi\,\sigma_2\sigma_3\sqrt{1-\rho^2}} \int_{-\infty}^{\infty} y_2 y_3 \exp\left[-\frac{1}{2}\left(\frac{y_3 + \mu_{1*}}{\sigma_{1*}}\right)^2\right] \\ & \times \int_0^{\infty} y_2 y_3 \exp\left[-\frac{1}{2}\left(\frac{y_2 - \rho\,(\sigma_2/\sigma_3)\,y_3}{\sigma_2\sqrt{1-\rho^2}}\right)^2\right] dy_2\,dy_3 \ . \end{aligned} \tag{C.65}$$

Then, change variables by letting

$$\tilde{s} = \frac{y_3 + \mu_{1*}}{\sigma_{1*}} \quad \text{and} \quad \nu = \frac{y_2 - \rho\,(\sigma_2/\sigma_3)\,y_3}{\sigma_2\sqrt{1-\rho^2}} \ .$$

Substitute into Eq. (C.65) and simplify,

$$\begin{aligned} II \ = \ & \frac{1}{2\pi}\frac{\sigma_2\sigma_{1*}}{\sigma_3} e^{-\Delta_1} \int_{-\infty}^{\infty} (\mu_{1*} + \sigma_{1*}\tilde{s}) \exp\left(-\frac{\tilde{s}^2}{2}\right) \\ & \times \int_{-\infty}^{\nu_U} \left[\left(\sqrt{1-\rho^2}\right)\nu + \left(\frac{\rho\sigma_{1*}}{\sigma_3}\right)\tilde{s} + \frac{\rho\mu_{1*}}{\sigma_3}\right] \exp\left(-\frac{\nu^2}{2}\right) d\nu\, d\tilde{s} \end{aligned} \tag{C.66}$$

where

$$\nu_U = -\frac{\rho}{\sigma_3\sqrt{1-\rho^2}}(-\mu_{1*} + \sigma_{1*}\tilde{s}) \qquad ;\ (0 \le \rho \le 1) \ . \tag{C.67}$$

Thus, the main difference with I is the new variable $\tilde{s}$ and the limits in ν. Upon rotation of axes through the angle Ω, as shown in calculation for I, the new upper limit of integration in x is

$$\begin{aligned} x_U \ &= \ \frac{\mu_{1*}}{\sigma_{1*}}\sin\Omega \ = \ -\frac{\mu_{1*}}{\sigma_{1*}}\left(\frac{\rho\sigma_{1*}}{\sqrt{\sigma_3^2(1-\rho^2)+\rho^2\sigma_{1*}^2}}\right) \\ &= \ \frac{\rho\mu_{1*}}{\Delta_2} \ = \ -x_L \ . \end{aligned} \tag{C.68}$$

Then,

$$\begin{aligned} II \ = \ & \frac{1}{2\pi}\frac{\sigma_2\sigma_{1*}}{\sigma_3} e^{-\Delta_1} \int_{-\infty}^{x_U}\int_{-\infty}^{\infty} [-\mu_{1*} + \sigma_{1*}(a_2 w + a_1 x)] \\ & \times \left[\sqrt{1-\rho^2}(-a_1 w + a_2 x) + \frac{\rho\sigma_{1*}}{\sigma_3}(a_2 w + a_1 x) - \frac{\rho\mu_{1*}}{\sigma_3}\right] \\ & \times \exp\left[-\frac{1}{2}(w^2 + x^2)\right] dw\, dx \ . \end{aligned} \tag{C.69}$$

Upon evaluation of the inner integral, we obtain

$$II = \frac{1}{\sqrt{2\pi}} \frac{\sigma_2 \sigma_{1*}}{\sigma_3} \mathrm{e}^{-\Delta_1} \times \left(a_3 \int_{-\infty}^{x_U} x^2 \mathrm{e}^{-x^2/2}\, dx + a_6 \int_{-\infty}^{x_U} x \mathrm{e}^{-x^2/2}\, dx + a_5 \int_{-\infty}^{x_U} \mathrm{e}^{-x^2/2}\, dx \right) \tag{C.70}$$

where $a_6 = -a_4$. The integrals are evaluated as follows:

$$\int_{-\infty}^{x_U} x^2 \mathrm{e}^{-x^2/2}\, dx = -x_U \mathrm{e}^{-x_U^2/2} + \sqrt{\frac{\pi}{2}} \operatorname{erfc}\left(-\frac{x_U}{\sqrt{2}}\right) \tag{C.71}$$

$$\int_{-\infty}^{x_U} x \mathrm{e}^{-x^2/2}\, dx = -\mathrm{e}^{-x_U^2/2} \tag{C.72}$$

$$\int_{-\infty}^{x_U} \mathrm{e}^{-x^2/2}\, dx = \sqrt{\frac{\pi}{2}} \operatorname{erfc}\left(-\frac{x_U}{\sqrt{2}}\right) \tag{C.73}$$

where erfc(·) is the complementary error function (see Appendix B, especially for its relation with the Gaussian cumulative distribution function). Substituting these forms back into (C.70), we obtain

$$II = \frac{1}{\sqrt{2\pi}} \frac{\sigma_2 \sigma_{1*}}{\sigma_3} \mathrm{e}^{-\Delta_1} \times \left[(a_3 + a_5) \sqrt{\frac{\pi}{2}} \operatorname{erfc}\left(-\frac{x_U}{\sqrt{2}}\right) + (-a_3 x_U - a_6) \mathrm{e}^{-x_U^2/2} \right] \tag{C.74}$$

which can also be written as

$$II = \frac{1}{\sqrt{2\pi}} \frac{\sigma_2 \sigma_{1*}}{\sigma_3^2} \mathrm{e}^{-\Delta_1} \times \left[\rho\, (\mu_{1*}^2 + \sigma_{1*}^2) \sqrt{\frac{\pi}{2}} \operatorname{erfc}\left(-\frac{x_U}{\sqrt{2}}\right) + (\mu_{1*} \Delta_2) \mathrm{e}^{-x_U^2/2} \right] . \tag{C.75}$$

• **Combine *I* and *II***

In combining Eqs. (C.62) and (C.75), note that

$$K_3 = I + II \quad , \quad x_U = -x_L$$

and

$$\left[1 + \operatorname{erf}\left(-\frac{x_L}{\sqrt{2}}\right)\right] = \left[1 - \operatorname{erf}\left(-\frac{x_U}{\sqrt{2}}\right)\right] = \operatorname{erfc}\left(-\frac{x_U}{\sqrt{2}}\right) .$$

Thus,

$$K_3 = \sqrt{\frac{2}{\pi}}\frac{\sigma_2\sigma_{1*}}{\sigma_3^2}\,\mathrm{e}^{-\Delta_1} \times \left[\rho\,(\mu_{1*}^2+\sigma_{1*}^2)\sqrt{\frac{\pi}{2}}\,\mathrm{erfc}\left(-\frac{x_U}{\sqrt{2}}\right)+(\mu_{1*}\Delta_2)\,\mathrm{e}^{-x_U^2/2}\right]. \tag{C.76}$$

Since

$$\frac{\sigma_{1*}}{\sigma_3}=\frac{\mu_{\zeta_2}}{\sqrt{2\sigma_3^2+\mu_{\zeta_2}^2}}, \tag{C.77}$$

K_3 can be rearranged in the form of Eq. (5.45):

$$K_3 = \frac{\mu_{\zeta_2}}{\sqrt{2\sigma_3^2+\mu_{\zeta_2}^2}}\frac{\sigma_2}{\sigma_3}\,\mathrm{e}^{-\Delta_1} \times \left[\rho(\mu_{1*}^2+\sigma_{1*}^2)\mathrm{erfc}\left(\frac{-x_U}{\sqrt{2}}\right)+\sqrt{\frac{2}{\pi}}\,\mu_{1*}\Delta_2\mathrm{e}^{-x_U^2/2}\right] \tag{C.78}$$

where x_U was defined as Δ_3 in Eq. (5.45).

C.3 Exponential Form With $|y_3|$

K_8 is selected to represent this group of integrals. Its expectation is

$$K_8 = E[y_2|y_3|^n y_3\ \mathrm{e}^{-(y_3\mathrm{sgn}(y_2)-qz_u)^2/\zeta_2^2}] = \int_{-\infty}^{\infty}\int_{-\infty}^{\infty} y_2|y_3|^n y_3\ \mathrm{e}^{-(y_3\mathrm{sgn}(y_2)-qz_u)^2/\zeta_2^2} f_{Y_2Y_3}\,dy_2dy_3\,. \tag{C.79}$$

The domain of integration can be divided into four regions ($y_2<0$, $y_2>0$, $y_3<0$ and $y_3>0$) resulting in

$$\begin{aligned} K_8 = {} & \underbrace{\int_{-\infty}^{0}\int_{-\infty}^{0}(-1)^n y_2 y_3^{n+1}\ \mathrm{e}^{-(-y_3-qz_u)^2/\zeta_2^2} f_{Y_2Y_3}\,dy_2dy_3}_{\mathcal{A}} \\ & + \underbrace{\int_{-\infty}^{0}\int_{0}^{\infty}(-1)^n y_2 y_3^{n+1}\ \mathrm{e}^{-(y_3-qz_u)^2/\zeta_2^2} f_{Y_2Y_3}\,dy_2dy_3}_{\mathcal{B}} \\ & + \underbrace{\int_{0}^{\infty}\int_{-\infty}^{0} y_2 y_3^{n+1}\ \mathrm{e}^{-(-y_3-qz_u)^2/\zeta_2^2} f_{Y_2Y_3}\,dy_2dy_3}_{\mathcal{C}} \\ & + \underbrace{\int_{0}^{\infty}\int_{0}^{\infty} y_2 y_3^{n+1}\ \mathrm{e}^{-(y_3-qz_u)^2/\zeta_2^2} f_{Y_2Y_3}\,dy_2dy_3}_{\mathcal{D}}\,. \end{aligned} \tag{C.80}$$

Letting $u_2 = -y2$ and $u_3 = -y3$, substituting into $\mathcal{A}$ and $\mathcal{B}$ in Eq. (C.80), we find that $\mathcal{A} \equiv \mathcal{D}$ and $\mathcal{B} \equiv C$, as in section C.1. Thus, K_8 simplifies to

$$K_8 = 2\left(\underbrace{\int_0^\infty \int_0^\infty y_2 y_3^{n+1}\ \mathrm{e}^{-(y_3 - qz_u)^2/\zeta_2^2} f_{Y_2Y_3}\, dy_2 dy_3}_{I} + \underbrace{\int_0^\infty \int_{-\infty}^0 y_2 y_3^{n+1}\ \mathrm{e}^{-(y_3 - qz_u)^2/\zeta_2^2} f_{Y_2Y_3}\, dy_2 dy_3}_{II}\right) . \tag{C.81}$$

As in sections C.1 and C.2, the integrals will be evaluated separately and then combined in the end.

- **Consider** I

Similar to K_3 in section C.2 and Eqs. (C.32) to (C.37), we can write I as

$$I = \frac{\mathrm{e}^{-\Delta_1}}{2\pi\,\sigma_2\sigma_3\sqrt{1-\rho^2}} \int_0^\infty y_3^{n+1} \exp\left[-\frac{1}{2}\left(\frac{y_3 - \mu_{1*}}{\sigma_{1*}}\right)^2\right] \times \int_0^\infty y_2 \exp\left[-\frac{1}{2}\left(\frac{y_2 - \rho\,(\sigma_2/\sigma_3)\,y_3}{\sigma_2\sqrt{1-\rho^2}}\right)^2\right] dy_2\, dy_3 \tag{C.82}$$

Change variable by letting

$$\nu = \frac{y_2 - \rho\,(\sigma_2/\sigma_3)\,y_3}{\sigma_2\sqrt{1-\rho^2}}$$

to obtain

$$I = \frac{\sigma_2}{2\pi\,\sigma_3}\mathrm{e}^{-\Delta_1} \int_0^\infty y_3^{n+1} \exp\left[-\frac{1}{2}\left(\frac{y_3 - \mu_{1*}}{\sigma_{1*}}\right)^2\right] \times \underbrace{\int_{\nu_L}^\infty \left(\sqrt{1-\rho^2}\,\nu + \frac{\rho}{\sigma_3} y_3\right) \exp\left(-\frac{\nu^2}{2}\right) d\nu}_{I_a}\, dy_3 \tag{C.83}$$

where

$$\nu_L = -\frac{\rho y_3}{\sigma_3\sqrt{1-\rho^2}} . \tag{C.84}$$

Consider the inner integral,

$$I_a = \sqrt{1-\rho^2} \int_{\nu_L}^\infty \nu \exp\left(-\frac{\nu^2}{2}\right) d\nu + \frac{\rho}{\sigma_3} y_3 \int_{\nu_L}^\infty \exp\left(-\frac{\nu^2}{2}\right) d\nu . \tag{C.85}$$

The integrals are evaluated as shown in Eqs. (C.57) and (C.58) to yield

$$I_a = \sqrt{1-\rho^2}\ \mathrm{e}^{-\nu_L^2/2} + \frac{\rho}{\sigma_3} y_3 \sqrt{\frac{\pi}{2}} \left[1 + \mathrm{erf}\left(-\frac{\nu_L}{\sqrt{2}}\right)\right] . \tag{C.86}$$

Substitute I_a back into Eq. (C.83),

$$\begin{aligned} I &= \frac{1}{2\pi}\frac{\sigma_2}{\sigma_3}\mathrm{e}^{-\Delta_1} \\ &\times \left\{ \sqrt{1-\rho^2} \underbrace{\int_0^\infty y_3^{n+1} \exp\left[-\frac{1}{2}\left\{\left(\frac{y_3-\mu_{1*}}{\sigma_{1*}}\right)^2 + \left(\frac{\rho y_3}{\sigma_3\sqrt{1-\rho^2}}\right)^2\right\}\right] dy_3}_{I_b} \right. \\ &+ \left. \sqrt{\frac{\pi}{2}}\frac{\rho}{\sigma_3} \underbrace{\int_0^\infty \exp\left[-\frac{1}{2}\left(\frac{y_3-\mu_{1*}}{\sigma_{1*}}\right)^2\right]\left[1+\mathrm{erf}\left(\frac{\rho y_3}{\sqrt{2}\sigma_3\sqrt{1-\rho^2}}\right)\right] y_3^{n+2}\, dy_3}_{I_c} \right\} \end{aligned} \tag{C.87}$$

where I_b can be solved in closed-form (which will be shown shortly), while I_c, which cannot be solved in closed-form, is rearranged to have a format compatible with the generalized Gauss-Laguerre quadrature as

$$\begin{aligned} I_c &= \int_0^\infty \exp\left[-\frac{1}{2}\left(\frac{y_3-\mu_{1*}}{\sigma_{1*}}\right)^2 + y_3\right] \\ &\quad \times \left[1+\mathrm{erf}\left(\frac{\rho y_3}{\sqrt{2}\sigma_3\sqrt{1-\rho^2}}\right)\right] \underbrace{y_3^{n+2}\,\mathrm{e}^{-y_3}}_{\text{weight}}\, dy_3 . \end{aligned} \tag{C.88}$$

To solve for I_b, let

$$p_{III} = \left\{\left(\frac{y_3-\mu_{1*}}{\sigma_{1*}}\right)^2 + \left(\frac{\rho y_3}{\sigma_3\sqrt{1-\rho^2}}\right)^2\right\} , \tag{C.89}$$

and rewrite p_{III} by expanding and completing the squares with respect to y_3 to obtain

$$p_{III} = \left(\frac{y_3-\mu_{2*}}{\sigma_{2*}}\right)^2 + \Delta_3^2 \tag{C.90}$$

$$\mu_{2*} = \frac{\mu_{1*}\sigma_3^2(1-\rho^2)}{\Delta_2^2} \tag{C.91}$$

$$\sigma_{2*} = \frac{\sigma_{1*}\sigma_3\sqrt{1-\rho^2}}{\Delta_2} \tag{C.92}$$

$$\Delta_3 = \frac{\rho\mu_{1*}}{\Delta_2} . \tag{C.93}$$

Substitute p_{III} back into I_b to obtain

$$I_b = e^{-\Delta_3^2/2} \int_0^\infty y_3^{n+1} \exp\left[-\frac{1}{2}\left(\frac{y_3 - \mu_{1*}}{\sigma_{1*}}\right)^2 + \left(\frac{\rho y_3}{\sigma_3\sqrt{1-\rho^2}}\right)^2\right] dy_3 \ . \tag{C.94}$$

Let

$$\check{s} = \frac{y_3 - \mu_{2*}}{\sigma_{2*}} \ ,$$

then,

$$I_b = \sigma_{2*}\, e^{-\Delta_3^2/2} \int_{-\mu_{2*}/\sigma_{2*}}^\infty (\mu_{2*} + \sigma_{2*}\,\check{s})^{n+1} \exp\left(-\frac{\check{s}^2}{2}\right) d\check{s} \ . \tag{C.95}$$

Note, however, that

$$(\mu_{2*} + \sigma_{2*}\,\check{s})^{n+1} = \sum_{k=0}^{n+1} \binom{n+1}{k} (\mu_{2*})^{n+1-k}\, \sigma_{2*}^k\, \check{s}^k \tag{C.96}$$

Substituting Eq. (C.96) back into (C.95), we obtain

$$I_b = \sigma_{2*}\, e^{-\Delta_3^2/2} \sum_{k=0}^{n+1} \binom{n+1}{k} (\mu_{2*})^{n+1-k}\, \sigma_{2*}^k \underbrace{\int_{-\mu_{2*}/\sigma_{2*}}^\infty \check{s}^k \exp\left(-\frac{\check{s}^2}{2}\right) d\check{s}}_{I_d} \tag{C.97}$$

where I_d can be shown, using the incomplete Gamma function integral (Appendix B), to be

$$I_d = (-1)^k\, (2)^{(k-1)/2} \left[\gamma\left(\frac{k+1}{2}, \frac{\mu_{2*}^2}{2\sigma_{2*}^2}\right) - \Gamma\left(\frac{k+1}{2}\right)\right] \tag{C.98}$$

where $\gamma(\cdot)$ is the incomplete Gamma function and $\Gamma(\cdot)$ is the complete Gamma function. Thus,

$$\begin{aligned} I_b \ = \ & \sigma_{2*}\, e^{-\Delta_3^2/2} \sum_{k=0}^{n+1} \binom{n+1}{k} (\mu_{2*})^{n+1-k}\, \sigma_{2*}^k\, (-1)^k\, (2)^{(k-1)/2} \\ & \times \left[\gamma\left(\frac{k+1}{2}, \frac{\mu_{2*}^2}{2\sigma_{2*}^2}\right) - \Gamma\left(\frac{k+1}{2}\right)\right] \ . \end{aligned} \tag{C.99}$$

Finally, I can be written as

$$I = \frac{1}{2\pi}\frac{\sigma_2}{\sigma_3}\, e^{-\Delta_1} \left(\sqrt{1-\rho^2}\ I_b \ + \sqrt{\frac{\pi}{2}}\frac{\rho}{\sigma_3}\ I_c\right) \tag{C.100}$$

where I_b and I_c are given by Eqs. (C.99) and (C.88), respectively.

- **Consider *II***

Similar to I, II can be written as

$$II = \frac{e^{-\Delta_1}}{2\pi\,\sigma_2\sigma_3\sqrt{1-\rho^2}} \int_0^\infty y_3^{n+1} \exp\left[-\frac{1}{2}\left(\frac{y_3+\mu_{1*}}{\sigma_{1*}}\right)^2\right] \times \int_0^\infty y_2 \exp\left[-\frac{1}{2}\left(\frac{y_2-\rho\,(\sigma_2/\sigma_3)\,y_3}{\sigma_2\sqrt{1-\rho^2}}\right)^2\right] dy_2\,dy_3 \tag{C.101}$$

$$= \frac{\sigma_2}{2\pi\,\sigma_3} e^{-\Delta_1} \int_0^\infty y_3^{n+1} \exp\left[-\frac{1}{2}\left(\frac{y_3+\mu_{1*}}{\sigma_{1*}}\right)^2\right] \times \underbrace{\int_{-\infty}^{\nu_U} \left(\sqrt{1-\rho^2}\,\nu + \frac{\rho}{\sigma_3} y_3\right) \exp\left(-\frac{\nu^2}{2}\right) d\nu}_{II_a}\, dy_3 \tag{C.102}$$

where $\nu_U = \nu_L$ [see Eq. (C.84)] and

$$II_a = -\sqrt{1-\rho^2}\; e^{-\nu_U^2/2} + \frac{\rho}{\sigma_3} y_3 \sqrt{\frac{\pi}{2}}\,\mathrm{erfc}\left(-\frac{\nu_U}{\sqrt{2}}\right) . \tag{C.103}$$

Then, following the procedure shown in Eqs. (C.87) to (C.99), II can be derived as

$$II = \frac{1}{2\pi}\frac{\sigma_2}{\sigma_3} e^{-\Delta_1}\left(-\sqrt{1-\rho^2}\; II_b + \sqrt{\frac{\pi}{2}}\frac{\rho}{\sigma_3}\; II_c\right) \tag{C.104}$$

where II_b has the form

$$II_b = \sigma_{2*}\, e^{-\Delta_3^2/2} \sum_{k=0}^{n+1} \binom{n+1}{k} (\mu_{2*})^{n+1-k}\, \sigma_{2*}^k\, (-1)^{n-k}\, (2)^{(k-1)/2} \times \left[\gamma\left(\frac{k+1}{2}, \frac{\mu_{2*}^2}{2\sigma_{2*}^2}\right) - \Gamma\left(\frac{k+1}{2}\right)\right] \tag{C.105}$$

and the Gaussian-Laguerre quadrature II_c is given by

$$II_c = \int_0^\infty \exp\left[-\frac{1}{2}\left(\frac{y_3+\mu_{1*}}{\sigma_{1*}}\right)^2 + y_3\right] \times \mathrm{erfc}\left(\frac{\rho y_3}{\sqrt{2}\sigma_3\sqrt{1-\rho^2}}\right) \underbrace{y_3^{n+2}\, e^{-y_3}}_{\text{weight}}\, dy_3 . \tag{C.106}$$

- **Combine *I* and *II***

In combining Eqs. (C.100) and (C.104), note that

$$K_8 = 2\,(I+II) \quad , \quad \nu_U = \nu_L = -\left(\frac{\rho y_3}{\sigma_3\sqrt{1-\rho^2}}\right)$$

and

$$\operatorname{erfc}\left(-\frac{\nu_U}{\sqrt{2}}\right) = \left[1 - \operatorname{erf}\left(-\frac{\nu_U}{\sqrt{2}}\right)\right] \ .$$

Thus, we can generalize I_b and II_b as

$$\begin{aligned} I_{sum}(f_i, n+1) &= \sigma_{2*}\, \mathrm{e}^{-\Delta_3^2/2} \sum_{k=0}^{n+1} \binom{n+1}{k} (\mu_{2*})^{n+1-k}\, \sigma_{2*}^k\, (2)^{(k-1)/2} \\ &\quad \times f_{sgn} \left[\gamma\left(\frac{k+1}{2}, \frac{\mu_{2*}^2}{2\sigma_{2*}^2}\right) - \Gamma\left(\frac{k+1}{2}\right)\right] \qquad \text{(C.107)} \\ f_{sgn} &= \begin{cases} (-1)^k & \text{if } f_i = 1 \text{ (i.e., } I_b) \\ (-1)^{n-k} & \text{if } f_i = -1 \text{ (i.e., } II_b) \end{cases} \ . \end{aligned}$$

Likewise, the Gauss-Laguerre quadrature can be expressed for both I_c and II_c as

$$\begin{aligned} I_{GL}(f_i, n+2) &= \int_0^\infty \exp\left[-\frac{1}{2}\left(\frac{y_3 - f_i\, \mu_{1*}}{\sigma_{1*}}\right)^2 + y_3\right] \\ &\quad \times \left[1 + f_i \operatorname{erf}\left(\frac{\rho y_3}{\sqrt{2}\sigma_3\sqrt{1-\rho^2}}\right)\right] y_3^{n+2}\, \mathrm{e}^{-y_3}\, dy_3 \qquad \text{(C.108)} \end{aligned}$$

where $f_i = 1$ for I_c and $f_i = -1$ for II_c. Then, K_8 is finally given as

$$\begin{aligned} K_8 &= \frac{1}{\pi}\frac{\sigma_2}{\sigma_3}\, \mathrm{e}^{-\Delta_1} \left\{\sqrt{1-\rho^2}\, [I_{sum}(1, n+1) - I_{sum}(-1, n+1)]\right. \\ &\quad \left. + \sqrt{\frac{\pi}{2}}\, \frac{\rho}{\sigma_3}\, [I_{GL}(1, n+2) + I_{GL}(-1, n+2)]\right\} \qquad \text{(C.109)} \end{aligned}$$

which is the same as that given in Eq. (5.50).

Appendix D

Digital Generation of White Noise

Simulation methods can be applied to the response and performance analyses of any systems subjected to random excitations, as long as computer algorithms to obtain the response to deterministic excitations are available. The most common type is the Monte Carlo simulation (MCS). Since each individual computation is deterministic, a large number of calculations are performed to infer about response statistics. Key to this method is the proper generation of sample functions of the excitation process. Clough and Penzien (1993) and Soong and Grigoriu (1993) present methods to generate samples of stochastic processes. Digital generation of the white noise excitation used in the present work follows that of Baber (1980).

1. A set of random variables uniformly distributed over (0,1) is generated; say w_1, $w_2, \ldots, w_n$.

2. The set of uniformly distributed random variable w_i is transformed to a set of standard Gaussian (or normal) random variable :

$$\begin{aligned} x_i &= \sqrt{-2\ln w_i}\,\cos(2\pi w_{i+1}) \\ x_{i+1} &= \sqrt{-2\ln w_i}\,\sin(2\pi w_{i+1}) \end{aligned} \tag{D.1}$$

   where x_i and x_{i+1} are independent Gaussian random variables with zero means and unit variances.

3. The x_i's are mapped to obtain new Gaussian random variables y_i with mean μ and standard deviation σ as follows:

$$y_i = \mu + \sigma x_i \tag{D.2}$$

$$\sigma = \sqrt{2\pi \frac{S_o}{\Delta t}} \tag{D.3}$$

where S_o is the Gaussian white noise power spectral density. In the case of zero-mean white noise excitation, μ is set to zero. In the limit as Δt approaches zero, the resulting sequence of y_i's becomes a white noise, *provided that* the time until the first pulse is taken as a random variable, uniformly distributed over (0,1). The limiting process is never allowed to occur, but for small Δt, Baber (1980) has shown that the actual power spectral density varies slowly, resulting to excitations that are nearly white in the range of interest.

Vita

(December, 1993)

Greg, born on June 18, 1964, received a Bachelor of Science degree in Civil Engineering in 1984 from the Mapua Institute of Technology in Manila, Philippines. He obtained a professional civil engineering license the following year. From 1985 to 1987, he worked as a researcher at the Philippine Forest Products Research and Development Institute. He was a three-time Philippine representative to seminar-workshops sponsored by the United Nations Development Program (UNDP/UNIDO) related to building materials, technologies and construction systems. He performed damage assessment surveys on houses damaged by typhoons or tropical cyclones and helped interested professionals to organize a national technical team for typhoon damage assessment.

He came to the United States as a graduate student at Virginia Polytechnic Institute and State University (Virginia Tech) in September 1987. He taught laboratory classes on mechanical properties of wood for the Department of Wood Science and Forest Products and an introductory class on microcomputing for the School of Forestry and Wildlife Resources. He received a Master's degree in Wood Mechanics and Engineering in November 1989 and continued studies in the PhD program. His master's research on the strength capacity of notched wood beams generated positive interest from timber code authorities and design practitioners. In June 1993, he received a second Master's degree in Civil Engineering (Structures).

Greg received the 1993 A.B. Massey Award, given by the School of Forestry and Wildlife Resources at Virginia Tech, for superior performance and professionalism as a graduate student. He is a member of the Honor Society of Phi Kappa Phi at Virginia Tech.